Università degli Studi di Palermo

AREA RICERCA E TRASFERIMENTO TECNOLOGICO
SETTORE DOTTORATI E CONTRATTI PER LA RICERCA
U. O. DOTTORATI DI RICERCA

D067 – TECHNOLOGIES AND SCIENCES FOR HUMAN HEALTH

Department of Biological, Chemical and Pharmaceutical Sciences and Technologies (STEBICEF)

S.S.D. - BIOS-14/A

Evaluation of DNA methylation role in regulating cell cycle progression and chromosome segregation

PhD STUDENT
Dr Salvatore Martino

COORDINATOR
Prof. Valeria Vetri

TUTOR
Prof. Salvatore Feo

CO TUTOR
Dr Viviana Barra

CYCLE - XXXVIII
2022/2025

Summary

Acronyms

5caC: 5-carboxylcytosine
5fC: 5-formylcytosine
5hmC: 5-Hydroxymethylcytosine
5hmU: 5-hydroxymethyluracil
5mC: 5-methyl-cytosine
9-1-1: Rad9-Rad1-Hus1 complex
ADD: ATRX–DNMT3–DNMT3L
AdoMet: S-adenosyl-l-methionine
AID: Activation-Induced cytosine Deaminase
AID: Auxin Inducible Degron
APC: Anaphase-Promoting Complex
APE1: AP Endonuclease 1
AS:Angelman Syndrome
ATM: Ataxia Telangiectasia Mutated
ATR: Ataxia Telangiectasia and Rad3-Related
ATRX: Alpha-Thalassemia/Mental Retardation Syndrome, X-linked
BASC: BRCA1-associated genome surveillance complex
BER: Base Excision Repair
BWS: Beckwith–Wiedemann Syndrome
CAP-Gly: Cytoskeleton-Associated Protein Gly-rich domains
CATD: Centromere Targeting Domain
CCAN: Constitutive Centromere-Associated Network
CDKs: Cyclin-Dependent Kinases
CDRs: Centromere Dip Regions
CENP-A: CENtromeric Protein A
CENP-B: CENtromeric Protein B
CENP-C: CENtromeric Protein C
CENP-E: CENtromeric protein E
CENP-T: CENtromeric Protein T
CGIs: CpG islands
CH: Calponin Homology domains
CHD: Chromodomain helicase DNA-binding
CKI: CDK Inhibitors
CPC: Chromosomal Passenger Complex
DBS: Double-Strand Breaks
DDR: DNA Damage Response
DiMeLo-seq: Directed Methylation with Long-read sequencing
DNMTs: DNA methyltransferase enzymes
DRM: Domains Rearranged Methylase
EBH: End-Binding Homology domains
ESC: Embryonic Stem Cells
FMRP: FMR1 protein
FRAXA: Fragile X syndrome
G0; Gap0
G1: Gap1 phase
G2: Gap2 phase

H3K9me3: tri-methylation of the histone H3 at the Lysine9
HATs: Histone acetyl transferases
HDAC: Histone deacetylases
Hec1: Highly Expressed in Cancer 1
HORs: Higher-Order Repeat units
HP1: Heterochromatic Protein 1
HYMAI: Hydatidiform Mole-Associated and Imprinted
IAA: Auxin or indole-3-acetic acid sodium salt
ICF: Centromere Instability and Facial anomalies syndrome
Igf-2: Insulin-like growth factor 2
Igf-2r: Igf-2 receptor
iPSC: Induced Pluripotent Stem Cells
IR: Ionizing Irradiation
ISWI: Imitation switch
K-fibers: kinetochore fibers
KMN: KNL1-MIS12-NDC80 complexes network
lnRNA: long non-coding RNA
LOI: Loss Of Imprinting
M: Mitosis
m6A: N6-Methyladenosine
m6Am: N6,2-O-dimethyladenosine
m7G: 7-methylguanosine
MAPs: Microtubule-Associated Proteins
MBD: Methyl-binding domain proteins
MCC: Mitotic Checkpoint Complex
MeCP2: Methyl-CpG binding protein 2
MRN: Mre11–Rad50–Nbs1 complex
MTCs: methyltransferase METTL3/METTL14 complex
NADNMT1: Auxin Inducible Degron (AID) and mNeon Green
ncRNA: Non-coding RNA
NHEJ: Non-Homologous End Joining
PCNA: Proliferating Cell Nuclear Antigen
PEFs: Polar Ejection Forces
PHP-Ib: Pseudo Hypoparathyroidism type Ib
piRNA: PIWI-Interacting RNA
PLAGL1: Pleiomorphic Adenoma Gene-Like 1
Plus-end: Microtubule plus extremity
Pol β: DNA polymerase β
pRB: RetinoBlastoma
pre-RC: pre-replicative complex
PWS: Prader–Willi syndrome
PWWP: Pro-Trp-Trp-Pro
RFTS: Replication Foci Targeting Sequence
RNAP II: RNA Polimerase II
ROS: Reactive Oxidative Species
ROS1: Repressor Of Silencing 1
RZZ: ROD-ZW10-ZWILCH
S: DNA Synthesis phase
S55p: Ser55

SAC: Spindle Assembly Checkpoint
Sat: Satellite DNAs
Sgo1: Shugoshin1
SLE: Systemic lupus erythematosus
SNURF: Small Nuclear Ribonucleoprotein Polypeptide N (SNRPN)/SNRPN Upstream Reading Frame
SRA: SET and RING finger-associated domain
STLC: S-Trityl-L-cysteine
SWI/SNF: Switch/sucrose non-fermentable
TADs: Topologically Associating Domains
TET: Tet-Eleven-Translocation
TIRs: Terminal Inverted Repeats
TLS: Translocated in Liposarcoma
TNDM: Transient Neonatal Diabetes Mellitus
UBE3A: Ubiquitin protein ligase E3A
UHRF1: Ubiquitin-Like PHD and Ring Finger Domain 1
WGS: Whole-Genome Shotgun reads
ZAC-AS: PLAGL1 antisense transcript
α Sat: α satellite DNA

Abstract

Background: Epigenetic regulation is important to ensure the fitness of the cells. To this regard, DNA methylation has the important role of regulating gene expression and heterochromatinization. DNA methylation pattern changes in cancer and during aging. Specifically, cancer cells are characterised by DNA hypermethylation at promoters of tumour suppressor genes, leading to improved proliferation in different microenvironments. Instead, DNA hypomethylation mostly occurs at repetitive sequences of the genome, which characterise the telomere and the centromere. The centromere sustains chromosome segregation through the recruitment of the kinetochore complex, which allows a strong connection with the microtubules and acts as an anchor to permit the movement of chromosomes. Impairment of chromosome segregation is known to be sensed as a stress by normal cells which undergo cell cycle arrest. Changes at the centromeric DNA methylation correlate with aneuploidy, suggesting the occurrence of alterations in chromosome segregation. However, how DNA methylation regulates the fidelity of chromosome segregation is not yet fully understood. To address this issue, a DNA hypomethylating inducible system was used.

Methods: To induce DNA methylation, I used Normal Retinal Pigment Epithelial hTert immortalized (RPE-1) and colon-rectum cancer cell line (DLD-1) engineered to trigger the degradation of the endogenous DNMT1 with an inducible degron. Prolonged DNMT1 absence leads to a global passive DNA methylation loss, which mimics the aging event. The system is not toxic and most importantly, it is reversible. The reversibility permits to discern the effect of the DNA methylation alteration from the combinatory effect achieved when the DNMT1, together with DNA methylation, is lost. To evaluate the effect of prolonged DNMT1 absence and DNA hypomethylation on the fitness of the cells and thus, the cell cycle progression and chromosome segregation, genetics, cell and molecular biology techniques were used.

Results: The performed experiments show that DNMT1 absence *per se* does not induce cell cycle arrest in both normal and cancer cells. Instead, prolonged DNMT1 absence and subsequent DNA hypomethylation are required to trigger p53/p21 cell cycle arrest.

In DLD-1 cancer cells, DNMT1 absence also correlates with difficulties in properly congressing the chromosomes, which fail in gaining a bioriented state with subsequent misaligned chromosomes. Moreover, DNMT1 absence or DNA hypomethylation favours the recruitment of CENP-A and CENP-C, which are important for centromere functioning. Ultimately, Aurora B, the kinase required to correct improper kinetochore-microtubule attachments, underwent altered dynamics: 1) increased activity when microtubules are disassembled; 2) reduced recruitment at the

metaphase plate, signature of mature end-on attachment; 3) no varied recruitment at misaligned chromosomes.

Conclusion: Prolonged DNMT1 absence generates cellular stress, due to the induced DNA hypomethylation. This stress culminates in the cell cycle arrest when the threshold sustainable minimal level of DNA methylation is reached. In cancer cells DNMT1 or DNA methylation regulates the recruitment of CENPs and Aurora B kinase. Interestingly, DNA methylation loss induces enhanced stability of the already in place kinetochore-microtubule attachments, while the misaligned chromosomes seem to be disregarded.

1 Introduction

In this introduction, I will provide a brief overview of epigenetics, with a particular emphasis on DNA methylation. I will discuss about the pathologies connected to the loss of DNA methylation which affects the human health. I will also present key knowledge about the cell cycle, focusing on mitosis and its regulatory mechanisms. This research aims to uncover novel molecular mechanisms that regulate cell cycle progression and in particular mitotic chromosome segregation.

1.1 DNA methylation "epi"-regulates the DNA

This chapter will focus on DNA methylation, a key epigenetic modification that contributes to the regulation of gene expression and chromatin architecture. It will outline the principles of epigenetic regulation, describe the molecular players involved in establishing and interpreting DNA methylation, and discuss its broader biological implications.

1.1.1 Chromatin organisation in the nucleus

DNA is the molecule where genetic information is stored, and it has a double helix structure [1]. The three-dimensional organisation of DNA within the nucleus is critical for regulating gene expression and cellular function. In eukaryotic cells, the DNA is organised with different levels of compaction to fit within the micro-sized nuclear space [2]. The DNA is characterised by a negative charge, due to the negatively charged phosphate groups, that repel each other, phenomenon that can be neutralised by salts; however, the DNA can fold even when lower salt concentrations are present [3,4], suggesting that the compaction of the DNA in higher-order structure is achieved when the negative charges of DNA phosphate are masked by proteins. Indeed, DNA compaction occurs thanks to different specialised proteins that help the DNA rearrange its three-dimensional configuration.

The DNA wraps around a complex of eight histone proteins, which constitute the nucleosome. A key role in this event is played by the histone proteins (H2A, H2B, H3 and H4) that form an octamer composed of two H2A-H2B dimers and one H3-H4 tetramer [5]. *Per se*, the octamer is unstable but gains stability when the DNA wraps around it. 147 bp long strings of DNA are wrapped in a 1.67 left-handed superhelix around the histone octamer, forming the so-called nucleosome [6]. To further compact the DNA, a lysine-rich histone (H1) interacts with the DNA located between 2 near nucleosomes (DNA "linker") [7]. The interaction between nucleosome, histone H1 and linker DNA generates a chromatin structure called chromatosome [7]. Different

theories and models were proposed on the rearrangement of the DNA in higher-order structures observed *in vitro*. Many nucleosomes are rearranged in a repetitive beads-on-a-string chain to create the 10 nm fiber known as chromatin that can reorganise into a 30 nm fiber at least *in vitro* (Figure 1) [8]. However, Ou and colleagues used ChromEMT, a modified osmium staining method for DNA, and observed the three-dimensional structures of chromatin in living cells. They noticed that disordered chains of 5- to 24-nm diameter particles are packed together at different concentration densities within the nucleus [9]. These particles are visualised as beads-on-a-string structures of nucleosomes and DNA characterised by short linear segments or helical twits with less frequent contacts between and within chains. In mitosis, chromatin chains bend back on themselves at interspersed intervals, creating dense interactions between chains. Together with proteins, this interaction induces a compaction that forms the chromosomes, where the fibers have a diameter of 5 to 12 nm and 12 to 24 nm depending on the specific dynamics [9]. A chromosome, then, is a structure of dense and compacted DNA characterised by important elements such as chromatid arms, centromere, which appears as a primary constriction and telomere, which are the extremities (Figure 1). Human cells have 23 pairs of chromosomes (22 pairs of autosomes and one pair of sex chromosomes), giving a total of 46 chromosomes per cell. Alteration in the number of chromosomes or in the sets of genes achieved due to arms breaks induces the so-called aneuploidy, which affects the fitness of cells.

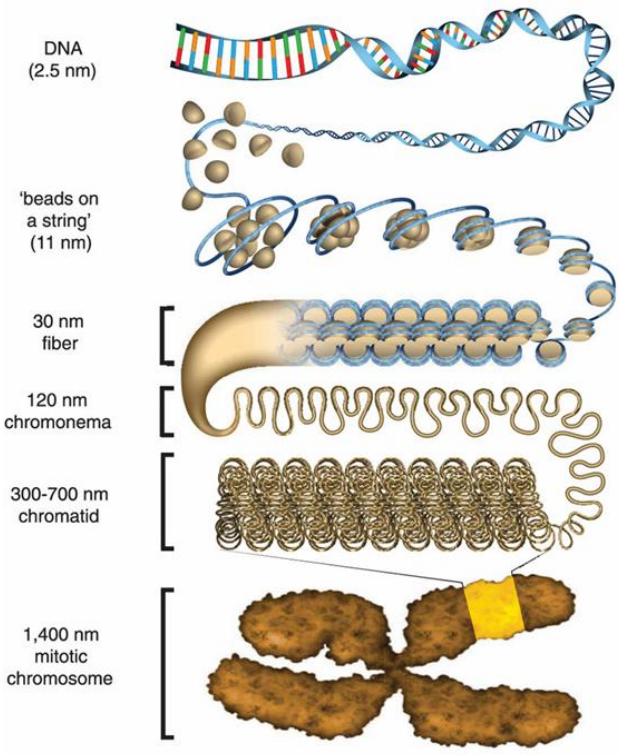

Figure 1: Hierarchical chromatin-folding model theorised by in vitro studies [9].

Ou and colleagues suggested that the fiber dimension is the same in both interphase nuclei and mitotic chromosomes, and they point out that it is the dynamics of the fibers that allows the compaction in highly chromatinic dense structures during chromosome formation (Figure 2). Indeed, chromatin dynamics is important for the establishment of the DNA three-dimensional configuration of the nuclei and chromosomes; however, despite the compaction of a fiber, interphase DNA must be accessible to proteins to initiate gene transcription when required. This implies the existence of chromatin remodelling and rearrangement of DNA accessibility. The discipline that studies all these changes to modulate gene expression without impacting the sequence of DNA is known as **epigenetics**.

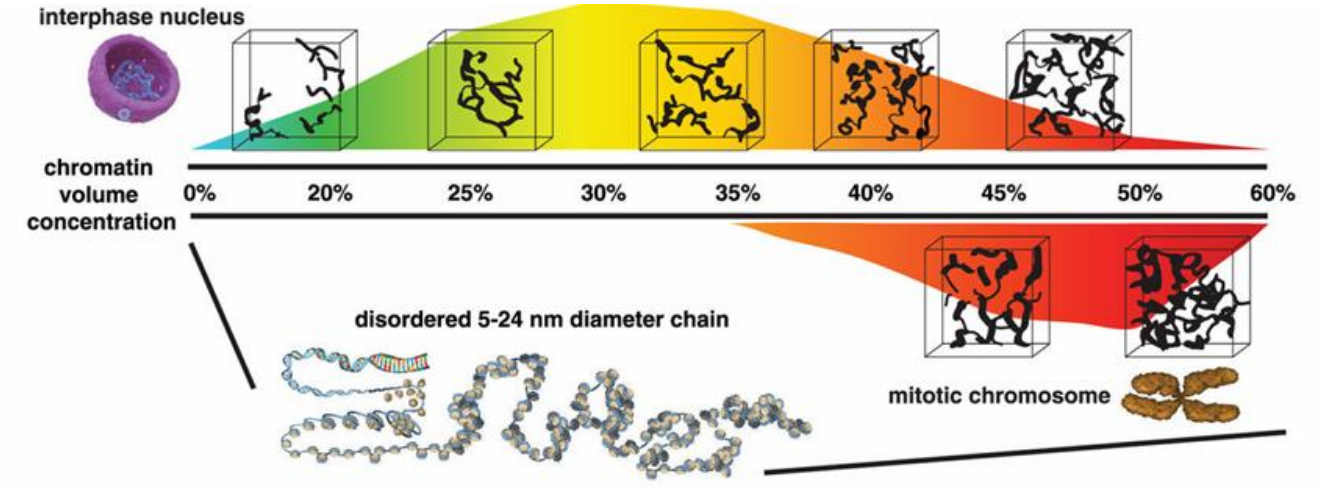

Figure 2: Chromatin chains can be packed together at different concentration densities in interphase nuclei and mitotic chromosomes [9].

1.1.2 Epigenetic modifications

Conrad Waddington coined the word Epigenetics in 1942 [10]. The prefix "epi" comes from Greek, meaning "on", and he defined epigenetics as the branch of biology that studies the causal interactions between genes, also named "*genotype*", and their products, which bring the "*phenotype*" into being [10]. However, the definition of epigenetics has been further extended to the heritable changes able to modulate gene function [11]. Since the fate of a cell is established by differential regulation of gene expression, cell differentiation is also studied by epigenetics [10,12]. Modifications of gene expression suggest a change in chromatin dynamics and DNA accessibility, and thus, all the players involved in chromatin remodelling must be considered as epigenetic

factors. Hence, epigenetic pathways modulating chromatin (epi-genetics), RNA (epi-transcriptomics), and proteins (epi-proteomics) work together to redirect the fate of the cell [13].

A single epigenetic modification involves several protein factors classified as writers (proteins that create the modification), readers (proteins that read the modification), and erasers (proteins that eliminate the modification when required) [14,15]. Different types of epigenetic modifications can occur, and they can be rearranged into multiple categories depending on their nature:

-Chemical modifications of DNA (Figure 3): DNA can undergo chemical modifications, mainly the 5-methyl-cytosine (5mC), which, with some exceptions, can regulate the DNA compaction and gene expression [16]. DNA methylation also characterises dinucleotide CpA, CpT, and CpC. The modification is highly present in embryonic stem cells however, upon differentiation, the non-CpG methylation is commonly lost, at least in part, in the differentiated cells [17]. The modification is mostly maintained at brain tissue, where non-CpG methylation still represents 25% of the overall DNA methylation level [18,19].

DNA methylation is catalysed by the DNA methyltransferase enzymes (DNMTs), which, as such, work as writers. DNA methylation of gene promoters usually inhibits gene expression, whereas DNA methylation of enhancers has highly variable effects on transcription [20]. Finally, DNA methylation of the gene body regulates the binding of proteins involved in the regulation of transcription and splicing events [20]. DNA methylation is read by proteins with the Methyl Binding Domain (MBD), such as Methyl-CpG binding protein 2 (MeCP2), which further regulates the compaction of chromatin by recruiting histone-modifying proteins, such as histone deacetylases (HDAC) [21]. Moreover, the presence of DNA methylation can block the binding of other proteins that read the DNA when not methylated, such as CTCF, which, instead, is involved in nuclear architecture remodelling [22]. Finally, erasing DNA methylation is possible; the active DNA demethylation is based on the TET-Eleven-Transferase (TET) or Activation-Induced cytosine Deaminase (AID) enzymes, which start a multi-step process that reconvert the 5mC into cytosine.

-Epi-proteomics and regulation of the chromatin (Figure 3): Histones are characterised by many variants that can be interchanged depending on the specific cellular function they have to exert. We can mention MacroH2A that localises predominantly to the inactive X chromosome, γ-H2A.X recruited in the presence of DNA damage, and CenH3 (also named CENtromeric Protein A CENP-A), which is specifically recruited at the centromere, establishing its functioning [23].
Post-translational modifications of the N-terminal tails of each histone variant occur with different effects on chromatin compaction, further enhancing their abilities in DNA reorganisation [24,25]. For example, the acetylation of histone lysine neutralises their positive charges and decreases histone-

DNA interactions [26,27]. Histone acetyl transferases (HATs) are the writers of this epigenetic modification, while up to 18 Histone deacetylases (HDACs) have been identified as the correlated epigenetic erasers [14,27]. Histone acetylation usually leads to the relaxation and opening of the chromatin, aiding the recruitment of transcriptional factors and, thus, the activation of gene expression [28,29]. Moreover, histones can be methylated by histone methyltransferases [15]. To remove this modification, specific demethylases are required [30,31]. Histone lysine can be mono-, di- or tri-methylated [32,33]. Di- and tri-methylation of lysine is usually gene-activating [33,34] except when located at Lysine in position 9 or 27 of the histone H3, mostly known for its repressive effect [33,35]. Histone modifications can be recognised by protein readers provided with specialised domains. Acetylation of histones is recognised by the bromodomain [27,36], whereas histone methylation is targeted by chromodomain [37]. Acting as a docking site for proteins, the modification rearranges the pool of enzymes around the DNA, for example, the methylation of H3 at lysine 9 is important for the recruitment of Heterochromatic Protein 1 (HP1), a protein involved in the compaction of the chromatin [38].

Histone modifications can affect DNA accessibility; however, the position of the histone itself can be modulated as well to allow proteins to bind the DNA. The enzymes involved in the histone sliding within the DNA are called chromatin remodelers. These proteins use an ATP-dependent mechanism, and they can be classified into four subfamilies: imitation switch (ISWI), chromodomain helicase DNA-binding (CHD), switch/sucrose non-fermentable (SWI/SNF) and INO80 [39]. ISWI and CHD remodelers aid in the formation of the octameric nucleosomes and form nucleosome arrays by spacing nucleosomes [39]. SWI/SNF remodeler is instead involved in sliding of nucleosomes along the DNA or in evicting nucleosome components, ejecting a full nucleosome [39]. Finally, the INO80 subfamily supports the replacement of histones with either a canonical or a variant histone [39].

-RNA and the epi-transcriptome (Figure 3): With the discovery of the many roles of the RNAs, including regulation of gene expression, the term epigenetics has been more recently broadened to include these pathways as well. For example, epigenetic factors are RNAs with an interfering effect (exogenous siRNA or endogenous miRNA) that can target and degrade mRNAs [40–42]. Also, long non-coding RNAs (lncRNAs) regulate both mRNA transcription, inducing a positive or negative regulation of gene expression by modulating the chromatin remodelers or transcriptional factor recruitment [43–45].

In addition, RNAs can also undergo different types of chemical modifications that have emerged as modulators of gene expression. Among these modifications, the best studied is the N6-Methyladenosine (m6A) at the 3' of mRNAs generated by methyltransferase METTL3/METTL14

complex (MTCs). This modification regulates gene expression by influencing localisation, stability, splicing or translation [46–49]. Also, through m6A-mediated structural changes, this modification allows the recruitment of the mRNA readers such as the YTH family, that regulate the splicing event [48,50]. Eukaryotic mRNAs also display a 7-methylguanosine (m7G) at 5' ends and near the mRNA cap, N6,2-O-dimethyladenosine (m6Am) can also be present [49]. In detail, the m7G stabilises mRNAs, improving the expression of the gene; instead, m6Am reduces translation of transcripts, negatively regulating gene expression [49]. Similarly to the epigenetic modifications on the DNA, RNA modifications are reversible; thus, demethylase enzymes exist to remove the methyl group [48,50].

-Topologically Associating Domains (Figure 3): Another layer of chromatin regulation is that both euchromatic and heterochromatic regions physically interact with each other. Through the contribution of architectural proteins and transcription factors, these interactions create the so-called Topologically Associating Domains (TADs), which are responsible for a higher and more elaborate system of gene regulation [51]. Indeed, the formation of loops to create the TADs further rearranges the chromatin, putting close or far away regulatory elements involved in gene regulation [52].

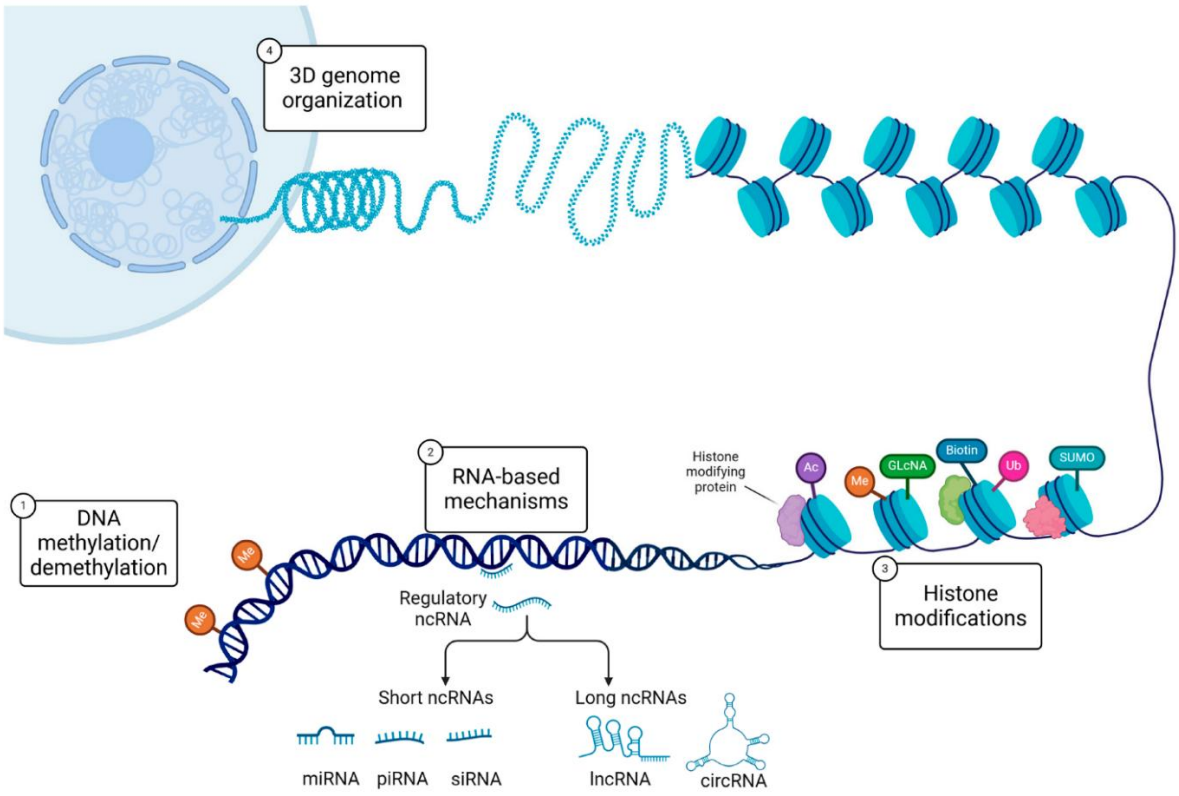

*Figure 3: Overview of the described epigenetic mechanisms. (**1**) Chemical addition or removal of DNA methylation. (**2**) RNA-based mechanisms: regulatory ncRNAs, including short ncRNAs (miRNAs, piRNAs, siRNAs) and long ncRNAs (lncRNAs, circular RNAs). (**3**) Histone modifications: post-translational modifications. (**4**) Three-dimensional (3D) genome organisation [52].*

By regulating chromatin accessibility and thus gene transcription, DNA methylation, histone modifications and RNAs form up to 2 different configurations of chromatin: the euchromatin is based on the easy accessibility of DNA with high chromatin remodelling and high chromatin dynamics which favours gene expression. The heterochromatin, on the contrary, is characterised by poor chromatin accessibility and dense packed chromatin structure [53]. Moreover, heterochromatin is distinguished in facultative, when it can be reverted to euchromatin, and constitutive, when it is always kept condensed and repressed, such as in the case of centromeric heterochromatin. During the cell cycle, chromatin is required to be highly dynamic from one side to favour the replication of DNA and from the other side to express different genes required for each phase of the cycle. Upon reaching mitosis, the chromatin is mostly heterochromatic, and the compaction of DNA reaches its maximum level as the DNA is not accessible anymore (Figure 4). The compaction of DNA and thus, the creation of the structure at mitotic chromosomes, is important to ensure a faithful segregation.

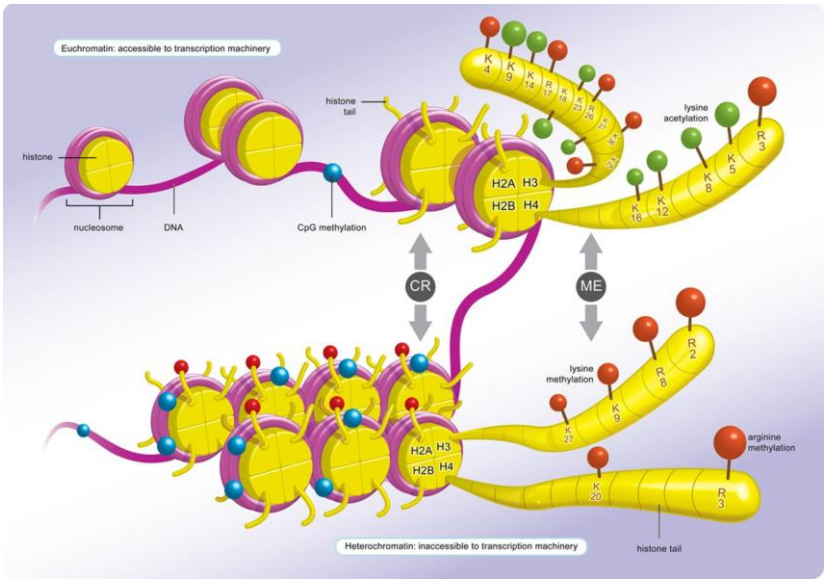

Figure 4: DNA methylation and Histone modifications support the compaction and the heterochromatinisation of DNA [54].

1.2 The writers and erasers of DNA methylation

This chapter will focus on the enzymes that catalyse and remove the methylation of DNA. I will discuss the pathologies where DNMTs and DNA methylation are involved.

1.2.1 DNA methyltransferases

DNA methylation refers to a chemical modification of the DNA, typically, the addition of a methyl group to cytosines. In 1984, the separation of amino acid mixtures by migration with organic solvents coupled with the ultraviolet detection at the spectrophotometer showed two cytosine populations characterised by different properties due to the presence of a methyl group in one population [55]. To differentiate the two types of cytosines, the methylated cytosine was initially named epi-cytosine or 5mC. The 5mC occurs at the dinucleotide CpG through the activity of DNMTs [56].

DNMTs are characterised by specific catalytic motifs used to generate 5mC, 4mC and 6mA, but the most observed is the 5mC within CpG di-nucleotides [57,58]. All DNMTs usually have a C-terminal-catalytic domain and an N-terminal regulatory domain [57,59], and the protein interaction with the DNA induces a change in the shape of DNA with subsequent rotation of the cytosine base into the catalytic pocket using a base-flipping mechanism [60]. The catalytic domain catalyses the covalent addition of a methyl group from *S*-adenosyl-l-methionine (AdoMet) to the C-5 of cytosine (Figure 5) [61]. In detail, a conserved cysteine mediates the nucleophilic attack on the C6 of the cytosine ring. Next, the methyl group is moved from the AdoMet to the carbon in position 5 of the cytosine (Figure 5) [57].

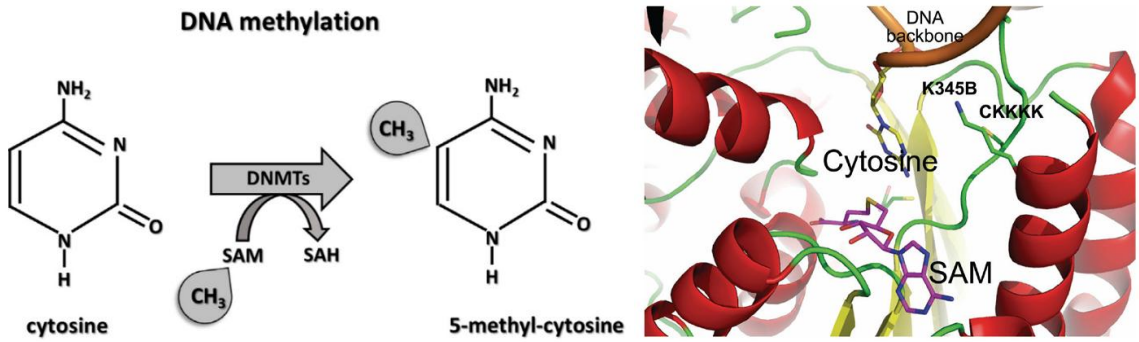

Figure 5: DNA methyltransferases use a base flipping mechanism to insert the cytosine in the catalytic pocket. Here, DNMTs transfer a methyl group from AdoMet to the cytosine and form the 5-methylcytosine at the residues in CpG dinucleotides [62,63].

The DNA can be methylated starting from a completely unmethylated state, and thus, it can occur *de novo*. Once established, DNA methylation can also be *maintained* across the cell cycle.

Different DNMTs play different roles in methylating the DNA, and their functioning is specified by their affinities with the DNA. In detail, *de novo* DNMTs have more affinity with non-methylated CpG dinucleotides, whereas the *maintenance* DNMTs are characterized by higher affinity for DNA methylated only on one strand (emi-methylated template).

In mammals, there are up to 4 members of the DNMT family, which include DNMT1, DNMT3A, DNMT3B, and DNMT3L [57,59]. DNMT2 has been considered in the past as a putative DNMT due to the similarities in structure with DNMT1, however, DNMT2 lacks the regulatory domain at the N-terminal [64,65] and it consists only of the 391 amminoacids of the catalytic domain, which has no activity *in vitro* [57,66]. Indeed, it has been observed to have no function on DNA methylation as it modifies tRNAs [61,67].

The *de novo* methylation is based on the DNMT3 group (Figure 6). The DNMT3 group is characterised by conserved domains such as the Pro-Trp-Trp-Pro (PWWP) domain and an ATRX-DNMT3-DNMT3L (ADD) domain used to interact with the chromatin [57,68]. DNMT3 group consists of DNMT3L, DNMT3A and DNMT3B. DNMT3L has no catalytic activity but stimulates the catalytic activity of the other DNMTs in cell culture systems [69]. Inactivation of both DNMT3A and DNMT3B disrupts *de novo* methylation but allows the survival of embryonic stem cells; nevertheless, the development of the embryo is impaired, thus DNMT3A and DNMT3B *de novo* DNA methylation is essential for mammalian development [70–72]. Once *de novo* DNMTs establish DNA methylation during development, the pattern of methylation of mammals is maintained by DNMT1 during subsequent cell cycles; thus, DNMT1 acts as the *maintenance* DNMT (Figure 6). DNMT1 is a multi-modular protein that consists of 1616 amino acids in humans. The maintenance of DNA methylation starts at the replication foci in S phase. Indeed, DNMT1 interacts with the Proliferating Cell Nuclear Antigen (PCNA) through the PIP box motif, thus, localising at the replication site [73]. Through the Replication Foci Targeting Sequence (RFTS) DNMT1 also associates with the replication fork but in an inactive state at first. Indeed, the RTFS is located at the N-terminus and directly inhibits the catalytic activity of the C-terminus [74,75]. Only the binding with Ubiquitin-Like PHD and Ring Finger Domain 1 (UHRF1) releases the inhibition. The RFTS domain consists, in fact, of a binding domain to UHRF1. Importantly, the SET and RING finger-associated domain (SRA) of UHRF1 binds the emi-methylated DNA template, ensuring that DNMT1 only methylates the new DNA strand exactly at the level of the methylated CpGs in the original strand. In addition, the CXXC domain of DNMT1 is a conserved zinc-finger domain that binds CpG dinucleotide within the DNA when unmethylated [76]. Once at the proper replication site, DNMT1 catalyses the covalent addition of a methyl group from AdoMet to the C-5 of cytosine only in these emi-methylated sites recognised by UHRF1. Moreover, DNMT1 also shows

interaction with heterochromatin during G2 and M phases of the cell cycle, suggesting a need to continue maintaining DNA methylation at these regions [77]. Even if DNMT1 is the *maintenance* DNMT, it also displays *de novo* activity. Mice depleted for DNMT3s revealed that DNMT1 can also *de novo* methylate repetitive and transposable elements [78]. These *de novo* spots are characterised by H3K9me3 and UHRF1 [78].

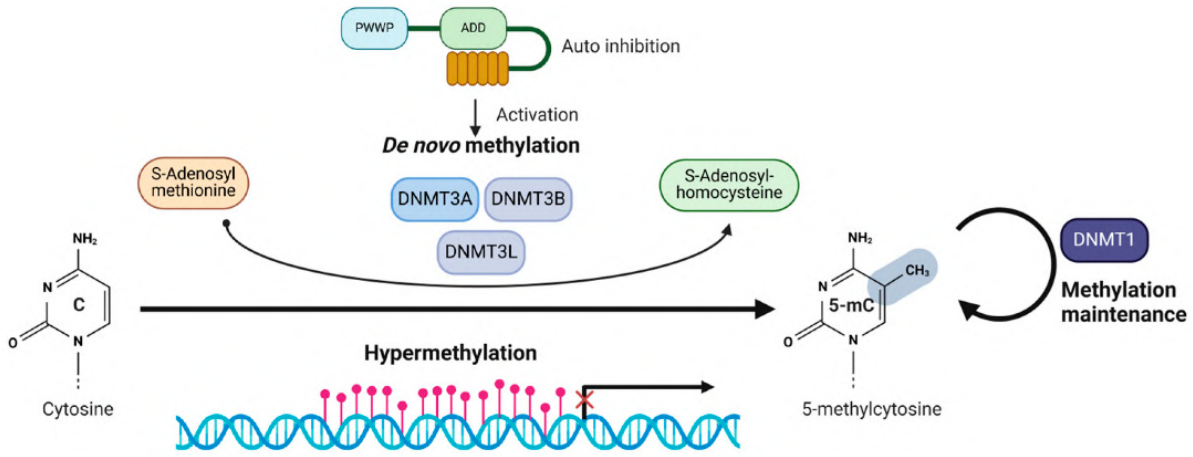

Figure 6: DNA methyltransferases methylate the cytosines within CpG dinucleotides. The methylation of DNA can occur through de novo or maintenance of the 5mC [79].

CpG dinucleotides can be located both at gene-poor DNA characterised by repetition of bases (repetitive DNA) and gene-rich regions [80,81]. Thus, DNA methylation must be finely regulated as both gene-poor and gene-rich regions may be affected by it. The genome is rich in highly methylated CpGs [80]; however, some CpG regions, called CpG islands (CGIs), are usually kept unmethylated [80,82]. Some organisms do not show DNA methylation. Yeast and *Caenorhabditis elegans* genomes, for example, lack detectable 5mC and do not have DNA methyltransferase [56,83,84]. Thus, the question that arises is: Is the methylation of cytosine that important? The-5mC is indeed indispensable in both plants and animals, with a particular relevance for mammals that will be the focus of my thesis [85,86]. Except for *Caenorhabditis elegans*, invertebrates also exhibit DNA methylation. For example, *Drosophila melanogaster* is characterised by a low amount of 5mC, which is difficult to identify and DNMTs are present. They are characterised by a function in chromatin compaction, suggesting that DNA methylation occurs even when it is not detectable [87].

1.2.2 Demethylation of the DNA

Loss of the DNA methylation process has dangerous implications in various diseases [88], and the enzymes involved are important for cell survival [57]. At the same time, DNA demethylation occurs

during development, during the establishment of the germline and post-fertilisation [89,90]. Thus, DNA demethylation is relevant as well as it affects cell's fate [91].

DNA demethylation can be achieved actively through multiple chemical reactions or passively in the absence of the DNA methylation maintenance. Passive DNA demethylation occurs during the zygote reprogramming or in the presence of DNMT1 pathologies, where DNMT1 cannot properly maintain the DNA methylation during the replication of DNA. This induces the formation of new DNA without 5mC; thus, DNA methylation will not be maintained and will be diluted over subsequent cell cycles. The loss of DNA methylation will not be total as *de novo* DNMTs activities can compensate for part of the loss by re-methylating specific regions of DNA.

While passive demethylation can only be achieved in certain scenarios, active demethylation is a continuous process that occurs during cell life. However, to remove the methyl group at the 5mC, the chemical bond between the cytosine and the methyl group must be broken. Breaking a C-C chemical bond is an endo-ergonic reaction, which is expensive and not energetically favourable. For this reason, up to today, no enzyme able to do this has been discovered in animals [90]. The only way to achieve active demethylation is to reduce such energy by creating a different chemical compound. As a first step, the 5mC base needs to be chemically modified either by deamination or by oxidation. Then, the modified methyl cytosine is excised through the Base Excision Repair (BER) DNA repair mechanisms [90]. The repair system is characterised by an AP Endonuclease 1 (APE1) that cleaves the phosphodiester backbone at the AP site, a DNA polymerase β (Pol β), which inserts the correct nucleotide, and finally by a ligase enzyme to form a phosphodiester bond between the newly inserted nucleotide and the existing DNA strand.

5mC deamination is induced by the Activation-Induced cytosine Deaminase (AID) (Figure 7), which is the only deaminase in charge of the DNA demethylation [90,92]. As such, the 5mC is deaminated into thymidine, generating an improper G-T interaction that triggers the thymidine DNA glycosylase and the BER mechanism to allow the replacement of a cytosine.

Tahiliani and colleagues were able to identify Tet-Eleven-Translocation 1 (TET1), which catalyses the oxidation of the 5mC into 5-Hydroxymethylcytosine (5hmC) (Figure 7) [93]. Both the 5mC and the 5hmC can be deaminated by the Activation-Induced cytosine Deaminase (AID) (Figure 7) [90,92] into thymidine and 5-hydroxymethyluracil (5hmU) respectively [90]. Moreover, two groups independently showed that TET enzymes are also able to further oxidise the 5hmC into 5-carboxylcytosine (5caC) or 5-formylcytosine (5fC) [94,95] (Figure 7).

The 5hmU, the 5caC, and the 5fC show structural similarity to a thymidine; thus, the presence of a thymidine or a similar compound, generates an improper G-T interaction that triggers the Base Excision Repair (BER) glycosylase, like the thymine-DNA glycosylase or the single-strand-selective monofunctional uracil-DNA glycosylase 1, to allow the replacement of a cytosine leading to DNA demethylation.

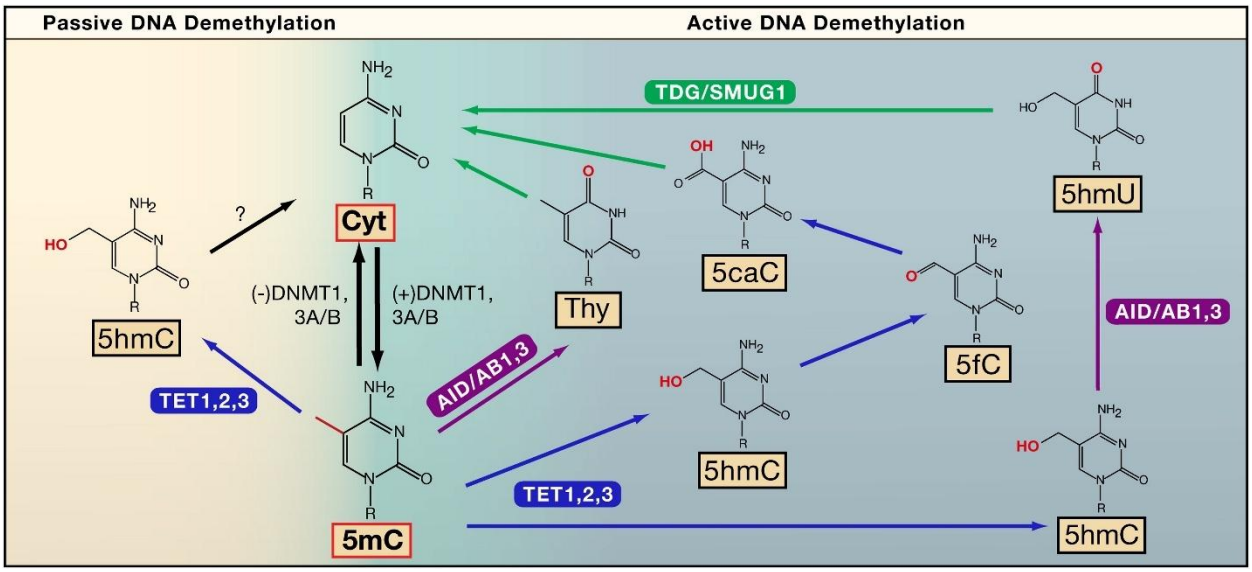

Figure 7: Active demethylation is induced by the TET family or by the AID family members. The generated Intermediates will recruit DNA repair system [96].

1.2.3 Human pathologies associated with defects in DNA methylation or DNMTs

Due to the significance of DNA methylation, any alteration of the enzymes responsible for methylating DNA, and consequently the abnormal loss or gain of DNA methylation, leads to different pathological conditions.

-DNMTs and global DNA methylation loss pathologies: Loss of DNMT1 activity directly correlates with a passive loss of DNA methylation and is involved in several types of human diseases. Mutations in the exons 20 or 21, for example, are known to induce neuropathological phenotypes such as cerebellar ataxia, dementia, deafness, and narcolepsy (Figure 8) [97,98]. These mutations occur in RFTS, thus impairing the binding of DNMT1 with the replication fork and leading to the inability to maintain the DNA methylation pattern through different cell cycles.

Subject	Symptom onset[a]	Age first examined[a]	Gender	First symptoms	Extremity sensory loss	Distal limb weakness	Cerebellar ataxia	Dementia onset[a]	Death[a]
K1 V7	30	59	F	Hearing loss	Yes[b]	No	No	40s	61
K1 V-12	35	48	M	Loss of sensation, hearing loss	Yes	No	No	42	Alive
K1 V-14	30	44	F	Hearing loss	Yes	No	No	41	–
K1 V-16	32	38	F	Loss of sensation, hearing loss	Yes	Yes	No	30s	Alive
K1 VI-11	20s	30	F	Hearing loss	Yes	No	No	30s	Alive
K1 VI-23	35	45	M	Hearing loss	Yes[b]	No	No	40	51
K1 VI-30	20s	30	M	Loss of sensation	Yes	No	No	30s	Alive
K1 V1-33	35	43	M	Hearing loss	Yes[b]	Yes	No	30s	46
K1 VI-36	35	42	M	Hearing loss	Yes[b]	No	No	40s	48
K1 VII 13	20s	18	F	Hearing loss	Yes	No	No	30s	Alive
K1 VII 15	20s	20	F	Loss of sensation	Yes	No	No	40s	Alive
K2 II-2	28	32	F	Hearing loss	Yes[b]	No	No	30s	46
K2 III-1	27	38	M	Hearing loss	Yes[b]	No	Yes	30s	Alive
K2 III-3	16	39	F	Hearing loss	Yes[b]	No	Yes	30s	Alive
K3 IV-16	35	47	F	Hearing loss	Yes[b]	No	No	40s	55
K3 IV-17	30s	40	M	Loss of sensation, hearing loss	Yes	No	Yes	40s	47
K3 V-1	30s	40	F	Loss of sensation, hearing loss	Yes[b]	No	Yes	40s	44
K4 III-3	30s	40s	M	Loss of sensation, hearing loss	Yes	No	No	30s	Alive

[a]Symptom onset, age, dementia onset and death in years. [b]Foot ulcers. – indicates that data was unavailable. K, kindred.

Figure 8: Phenotypic characteristics observed in patients with DNMT1 mutations and DNA methylation loss [97].

DNA methylation correlates with DNA compaction and heterochromatinization. Consequently, DNA hypomethylation deregulates such events, leading to the opening of chromatin and favouring gene expression. Sometimes this allows the transcription of unscheduled ncRNAs that can induce the production of autoantibodies, leading to inflammation in tissues and organs, which, in turn, can contribute to pathologies such as Systemic Lupus Erythematosus (SLE) [99,100].

Also, a change in the DNA compaction may affect the structures of chromosomes important for segregation. Indeed, mutation in the DNMT3B or loss of DNA methylation at the centromeric repetitive DNA correlates with the Immunodeficiency in association with Centromere Instability of chromosomes 1, 9, and 16 and Facial Anomalies (ICF) syndrome, a rare disorder characterised by a deficiency of IgA, IgG, IgM immunoglobulin, facial dysmorphisms, telecanthus, flat nasal bridge, macroglossia and mild micrognathia [100–102]. Specifically, DNA methylation is lost mainly at the centromeric repetitive DNA satellite (Sat) II and III (see paragraph for details on the centromere structure); however, in some patients, DNA methylation loss also characterizes the α Sat and Sub-telomeric regions [100,101,103–106]. DNA compaction in these regions supports the chromosome structure, and the loss of DNA methylation correlates with chromosome anomalies in ICF patients (Figure 9). Indeed, DNA methylation loss at the Sat induces nuclear defects and mitotic errors with subsequent chromosome loss, leading to genome instability [100,107].

Figure 9: Examples of pericentromeric anomalies in metaphases from ICF cells compared to a normal chromosome. From left to right:normal chromosome; chromosome with decondensation at the centromere; triradial chromosome; hexaradial chromosome; chromosome with a deletion and decondensed region below the centromeric constriction [108].

-Loss of Imprinting pathologies: Imprinted regions are regulated by imprinted-based-DNA methylation that occurs during embryo development. Alterations in DNA methylation at imprinted loci can disturb the normal balance between maternal and paternal gene expression, leading to several imprinting-related disorders (Figure 10). In Prader-Willi syndrome (PWS), loss of paternal expression within the *SNRPN/SNURF* region is commonly associated with abnormal methylation at its promoter and first exon, resulting in developmental and behavioural defects [88]. In contrast, Angelman syndrome (AS) arises when the maternally expressed *UBE3A* gene loses its methylation imprint, leading to silencing of the maternal allele and severe neurodevelopmental impairment [88]. Transient Neonatal Diabetes Mellitus (TNDM) is another imprinting disorder caused by loss of methylation on the maternal allele within the *HYMAI/PLAGL1* region, which results in overexpression of paternally active genes and transient neonatal hyperglycaemia [88]. In Beckwith-Wiedemann syndrome (BWS), loss of maternal methylation at the *KCNQ1/KCNQ1OT1* and *CDKN1C* loci disrupts imprinting control, leading to deregulated expression of paternal genes and fetal and postnatal overgrowth [88]. Similarly, Pseudohypoparathyroidism type Ib (PHP-Ib) involves loss of maternal methylation at exon 1A of the *GNAS* gene, which interferes with G-protein signalling and causes metabolic and skeletal abnormalities [88].

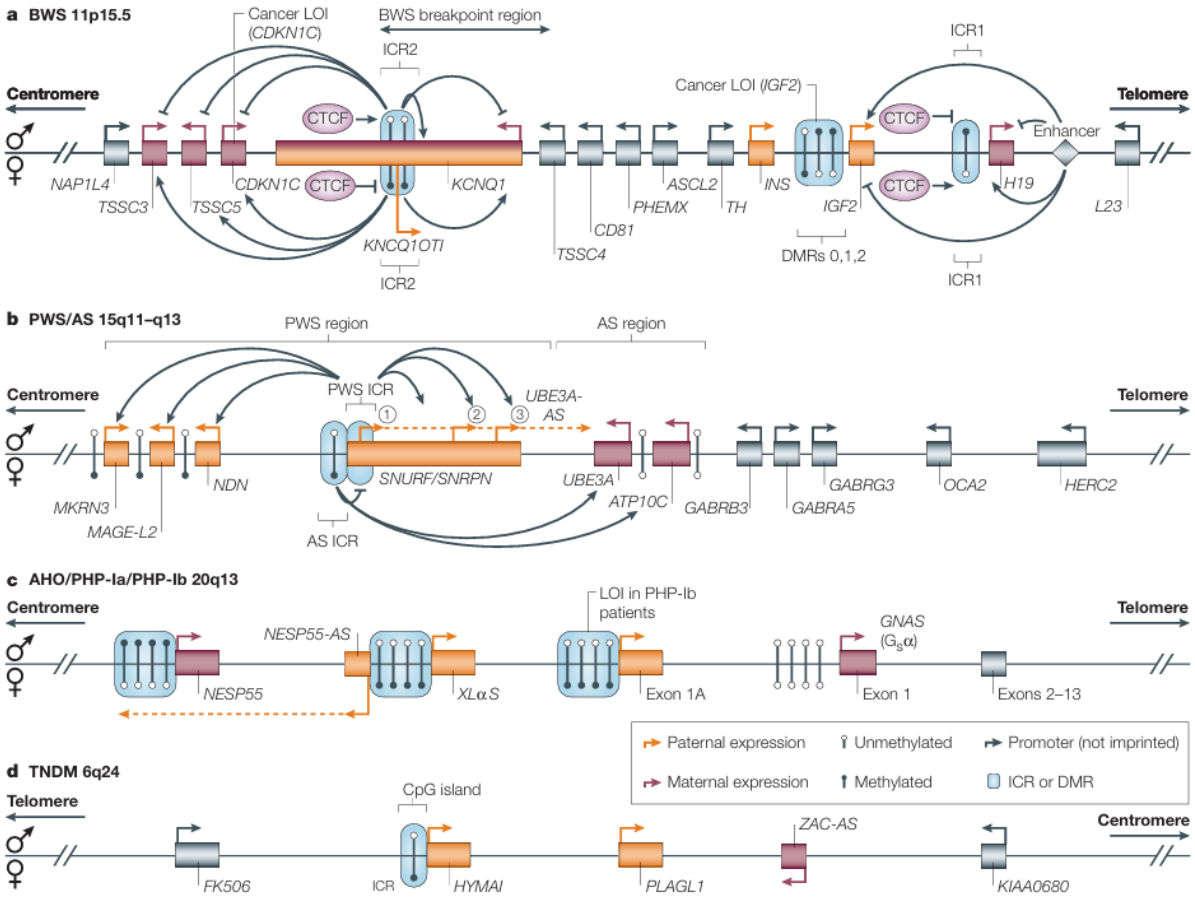

Figure 10: Regions that induce diseases characterized by loss of gene imprinting [88].

-Aging and neurodegenerative diseases

A change in epigenetic modifications is observed during aging. Changing of DNA methylation at the CpG dinucleotide was confirmed by different groups that analysed several cell tissues in both humans and mice [109–116]. The change in DNA methylation upon aging also affects non-CpG dinucleotides. Indeed, more than 50% of the methylated non-CpG are hypomethylated in the hippocampal genome of old mice [117,118]. Age-related DNA hypomethylation characterises repetitive elements such as Alu sequences but not LINE-1 repetitive DNA [119]. Indeed, when the cells undergo aging-based arrest, repetitive DNA starts to be more active [120,121], which favors cancer and neurodegenerative diseases [115]. In particular, due to the importance of DNA methylation in maintaining neurons and brain tissue, changes in DNA methylation patterns indeed, correlate with neurodegenerative diseases such as Parkinson's and Alzheimer's disease [122–127].

Parkinson's disease is characterised by motor symptoms such as tremor, rigidity, and postural instability, but also depression, anxiety, sleep disorders and cognitive impairment. Parkinson's

disease is observed when α-synuclein, parkin, PTEN induced putative kinase 1, parkinson protein 7, leucine-rich repeat kinase 2 , and glucosidase-ß acid genes are mutated [128]. At the same time, DNA methylation plays a role in regulating α-synuclein when not mutated [129]. The locus is characterised by two CpG islands [130]. The first, CpG-1, is in the first exon, whereas the CpG-2 is in the first intron. When DNA methylation is present at the CpG-2 dinucleotide, the gene is repressed [129]. Indeed, patients characterised by Parkinson's disease display hypomethylation of the first intron [129,131,132]. In Parkinson's disease, other genes are hypomethylated as well. For example, hypomethylation of NPAS2, CYP2E1, and NOS2 characterises the disease [129]. Parkinson's disease, is also characterised by genes such as PGC1-α, with a hypermethylated condition [129].

Alzheimer's disease is a disease characterized by cognitive decline and memory deficits due to amyloidogenesis. During Alzheimer's disease, different foci undergo DNA demethylation. In detail, PSEN1, BACE1, and Amyloid β Precursor Protein are overexpressed during the disease [133,134]. So far, researchers have discovered PSEN1 and Amyloid β Precursor Protein as the main hypomethylated loci in Alzheimer's disease patients and in mice affected by the pathology [133]. BACE1 is, instead, regulated by miR-29a, which is, in turn, regulated by DNA methylation. Indeed, DNA methylation upregulates miR-29a. When expressed, the miR-29a targets BACE1 mRNA, reducing the amyloidogenesis [135]. Alteration of the DNA methylation correlates with alteration of such miR-29a, leading to Alzheimer's disease. At the same time, other genes, such as ANK1, RPL13, RHBDF2, DUSP22, and SORL1, were found instead, hypermethylated in the patients [136,137]. Finally, a recent analysis of the cortex revealed a differentially methylated region of the ZFPM1 gene, which is strongly connected to the pathology [138]. Alteration in the DNA methylation pattern strongly correlates with Alzheimer's disease.

Alteration of the DNA methylation pattern correlates with other neurodegenerative and neuropsychiatric diseases as well [137 137,139].

-DNA methylation in cancer: Tumours display a high variability of epigenetic rearrangements, including variations in DNA methylation. Hypermethylation of tumour suppressor genes is often observed in cancer cells, leading to repression of transcription (Figure 11) [140], whereas hypomethylation occurs mainly at repetitive DNA (Figure 11) [141] which might have an effect on chromosome segregation and altered mitotic segregation as discussed before. DNA methylation pattern varies based on the cell line and type observed [142–146].

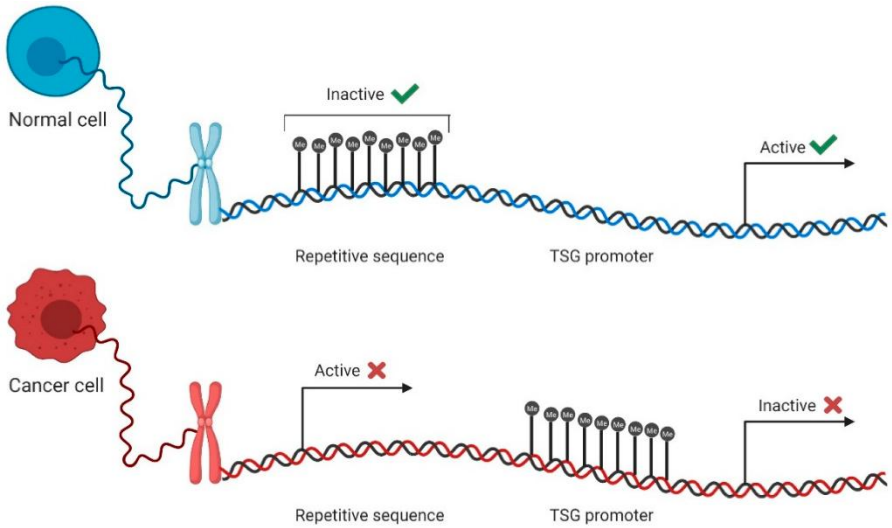

Figure 11: Cancer cells are characterized by high variability in repetitive DNA methylation compared to normal cells [147].

-

1.3 The role of DNA methylation

This chapter will focus on DNA methylation functioning. It will outline the effects on the gene expression and the heterochromatinization of the DNA. Moreover, I will describe the demethylation event that occurs during the development.

How does DNA methylation work? Dinucleotides containing Cs and Gs are located everywhere in the genome [80]. Moreover, mammalian genomes are characterised by a high frequency of CGIs, which are physically connected with gene promoters and usually lack DNA methylation [82]. Tompkins elegantly suggested that DNA methylation represents a form of "molecular braille" [148], and, thus, it is used by the cell to read and specify a change, a regulation, and finally a fate. All the cells in the body contain the same genome, and each type of cell is regulated in such a way that only specific proteins are expressed. Specialised cells are characterised by gene expression and chromatin regulation optimised for their functioning (Figure 12).

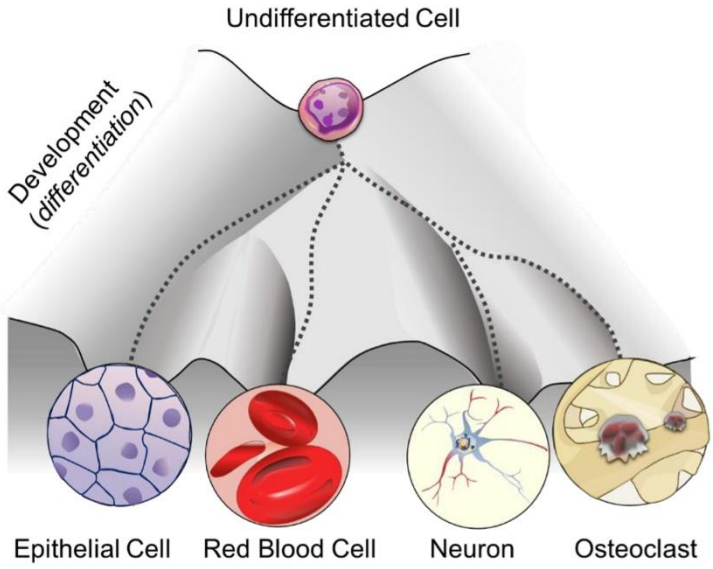

Figure 12: An outline depicting cell-fate plasticity according to the Waddington's epigenetic landscape (inspired by the model proposed by Waddington [149].

DNA methylation supports the fate of cells through multiple ways that will be described individually.

1.3.1 DNA methylation and gene regulation: Based on the cell line taken in analysis, some promoters may be unmethylated in a cell line, whereas methylated in another one. This is due to

the different gene expression program peculiar to each cell type, depending on their function in the organism (Figure 13).

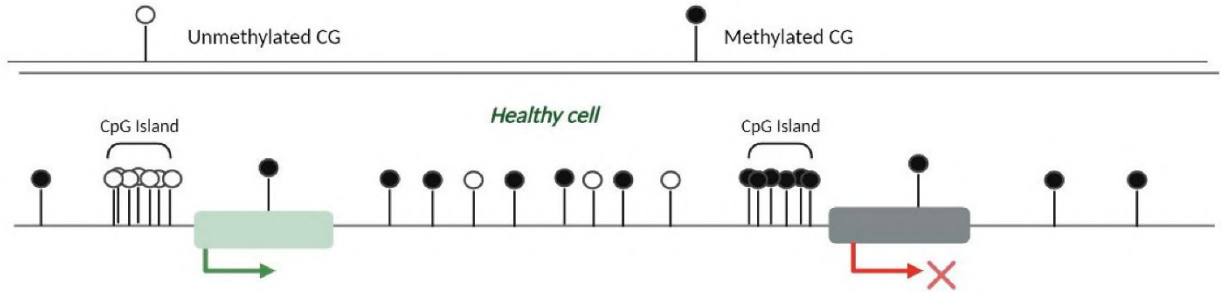

Figure 13: CpG islands of promoters are rarely methylated in healthy cells; thus, gene expression is permitted. DNA methylation at the promoters regulates gene expression [150].

Non-CpG methylation regulates gene expression, and it occurs mostly on regulatory regions [151]. At the promoters, it impairs gene expression in a similar manner to the CpG methylation [152]. The methylation of non-CpG dinucleotide also, has been proven to favour the interchromosomal interaction between genes and enhancer [153] favouring, in this way, gene expression.

Moreover, non-CpG can also be recognised by MeCP2 when DNA methylation is present, especially in neurons with a repressive role required for the maintenance of the neuron itself [18,154].

CpG sites are also located at regulatory elements both upstream and downstream of transcription initiation, and sometimes in the gene body. The enhancer and silencing elements are mostly CpG-poor, with a variable methylation [20,155]. In glioblastoma tumour DNA methylation at these regions has been shown to have no negative effect on the regulatory function, but at the same time, it has been correlated with a change in the regulatory element activity depending on the region analysed [156]. Indeed, the cell is characterised by methylation-sensitive and methylation-insensitive sites, and those regulated by DNA methylation switch their activity. The repression of an enhancer through 5mC could occur through the repression of transcriptional factor binding, and the recruitment of MBD proteins, which induce heterochromatinisation and chromatin closure [157]. At the gene body, DNA methylation has been proven not to impair gene expression as observed in genes in the chromosome X [158] and in other chromosomes [159]. DNA methylation protects, together with H3K36me3 and DNMT3B, the gene from RNA Polimerase II (RNAP II) entry at cryptic starting sites [160]. DNA methylation can recruit HP1 and CTCF as discussed above; thus, it can regulate the transcriptional event, favouring alternative splicing [161] and modifying the architecture of the chromatin [22]. Since CTCF is involved in the rearrangement of chromatin loops (Figure 14), the loss or the formation of loops may favour or not the enhancer-promoter interactions and thus, DNA methylation regulates gene expression by affecting the chromatin structure through CTCF

regulation [162]. Also, by regulating the binding of CTCF, the presence of DNA methylation can control the inclusion of an exon during the splicing event, further regulating the gene expression [163].

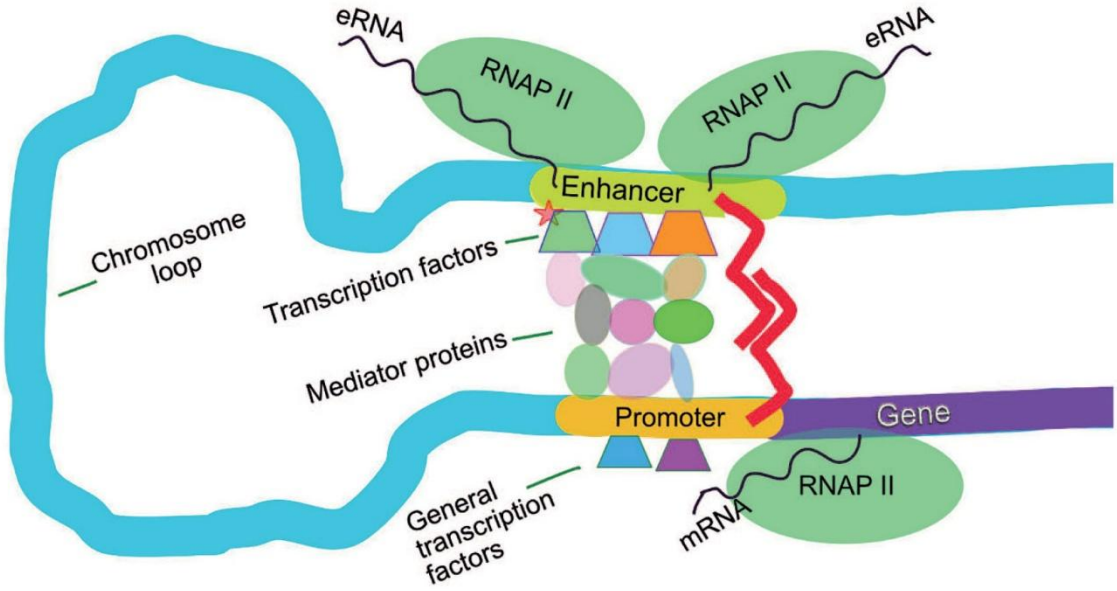

Figure 14: Loop formation through CTCF favours the interaction between enhancer and promoter and thus, gene expression [164].

1.3.2 DNA methylation and compaction of DNA. Nucleosomes are positioned where the sequence of DNA generates a structural bending that can accommodate the histones. Sequences like repetition of Ts or As generate too much stiffness, which does not allow the inclusion of nucleosomes or, eventually, it generates histone instability [165,166]. Instead, a periodic distribution of short G/C-rich and A/T-rich motifs favours the inclusion of histone proteins [167]. The methyl group of 5mC occupies space; therefore, depending on its location, it influences DNA structural properties, potentially affecting nucleosome formation. Depending on the DNA sequence, histone proteins may be less likely to bind to methylated DNA and thus, CpG methylation forces them to bind elsewhere or close by [168,169]. Also, the methyl group reduces the amplitudes of motions of the phosphate-sugar backbone, creating less dynamicity in the DNA [170]. On one side, the 5mC can impair the recruitment of histones; On the other, some methylated DNA sequences can still wrap to histones, but this time the methylated DNA interacts with them, generating a shorter end-to-end DNA length and thus, a more tightly wrapped DNA on the nucleosome [169,171]. Hence, the methyl group at the cytosine induces compaction by affecting the bending of DNA and nucleosome rearrangement. This is further enhanced by the cooperative work between DNA methylation and histone modifications.

DNA methylation can further rearrange the chromatin as it can be bound by many proteins with MBDs, such as MeCP2 or HP1. *In vitro*, MeCP2 can bind nucleosomes and compact the chromatin when the DNA is not methylated [172]; however, DNA methylation favours the affinity of MeCP2 to methylated DNA [173]. MeCP2 is known to interact with RNAP II in neurons, potentially positively regulating gene expression [174]. Also, MeCP2 represses the expression of long genes when they are methylated [175]. The MeCP2 mutations can cause the RETT syndrome, whose worst phenotype arises from mutations that affect the ability of the protein to bind methylated DNA [176]. Other than regulating gene expression, MeCP2 regulates chromatin loop formation and nuclear architecture [177–179], a similar role observed for DNA methylation itself.

HP1 family, while can interact with histone H3 trimethylated on Lys9, binds methylated DNA as well, with the possibility to splicing factors at alternative exons, thus regulating mRNA splicing [180]. Moreover, HP1 can also rearrange the chromatin [181,182], ensure proper mitotic exit and preserve chromatids cohesion and segregation through the recruitment of Shugoshin1 (Sgo1) [183]. Any change in the DNA methylation pattern may rearrange the HP1 pattern as well, deregulating all these events. By the presence of DNA methylation, or through the direct recruitment of other proteins, heterochromatinisation and DNA compaction are favoured to establish the perfect conditions for the fitness of the cells.

1.3.3 DNA methylation and development: DNA methylation at the 5mC is important during the development of mammals, as several studies demonstrated that DNA hypomethylation, due to mutations of DMNTs, induces lethality in mouse embryos [184]. The parental genomes are characterised by gamete-specific differential modification, a substantial difference called genomic imprinting. Non-CpG methylation is also important for the imprinting event, as different loci are methylated in the oocytes [152,185] and in brain tissue in a sex specific manner [186].

DNA methylation is, indeed, involved in genomic imprinting; alleles may be differentially methylated based on the sex of the organism. For example, the non-coding RNA (ncRNA) *H19* is silent in the paternal allele. Insulin-like growth factor 2 *(Igf-2)* is, instead, expressed in the paternal allele [187], and Igf-2 receptor *(Igf-2r)* is expressed in the maternal allele [188,189]. Interestingly, the organisms themselves induce a rearrangement of the epigenome during fertilisation. The paternal genome is highly compacted in the sperm; thus, a loss of compaction is required to achieve an ideal condition to merge with the maternal genome. The demethylation of the mammalian paternal genome is observed to be a conserved mechanism between different organisms [190]. However, this is not the case with the maternal genome because it does not become actively demethylated in the zygote. Still, the zygote is characterised by sequential stepwise demethylation through passive

demethylation during the first cleavage divisions [190–193]. Indeed, upon the regulated interaction between female and male pronuclei, the zygote is characterised by a loss of DNA methylation till the stage of blastocyst, where the 5mC reaches the lowest amount [194]. The loss of DNA methylation during embryogenesis is an important event because the embryo must start from a "clean" epigenetic blackboard (Figure 15). From this moment on, DNA methylation will progressively reappear to allow differentiation of the cell fate. This is not the case for the formation of the primordial germ cells. Indeed, based on the sex of the organism, gametogenesis will produce sperm or oocyte. Since these two are characterised by different phenotypes, epigenetic regulation must be different. To achieve that, after the first wave of DNA demethylation, a second wave is required to remove specific DNA methylation marks [194]. From now on, DNA methylation reappears to regulate the gamete-specific epigenetic changes required for gametogenesis, a process named genomic imprinting (Figure 15). Another important event that occurs during embryogenesis is X chromosome inactivation in females. To obtain the inactivation, different strategies are used by the cells: *Xist* RNA coating, which compacts the DNA and recruits macroH2A histone variant; chromatin changes such as histone modifications that further compact the DNA; and finally, DNA methylation that compacts the DNA and represses gene promoters [195].

The genome is characterised by the presence of viral and retroviral elements that originated during the evolution and the interaction with viruses. These DNA elements are characterised by repetitive DNA and constitute approximately 45% of the human genome [196]. They are considered selfish elements because transposon DNA encodes enzymes that allow them to excise and insert into another part of the genome. The classification and the molecular mechanism will be discussed in the repetitive DNA paragraph. In all scenarios, their DNA integration from one region to another can affect the gene expression if they are introduced in one exon [197,198]. During the development reprogramming, the loss of compaction may favour the activation of such selfish elements, which would affect the fitness of cells and the embryo. To overcome this and be protected, cells have developed multiple mechanisms to avoid these. The defense against these selfish replicating elements starts with PIWI-Interacting RNAs (piRNAs), which are small silencing RNAs [199]. When transcribed, these piRNAs recruit the protein PIWI, where the viral element is expressed. In mouse, a lack of piRNAs induces a loss of DNA methylation, suggesting that piRNA and DNA methylation may be closely related [200]. Indeed, DNA methylation, together with the repressive histone modifications, acts by compacting the DNA and silencing the mobility of such elements [196].

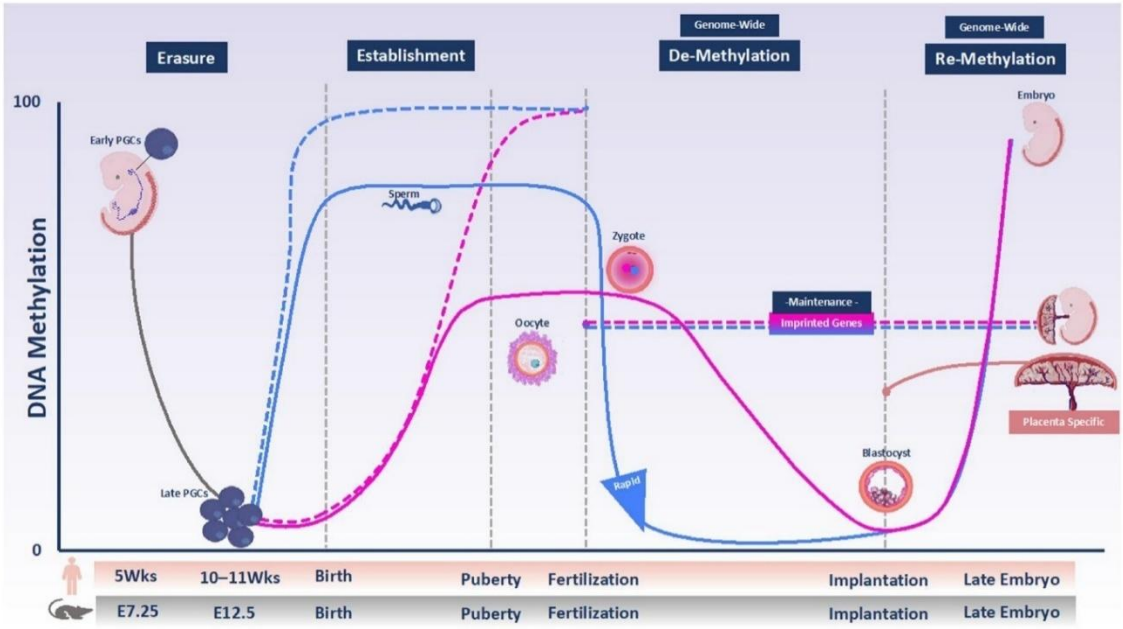

Figure 15: DNA methylation programming and reprogramming during development in humans and mice [201].

Artificial reprogramming, which is the acquisition of pluripotency by a differentiated somatic cell, requires an epigenetic rearrangement of histone modifications and DNA methylation pattern. First, the reprogramming is characterised by a change in histone modification patterns at all stages taken into consideration; instead, DNA methylation patterns change at the promoters is observed only at the late stage of the reprogramming event [202]. However, even when reprogramming is induced, the DNA methylation pattern of the induced Pluripotent Stem Cells (iPSC) is never identical to the one observed in the Embryonic Stem Cells (ESC) [203]. Lister and colleagues observed 1175 differentially methylated regions between the two cell lines. A never-identical condition was also observed *in vivo* with the animal cloned embryos that did not show the same DNA methylation pattern as the normal condition during development [190].

1.4 The cell cycle: A program to sustain the proliferation

Cells undergo an ordered series of events to grow, duplicate their genetic material, and divide it into genetically identical daughter cells. This process is known as the cell cycle, which consists of different phases that allow a perfect and balanced division. Alteration of any of these events affects the life of the cells, with sometimes catastrophic effects such as cell death.

Four phases are required to complete a cycle (Figure 16).

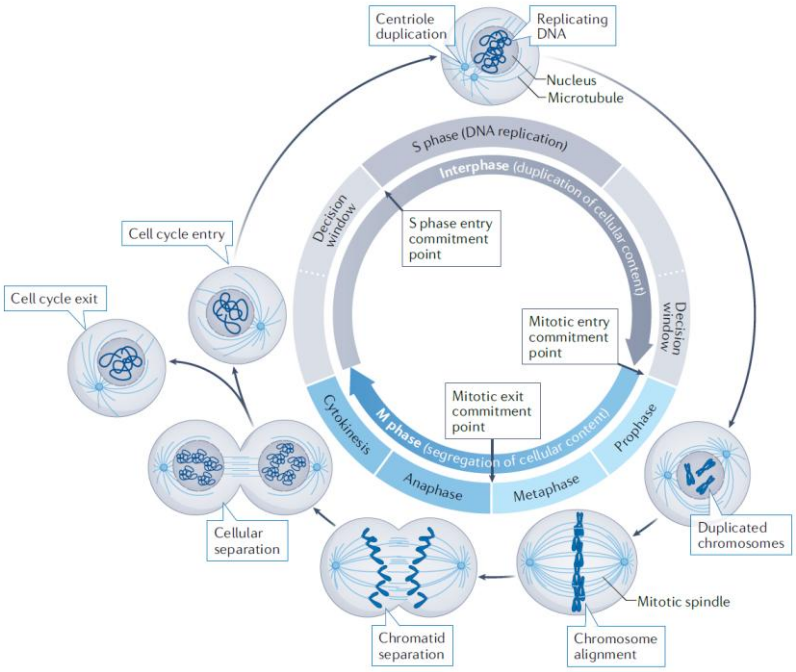

Figure 16: The cell cycle consists of multiple phases to regulate cell proliferation [204].

The **Gap1 phase (G1)** is the initial phase, when the cells are small in size and sense the nutrients present in the environment or the interaction with other cells [205]. If the sum of these signals induces proliferation, the proliferation genes turn on their expression, causing the duplication of organelles such as the Golgi and the activation of factors required to enter the next phase, the S phase [205].

Upon entering the **DNA Synthesis phase (S)**, cells begin the replication of their DNA starting from specific sites called replication origins. This process requires a specific enzymatic complex, the replisome, characterized by the presence of DNA polymerase and other proteins, among which there is DNMT1. The maintenance of the DNA methylation pattern, peculiar of each cell type, is accomplished in this phase and is essential for cell health.

The **Gap2 phase (G2)** is the second phase where the cells duplicate organelles, especially the centrosomes, which are crucial for chromosome segregation. Also, during the G2 phase, cells begin to express genes necessary for the next phase, mitosis.

Mitosis (M) is the last phase of the cell cycle. The first person to observe the mitosis in detail was a German biologist, Walther Flemming (1843-1905), who used aniline dyes to stain the chromosomes [206]. Together with the replication of DNA, the mitosis event is important to enable cell proliferation, to ensure the faithful segregation of the genetic material to the two daughter cells, and to allow growth and tissue repair of multicellular organisms. Mitosis consists of different subphases (Figure 17):

- In prophase, the nuclear envelope starts to disassemble, and the DNA compacts into chromosomes.
- In prometaphase, the mitotic spindle assembles in a bipolar configuration, and centromeres interact laterally with the microtubules that arise from the poles of the mitotic spindle.
- Upon this lateral interaction, the chromosomes are moved to the equatorial plate, reaching the metaphase. Once all chromosomes are aligned in metaphase, the Spindle Assembly Checkpoint (SAC) ensures that kinetochores and microtubules are properly attached and stabilised before anaphase.
- If everything is functioning correctly, the checkpoint is satisfied, allowing the chromosomes to segregate during anaphase towards the two poles of the mitotic spindle in the two daughter cells. The transition in anaphase requires the degradation of different components involved in the chromatid cohesion and also cyclin B1 [207,208].
- Finally, cytokinesis occurs, an event characterised by the decompaction of chromosomes, reformation of the nuclear envelope, and constriction of the cytoplasmic membrane by a ring of myosin to finally split the cells into two.

Mitosis with the proteins that are involved and the molecular mechanisms behind the process, will be discussed in detail in the next chapter.

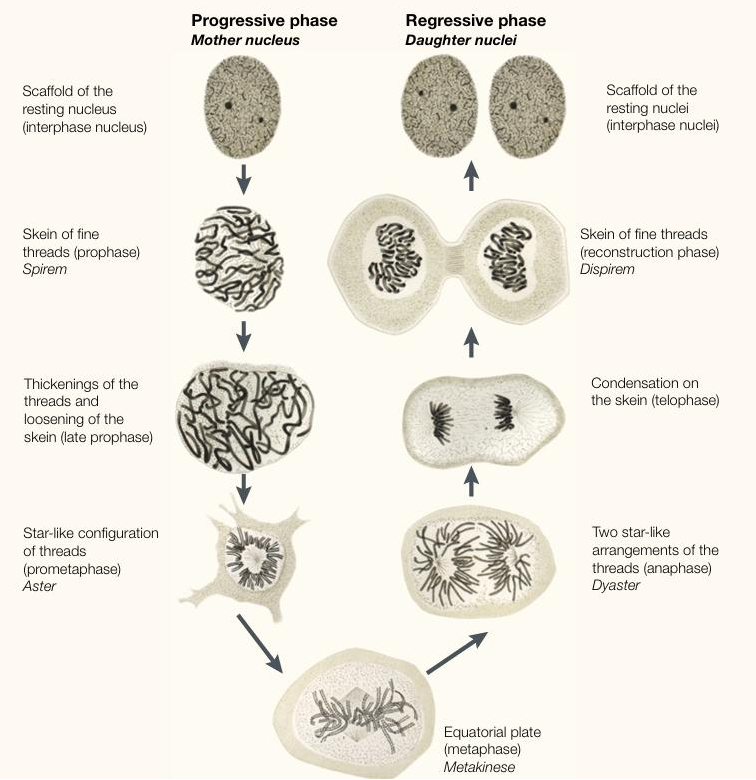

Figure 17: Mitosis is characterized by chromosome congression to the metaphase plate. Chromosomes will later segregate to the poles into the 2 daughter cells [206].

When mitosis is completed, the daughter cells are once again in G1 phase, and the cell cycle restarts. However, DNA damage, drugs, and telomere shortening all trigger signals of cell cycle arrest, leading to a Gap phase with a completely different profile of gene expression and metabolism [209]. This senescent phase is called Gap0 (G0), and it can be both reversible and not. If senescence is reversible, the cells will be able to cycle back again through the different phases. G0 phenotype is achieved when the cells sense some stress (i.e. DNA Damage, lack of nutrients, cell-to-cell contact inhibition), but also when the cells age. Upon aging, in fact, telomere extremities are shortened, and this activates G0 entry (replicative senescence) [209].

1.4.1 Cell cycle regulation

The cell cycle is highly regulated, and this is based on two main protagonists. The cyclins and the Cyclin-Dependent Kinases (CDKs). While CDKs are always present and ubiquitously expressed, the cyclins are expressed only in specific phases, which allows the timely regulation of the progression of the cell cycle (Figure 18).

Starting from the G1 phase, growth factors stimulate the expression of D-type cyclins [210], which specifically activate the cyclin D-dependent CDK4 and CDK6 during this cell cycle phase [211,212]. As a result, cyclin D/CDK complex phosphorylates substrates required for the next phase, such as the RetinoBlastoma protein (pRB), which is a tumour suppressor [213]. pRB normally binds the transcription factors of the E2F family. The resulting pRB-E2F complexes repress the binding of E2F to gene promoters, thus pRB regulates the cell cycle progression [214–216]. When cyclin D/CDK phosphorylates pRB, E2Fs are released, which allows the activation of the genes regulated by E2Fs [214,217]. One of the gene targets is cyclin E, which, once expressed, binds CDK2 to further phosphorylate pRB [218,219]. This event is required to reach the G1-S boundary. Once cells enter S phase, a rapid turnover of cyclin E is observed with a subsequent decrease in E2F activity. Instead, cyclin A is expressed, and it can bind CDK2 [220]. The cyclin A/CDK2 complex further phosphorylates the E2F family [221].

During the S phase, the pre-replicative complex (pre-RC) is activated for DNA replication. It is constituted by ORC (origin recognition complex) proteins [222]. ORC proteins are activated by CDK2-based phosphorylation. Specifically, on one side, the phosphorylation is speculated to initiate replication of DNA; on the other side, it leads to a loss of affinity with the chromatin. This mechanism guarantees that each replication origin is activated only once per cell cycle [222,223]. Also, cyclin A-dependent CDK2 signaling induces activation of new factors required to enter G2 and M phase [224–226].

Upon G2 phase entry, the cyclin A associates with the CDK1 and cyclin B1 starts to be expressed. Cyclin B1 stays in the cytoplasm bound to CDK1 but inactive due to the phosphorylation induced by Wee1 and Myt1 kinases [227,228]. Cyclin B1 is translocated to the nuclei only in early mitosis, where it triggers a cascade of phosphorylation events essential for mitotic entry, progression, and permanence [229–231]. The cyclin A/ CDK1 will persist till the mitosis, where it plays a role in congressing the chromosome and in regulating the SAC [232].

- Cyclin B1 is also transcribed during mitosis [233], and its absence in mitosis stops mouse embryos from proliferating [234]. In mitosis, the cyclin B1/CDK1 complex is required to promote chromosome condensation, nuclear envelope breakdown, and nuclear lamina solubilization, mitotic aster assembly, and Golgi breakdown [230,231]. Most importantly, cyclin B1/CDK5 complex regulates mitotic spindle stability and chromosome segregation, thus preventing mitotic errors [235]. Finally, during mitosis cyclin B1/CDK1 complex is located at the kinetochore complex, which is a protein complex that interacts with microtubules to permit chromosome segregation during mitosis. Cyclin B1/CDK1 is stripped away when

microtubules attach to kinetochores (Bentley *et al.*, 2007; Chen *et al.*). Indeed, when the attachments are made and thus, the cells are ready to segregate the chromosomes, cyclin B1 is removed from the kinetochores and can be degraded by the Anaphase-Promoting Complex (APC) ensuring the mitotic exit (Yamano *et al.*, 2004; Bentley *et al.*). Another target for degradation is Securin, which inactivates Separase. Separase is, then, able to cleave Cohesins that physically connect sister chromatids, allowing their separation and thus, chromosome segregation [238]. Details of this cell cycle phase will be discussed in the next section.

1.4.1.1 Regulation of CDKs

The central machines that drive cell cycle progression are the CDKs. The catalytic subunits lack activity until the protein is bound by their cognate cyclin subunits, which are tightly regulated at both the levels of synthesis and ubiquitin-dependent proteolysis. Thus, the transition between one phase and the other of the cell cycle is based on the cell cycle expression of cyclin. However, cells employ an additional security plan, which is the regulation of the activity of the cyclin/CDK complexes through post-translational modification and CDK Inhibitors (CKI).

Cyclin/CDKs are not fully active until phosphorylation on specific conserved threonine residues [239]. Loss of such modification inactivates the CDKs. At the same time, phosphorylation at other specific residues, caused by CDC25, displays a negative effect on CDKs activities [239]. CDK activity can also be negatively regulated by the binding of small inhibitory proteins, the CKI. The CKI consists of different families that inhibit the CDK in different ways [240,241]. INK4 family consists of p16 INK4a, p15 INK4b, p18 INK4c and p19 INK4d, whereas the Cip/Kip family consists of three proteins, p21waf1/cip1, p27kip1, and p57kip2 (Figure 18) [240,241]. While the INK4 family blocks the progression of the cell cycle by competing with cyclin D in binding to the CDKs, the Cip/Kip family, instead, does not allow the phosphorylation of CDKs, which, thus, remain inactive. P21waf1/cip1 gene expression is regulated by p53, which is a transcription factor maintained at low levels by MDM2, which functions as a p53 ubiquitin ligase [242,243]. Oncogene signaling, DNA damage, and replication stress induce p53 post-translational modifications to stabilize p53, which will tetramerize and be activated as a transcription factor [243,244]. P53 regulates many biological processes according to the origin of stress. In detail, p53 promotes the transcription of genes involved in DNA repair and in cell cycle arrest, thus, p53 was named "Guardian of the genome" [244,245]. Since p53 induces the transcription of p21waf1/cip1, cell cycle arrest through p21waf1/cip1expression is observed in many situations. Indeed, p21waf1/cip1 interacts with the PCNA at the replicative fork; regulates the transcription event by binding and

inhibiting proliferative transcriptional factors E2F1, c-Myc, and STAT3, modulates the cytoskeleton and aids in the DNA repair establishing the fate of cells between arrest or apoptosis [216,246–254].

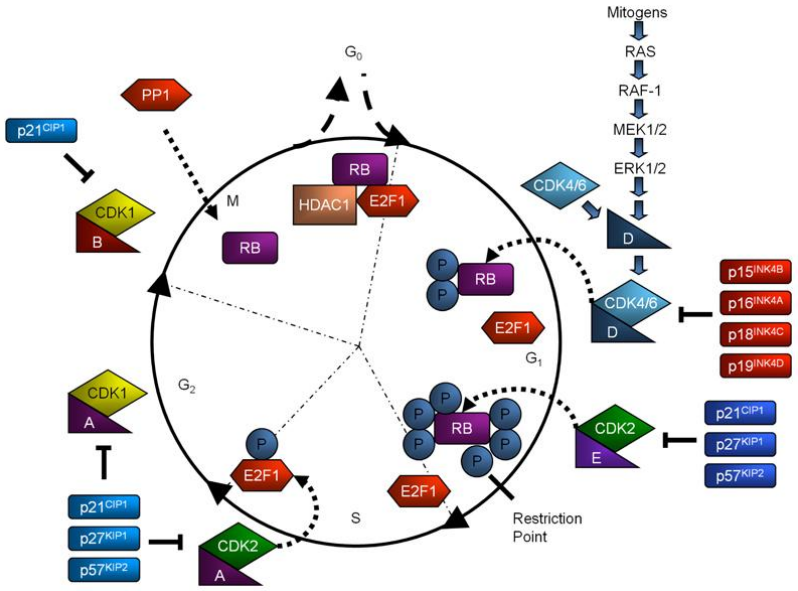

Figure 18: The cell cycle is regulated by the cyclin/CDK complexes. The INK4 and CIP/KIP proteins modulate CDK activity at different stages [255].

1.4.2 DNA Damage response and cell cycle checkpoints

Cells can be arrested during the cell cycle to repair DNA damage, resolve structural problems, or in response to stress signals, which includes the lack of essential growth factors, hormones, or nutrients. The presence of DNA damage or replication stress triggers the recruitment of the DNA Damage Response (DDR) enzymes, which consist of Ataxia Telangiectasia Mutated (ATM), Ataxia Telangiectasia and Rad3-Related (ATR) and DNA-PK [223,256,257]. These enzymes belong to the phosphoinositide-3 kinase-related protein kinase (PIKK) family of serine/threonine kinases that induce a cascade of events to promote cell cycle arrest and DNA/Replication repair.

DNA-PK is crucial for the repair of Double-Strand Breaks (DBS). DNA-PK is recruited through Ku80 binding to the DBS region, where DNA-PK will repair the lesion by the Non-Homologous End Joining (NHEJ), which involves ligation of two broken DNA ends without needing a repair template [257–259].

ATM and ATR (Figure 19) both sense DNA damage. However, ATM responds mostly to double-strand break ends induced in the presence of Ionizing Irradiation (IR), while ATR, which senses double-strand break as well, also reacts to UV or stalled replication upon replication stress [260,261].

ATR and ATM phosphorylate and activate, respectively Chk1 and Chk2 which, in turn, phosphorylate and inactivate Cdc25 phosphatases. Moreover, Chks induce other effects, which include, for example, p53 activation through phosphorylation [223]. Consequently, p53 activation leads to the expression of p21waf1/cip1, which triggers the cell cycle arrest [242].

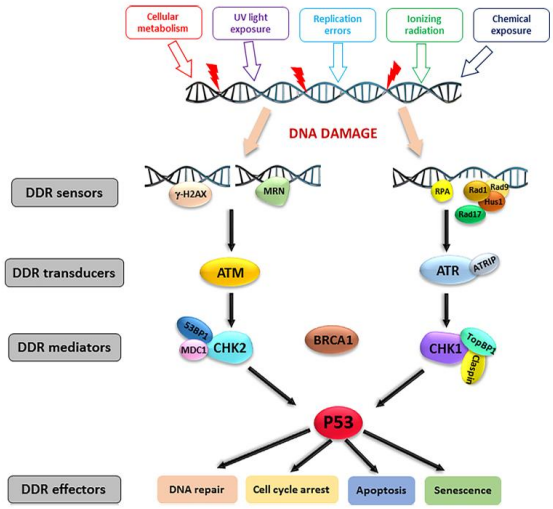

Figure 19: Different types of DNA damage induce the recruitment of DDR sensor and trigger the DDR pathway[262].

The regulatory mechanisms within the eukaryotic cell cycle that ensure the accurate and timely progression of cellular events are called checkpoints:

- During the G1 phase, the sensors monitor the cells prior to the phase S (Figure 20). They establish the fate of the cells and regulate the transition G1/S;
- S phase is characterized by an intra-phase checkpoint to support DNA replication (Figure 20);
- G2 phase regulators ensure that everything is ready for mitosis (Figure 20);
- Mitotic checkpoint SAC ensures the perfect condition for chromosome segregation (The SAC will be discussed in the dedicated paragraph).

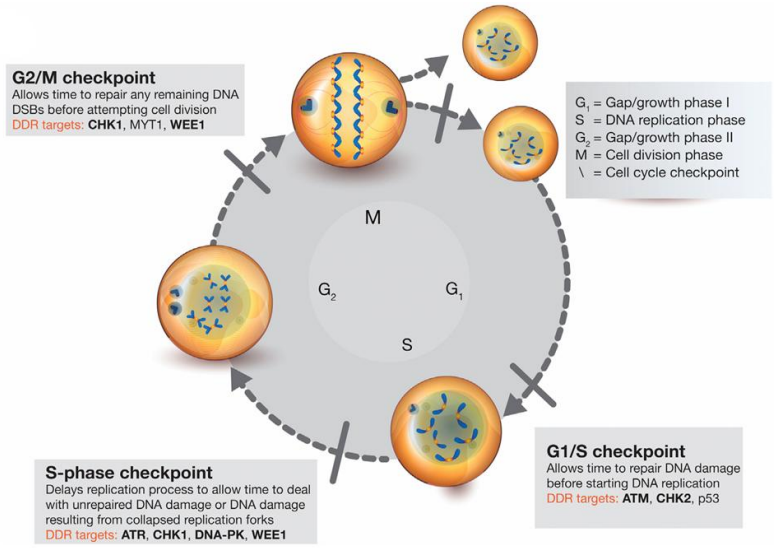

Figure 20: Interphase checkpoints are connected to the DDR response to regulate the cell cycle progression [263].

-G1/S transition checkpoint: During G1, the cells monitor the presence of nutrients and growth factors because, without them, the cells cannot proliferate. Upon reaching the G1/S phase transition, the checkpoint controls if the cells are ready to undergo the duplication of DNA in S phase. Once the cell surpasses such a restriction point, it cannot return to G1 anymore. The G1 to S transition is controlled by the p16-pRb pathway. P16 binds to CDK4/6, inhibiting its kinase activity, thereby preventing Rb phosphorylation [264].

Interaction with other cells is known to affect cell behaviour. Indeed, contact inhibition triggers signals that stop cell proliferation even in the presence of nutrients [265]. Moreover, upon aging, the telomere extremities shrink in length and trigger the replicative senescence in G0 [209,266]. In both scenarios, contact inhibition and senescence, the cells stop proliferating due to the presence of p21waf1/cip1 protein [267,268]. When DNA damage occurs during the G1 phase due to, for example, exposure to chemical compounds or Reactive Oxidative Species (ROS), it must be resolved before the S phase entry to avoid that mutated DNA is inherited by the daughter cells. Indeed, the checkpoint at G1/S transition monitors this aspect and blocks the cell cycle through the DDR if DNA damage is present ensuring that the damage is repaired in time before the S phase.

-Intra-S checkpoint: During the S phase, an intra-S checkpoint regulates the replication event to ensure that the DNA is replicated in the proper manner. Lack of nucleotides, proteins, or the formation of mismatches and DNA secondary structures, the presence of nicks and gaps during DNA replication are known to cause replication stress. All these problems are handled by the DDR [269,270].

-G2/M transition checkpoint: The G2 phase is characterised by a major checkpoint to control the cell state prior to mitosis entry, and it includes the surveillance on eventual DNA damage. When DNA damage is produced during the S phase and not resolved, the cell can reach the G2 phase which triggers, once again, the DDR.

-SAC: SAC monitors the attachment between the microtubules of the mitotic spindle and the kinetochore complex and impairs the progression from metaphase to anaphase until every chromosome is correctly contacted by the mitotic spindle. Chromosome segregation is a crucial event highly regulated to ensure the correct number of chromosomes in the new generation of cells. Indeed, alteration of the chromosome segregation fidelity correlates with an alteration in the number of chromosomes and thus in the genome. For this reason, active control of the chromosome segregation dynamics is required to achieve perfect fitness.

1.5 The mitosis

This chapter will focus on the mitosis, a key event required for the cell proliferation. It will outline and describe the structure and the molecular players involved in chromosome segregation.

Mitosis is a critical process for ensuring genome stability. When mitotic errors arise, like a chromosome that is not aligned at the metaphase plate (misaligned chromosome) or does not segregate in time (lagging chromosome) during anaphase, aneuploidy can be induced and the proper balance of genes altered, thus jeopardising cell fitness, potentially leading to cell transformation. Therefore, proper regulation of mitosis is essential.

Chromosome segregation relies on the interaction of microtubules with the kinetochore complex. Microtubules arise from the mitotic spindle. Instead, the kinetochore complex is recruited to the centromere. Each of these two components will be discussed in the next paragraphs.

1.5.1 The mitotic spindle

Upon entry into mitosis, the mitotic spindle starts to be assembled thanks to centrosome nucleation and duplication, which are regulated, among others, by Aurora A kinase [271]. The centrosome is composed of pericentriolar material and the centrioles, which are barrel-shaped arrays of microtubules [272]. The centrosome acts as the primary site of microtubule nucleation. Microtubules, in turn, are composed of α- and β-tubulin subunits that together generate long and dynamic filaments. The dynamics of polymerisation and depolymerisation of the microtubules generate the forces required to push and pull the chromosomes towards the equatorial plate in metaphase and to the opposite poles of the mitotic spindle in anaphase, respectively. Thus, the mitotic spindle formation is a crucial event for both chromosome congression and segregation. The microtubules that arise from the mitotic spindle are divided into 3 groups (Figure 21) [273]:

-Astral microtubules are able to place the poles to the cortex of the cell,

-Kinetochore fibers physically interact with chromosomes at the kinetochore (k-fibers),

-Interpolar microtubules extend from one spindle pole and reach the other spindle pole.

To regulate microtubule fibers, different proteins are involved. The Microtubule-Associated Proteins (MAPs) interact with microtubules to rearrange their dynamics. Microtubules are characterised by a stable minus extremity, which fixes the microtubule in a specific position, and a plus extremity (plus-end), which is characterised by dynamicity and polymerisation. To this

regard, it is important to stabilise the microtubules plus-end when it is located at the kinetochore to achieve the kinetochore-microtubule attachment. To do this, the MAPs, such as +TIPs, move along the microtubule to locate at the plus-end favouring the stability and the loss of dynamics of tubulin [273,274].

MAPs can also induce the stabilization of the microtubules, allowing the formation of the kinetochore-microtubule attachment. However, MAPs can also destabilise the microtubules, which is required both during the maturation of kinetochore-microtubule attachments and chromosome segregation.

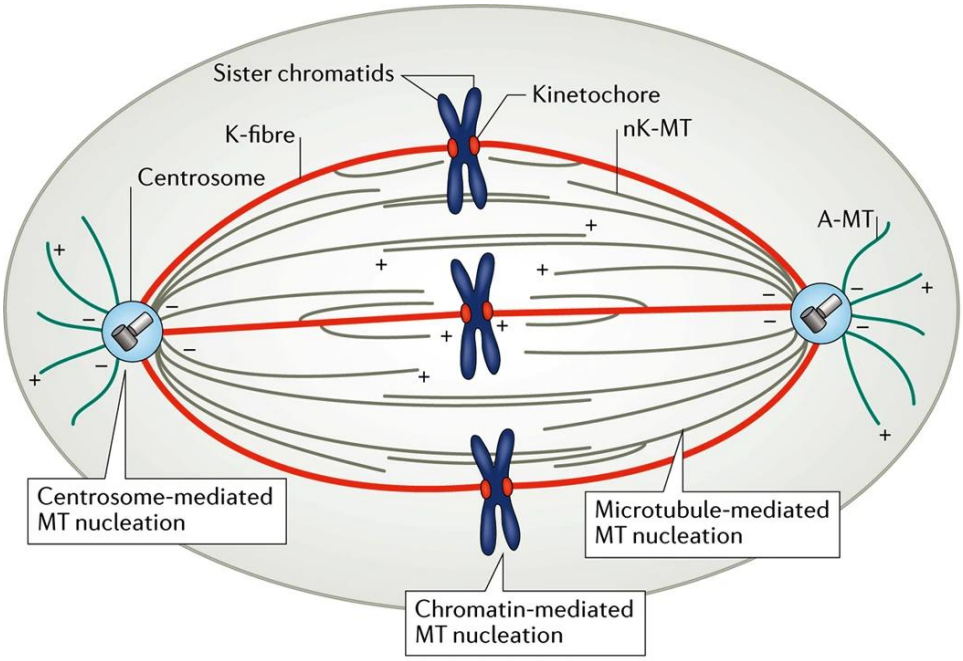

Figure 21: The spindle is characterised by microtubules with different roles. Astral microtubules aid in the positioning of the pole; K-Fibers interact with the kinetochore, and interpolar microtubules nucleate new microtubules [275].

The stability of the microtubule plus end, namely the reduction of the depolymerisation speed, is important to ensure the building of microtubules and to avoid catastrophic events that can be generated when the depolymerisation speed surpasses the polymerisation one. The stability of the microtubules is ensured by several proteins, such as P150Glued and CLIP170.

P150Glued is the largest subunit of the dynactin complex and is responsible for the binding to the microtubules. By regulating dynein, P150Glued has a fundamental role in regulating the mitosis [276–279]

CLIP170, the best-known exponent of the CLIP family, consists of cytoplasmic linker proteins that mediate the interaction of organelles with microtubules. CLIP170 supports cargo movements and metaphase chromosome alignment along the microtubules [280,281]. The C-terminal domain of

CLIP-170 is responsible for its interaction with the kinetochore, whereas the binding of CLIP-170 to microtubules requires the CAP-Gly domain [280,282]. The CAP-Gly domain found at the N terminus also allows interactions with the EB family [273,274,283].

If on one side the stability of the kinetochore-microtubule attachment is important, at the same time, the cell requires a dynamicity to allow chromosome segregation and movement. In this regard, MCAK recruited at the plus end of microtubules at the centromere, destabilises microtubules [284]. MCAK is a kinesin 13 family member and, by forcing the depolymerisation of microtubules, is involved in the increase of the tubulin dynamics [285–287]. To ensure that microtubule stabilisation is maintained up to anaphase, MCAK is inactive during the transport to the microtubule-plus end close to the kinetochore. and is phosphorylated on Ser92 and Ser186 by Aurora B [288–290]. At the centromere, when bi-orientation of the kinetochore-microtubule attachment is achieved for all the chromosomes, the MCAK phosphorylation will be removed by PP1, a phosphatase that activates MCAK; thus, MCAK will localise to the kinetochore to depolymerise the microtubules for chromosome segregation.

1.5.2 The Repetitive DNA along the chromosome

In 1972, Susumu Ohn considered it "junk" DNA with no biological meaning (non-protein-coding DNA) [291]. However, in 1992, Emile Zuckerkandl revised the "junk" DNA, revealing that some sequences are still bound by proteins even if no functions were known [292].

Until 2000, very little was known about repetitive DNA. Starting in 2001, the sequencing of the human genome [293,294], had difficulties in analysing the complexity of the repetitive DNA especially at the centromere and telomere [295]. Using a database of Whole-Genome Shotgun (WGS) reads and frequency vectors [296], in the latest years, the researchers finally obtained the sequence of the human genome and thus, the sequence of an entire chromosome from one telomere to the other with the repetitive DNA included [297].

Repetitive DNA can be divided into two categories (Figure 22): interspersed repeats and tandem repeats. Tandem repeats are Satellite DNA classified depending on the monomeric repeat length into microsatellites, minisatellites, satellites, and macrosatellites [298,299]. Satellites consist of units up to megabases long, and characterise the centromeric region [298,300–302].

The Interspersed repeats, instead, consist of mobile DNA sequences capable of transcribing, expressing, and excising themselves to insert into another region of DNA within genomes. Due to

their potentially dangerous nature, these elements are normally kept silenced by piRNAs and DNA methylation.

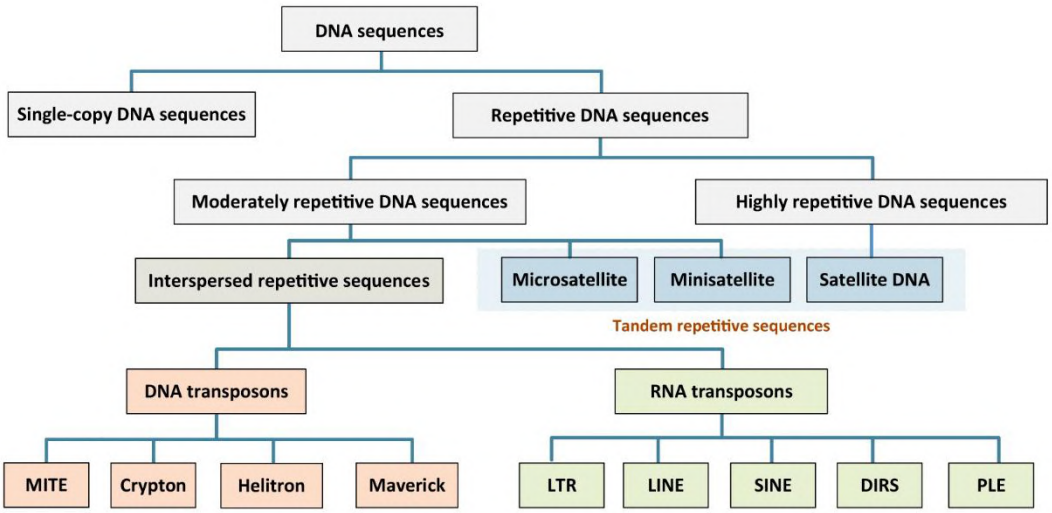

Figure 22: Classification of repetitive DNA in the human genome [299].

1.5.3 The Centromere

The centromere appears as a constriction that divides the chromosome into two arms. Depending on centromere position, we distinguish metacentric chromosomes, when the centromere is located in the center of the chromosome, submetacentric when the centromere is slightly off-center, acrocentric if the centromere is located almost at the chromosome end, and telocentric if the centromere is instead located at the very end of the chromosome [303]. The evaluation of a chromosome can occur in many ways. Chromosomes can be rearranged based on their length, on their centromere localisation, and finally through a band pattern staining. Moreover, the number of chromosomes can also be analysed. All these evaluations realise the Karyotyping of the cell. This technique is often studied to check for human pathologies (Figure 23).

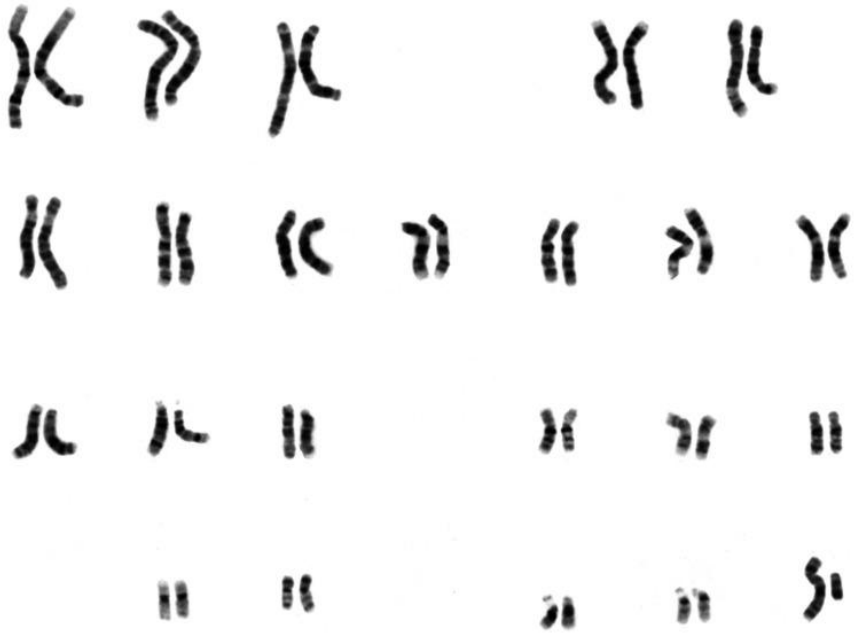

Figure 23: The Karyotype is an individual's complete set of chromosomes, achieved through alignment of chromosomes based on their length and centromere location. Moreover, chromosomes can also be organised based on the pattern of bands [304].

The centromere is fundamental to cell fitness as it is involved in kinetochore recruitment and chromosome segregation [305]. Two regions can be distinguished: the pericentromere and the centromere core. The centromere core is characterised by long arrays of AT-rich α Sat repeated in tandem and provided with an epigenetically defined chromatin structure that contains CENP-A, which replaces canonical histone H3 [306,307]. Each monomer of α Sat DNA is composed of 171bp repeat units organised in Higher-Order Repeat units (HORs) (Figure 24 and 25) or in monomers that lack a higher organisational pattern [306–309]. Moreover, α Sat arrays differ in HOR size and sequence based on the chromosome but only one HOR repeat per chromosome is characterised by the kinetochore recruitment and thus is active [306,307]. The activation of α Sat HOR is based on a high level of methylated CpG in comparison to the inactive arrays, where, instead, CpG methylation is at low levels. At the same time, the active HOR is characterised by region with low amount of DNA methylation [307,310–312].

The pericentromeric region, which flanks the centromere core, lacks CENP-A and is characterized by transposable elements and smaller arrays of diverged α Sat monomers that lack HORs [307,313,314]. Moreover, at the pericentromere, we can observe non-α Sat repeat families, such as HSat2 and HSat3 that are present in every chromosome, especially on chromosome 9 [296,307,315].

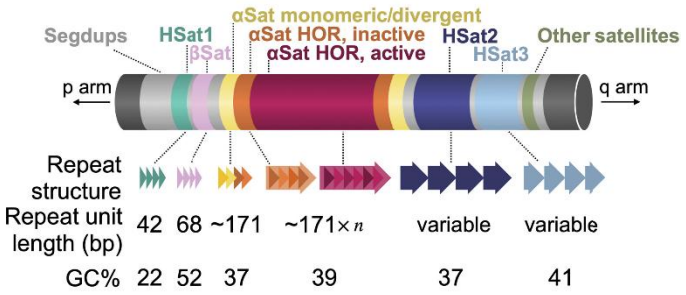

Figure 24: Schematic of a generalized human peri and centromeric region. α Sat DNA characterizes the HORs of the centromere [307].

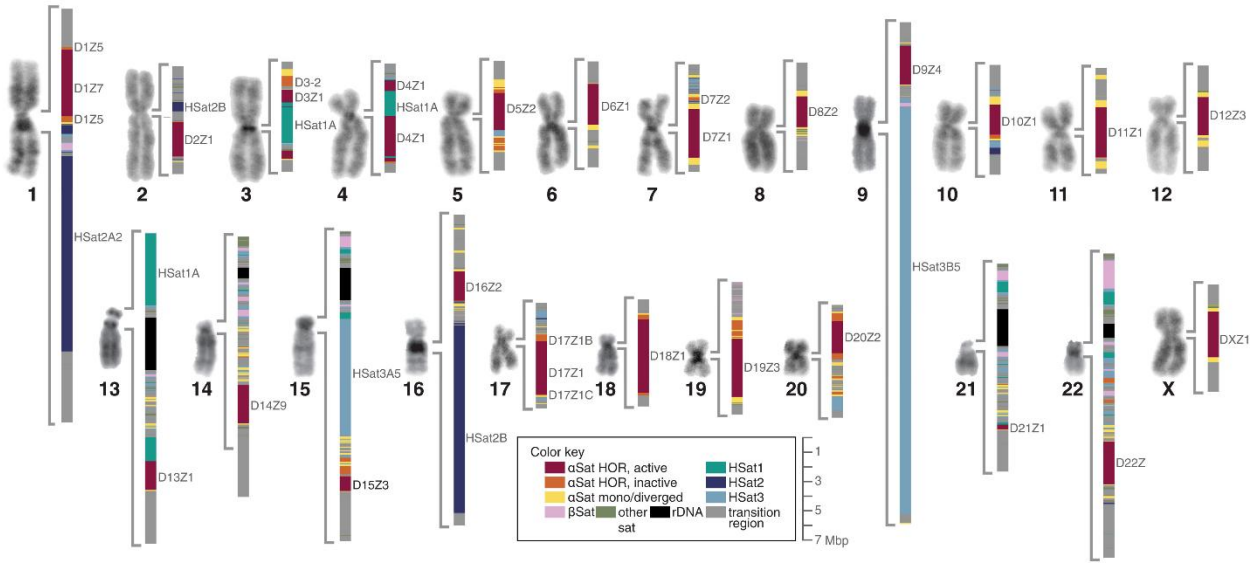

Figure 25: Different types of repetitive DNA characterise the chromosomes [307].

1.5.3.1 CENtromeric proteins CENP-A and CENP-B

CENP-A is a histone H3 variant that defines centromere identity, being essential for kinetochore assembly but dispensable for maintaining its function once established [316–325]. Interestingly, CENP-A localises to the centromere core thus, at alpha satellites organised in HOR expansions (eight sites of identical duplications within a ~365-kb region) and characterized by low DNA methylation [306,307,311,312]. CENP-A can show heterogeneity in its positioning between the same clone population at the boundary of the CDR [326]. However, it is not the DNA sequence identifies CENP-A position nor the centromere functioning. This has been demonstrated with the existence of neocentromeres and with artificial centromeres that are built in non-repetitive DNA still allowing a functional kinetochore, due to the presence of CENP-A [322,327,328]. Neocentromere, which occurs in the chromosome arms and not at the standard region, are still characterized by CENP-A enrichment and functionality. Directed Methylation with Long-read sequencing (DiMeLo-seq) for CENP-A, revealed that CENP-A enrichment at the neocentromere coincides

with a reduction in DNA methylation, suggesting that DNA methylation low levels contributed to the distribution pattern of CENP-A at the neocentromere and native centromere [326]. Also, at the human native centromere heavily methylated inactive centromere is characterized by no CENP-A enrichment or kinetochore formation confirming that DNA methylation somehow regulates CENP-A positioning [326]. Maintenance of the heterogeneity of CENP-A chromatin is also supported by H3K9me3 heterogeneity, which creates the boundaries for CENP-A recruitment [326].

CENP-A loading at the centromere is mediated by the chaperone activity of HJURP [303,329–331]. In this regard, lncRNAs, specific transcription at the centromere, and other protein complexes such as Mis18 are also required for the loading of CENP-A [332–335].

CENP-A has a central histone fold domain similar to histone H3, flexible N- and C-terminal tails, and a specific Centromere Targeting Domain (CATD). The CATD interacts with the HJURP chaperone, which ensures CENP-A is incorporated into the centromeric chromatin (Figure 26). The flexible N-terminal or C-terminal tails, instead, bind to the CENtromeric Protein B (CENP-B) or the CENtromeric Protein C (CENP-C), respectively (Figure 26) [324,336,337]. In fact, in RPE-1 cells, the CATD was enough to establish the epigenetic conditions required for cell cycle-dependent loading, but that condition was not enough to maintain CENP-C at the kinetochore [337]. CENP-C was maintained at the centromere, suggesting a functional kinetochore. This is also confirmed by Longdson and colleagues, who induced the formation of a neocentromere and observed that the establishment of the centromere requires the CATD domain and a N-terminal region [328].

Differently from the other histones that are loaded onto the DNA during replication, CENP-A incorporation occurs during late telophase and the following early G1 phase in humans. Instead, during the S phase, pre-existing CENP-A is redistributed onto newly replicated centromeric DNA, thus diluting the amount of CENP-A to half [306,337–340]. Since the deposition of CENP-A occurs in the early G1 phase, this suggests a cell cycle-based regulation of CENP-A recruitment to the centromere. Indeed, CDK1 and CDK2 regulate Mis18BP1, HJURP, and CENP-A itself through phosphorylation [303,341–344]. While phosphorylation by CDKs usually prevents kinetochore assembly, phosphorylation of CENP-A by PLK1 favours CENP-A loading at the centromere [342].

CENP-B is the only centromeric protein that binds a specific 17-bp repetitive DNA sequence known as CENP-B box [303,345]. Even if cells can survive without CENP-B and viable mice can be generated in its absence [346–348], this protein has been observed to support the faithful segregation of chromosomes, likely by influencing the recruitment of CENP-A through CENP-B N-terminal domain [349,350]. Importantly, CENP-B can interact with CENP-C, strengthening the connection

between CENP-A and CENP-C, and thereby promoting the subsequent recruitment of the kinetochore complex [349,351].

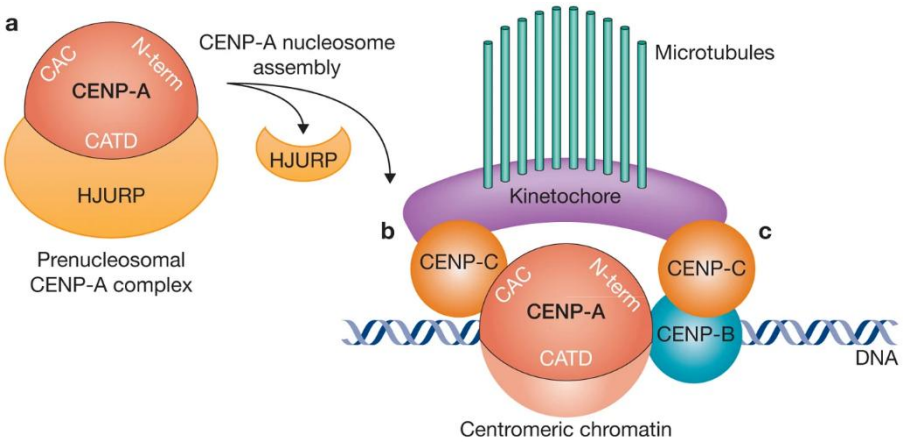

Figure 26: HJURP recruits CENP-A at the centromere. CENP-A, in turn, recruits CENP-C and CENP-B to ensure the assembly of the kinetochore complex [352].

1.5.3.2 Epigenetic regulation of the centromere

A peculiarity of repetitive DNA is its high dynamics in opening and closing the state of chromatin. Indeed, transcriptional event still occurs at the centromere core. The presence of the RNAP II at the centromeric region confirms that transcription is still performed in this region despite the heterochromatinization of DNA [353,354]. However, the centromere is a gene-poor region; still, transcription occurs at the repetitive DNA. Depending on which repetitive DNA locus is transcribed, transcripts have distinct molecular functions. There are transcripts arising from α Sat of active centromeres that are physically associated with CENP-A and CENP-C. Instead, α Sat transcripts arising from inactive arrays interact with CENP-B [335]. Moreover, in X*enopous Laevis* egg extracts, centromeric ncRNA are required for the localisation of the kinetochore and Aurora B kinase, which is involved in the correction of the wrong attachment, reinforcing the idea that centromeric transcripts are required to preserve the cell fitness [355,356].

If from one side the transcription event is important, on the other side, centromere DNA is mainly characterised by repressed heterochromatin. Thus, a balance between open and closed chromatin is necessary. The pericentromere is composed of constitutive heterochromatin, which, as previously discussed, is important to preserve the fitness and genome stability [357,358]. Constitutive heterochromatin is characterised by the tri-methylation of the histone H3 at the Lysine9 (H3K9me3) performed by the histone methyl transferase SUV39h1 [359]. H3K9me3 is

mostly located at interspersed repeats of the pericentromere [360,361]. HP1 also characterises the DNA of the centromere and, together with SUV39h1, it further improves heterochromatinization by recruiting DNMTs and inducing DNA methylation [362].

At the same time, DNA methylation can also attract more HP1 proteins that will increase the recruitment of SUV39h1. It is important to mention that ncRNA also stabilizes SUV39h1, showing once again that transcription of centromeric repetitive sequences is important for centromere biology [363].

Despite the recruitment of DNMTs at centromeres, DNMT1 single null or DNMT3A/DNMT3B double null mouse embryonal stem cells do not alter H3K9me3 and HP1 localization at long Sat of pericentromeric heterochromatin [360]. In the absence of DNMTs or SUV39h1, however, MeCP2 is reduced at the centromere [360]. These studies suggest that it is important to maintain the compaction of DNA and that the cell has a mechanism to compensate for defects that would lead to a loss of constitutive heterochromatinization at the centromeric region. However, the absence of DNA methylation correlates with a change in histone modification due to transcriptional activation [360,364]. DNMT3A/DNMT3B double null phenotype has a non-complete loss of DNA methylation due to the presence of DNMT1; thus, Lehnertz and colleagues, do not exclude that the complete absence of DNA methylation could affect the centromere heterochromatinization. Indeed, triple DNMTs null mice die at early stages of development which confirms the importance of DNA methylation.

1.5.3.3 The Kinetochore assembly

At the centromere, CENP-A serves as the foundation for a hierarchical protein assembly that culminates in the recruitment of the outer kinetochore complex and fibrous corona proteins. Specifically, three complexes are sequentially recruited starting from CENP-A:

- The Constitutive Centromere-Associated Network (CCAN),
- The KNL1-MIS12-NDC80 network (KMN),
- The fibrous corona.

-CCAN: The CCAN is the first protein complex to interact with CENP-A, acting as a bridge for the recruitment of the kinetochore. Indeed, the CCAN may be considered part of the inner kinetochore complex, which interacts with the centromere. At least 16 CENPs non-histone proteins craft the CCAN (Figure 27) [365] and they can be grouped into five sub-complexes: CENP-C, CENP-L-N, CENP-H-I-K-M, CENP-T-W-S-X, and CENP-O-P-Q-U-R [366]. CRISPR/Cas9 knockdown

experiments have shown that depletion of each one of these proteins disrupts the stability of the network, demonstrating that these proteins interact and depend on one another [366]. Among them, the most relevant proteins that I will focus on are the centromeric protein CENP-C and CENP-T as they are able to recruit the outer kinetochore complex independently [367–370].

CENP-C is the most important upstream component of the CCAN network [371,372] because it directly interacts with CENP-A to mediate kinetochore recruitment [373–375]. Indeed, CENP-C contains a centromeric targeting domain required both for targeting CENP-C to the centromere and for binding heterochromatin [350,375–377] . The C-terminal domain allows CENP-C dimerization [378,379] and interactions with histone H3 and, preferentially, CENP-A [350,377]. In humans, CENP-C is characterised by an N-terminal region that interacts with the CENP-K and MIS12 complex, which, in turn, is a component of the KNM complex. This interaction is necessary for the full recruitment of the kinetochore complex at the centromere [380–383]. CENP-C supports the recruitment of other CENP complexes, such as CENP-H-I-K-M and CENP-T-W-S-X complexes [350,384]. CENP-C is also required for CENP-L-N localization [366]. Vice versa, CENP-L-N supports the recruitment of CENP-C during G1/S phase [366].

CENP-T is the second important upstream element for CCAN formation. Indeed, CENP-T interacts with centromeric DNA in a CENP-A-independent manner to establish an alternative pathway for the recruitment of the CCAN [385,386]. When CENP-T interacts with CENP-W, the CENP-T-W complex recruits the CENP-S-X to create the CENP-T-W-S-X complex, which is recruited at the centromere via the CENP-H-I-K-M, CENP-L-N complexes and CENP-C [366]. Loss of CENP-T by an inducible degron leads to a reduction of the CENP-H-I-K-M and CENP-L-N complex suggesting a mutual needs [366]. Finally, CENP-T interacts with NDC80 and MIS12 complexes to recruit them to the kinetochore complex [367,369,370,387].

-KMN: Once the CCAN is recruited, from the late G_2 phase to mitosis, the KMN can localize to the centromere. The KMN is a complex that, together with the fibrous corona, forms the outer kinetochore (Figure 27 and 28). The KMN interacts with the microtubules arising from the mitotic spindle to ensure the chromosome segregation event. It is made up of ten subunits, which create 3 complexes KNL1, MIS12 and NDC80. The KMN is recruited by both CENP-C and CENP-T.

KNL1 complex contains the Knl1 and Zwint subunits [303,388]. Via the C-terminal region of Knl1, the complex interacts with MIS12 [389,390]. Instead, Zwint interacts with the C-terminal region of Knl1 to recruit ROD-ZW10-ZWILCH (RZZ), which characterises the fibrous corona [390–392].

MIS12 complex is composed of Mis12, Pmf1, Nsl1, and Dsn1 subunits [303,388]. The binding to CENP-C occurs through the Dsn1 and Nsl1 subunit [388]. Also, via the C-terminal tail of Nsl1, Mis12

recruits KNL1 and NDC80 complexes [390]. MIS12 acts as a bridge between CENP-C, KNL1, and NDC80, thus supporting kinetochore functioning [368,390,393]. Importantly, MIS12 recruits components of the SAC, both Bub1 and BubR1, and thus, it also acts as a hub for cell signaling [389].

NDC80 complex consists of four subunits Highly Expressed in Cancer 1 (Hec1), Nuf2, Spc24, and Spc25 subunits [303,388]. Hec1 CH domain at the N-terminal region interacts with the C-terminus of the microtubule and Nuf2 subunit [394,395]. Instead, the C-terminus of the Spc24 and Spc25 subunits is used for the interaction with MIS12 [303,394–397]. Moreover, components of the SAC, such as MAD1 and MAD2, locate near Hec1 [398].

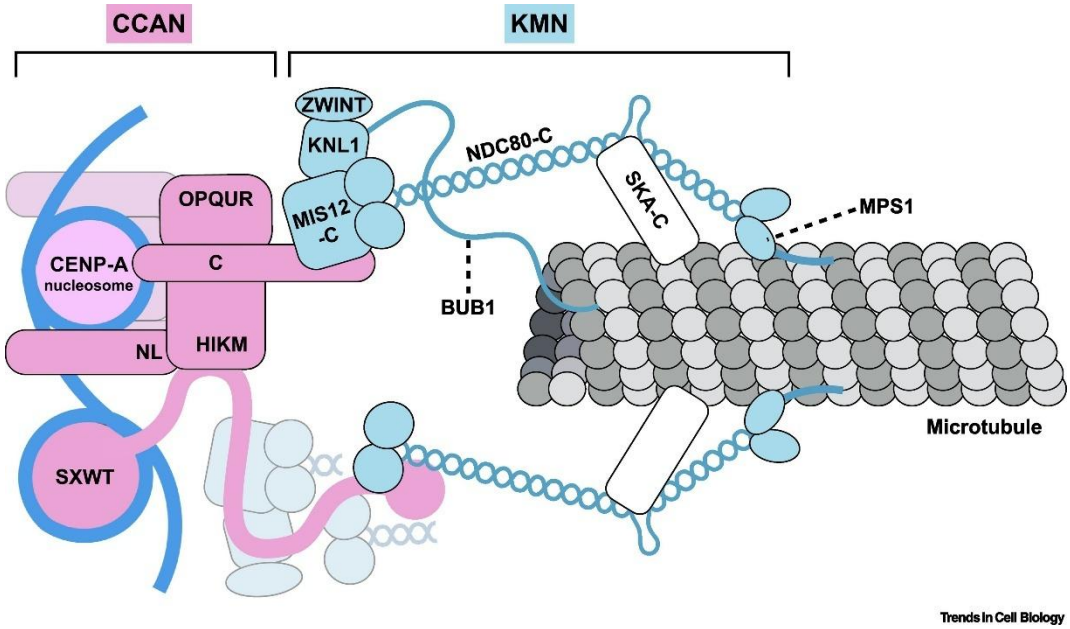

Figure 27: Schematics of the most important elements of the kinetochore complex. In pink the CCAN which interacts with the centromere and in light blue the KMN network which interacts with the CCAN and the microtubules [399].

-The fibrous corona: The fibrous corona (Figure 28) acts as a scaffold for the recruitment of different proteins involved in the attachment to the microtubules. Indeed, the fibrous corona promotes chromosome alignment and SAC signalling [400]. To form the fibrous corona, different proteins are recruited at the kinetochore, such as the RZZ complex and Spindly. However, once the fibrous corona is established, SAC proteins, dynein, the CENtromeric protein E (CENP-E), and MAPs characterise the fibrous corona as well [399].

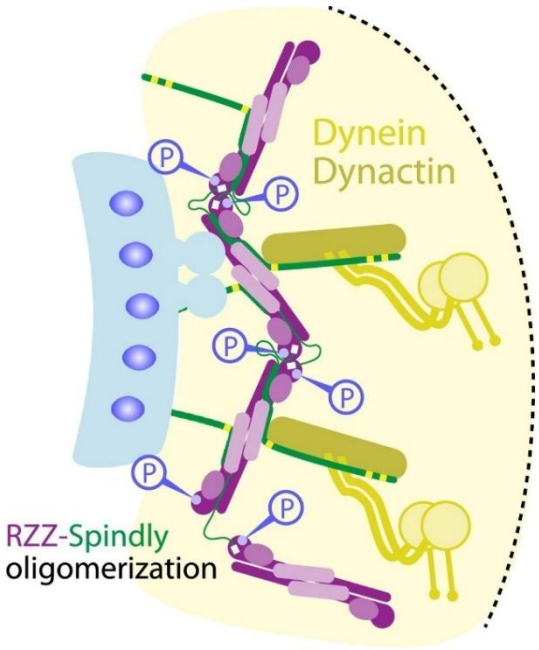

Figure 28: Schematics of the fibrous corona RZZ-Spindly complex. Dynein and Dynactin are located at the fibrous corona when the kinetochore is not bound to the microtubules [399].

Dynein, a cell motor, localises at the kinetochore complex thanks to an interaction with P150Glued [276,401–403]. Specifically, P150Glued supports the kinetochore localisation of dynein by allowing the interaction with microtubules [273,403,404]. Another important cell motor that locate at the fibrous corona is CENP-E (or kinesin 7) [405]. CENP-E is important from one side, to allow chromosome congression in metaphase and, from the other side, to permit the realisation of the first, yet immature, lateral kinetochore-microtubule attachments.

1.5.4 Chromosome congression

Upon mitosis entry, the density of microtubules favours numerous lateral interactions with the unattached kinetochores, which allows chromosomes to move and congress to the mitotic spindle equator [399,406,407]. The chromosomes that locate in the middle region between the spindle poles can be more easily attached by microtubules arising from the opposite spindle poles (bioriented state) and reach the equator. However, some chromosomes are located near the astral tubulin and have a mono-oriented state. These chromosomes can still interact with the microtubules from the other pole and thus, move to the chromosome plate. To do this, the chromosome located at the pole must overcome the Polar Ejection Forces (PEFs) applied by spindle pole microtubules, which push the arms of chromosomes away from the spindle. These forces are both based on microtubules dynamics and cell motor chromokinesin [408,409]. To counteract these forces, CENP-E and dynein play antagonistic roles at the kinetochore, independently from the chromosome biorientation (Figure 29). Dynein allows the peripheral movement of the chromosome towards the spindle pole

[277,278,409]. Once the spindle pole is surpassed, and the chromosome is located between the two spindle poles, CENP-E interacts with the microtubules allowing the chromosome to move and congress towards the equatorial plate, even if there is no bi-oriented attachment yet [410,411]. CENP-E function is regulated by Aurora A and Aurora B kinases-dependent phosphorylation. Although the phosphorylation occurs at the same residue, Aurora A dependent phosphorylation promotes chromosome congression from the pole to the equatorial plate, while Aurora B dependent phosphorylation prevents premature CENP-E removal from the kinetochore [411]. Indeed, inhibition of Aurora B kinase leads to a loss of CENP-E from the kinetochore during early mitosis [412]. Both Aurora kinases are active during mitosis, however, Aurora A is located at the spindle pole, while Aurora B is at the kinetochore. This positioning creates a gradient of kinases that can efficiently regulate CENP-E and the process of mitosis itself.

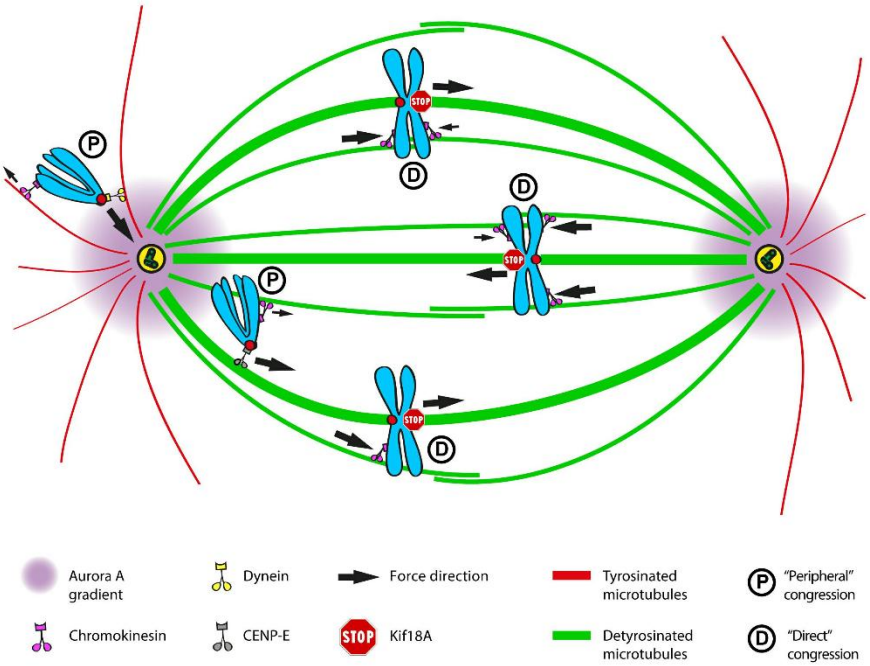

Figure 29: Representative image of the peripheral and direct congression generated by dynein and CENP-E [409].

CENP-E facilitates the establishment of kinetochore-microtubule attachments, as depletion of CENP-E in human HeLa cells reduces the efficiency of chromosome congression and abolishes detectable interactions between kinetochores and microtubules [410,413]. CENP-E plays a fundamental role in creating lateral attachments, which must subsequently be converted into stable end-on attachments [413]. Notably, depletion of Hec1 by siRNA impairs the formation of end-on kinetochore-microtubule attachments without affecting the lateral chromosome interactions, indicating that lateral attachments represent an immature intermediate state preceding end-on connections [413,414].

1.5.5 Kinetochore-microtubule end-on attachment

The exact mechanism to convert the lateral into an end-on attachment is not known yet, however, it was observed that MCAK and CENP-E play a role in kinetochore-microtubule attachment maturation from the lateral interaction to an end-on interaction [413]. Since lateral kinetochore-microtubule attachments are not the correct configuration, Aurora B kinase remains active [415]. At the outer-kinetochore, two major phosphatases (KNL1 associated PP1 and BubR1 associated PP2A) counteract Aurora B activity and are required to ensure stable kinetochore-microtubule attachments. Shrestha and colleagues, observed that both phosphatases are required for end-on attachment, however, the phenotype was stronger when PP2A was mutated [415].

Once the kinetochore-microtubule end-on attachments are established, many factors step in to maintain the stability, such as Astrin, SKA complex and, as described above, Hec1 [416–423].

Astrin is recruited at the kinetochore-microtubule end-on interaction in a microtubule-dependent manner [413,424,425]. Via its C-terminal domain, Astrin interacts with Hec1 (Figure 30). Moreover, since Astrin is in a complex with PP1, Astrin localization at the kinetochore, enables the recruitment of the PP1 that, in turn, promotes the recruitment of more Astrin strengthening kinetochore-microtubule stability (Figure 30) [421]. Also, PP1 can counteract Aurora B function by directly interacting with KNL1 and CENP-E to interfere with the substrates phosphorylated by Aurora B [411,426]. Impairment of Astrin has been correlated with improper kinetochore-microtubule attachments and, thus, SAC activation and impairment of chromosome segregation [415,421,425].

Ska subunits 1,2, and 3 compose the SKA complex, which, by interacting with Hec1, are able to stabilise kinetochore-microtubule end-on attachment (Figure 30) [423]. SKA complex is not part of the kinetochore complex as it is not required for the structural formation of the kinetochore, instead, depletion of one of SKA components impairs kinetochore-microtubule attachments, increases mitotic errors, and induces cold sensibility of kinetochore-microtubule attachments [419,423,427,428]. Moreover, loss of the Ska subunits through RNA interference induces a higher recruitment of SAC proteins confirming the realisation of non-stable kinetochore-microtubule attachment when SKA complex is missing [427,429].

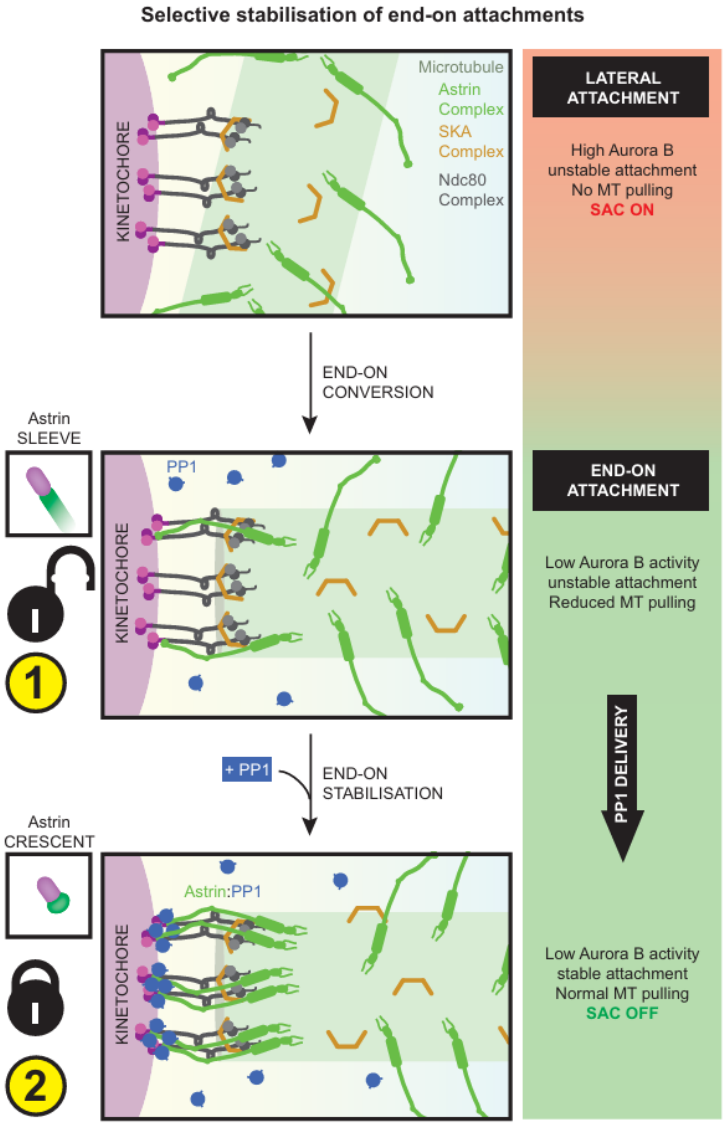

Figure 30: Schematics of Astrin, PP1 and SKA recruitment in the realisation of stable kinetochore-microtubule attachments. The stable attachments occurs when Aurora B activity is reduced [421].

Another event that stabilises the kinetochore-microtubule end-on attachment is corona shedding, which is the removal of the corona and SAC components away from kinetochores mediated by the Dynein motor [399]. CENP-E also seems to be characterised by a stripping process, because unattached kinetochores correlate with an increase in CENP-E signal at the kinetochore [430]. Also, once the kinetochore-microtubule end-on attachment is established, the kinetochore-microtubule attachment persists during mitosis. However, chromosome segregation can occur only when all kinetochores are attached, stabilised, and correctly oriented. This is ensured by Aurora B kinase, which corrects wrong attachment. Once the kinase concludes its work, Aurora B gradient will be adjusted to allow dephosphorylation of Aurora B substrates.

1.5.6 Correction of the kinetochore-microtubule attachments

Accomplice the fact that mitosis is a rapid event within the cell cycle, different erroneous attachments can arise during chromosome segregation (Figure 31). For example, microtubules originating from the same spindle pole may attach to the kinetochores of both sister chromatids, generating a syntelic attachment [431]. Moreover, microtubules from both spindle poles may attach to a single kinetochore, resulting in a merotelic attachment, which generates unbalanced forces [431]. In other cases, only a single microtubule attaches to a single kinetochore, producing a monotelic attachment. All of these erroneous configurations must be resolved to establish the correct bi-oriented or amphitelic attachment [431]. The correct orientation ensures a balance in the kinetochore-microtubule tension forces that turn off the SAC and allow the progression of mitosis from metaphase to anaphase.

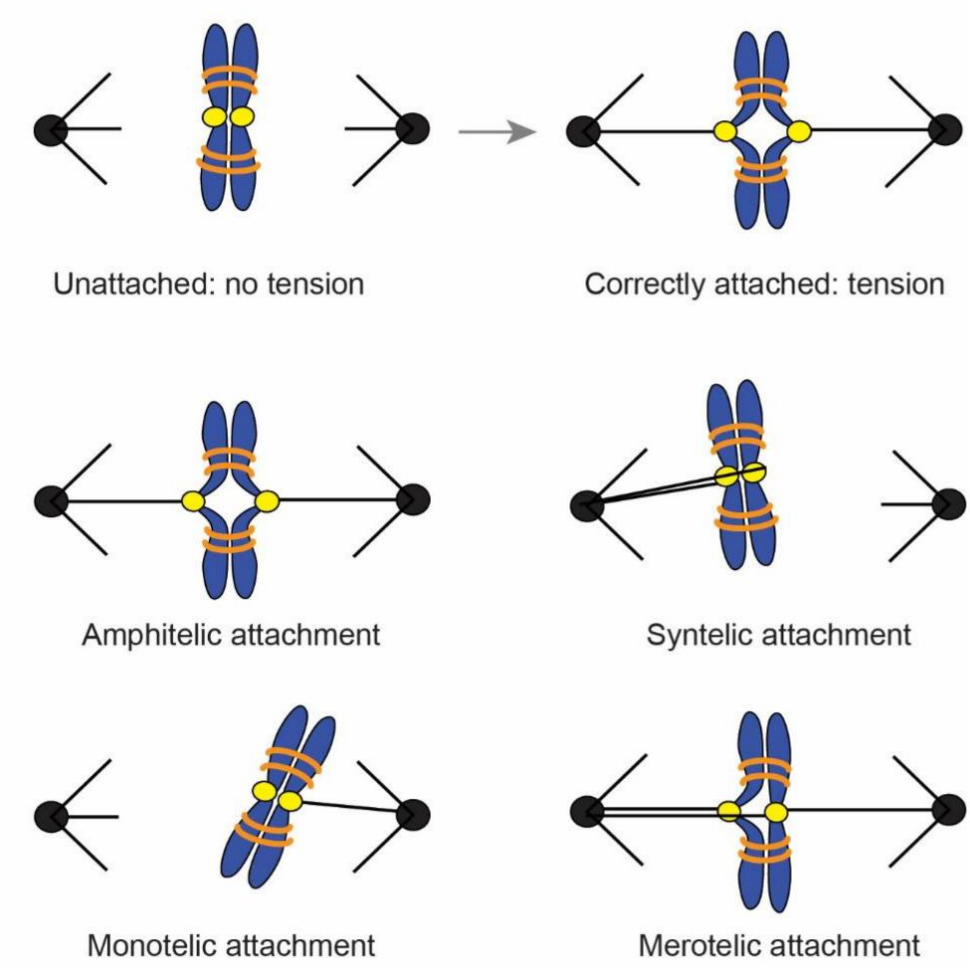

Figure 31: Schematics of different types of attachment. Wrong attachments affect mitosis and thus they must be corrected to favour amphitelic attachment, which is characterized by balanced tension between microtubules and chromosomes [431].

Once microtubules interact with the kinetochore complex through Hec1, the Chromosomal Passenger Complex (CPC) takes care that the attachment is correct. The CPC is composed by Aurora B kinase and three non-enzymatic subunits: INCENP, Survivin, and Borealin [432]. INCENP serves as a scaffold protein that interacts with and coordinates the assembly of the other three components [432]. During prometaphase and metaphase, INCENP associates with chromosome arms and subsequently relocates to the kinetochores, thereby increasing the local pool of Aurora B kinase in this region. Survivin and Borealin ensure the correct localisation and activity of the CPC complex [432]. Aurora B is a Ser/Thr kinase that binds the IN box of INCENP, which is close to its C terminus. As such, INCENP can be phosphorylated thus, enhancing the kinase activity of Aurora B in the complex (Ruchaud, Carmena, and Earnshaw, 2007). Aurora B specifically inhibits the formation of mature kinetochore-microtubule end-on attachments favouring the lateral attachments [415]. When the bi-orientation and appropriate kinetochore-microtubule tension are achieved, the gradient of Aurora B kinase reduces, as previously discussed, preventing interaction and phosphorylation of targets at the outer kinetochore (Figure 32) [433]. The change of the Aurora B gradient is also important to regulate proteins like MCAK, which, depolymerise the microtubules to ensure chromosome segregation, as discussed above [288,290]. Similarly, Aurora B phosphorylates Hec1 when tension is low, and this leads to kinetochore-microtubule detachment allowing the possibility to correct the unstable attachment [431,434,435]. However, this process is quite dynamic as different serine residues of Hec1 (Ser55, Ser44, Ser15, and Ser8) can be phosphorylated by Aurora B [433]. Strikingly, once chromosomes are congressed and Hec1 phoshorylation is removed, Aurora B is not able to phosphorylate these residues again if microtubules are exposed to microtubule-depolymerising drugs [433].

As discussed above, Aurora B activity interferes with PP1 activity within the Astrin:PP1 and the KNL1 complexes [425] inducing instability of kinetochore-microtubule attachments [426]. Also, Aurora B mediated phosphorylation of CENP-E reduces its affinity for microtubules and impairs PP1 binding, further destabilizing the attachments [411].

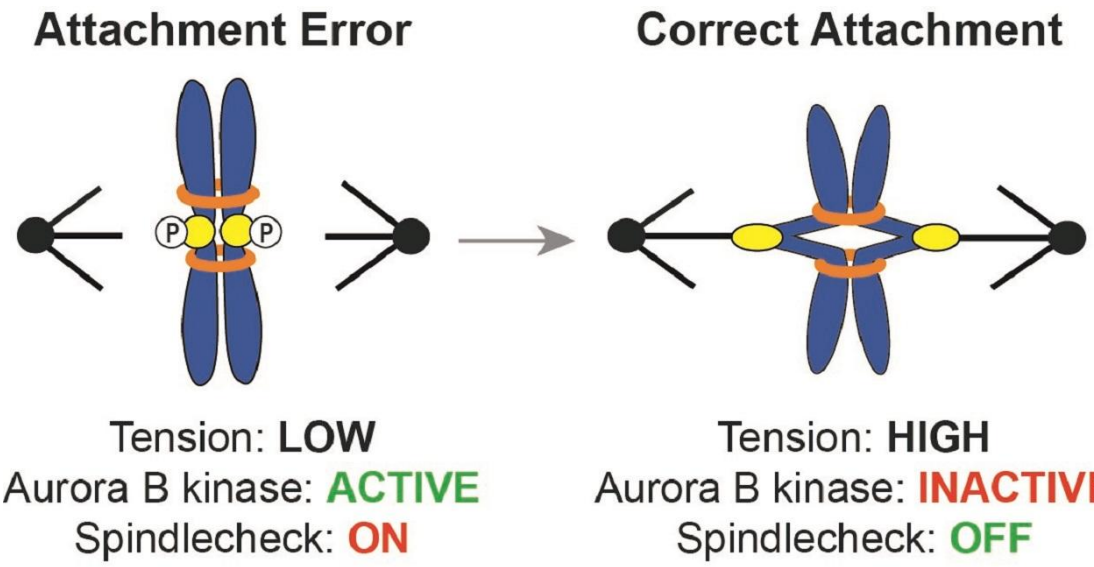

Figure 32: Tension from the correct attachment negatively regulate Aurora B kinase and SAC activities [431].

Aurora B has been observed to be regulated by transcripts arising from the SatI which associate with it in mitotic HeLa cells [436]. This type of transcripts, when absent, induce up-regulation of Aurora B and delocalization of the CPC from the centromere region. Interestingly, cells have a grape-shape phenotype of the nuclei, a phenotype also achieved when Aurora B is silenced [436]. The same happens in *Xenopus Laevis,* where treatments with RNAse or inhibitor of RNAP II affect Aurora B activity and localization at the centromere [354,437].

1.5.6.1 Role of Aurora A in error correction

During mitosis, once a K-Fiber attaches to a kinetochore, it undergoes depolymerization to move the chromosome to the metaphase plate. The depolymerization pulls the attached sister kinetochore toward one of the spindle poles, [438]. This movement generates tension within the inter-kinetochore space, which is defined by the centromere and cohesins. The other sister kinetochore is also subjected to these forces through the physical linkage maintained by cohesins. The movement of the chromosomes or the kinetochore at the metaphase plate is an event named chromosome or kinetochore oscillation (Figure 33). Loss of the chromosome oscillation dynamicity correlates with high rates of chromosome missegregation in cancer. Thus, chromosome oscillation favours instabilities to actively correct the errors [438].

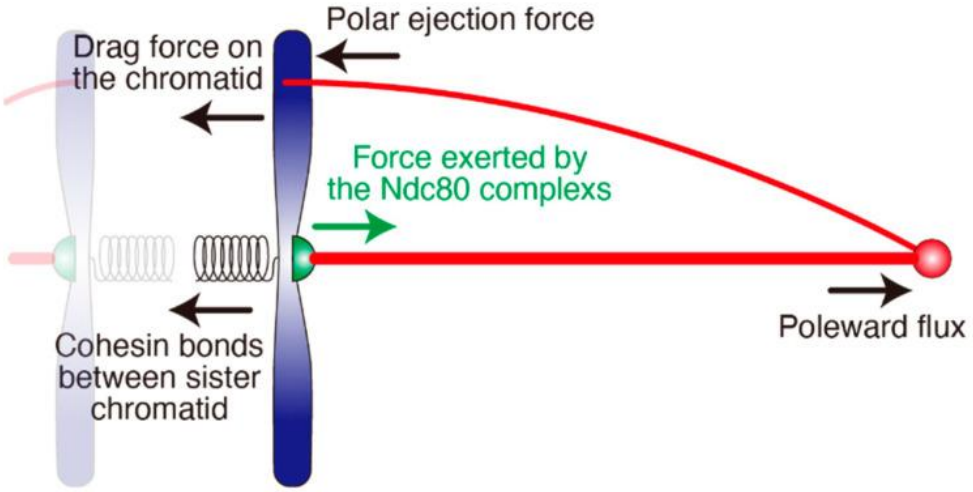

Figure 33: examples of forces that occurs at the chromosome [438].

Chromosome oscillation at the metaphase plate induces the phosphorylation of Hec1 at the Ser55 (S55p). This phosphorylation is generated by Aurora B, but it is also ensured by Aurora A kinase activity as chromosomes approach the spindle poles [433,438]. Indeed, the chromosome oscillation and Hec1 phosphorylation are lost when microtubules are stabilized with depolymerization-inhibiting drugs. Although Aurora A is primarily concentrated at the spindle poles, a small fraction localizes to the centromere through INCENP, where it phosphorylates Hec1 to stimulate kinetochore oscillations [439]. Iemura and colleagues further demonstrated that, in normal cells, Hec1 S55p occurs at the edges of the metaphase plate [438,440]. By contrast, HeLa cells lack this phosphorylation at the metaphase plate and display reduced oscillatory dynamics compared to normal cells [440]. Consistently, cancer cells with high rates of mitotic errors also exhibit reduced oscillations relative to cancer cells with fewer errors [438]. Since Hec1 S55p correlates with less mitotic errors, Aurora A activity at the metaphase plate seems to contribute to error correction. Inhibition of Aurora A results in merotelic attachments and missegregating or lagging chromosomes [439,440]. Thus, Aurora A- and Aurora B-based phosphorylation of Hec1 at serine 55 improves error correction and promotes mitotic fidelity.

1.5.7 The Spindle Assembly Checkpoint (SAC)

To ensure faithful chromosome segregation, cells rely on the SAC. This surveillance mechanism continuously monitors mitotic progression and halts it if proper amphitelic attachments are not established. Once correct kinetochore-microtubule attachments are achieved and the resulting tension is generated, the SAC is satisfied, and it will allow the mitosis to proceed. Alteration of

the fidelity and thus, SAC defects, leads to aneuploidy with potential proteotoxic and tumorigenic effects [441].

In the 1990s, two main models were proposed to explain SAC activation during mitosis. Rieder and colleagues proposed that the checkpoint responds to the absence of kinetochore-microtubule attachment, whereas McIntosh and Li and colleagues emphasised the role of missing tension [442–444]. Current evidence indicates that attachment stability and tension are interconnected, and both mechanisms contribute to the fine regulation of mitotic progression.

The SAC signal is primarily generated at unattached kinetochores and transmitted by the Mitotic Checkpoint Complex (MCC), which includes conserved proteins such as MAD1, MAD2, MAD3 (BubR1 in humans), Bub1, Bub3, and Mps1 [392,445–448]. While MAD proteins monitor attachment, Bub1, BubR1, Bub3, and CENP-E additionally sense tension and are removed from kinetochores upon stable end-on microtubule attachment through dynein-mediated stripping [449].

MAD1 and MAD2 play a central role in SAC signaling. Both are expressed from the G1 phase, with MAD2 expression peaking in G2/M phases [450,451]. MAD1 localizes to unattached kinetochores, where it recruits MAD2 [399,452,453]. MAD2 can adopt two distinct conformations: the open cytosolic form (O-MAD2) and the closed active form (C-MAD2). The binding of O-MAD2 to MAD1 or Cdc20 converts it into the closed conformation [445,454], which, instead, is recruited to kinetochores. C-MAD2, in complex with MAD1, can still dimerise with O-MAD2 which, then, captures Cdc20, forming a C-MAD2-Cdc20 complex that inhibits the APC/C and blocks anaphase onset (Figure 34) [445,452,454–457]. Once all kinetochores achieve proper attachment, the MAD1/MAD2 complex is removed, and thus, no more MAD2 is recruited at the kinetochore. As a result, Cdc20 is released to activate the APC/C, allowing progression into anaphase (Figure 34).

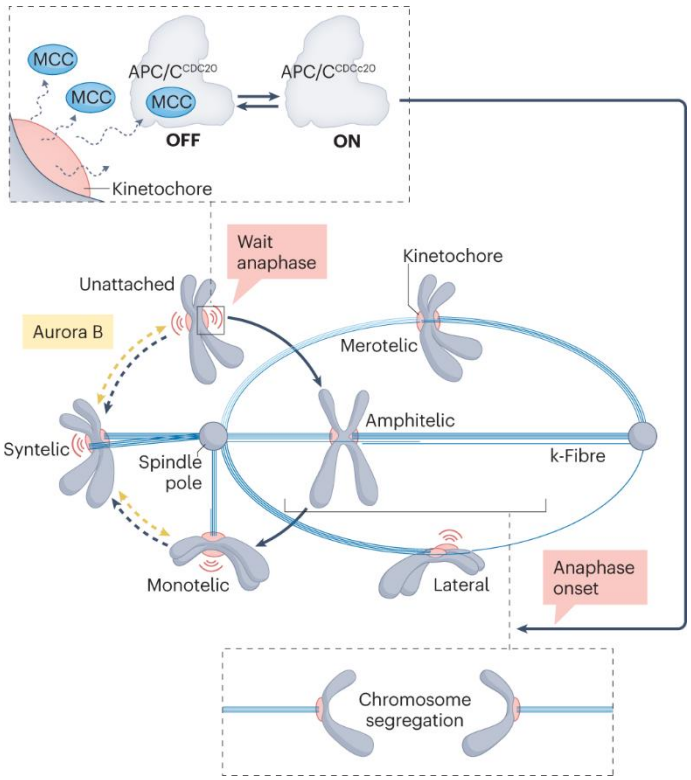

Figure 34: MCC blocks the activity of the APC/C when the kinetochore-microtubule attachment is absent. The realization of the correct attachments results in chromosome bi-orientation, and in the removal of MCC from the kinetochore, which leads to activation of the APC/C and progression to anaphase [458].

Many proteins further regulate this complex process, such as MPS1. MPS1 interacts with Hec1 at unattached kinetochores. Here, it phosphorylates the KNL1 complex to trigger the recruitment of Bub1/3 and MAD2 [445,459–466]. Once again, when kinetochore-microtubule end-on attachments are formed, MPS1 is not able to interact anymore with the kinetochore [464].

Aurora B ensures proper SAC function by regulating kinetochore-microtubule attachment. It promotes the correction of erroneous attachments (see above) and the recruitment of SAC proteins such as BubR1, MAD2, CENP-E, and Dynein at the kinetochore [467–470].

Once SAC is satisfied, APC/C is active and degrades cyclin B1 to ensure the exit of mitosis and Securin. The degradation of Securin activates the Separase, which cleaves the cohesins to allow sister chromatids separation and chromosome segregation [238]. The cohesins are further protected by SGO1 which is also a target of the APC/C complex. Sgo1 prevents chromosome segregation before reaching anaphase and blocks SAC satisfaction by recruiting the phosphatase PP2A to protect cohesin from degradation.

2 AIM of the thesis

DNA methylation pattern changes upon aging and in cancer. In cancer cells, promoters of tumour suppressor genes are often hypermethylated, whereas repetitive DNA is frequently hypomethylated. Different approaches in recent studies correlated DNA methylation loss with aneuploidy [471–473] which is a hallmark of cancer cells. However, the mechanisms that connect DNA methylation and aneuploidy are not fully understood yet. By using the Auxin Inducible Degron (AID) system approach to remove DNMT1 and achieve a global DNA methylation loss, I focused on the following goals:

- evaluate the effect of DNMT1 absence in normal Retinal Pigment Epithelial hTert immortalized (RPE-1) cells, distinguishing between the effect of the enzyme absence *per se* and of the loss of DNA methylation. the results of this part of the thesis have already been published, and I will attach here the published version of the article (I performed the majority of the experiments, and I participated in the writing of the draft). RPE-1 cells have been used only for cell cycle analysis because this cell line is not suitable for the second goal of the thesis.
- study the chromosome segregation event in colon-rectum DLD-1 cancer cells upon DNA methylation loss and understand the molecular mechanism behind the acquisition of aneuploidy during DNA hypomethylation.

3 Materials and methods

3.1 Cell culture

Normal Retinal Pigment Epithelial hTert immortalized (RPE-1) cells were previously engineered to express the F-box protein TIR1 and the endogenous DNMT1 tagged at the N-terminus with Auxin Inducible Degron (AID) and mNeon Green (^{NA}DNMT1) [472]. RPE-1 culture media, and RPE-1-related experiments are discussed in the paper that is attached to the thesis.

The attached paper discusses the results I achieved analysing RPE-1 during my thesis; instead, the following part of the thesis will focus on the analysis of cancer cell line DLD-1

Colon-rectum cancer cell line DLD-1 was previously engineered to express the F-box protein TIR1 and the endogenous DNMT1 tagged at the N-terminus with AID and mNeon Green (^{NA}DNMT1) [472]. DLD-1 ^{NA}DNMT1 cells were cultured in Dulbecco's modified Eagle's medium (DMEM; Corning/Gibco) supplemented with 10% bovine fetal serum, 1% L-Glutamine and occasionally Penicillin and Streptomycin mix. Cells were grown at 37 °C in a humidified atmosphere with 5% CO.

Used drugs: Water-soluble auxin (indole-3-acetic acid sodium salt (IAA) (I5148; Sigma-Aldric)) was used at 500 µM. This low concentration of IAA has already been documented not to affect RPE-1 cell growth [474,475]. For the IAA washout, DLD-1 ^{NA}DNMT1 cells were washed twice with 1x PBS and incubated for 5 min with cell media. After the incubation, the cells were washed again twice with 1x PBS and left in warm fresh cell media.

Depending on the experiments, different mitotic drugs were also used. *S*-Trityl-L-cysteine (STLC) at a concentration of 20 µM for 12h; MG132 at the concentration of 10 µM for up to 3h; Colcemid at the concentration 0,2 µg/ml for 3h; Nocadozole at the concentration of 10 µM for 3h. The STLC release was achieved by washing with warm media 3 times with 5 minutes incubation with media. This wash step was repeated up to 4 times.

3.2 Cell growth measurement

DLD-1 ^{NA}DNMT1 cells were seeded in 12-well plates and treated with IAA for up to 10 days. At the indicated time points, the cells were detached by trypsinization, stained with Trypan Blue solution at a 1:1 ratio, and counted with a Burker chamber. The experiment was performed in triplicate for each condition.

3.3 Colony Assay

DLD-1 ^{NA}DNMT1 cells were seeded in 100 mm dishes treated with IAA for up to 7 days. On the 7th days, the cells were trypsinised and seeded at low confluency (500, 1000 or 2000 cells per well) in a 6-well multiwell and treated for additional 14 days. The cells were then washed with 1x PBS, fixed with cold methanol for 5 min, and stained with Crystal Violet solution for 1 min. Finally, the cells were washed with 1x PBS until the colonies were visible. The experiment was performed in triplicate for each condition.

3.4 Immunoblot

DLD-1 ^{NA}DNMT1 cells were grown in 100 mm dishes and split before reaching the 80/90% confluency. On the established day, the cells were collected by trypsinization, washed with PBS, and lysed in 1X Laemmli buffer (0.05 M Tris-HCl pH 6.8, 2% SDS, 10% glycerol, 0.01% bromophenol blue, 50 mM β-mercapto-ethanol).

The samples were loaded in a 6%, 10% polyacrylamide gel or in a 4 to 15% precast gel. The gels were blotted on a PVDF membrane overnight at 30V or for 1h at 100V. After 30 min of Blocking with 5% milk in PBS with 0.1% Tween-20, the membranes were incubated with the following antibodies diluted in the blocking solution overnight at 4°C or for 1h at room temperature: DNMT1 (1:100, SantaCruz H-12: sc-271729), p21waf1/cip1 (1:200; SantaCruz F-5: sc-6246), p53 (1:200; SantaCruz DO-1: sc-126), Vinculin (1:1000; Gene Tex: GTX109749-S), Actin (1:2000; Invitrogen: 5047778), GAPDH (1:5000; Proteintech: 80570-1-RR), β-Tubulin (1.200; Sigma) CENP-A (1:1000; Enzo; #Adi-kam-cc006-E), CENP-E (1:100; SantaCruz; sc-376685), Hec1 (1:500; SantaCruz; sc-515550), phospho S55-Hec1 (1:1000; Genetex; Gxgtx640829-s), MAD2 (1:500; SantaCruz; sc-47747), Aurora B (1:1000; BD bioscience; #611082), Sgo1 (1:200; SantaCruz; sc-393993), P150Glued (1:1000; BD bioscience; #610473). Upon primary antibody incubation, the membranes were washed with PBS with 0.1% Tween-20 and incubated with HRP-conjugated secondary antibody either anti-mouse or anti-rabbit (Invitrogen and Promega) diluted in 5% milk in PBS with 0.1% Tween-20 for 1h. After the incubation, the membranes were washed again and incubated with 1:1 Luminol-Enhancer solution (Femto, Invitrogen or ECL, Biorad), and the chemiluminescence signal was then visualized at the Bio-Rad ChemiDoc™ Imager. When the proteins shared the same molecular weight (Hec1 and Hec1 S55p) the membrane was incubated first with the antibody anti-phospho S55-Hec1 produced

in rabbit. After the image acquisition, the membrane was stripped with a Restore western blot stripping buffer (Pierce) and reblocked with 5% milk in PBS with 0.1% Tween-20. After blocking, the membrane was incubated with the antibody anti-Hec1 produced in mouse. The images were quantified with IMAGEJ. The experiment was performed at least in triplicate for each condition.

3.5 RTqPCR

RNA was extracted with TRIzol Reagent (Thermo Fisher Scientific) following the manufacturer's instructions.

Purified RNA was then quantified using Nanodrop™ and loaded on 1% agarose gel to verify its integrity. For each sample, 1 µg of RNA was reverse-transcribed using the High-Capacity cDNA Reverse Transcription Kit (Thermo Fisher Scientific, Milan, Italy) with the following conditions, according to the manufacturer's instructions:

	Step 1	**Step 2**	**Step 3**	**Step 4**
Temperature (°C)	25	37	85	4
Time	10 min	120 min	5 min	∞

RT-qPCR was performed using Applied Biosystems 7300 Real-Time PCR System. Each sample was amplified in triplicate (50 ng of cDNA/sample) in a final volume of 15 µL 1X Master Mix SyBR Green (Thermo Fisher Scientific, Milan, Italy) supplemented with 150 nM primer mix and with the following thermal cycle: 95 °C for 15 s, 60 °C for 60 s repeated for 40 cycles. Relative gene expression was quantified by comparing the $2^{-\Delta\Delta Ct}$ of each analyzed gene to that of the *GAPDH* gene used as the internal control. The experiment was performed in triplicate for each condition. The used primers are indicated in the following table:

p21waf1/cip1 Forward primer	5′-CTGGAGACTCTCAGGGTCGA-3′
p21waf1/cip1 Reverse primer	5′-CGGATTAGGGCTTCCTCTTG-3′
CENP-E Forward primer	5′-GTGGGACCAGTTCAGCCTGATA-3′
CENP-E Reverse primer	5′-CCAAGTGATTCTTCTCTGCTGTTC-3′

CENP-A Forward primer	5′-GATTCTGCGATGCTGTCTGG-3′
CENP-A Reverse primer	5′-CAGGCCTTTGGAACGTGTT-3′
GAPDH Forward primer	5′-CTCATGACCACAGTCCATGCC-3′
GAPDH Reverse primer	5′-CAATCCACAGTCTTCTGGGT-3′

3.6 Cytogenetic analysis and Mitotic index evaluation

DLD-1 ^{NA}DNMT1 cells were harvested and collected with PBS. Cell pellets were then resuspended drop by drop at vortex with pre-warmed 75 mM KCl hypotonic solution and incubated at 37 °C for up to 20 min. After the incubation, cell pellets were fixed at least 3 times with cold Carnoy fixative (3:1, Methanol: Glacial Acetic Acid). The samples were dropped onto cold glass slides and left to air dry overnight. Once dried, the slides were stained with 3% Giemsa Gurr staining solution and then observed at an upright microscope with transmitted light. The ploidy of DLD-1 ^{NA}DNMT1 cells was evaluated using a 63x magnification.

To evaluate the mitotic index of DLD-1 ^{NA}DNMT1 cells, the cells were seeded onto coverslips inside a 6-well multiwell, washed with 1x PBS and fixed with 4% PFA. After one wash with 1x PBS, the coverslips were mounted with a DAPI-provided mountant (IBIDI) onto a glass slide. The cells were then observed with a Zeiss Axioskop microscope with fluorescent light with 20x magnification.

3.7 Immunofluorescence (IF) assays

3.7.1 IF for 5-Methylcytosine

DLD-1 ^{NA}DNMT1 cells were grown onto coverslips, then washed with 0.1% Tween-20 in PBS and fixed with 4% formaldehyde in PBS for 10 min in the dark.

For the staining on the chromosomes, DLD-1 ^{NA}DNMT1 cultured cells were incubated prior to fixation with colcemid for 3h at the concentration 0,2 μg/ml; then, the cells were washed and incubated with a hypotonic solution (0.25x PBS) for 20 min. The hypotonic solution was removed without completely drying the well and the cells were centrifuged at 1500 RPM for 3 min. After centrifugation, the cells were gently washed with cold 1x PBS on ice and fixed with cold 4%

formaldehyde in PBS for 10 min in the dark. After fixation, the cells were permeabilized with 0.5% Triton X-100 diluted in PBS for 30 min and then treated with 2 M HCL for 30 min at room temperature. After washing with 0.1% Tween-20 in PBS and blocking for 1 h with 2% BSA in 1% Tween-20 in PBS, cells were incubated with the primary antibody anti-5-Methylcytosine (5mC) (1:500; Epigentek, Farmingdale, NY, USA, clone 33D3; A-1014) in 0.1% Tween-20 in PBS overnight at 4 °C. The cells were then washed and incubated with antibody anti-mouse Cy3-conjugated (1:500) diluted in 0.1% Tween-20 in PBS for 1 h at 37 °C. After washing 3 times and counterstaining with DAPI for 3 min, the slides were mounted with ProLong™ Gold Antifade Mountant and observed with Zeiss Axioskop microscope.

3.7.2 IF for nuclear and chromosome proteins

DLD-1 ^{NA}DNMT1 cells were treated for different time points with IAA to induce DNMT1 degradation and DNA hypomethylation. The day before the analysis, the cells were washed, trypsinized, and seeded onto coverslips in a 12 multiwell plate. Depending on the analysis, two different protocols were used to reduce the aspecific signal and optimize primary antibody binding:

- For the CENP-A and CENP-C proteins, the cells were washed with 1x PBS and treated with a Triton block solution (0,2 M Glycin, 2,5% FBS, 0,1% Triton-X diluted in PBS 1x) for 1 min. After incubation, the cells were fixed with 4% PFA in PBS for 10 min in the dark. The cells were washed 3 times with 1x PBS 0,5% Triton-X and incubated with 1% BSA (Sigma) in PBS for at least 30 min. Then, the cells were incubated overnight at 4ºC with primary antibody anti-CENP-A (1:1000; Enzo; #Adi-kam-cc006-E), -CENP-C (1:750; Sigma, HPA058252) in 1% BSA in PBS. The next day, the cells were washed 3 times with 1x PBS 0,5% Triton-X and incubated with secondary antibodies anti-mouse Cy3-conjugated (1:1000) and anti-rabbit Alexa647-conjugated (1:1000) diluted in 1% BSA in PBS for 50 min at room temperature and in the dark. After 3 washes with 1x PBS 0,5% Triton-X, cells were counterstained with DAPI for 3 min. After 3 washes with PBS 0,5% Triton-X, the cells were finally mounted with a ProLong™ Gold Antifade Mountant. The images were observed with Zeiss Axioskop microscope.

- For Astrin and Hec1, the seeded cells were washed with 1x PBS and fixed with cold methanol for 60 seconds and then washed 3 times with 1x PBS and incubated with 1% BSA (GE Healthcare code K41-001) in PBS for at least 30 minutes. Then, cells were incubated overnight

at 4ºC with primary antibody anti-Astrin (1:500; Novus; NBP-185262), -Hec1 (1:500; SantaCruz; sc-515550), and Crest Sera (1:1000 Human) diluted in 1% BSA in PBS. The next day, after 4 washes with PBS, cells were incubated with antibodies anti-mouse Dylight488-conjugated (1:1000), anti-rabbit Alexa590-conjugated (1:1000) and anti-human Alexa647-conjugated (1:1000) secondary antibody diluted in 1% BSA in PBS for 1.45h at room temperature and in the dark. The cells were counterstained with DAPI, washed 4 times with 1x PBS and 1 time with distilled H2O. Finally, the cells were mounted with Vectashield (Vector H-1000). The images were acquired with DeltaVision Elite microscope. The quantification was performed on a Max Projection of the raw data image. The representative images are deconvolved through the program provided by DV Elite.

- To optimize the signal of CENP-A together with CENP-T, a dedicated protocol was created. The coverslip with seeded cells was treated with STLC overnight, released, and treated with MG132 for 2.50h. The coverslips were washed with 1x PBS and fixed with 4% PFA in PBS for 10 minutes in the dark. After 3 washes with 1x PBS (5 minutes incubation each), the cells were permeabilised with PBS 0.1% Triton-X for 5 minutes. After 3 washes, the cells were incubated with blocking solution 3% BSA (GE Healthcare code K41-001) in PBS for 3h. Then, the cells were incubated overnight at 4ºC with primary antibodies anti-CENP-A (1:750; MBL; D115-3) and -CENP-T (1:500; Abcam; ab220280). The next day, the cells were washed 3 times and incubated with DAPI and antibodies anti-mouse Dylight488-conjugated (1:1000), anti-rabbit Alexa590-conjugated (1:1000) diluted in 3% BSA in PBS for 1.45h at room temperature in the dark. Then, the cells were washed 3 times with 1x PBS and once with distilled H2O, and mounted with Vectashield (Vector H-1000). The images were acquired with DeltaVision Elite microscope. The quantification was performed on a Max Projection of the raw data image. The representative images are deconvolved through the program provided by DV Elite.

- For the staining of Hec1 S55p together with Aurora B kinase on metaphase chromosomes, the cells cultured onto coverslips were washed with 1x PBS and fixed with 4% PFA in PBS for 10 min. After fixation, the cells were washed 2 times with 1x PBS and permeabilised with 0,05% Triton X-100 in PBS for 10 min. After permeabilisation, the cells were blocked in 1% BSA (Sigma) in PBS for 30 min. Then, the cells were incubated overnight at 4ºC with primary antibodies anti-phospho S55-Hec1 (1:1000; Genetex; Gxgtx640829-s) and anti-Aurora B (1:1000; BD bioscience; #611082) diluted in 1% BSA in PBS. The next day, the cells were washed 4 times with 1x PBS and incubated with secondary antibodies anti-mouse Cy5-

conjugated (1:1000) and anti-rabbit Cy3-conjugated (1:1000) diluted in 1% BSA in PBS for 50 min at room temperature in the dark. The cells were washed 4 times with 1x PBS and mounted with DAPI-provided mounting media (IBIDI). The images were observed with Zeiss Axioskop microscope.

- For target protein staining on the chromosomes in cytospin, DLD-1 ^{NA}DNMT1 cells were incubated either with nocodazole or with colcemid for 3h and fixed after cytospinning as described for 5-methylcytosine staining. After fixation, the cells were washed with 1x PBS with 0,1% Triton-X or (3 times with 1x PBS for MAD1 staining) and blocked with Triton block solution for 30 min (3% BSA (GE Healthcare K41-001) in PBS for 3h in the case of MAD1 staining). For MAD1 staining, cells were also first permeabilised with 5 min incubation with PBS 0.1% Triton-X, then washed 3 times with 1x PBS and incubated for 5 min with each wash. The cells were then incubated overnight at 4ºC with primary antibodies anti-CENP-A (1:1000; Enzo; #Adi-kam-cc006-E), -Aurora B (1:1000; BD bioscience; #611082) and -INCENP (1:1000, Sigma; HPA070550-25), or -MAD1 (1:500; Genetex; GTX105079) and -Hec1 (1:500; SantaCruz; sc-515550). After the incubation, the cells were washed 3 times with 0,1% Triton-X (4 times with PBS in the case of MAD1 staining with 5 min incubation for each wash) and incubated with the secondary antibodies anti-rabbit Cy2-conjugated (1:1000), anti-mouse or anti-rabbit Cy3-conjugated (1:1000), and anti-mouse Cy5-conjugated (1:1000) diluted in Triton block for 50 min at room temperature and in the dark. For MAD1/Hec1 staining cells, instead, were incubated with antibodies anti-mouse Dylight488 (1:1000) and anti-rabbit Alexa590 (1:1000) diluted in 3% BSA in PBS for 1.45h at room temperature and in the dark. DAPI was used to counterstain the DNA. After 3-4 washes, coverlips were mounted with ProLong™ Gold Antifade Mountant or Vectashield. The images were acquired with DeltaVision Elite microscope. The quantification was performed on a Max Projection of the raw data image. The representative images are deconvolved through the program provided by DV Elite.

3.7.3 Cold treatment assay

DLD-1 ^{NA}DNMT1 cells were treated for 4 and 7 days with IAA to induce DNMT1 degradation and DNA hypomethylation. The day before the analysis, the cells were washed, trypsinized, and seeded on coverslips in a 12-multiwell dish. The next day, the cells were put inside an isolated tank-box provided with ice and cold water. As such, the cells were incubated on ice in cold water

for 15 minutes. After incubation, the cells were washed with 1x PBS and fixed with cold methanol. After 3 washes with 1x PBS and incubation with 1% BSA (GE Healthcare code K41-001) for at least 30 min, the cells were left overnight and at 4ºC with the primary antibodies anti-Tubulin (1:1000; Abcam; ab6160) and -Hec1 (1:500; SantaCruz; sc-515550). The next day, the cells incubated, after 4 washes, with DAPI and secondary antibodies anti-rat Dylight488 (1:1000) and anti-mouse Alexa590 (1:1000) diluted in 1% BSA in PBS for 1.45h at room temperature in the dark. After 4 washes in PBS and one with distilled H20, the coverslips were mounted with Vectashield (Vector H-1000). The images were acquired with DeltaVision Elite microscope. The quantification was performed on a Max Projection of the raw data image. The representative images are deconvolved through the program provided by DV Elite.

For the experiments at 10 days of IAA, a different protocol was used. The seeded cells were incubated on ice for 15 min. After the incubation, the cells were treated for 30 sec with a microtubule buffer (100nm PIPES, pH 6.9 with KOH, 0,1 mM $CaCl_2$, 1mM $MgCl_2$, and 0,1% Triton X-100). After the incubation, the cells were fixed for 15 minutes with 4% PFA diluted in the microtubule buffer. After 3 washes with 0,1% Triton X-100 in PBS and incubation with 0,5% BSA (Sigma) diluted in PBS 0,1% Triton X-100 for 1h at room temperature, the cells were left with primary antibody anti-β-Tubulin overnight at 4°C. After 3 washes with 0,1% Triton X-100 in PBS the cells were incubated with secondary antibody anti-mouse Cy3-conjugated diluted in 0,5% BSA in PBS 0,1% Triton X-100 for 30 min at room temperature and in the dark. The cells were washed 3 times with 0,1% Triton X-100 in PBS and stained with DAPI for 3 min. After the staining, the coverslips were washed 3 times with 0,1% Triton X-100 in PBS and mounted with ProLong™ Gold Antifade Mountant. The images were observed with Zeiss Axioskop microscope.

3.8 Statistical analysis

For all the performed sets of experiments, I applied statistical analyses by using Prism software (GraphPad). As indicated in the figure legends, the statistical significance of comparisons between two samples or experimental conditions was assessed by the two-tailed unpaired Student's t-test. We generally assumed a standard normal distribution, but this was not formally tested. I considered it significant if the calculated P value was ≤ 0.05. P values were indicated as follows: *$P \leq 0.05$; **$P < 0.01$; ***$P < 0.001$; ****$P < 0.0001$; ns = not significant.

Cellular and Molecular Life Sciences (2025) 82:7
https://doi.org/10.1007/s00018-024-05547-y

ORIGINAL ARTICLE

DNMT1 prolonged absence is a tunable cellular stress that triggers cell proliferation arrest to protect from major DNA methylation loss

Salvatore Martino[1] · Serena Gargano[1] · Pietro Salvatore Carollo[1] · Aldo Di Leonardo[1,2] · Viviana Barra[1]

Received: 23 July 2024 / Revised: 16 November 2024 / Accepted: 11 December 2024

Abstract

Methylation of cytosine in CpG dinucleotides is an epigenetic modification carried out by DNA-methyltransferases (DNMTs) that contributes to chromatin condensation and structure and, thus, to gene transcription regulation and chromosome stability. DNMT1 maintains the DNA methylation pattern of the genome at each cell cycle by copying it to the newly synthesized DNA strand during the S-phase. DNMT1 pharmacological inhibition as well as genetic knockout and knockdown, leads to passive DNA methylation loss. However, these strategies have been associated with different cell fates, even in the same cell background, suggesting that they can question the interpretation of the obtained results. Using a cell system in which endogenous DNMT1 is fused with an inducible degron and can be rapidly degraded, we found that in non-tumoral RPE-1 cells, DNMT1 loss progressively induced cell proliferation slowing-down and cell cycle arrest at the G1/S transition. The latter is due to p21 activation, which is partly mediated by p53 and leads to a global reduction in DNA methylation. DNMT1 restoration rescues cell proliferation, indicating that its deregulation is sensed as tunable cellular stress.

Keywords Epigenetics · Auxin-Inducible Degron · Genome stability · Cell cycle arrest · γH2AX

Abbreviations

DNMT1	DNA methyltransferase 1
DAC	2′-Deoxy-5-azacytidine
AZA	5-Azacytidine
AID	Auxin Inducible Degron
^{NA}DNMT1	mNeonGreen-AID-DNMT1
IAA	Indole Acetic Acid
EdU	5-Ethynyl-2′-deoxyuridine
5MeC	5-Methylcytosine
p21	p21waf1/cip1

Introduction

DNA methylation is an epigenetic mechanism that occurs mainly at CpG dinucleotides, which cells use to condense the chromatin. As such, it is involved in many cellular processes, including gene transcription regulation, embryonic development, X chromosome inactivation, gene imprinting, chromosome stability, and chromatin structure [1–8]. DNA methyltransferase 1 (DNMT1) is a DNA methyltransferase of maintenance since it preserves DNA methylation patterns by associating with replication foci and methylating hemimethylated DNA generated during each phase of DNA replication.

To investigate the critical role of DNMT1 further, various experimental approaches have been employed to impair its function, revealing its importance in genome stability. As observed by our laboratory and other groups, disabling DNMT1 function via treatments with 2'-deoxy-5-azacytidine (DAC) or 5-azacytidine (AZA), genetic knockout, or knockdown by RNA interference induces passive DNA demethylation after multiple cell cycles, DNA double-strand breaks, mitotic errors, and aneuploidy in both humans and mice [4, 9–13]. These results support the importance of DNMT1 in maintaining genome stability. Importantly, DNMT1 impairment usually leads to a reduction in cell proliferation, often culminating in cell cycle arrest and apoptosis, both in vivo and in vitro [10, 12, 14–16]. This is in agreement with DNMT1 being an essential gene [17–19]. However, cell behaviour and fate differ depending on the cell type and the strategy used to inhibit DNMT1. Clarifying the effects of

✉ Viviana Barra
viviana.barra@unipa.it

[1] Department of Biological, Chemical and Pharmaceutical Sciences and Technologies (STEBICEF), University of Palermo, 90128 Palermo, Italy

[2] Centro Di Oncobiologia Sperimentale (C.O.B.S.), Viale Delle Scienze, 90128 Palermo, Italy

Published online: 18 December 2024

DNMT1 depletion per se in normal human cells can provide important details on the functioning of DNMT1, elucidating whether and why DNMT1 is essential in differentiated cells. This could also have implications in cancer therapy, as DNMT1 inhibitors are used for the treatment of myelodysplastic syndrome (MDS) and hematological tumors, and the development of new ones is ongoing [20].

DAC and AZA have been widely used to inhibit DNMT1, as they are incorporated in the DNA to replace the cytosine and sequester DNMT1 by forming covalent bonds with it. Both drugs are able to induce DNA hypomethylation but they lead to different outcomes. Indeed, DAC induced G2-phase arrest in HeLa and HCT116 cell lines [21] while in A549 and T24 cells it led to G1-phase arrest and in KG1a cells to a subG1 arrest and an accumulation of cells in G2/M phase [11, 22, 23]. DAC was also able to induce G2-phase arrest with subsequent cell death and accumulation in the G2/M phase in MDS-L and MPM cell lines respectively [24, 25]. Surprisingly, AZA did not influence the cell cycle of the MDS-L cell line [25]: instead, it had an effect similar to that of DAC in KG1a cells causing accumulation of cells in the subG1-phase and apoptosis [11].

Chen et al. generated the DNMT1 conditional allele in HCT116 cells to evaluate the impact of DNMT1 inactivation. HCT116 cells, upon DNMT1 disruption, underwent G2-phase arrest that eventually resulted in a mitotic catastrophe [26], On the contrary, genetic knockout through homologous recombination in the same cell line did not affect cell growth as reported by Rhee and colleagues [27].

Similarly, exploring DNMT1's role in cell cycle progression through alternative methods, our laboratory observed by RNA interference that DNMT1 post-transcriptional silencing induced a G1-phase arrest in normal human fibroblasts IMR90 [12]. The silencing of DNMT1 in HCT116 cells, in contrast to the usage of DAC observed by Palii and colleagues, induced accumulation in the S-phase. DNMT1 silencing by a short hairpin in MPM cells only slightly increased the number of cells in the S-phase [24]. Finally, it was observed a proliferation arrest with increased cells in the S-phase in hepatocellular carcinoma upon DNMT1 post-transcriptional silencing [28]. Antisense oligonucleotides targeting DNMT1, instead, caused an intra-S-phase arrest in A549 cells [29], while they induced a severe reduction in the number of BrdU-positive cells in zebrafish posterior lateral line neuromasts [15].

Noncoding RNA can also directly regulate DNMT1 expression when overexpressed. DNMT1 targeting by mir342 has been demonstrated to induce a G1-phase arrest in SW480 cells [30].

The different effects observed upon DNMT1 impairment are probably the result of different genetic backgrounds (most of the cell lines used were tumoral) but also of the method used to disable DNMT1. Genetic disruption of DNMT1 might be too harsh, considering that DNMT1 is an essential gene, leaving the possibility for the cells to adapt depending on their genetic background. Post-transcriptional silencing on the other hand may be insufficient to efficiently deplete DNMT1 [12]. Also, the use of AZA or DAC, which are base analogs, is closely associated with side effects such as DNA damage [16, 31]. Thus, it is difficult to distinguish between the direct effect of the absence of DNMT1 protein/activity and secondary/side effects. To overcome this issue, we decided to use the non-tumoral cell line RPE-1 engineered to express the endogenous DNMT1 tagged with an Auxin-Inducible Degron (AID) [32]. The AID allows the rapid and complete degradation of DNMT1 (in approximately one hour) in the presence of auxin. Using this approach, we evaluated cell proliferation and activation of a cell cycle checkpoint. Altogether, our results demonstrate that DNMT1 is important for cell fitness, as its rapid degradation gradually leads to p53- and p21waf1/cip1-dependent cell cycle arrest at the G1/S transition in normal human cells. While the consequent passive DNA methylation loss has occurred, the restoration of DNMT1 can promote the reinitiation of cell proliferation.

Materials and methods

Cell culture

Retinal Pigment Epithelial cells (RPE-1), h-TERT immortalized, were previously engineered to express the F-box protein TIR1 and the endogenous DNMT1 tagged at N-terminus with AID (Auxin inducible degron) and mNeon Green (^{NA}DNMT1) [32]. Cells were cultured in Dulbecco's modified Eagle's medium (DMEM; Corning) supplemented with 10% bovine fetal serum and 1% L-Glutamine. Water soluble auxin indole-3-acetic acid sodium salt (IAA) (I5148; Sigma-Aldric) was used at 500 µM. This low concentration of IAA has been already documented not to affect RPE-1 cell growth [33, 34]. Cells were grown at 37 °C in a humidified atmosphere with 5% CO_2. For the IAA washout, RPE-1 ^{NA}DNMT1 cells were washed twice with 1X PBS and once with cell media.

Cell transfection

Cells were treated for 1 or 3 days with IAA to induce DNMT1 degradation and transfected as previously done [35]. The day before the transfection the cells were seeded in a 12-well plate. On the day of the transfection, specific siRNAs duplex (see the table below) were mixed with Lipofectamine 3000 Reagent (Invitrogen, Life Technologies) in Optimem media (Gibco), according to the manufacturer's recommendation, and added to the cells. At least after 5 h of incubation with

the siRNA mixture, the culture media was changed, and IAA was replaced every 2–3 days till day 4 or 6.

Target gene	siRNA sequence	References
p53	5′-GCA UGA ACC GGA GGC CCC AUtt-3′	[12]
Luc (control)	5′-CGTACGCGGAATACT TCGA-3′	[36]

Cell growth curves

Cells were seeded in 12 well plates and treated or not (control cells) with IAA for up to 7 days. At the indicated timepoints the cells were detached by trypsinization and counted with a Burker chamber. The experiment was performed in triplicate for each condition.

Immunoblot

Cells were collected by trypsinization, washed with PBS, and lysed in 1X Laemmli buffer (0.05 M Tris–HCl pH 6.8, 2% SDS, 10% glycerol, 0.01% bromophenol blue, 50 mM β-mercapto-ethanol) as previously performed [37]. The samples were loaded in a 10% polyacrylamide gel and blotted in a PVDF membrane. After 30 min of Blocking, the membranes were incubated with the following antibodies: DNMT1 (1:100, SantaCruz H-12: sc-271729), p21 (1:200; SantaCruz F-5: sc-6246), p53 (1:200; SantaCruz DO-1: sc-126) [38], phospho S15-p53 (1:1000; Abcam: ab1431), γH2Ax (1:500; Merck: 05-636), Vinculin (1:1000; Gene Tex: GTX109749-S), Actin (1:2000; Invitrogen: 5047778), GAPDH (1:5000; Proteintech: 80570-1-RR). The chemiluminescence signal was then visualized at the Bio-Rad ChemiDoc™ Imager and quantified with IMAGEJ. The experiment was performed in triplicate for each condition.

RTqPCR

RNA was extracted with TRIzol Reagent (Thermo Fisher Scientific) following the manufacturer's instructions.

Purified RNA was then quantified using Nanodrop™ and loaded on 1% agarose gel to verify its integrity. For each sample, 1 µg of RNA was reverse-transcribed using the High-Capacity cDNA Reverse Transcription Kit (Thermo Fisher Scientific, Milan, Italy) with the following conditions, according to the manufacturer's instructions:

	Step 1	Step 2	Step 3	Step 4
Temperature (°C)	25	37	85	4
Time	10 min	120 min	5 min	∞

RT-qPCR was performed using Applied Biosystems 7300 Real-Time PCR System as previously described [39]. Briefly, each sample was amplified in triplicate (50 ng of cDNA/sample) in a final volume of 15 µL 1X Master Mix SyBR Green (Thermo Fisher Scientific, Milan, Italy) supplemented with 150 nM primer mix and with the following thermal cycle: 95 °C for 15 s, 60 °C for 60 s repeated for 40 cycles. Relative gene expression was quantified by comparing the $2^{-\Delta\Delta Ct}$ of each analyzed gene to that of the *GAPDH* gene used as the internal control. The experiment was performed in triplicate for each condition. The used primers are indicated in the following table:

$p21^{waf1/cip1}$ Forward primer	5′-CTGGAGACTCTCAGGGTC GA-3′
$p21^{waf1/cip1}$ Reverse primer	5′-CGGATTAGGGCTTCCTCT TG-3′
GAPDH Forward primer	5′-CTCATGACCACAGTCCAT GCC-3′
GAPDH Reverse primer	5′-CAATCCACAGTCTTCTGG GT-3′
p14ARF Forward primer	5′-TGATGCTACTGAGGAGCC AGC-3′
p14ARF Reverse primer	5′-AGGGCCTTTCCTACCTGG CTC-3′

Cell cycle analysis by flow cytometry

Cell cycle analysis was conducted as previously done [40]. Briefly, after the indicated treatment asynchronously growing cells were collected in PBS, then fixed in 70% ice-cold ethanol and incubated at 4 °C at least overnight. On the day of the analysis, cell pellet was resuspended in Propidium Iodide/RNase staining buffer in the dark (20 µg/mL PI and 40 µg/mL RNase) and incubated for at least 30 min. The samples were acquired on FACSAriaIII by AteN Center, University of Palermo. Experiments were repeated twice and at least 10,000 events were analysed for each sample. Flow cytometry data were then analyzed with FCS Express 7 (De Novo Software).

Click-iT EdU imaging

S phase evaluation was performed using the Click-iT Plus EdU Alexa Fluor 555 Imaging Kit (Invitrogen, C10638) following the manufacturer's instructions. Cells were seeded on round glass coverslips in a 12-well plate and treated (or not) with the hormone IAA. On the day of the analysis, cells were incubated with EdU (10 µM). After 2 h of incubation, cells were fixed with 3.7% formaldehyde in 1X PBS for 15 min at room temperature and permeabilized with 0.5% Triton X-100 in 1X PBS for 20 min at room temperature. All the washing steps were performed with 3% BSA in 1X PBS. A

click reaction was catalyzed to label and detect the EdU: cells were incubated with the Click-iT Plus reaction cocktail for 30 min at room temperature, protected from light. Nuclei were counterstained with Hoechst 33342 (5 µg/mL). The slides were mounted with ProLong™ Gold Antifade Mountant (Thermo Fisher Scientific) and cells were imaged using a 10× and a 63× objectives in a Zeiss Axioskop microscope.

Mitotic index evaluation

Cells were harvested and collected with PBS. Cell pellets were then resuspended drop by drop at vortex with pre-warmed 75 mM KCl hypotonic solution and incubated at 37 °C for up to 20 min. After the incubation, cell pellets were fixed at least 3 times with cold Carnoy fixative (3:1, Methanol: Glacial Acid Acetic). The samples were dropped onto cold glass slides and left to air dry overnight. Once dried, the slides were stained with 3% Giemsa Gurr staining solution and then observed at an up-right microscope with transmitted light with 20× magnification. At least 10 images were taken for each condition to evaluate the mitotic index (number of mitoses/total number of cells). The experiment was performed as three independent replicates.

Immunofluorescence assays

MPM2

MPM2 staining was performed as previously [41]. Cells were seeded onto glass slides. On the day of the analysis, the cells were washed with 1X PBS and fixed on ice with cold methanol for 5 min. The methanol was then discarded, and the cells were washed 3 times with 1X PBS. The cells were then blocked for 1 h with 1% BSA diluted in PBS and then incubated overnight at 4 °C with antibodies anti-MPM2. (1:100; Merck, Milan, Italy, 05-368). The next day, the cells were washed with PBS, and then incubated for 1.5 h at 37 °C with the secondary antibody 1:1000 anti-mouse Cy3-conjugated (Jackson ImmunoResearch; 715-225-150) in 1X PBS. Nuclei were then counterstained with DAPI for 3 min, the slides were mounted with ProLong™ Gold Antifade Mountant, and cells were imaged with a Zeiss Axioskop microscope.

5-Methylcytosine

Cells were grown onto coverslips, then washed with 0.1% Tween-20 in PBS and fixed with 4% formaldehyde in PBS for 10 min in the dark. Upon fixation, the cells were permeabilized with 0.5% Triton x-100 diluted in PBS for 30 min and then, treated with 2 M HCL for 30 min at room temperature. After washing with 0.1% Tween-20 in PBS and blocking for 1 h with 2% BSA in 1% Tween-20 in PBS, cells were incubated with the primary antibody anti-5-Methylcytosine (5MeC) (1:500; Epigentek, Farmingdale, NY, USA, clone 33D3; A-1014) overnight at 4 °C. The cells were then washed and incubated with 1:500 anti-mouse Cy3-conjugated in 0.1% Tween-20 in PBS for 1 h at 37 °C. After washing 3 and counterstaining with DAPI for 3 min, the slides were mounted with ProLong™ Gold Antifade Mountant and observed with Zeiss Axioskop microscope.

Statistical analysis

For all the performed sets of experiments, we applied statistical analysis by using Prism software (GraphPad). As indicated in the Figure legends, the statistical significance of comparisons between two samples or experimental conditions was assessed by the two-tailed unpaired Student's t-test. For the proliferation curve in Fig. 1B, instead, we used a 2way ANOVA test. We generally assumed a standard normal distribution, but this was not formally tested. We considered it significant if the calculated P value was < 0.05. P values were indicated as follows: *$P < 0.05$; **$P < 0.01$; ***$P < 0.001$; ****$P < 0.0001$; ns = not significant.

Results

Prolonged DNMT1 absence induced proliferation defects and cell cycle arrest in the G1-S phase of the cell cycle in normal human cells

To study DNA hypomethylation effects on normal cells, we took advantage of the RPE-1 cell line (Retinal Pigment Epithelial cells) engineered to express endogenous DNMT1 tagged with both mNeonGreen and auxin-inducible degron AID (RPE-1 ^{NA}DNMT1) [32]. Upon the addition of auxin indole Acetic Acid (IAA), the system allowed DNMT1 degradation (Fig. 1A, Suppl. Fig. 1A, B). Nevertheless, by live microscopy observation, we found that approximately 0.8% of the cells did not respond to IAA (escapers) (data not shown), which could be responsible for the low residual level of DNMT1 in the immunoblot (Suppl. Fig. 1B).

We first assessed DNMT1's importance in cell proliferation and cell cycle over a timeframe of 7 days upon IAA treatment. RPE-1 ^{NA}DNMT1 cells underwent a progressive slowing-down in cell proliferation, which became significant over time (Fig. 1B). To ensure that the presence of escapers in the cell population did not alter our results, we analyzed the growth of one clone obtained from a single cell of the population (clone5). The clone5 treated with IAA showed a slowing down of cell proliferation as well as the entire population (Supp. Fig. 1C).

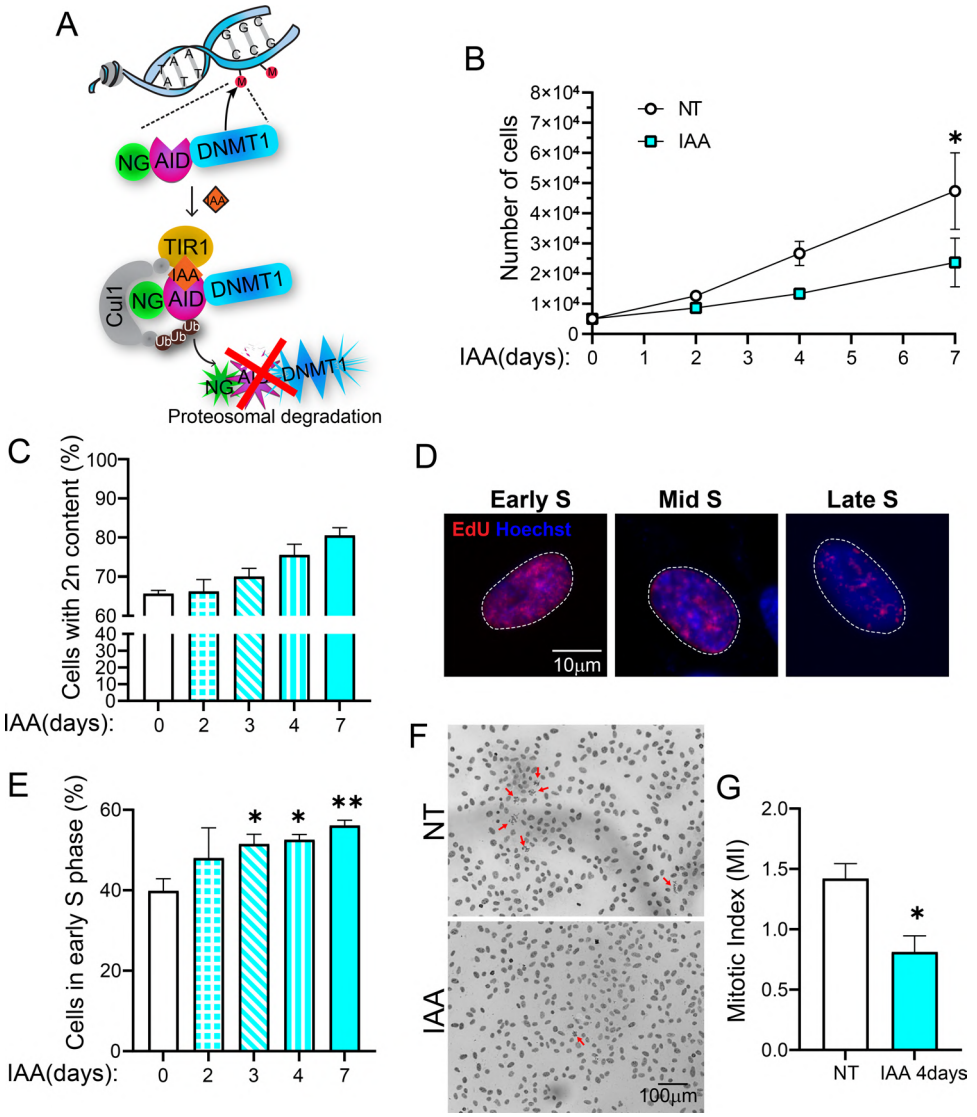

Fig. 1 Antiproliferative effect of DNMT1 degradation. **A** Schematics of ^{NA}DNMT1 degradation due to AID system, in the presence of IAA. **B** Cell growth curves showing the proliferation defects of IAA-treated RPE-1 ^{NA}DNMT1 cells in respect to the untreated ones. The graph shows the mean of 3 independent experiments. The error bars represent the standard error of the mean, SEM. 2way ANOVA between the samples: $*\leq 0.05$; ns > 0.05. **C** Histogram summarising flow cytometry analysis of Propidium Iodide-stained cells showing the increased percentage of IAA-treated RPE-1 ^{NA}DNMT1 cells with 2n DNA content. The graph shows the mean of 2 independent experiments. **D** Representative images of immunostaining for EdU (red) showing the differences between the S phase stages (early S, mid-S, late S). Nuclei were counterstained with Hoechst. **E** Quantification of RPE-1 ^{NA}DNMT1 cells (treated or not with IAA) positive for EdU showing the accumulation of cells in the early S phase starting from 3 days of treatment. The graph shows the mean of 3 independent experiments. At least 150 nuclei for each condition were evaluated. The error bars represent the standard error of the mean, SEM. Unpaired t-test between the samples: $**<0.01$; $*\leq 0.05$; ns > 0.05. **F** Representative images of mitotic spreads of untreated and IAA-treated RPE-1 ^{NA}DNMT1 cells. The nuclei and chromosomes were stained with Giemsa. Red arrows point to cells in mitosis. **G** Mitotic index quantification of untreated and 4-day IAA-treated RPE-1 ^{NA}DNMT1 cells. The graph shows the mean of 3 independent experiments; at least 150 nuclei were analyzed for each sample. The error bars represent the standard error of the mean, SEM. Unpaired t-test between the samples: $*\leq 0.05$; ns > 0.05

To assess whether the observed slow cell proliferation was due to cell cycle arrest, flow cytometry analysis with Propidium Iodide staining was performed. The histogram in Fig. 1C shows the progressive accumulation of cells with 2n DNA content starting from the third day of treatment. This result suggests possible cell cycle arrest in the G1 phase or at the G1/S transition. To quantify cells actively replicating DNA (S phase) EdU assay was performed on RPE-1 ^{NA}DNMT1 cells upon IAA treatment. As shown in Supp. Fig. 1D, the percentage of cells in the S phase did

not change in IAA-treated cells compared with that in the untreated control. However, we took advantage of the pattern of the incorporated EdU to identify cells in different stages of the S phase [42] (Fig. 1D). The graph in Fig. 1E reveals a significant increase in the percentage of cells in the early S phase, starting from the third day of treatment (Fig. 1E, Supp. Fig. 1E), which is consistent with the accumulation of cells with a 2n DNA content (Fig. 1C). To further confirm this, we synchronized the cells in the G1 phase (2n DNA content) by serum starvation for 48 h, and then released the cells in the presence or absence of IAA for an additional 4 and 6 days (Supp. Fig. 2A), and evaluated the cell cycle progression with flow cytometry (Supp. Fig. 2B). These results showed that once synchronized, RPE-1 ^{NA}DNMT1 cells had mainly a 2n DNA content (~ 80%) after release in IAA for 4 and 6 days (Release IAA 4d and 6d). In contrast, the cells released for 4 days in normal media (Release NT) re-entered the cell cycle with a profile similar to that of asynchronous cells (NT async).

Taken together, these results strongly suggest that RPE-1 ^{NA}DNMT1 cells arrest their proliferation at the G1/S transition when DNMT1 absence is prolonged.

To confirm the cell cycle arrest of RPE-1 ^{NA}DNMT1 cells, the mitotic index was also evaluated (Fig. 1F) which showed a significant reduction in the RPE-1 ^{NA}DNMT1 cell population in mitosis after 4 days of IAA treatment (Fig. 1G).

Cell cycle arrest induced by DNMT1 prolonged absence is due to p21 p53-dependent activation

It was previously observed that DNMT1 acute depletion induces activation of the p53-p21(waf1/cip1) pathway via p14ARF upregulation [12]. Similarly, we observed an increase in p21, both at the transcriptional and protein levels, in RPE-1 ^{NA}DNMT1 cells from the third day of treatment (Fig. 2A, B, D). Instead, while the total fraction of p53 protein did not change upon the treatment (Suppl. Fig. 1F), the fraction of activated p53 phosphorylated at S15 increased from the fourth day of IAA treatment (Fig. 2A and C). However, the p14ARF transcript level increased only on the 7th day of treatment (Suppl. Fig. 1G), suggesting that its activation and involvement in p53 and p21 triggering is not an early event following DNMT1 protein degradation.

To test the involvement of p53 in p21 upregulation, we knocked down p53 by RNA interference during IAA treatment (Fig. 2E). Following p53 reduction, the p21 protein increase in IAA-treated cells was reduced (from 2.2 of IAA siLuc to 1.5 of IAA sip53) (Fig. 2F–G and Suppl. Fig. 1H). However, the p21 protein level was not lowered down to that of the untreated condition, suggesting that either the residual p53 (Fig. 2F) keeps activating p21, or p53 could not be the only regulator of p21 activation in a DNMT1-depleted context. Nevertheless, MPM2 staining revealed that, while only 1.7% of RPE-1 ^{NA}DNMT1 control cells treated with IAA were in G2 phase/mitosis (G2/M) (in accordance with the mitotic index shown in Fig. 1G), 8.7% of the p53-depleted cells (sip53) were in G2/M when treated with IAA (Fig. 2H, I). Importantly, the percentage of IAA-treated RPE-1 ^{NA}DNMT1 sip53 cells in the G2/M was similar to that of the untreated control cells (Fig. 2I). These data indicated that p53 reduction was sufficient to rescue the proliferation arrest observed following DNMT1 prolonged degradation.

DNMT1 rescue restores normal levels of p21 and cell proliferation arrest

We then sought to evaluate whether or not cell proliferation defects were reversible. We, thus, washed out IAA and checked the effect of ^{NA}DNMT1 rescue after 24 h (Fig. 3A, B and Supp. Fig. 2C). We observed the reduction of p21 protein in the washout (WO) condition with respect to both IAA- and untreated samples suggesting that DNMT1 recovery even for only 24 h is sufficient to shut down p21 activation (Fig. 3C, D).

We, then, analyzed EdU staining and observed no significant difference in the percentage of cells in the S phase or early S after IAA washout with respect to the untreated cells, suggestive of no changes in the cell cycle progression (Fig. 3E and Supp. Fig. 2D). However, the reduction of the percentage of washed-out cells in the early S phase was not statistically different from the one of IAA treatment, probably suggesting that 1 day of DNMT1 rescue might be not enough to completely recover the G1/S arrest.

To have a better understanding of the progression of the cell cycle after IAA washout, we evaluated G2 and mitosis. MPM2 staining showed no significant difference in the percentage of cells in G2/M between the washout and the untreated samples, suggesting a recovery of cell proliferation when DNMT1 is restored (Fig. 3F). However, there was no significant increase in the percentage of cells in G2/M between the washout and the IAA-treated conditions (Fig. 3F). On the other hand, by analyzing the mitotic index, we observed a full recovery of the cells in mitosis after IAA washout with respect to the IAA treatment (Fig. 3G, H). Also, the mitotic index was comparable to the one of untreated RPE-1 ^{NA}DNMT1 cells. To evaluate the possibility that 1 day of release from IAA might be not enough to fully restore the cell cycle, we repeated the experiments on the RPE-1 ^{NA}DNMT1 cells clone5 extending the wash out to 2 days and we named this condition WO2d (Supp. Fig. 2E). Immunoblotting confirmed the complete rescue of DNMT1 (Supp. Fig. 2F) and MPM2 staining also revealed a significant increase in the percentage of cells in G2/M upon two days of release from IAA (WO2d) with respect

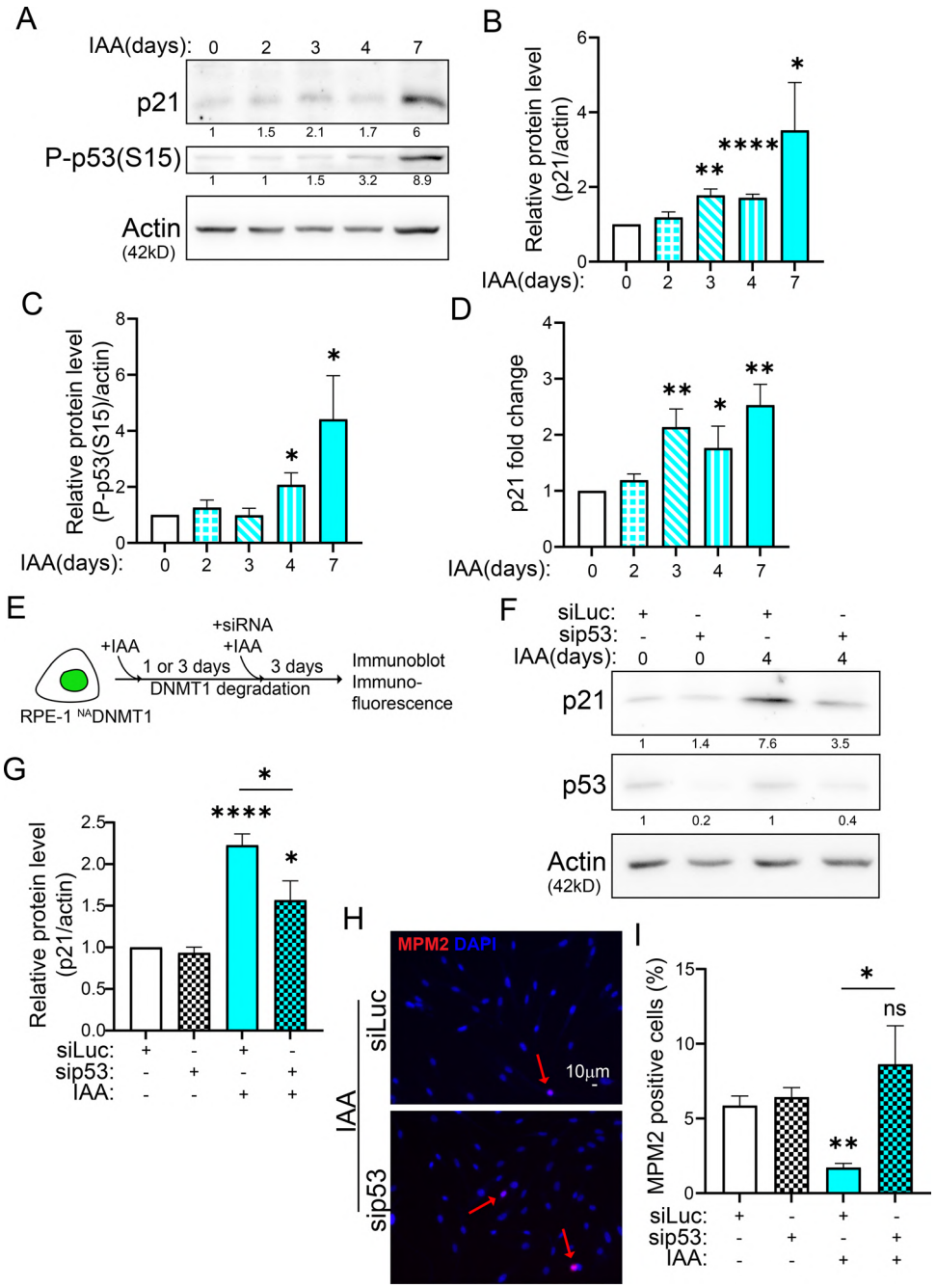

Fig. 2 DNMT1 degradation induces cell proliferation arrest that is dependent on p53 and p21. **A** Immunoblot showing the level of p21 protein and phosphorylated p53 on serine 15 (P-p53(S15)) at the indicated time points during IAA treatment. **B** Quantification of **A** showing p21 increase during IAA treatment. The graph shows the mean of at least 3 independent experiments. The error bars represent the standard error of the mean, SEM. Unpaired t-test between the samples: **** < 0.0001; ** < 0.01; * ≤ 0.05. **C** Quantification of **A** showing P-p53(S15) increase upon IAA treatment. The graph shows the mean of at least 3 independent experiments. The error bars represent the standard error of the mean, SEM. Unpaired t-test between the samples: * ≤ 0.05. **D** Histogram summarising RT-qPCR results of p21 transcript levels in RPE-1 ^{NA}DNMT1 cells during IAA treatment. The graph shows the mean of at least 3 independent experiments. The error bars represent the standard error of the mean, SEM. Unpaired t-test between the samples: ** < 0.01; * ≤ 0.05. **E** Schematics showing how sip53 experiments were performed. **F** Representative immunoblot of p21 and p53 in the indicated samples. **G** Graph summarising the results of **F** shows that sip53 transfection reduces p21 protein level in RPE-1 ^{NA}DNMT1 cells upon IAA treatment. The graph shows the mean of at least 3 independent experiments. The error bars represent the standard error of the mean, SEM. Unpaired t-test between the samples: **** < 0.0001; * ≤ 0.05. **H** Representative images of immunofluorescence assay targeting MPM2 in IAA-treated RPE-1 ^{NA}DNMT1 cells transfected with siLuc (control) or with sip53. Nuclei were counterstained with DAPI. **I** The graph is the quantification of **H**. The graph shows the mean of 3 independent experiments. At least 100 nuclei for each sample were evaluated. The error bars represent the standard error of the mean, SEM. Unpaired t-test between the samples: ** < 0.01; * ≤ 0.05; ns > 0.05

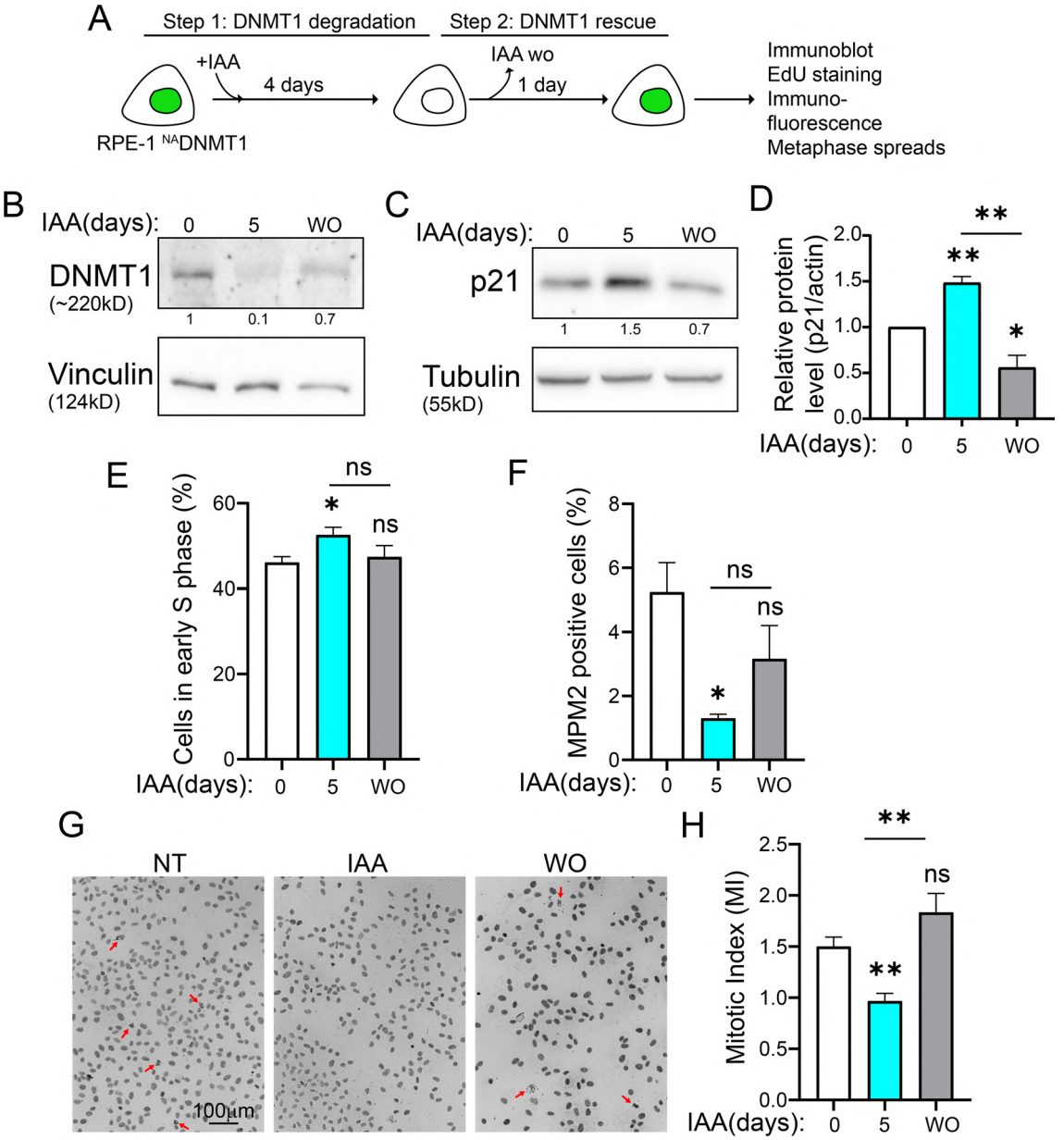

Fig. 3 DNMT1 restoration rescues cell proliferation. **A** Schematics showing how washout experiments were performed. **B** Immunoblot shows ^{NA}DNMT1 successfully recovered upon 1 day of IAA washout. **C** Immunoblot of p21 level in the untreated, IAA-treated, and washed-out RPE-1 ^{NA}DNMT1 cells. **D** Graph summarising the results in **C** highlights that ^{NA}DNMT1 rescue reduces p21 level in RPE-1 ^{NA}DNMT1 cells. The graph shows the mean of 3 independent experiments. The error bars represent the standard error of the mean, SEM. Un-paired t-test between samples ** < 0.01; * ≤ 0.05; ns > 0.05. **E** Graph summarising EdU staining data in the washout experiments. The graph shows the mean of 3 independent experiments. The error bars represent the standard error of the mean, SEM. At least 200 nuclei for each condition were evaluated. Unpaired t-test between samples: * ≤ 0.05; ns > 0.05. **F** Graph summarising data of MPM2 staining in the untreated, IAA-treated, and washed-out conditions. MPM2-positive cells increase after ^{NA}DNMT1 rescue. The graph shows the mean of 3 independent experiments. At least 150 cells were analyzed for each sample. The error bars represent the standard error of the mean, SEM. Unpaired t-test between the samples: * ≤ 0.05; ns > 0.05. **G** Representative images of mitotic spreads of untreated, IAA-treated, and washed-out RPE-1 ^{NA}DNMT1 cells. The nuclei and chromosomes were stained with Giemsa. Red arrows indicate cells in mitosis. **H** Graph summarising the data in **G**. Increased mitoses are observed in the IAA-washout condition. The graph shows the mean of 3 independent experiments. The error bars represent the standard error of the mean, SEM. At least 450 cells were evaluated. Unpaired t-test between the samples: ** < 0.01; ns > 0.05

to the IAA-treated condition (Supp. Fig. 2G). These results suggest that the proliferation arrest induced by prolonged DNMT1 absence can be progressively rescued by DNMT1 restoration.

DNMT1 inducible degradation causes global DNA demethylation

To evaluate whether DNMT1 inducible degradation affects global DNA methylation levels, a 7-day time-course analysis was carried out on RPE-1 ^{NA}DNMT1 cells (Fig. 4A, B). Similar to previous observations in DLD-1 ^{NA}DNMT1 cells [32], 5-methylcytosine (5MeC) immunostaining showed a progressive reduction in global DNA methylation starting from 2 days after IAA addition. The maximum degree of methylation loss is reached after 4 days of treatment, remaining unchanged up to 7 days of treatment. This finding is in accordance with the G1/S cell cycle arrest at both 4 and 7 days after IAA addition (Fig. 1C, E).

Given the association between global DNA demethylation and DNA damage signaling [11, 16, 43], we also wanted to address whether decreased levels of 5MeC could possibly trigger phosphorylation of histone H2AX on serine 139 (γH2AX), one of the earliest markers of the DNA damage response. However, we did not find any increase of γH2AX by immunoblotting (Supp. Fig. 2H), as we previously reported [12], suggesting no occurrence of DNA damage.

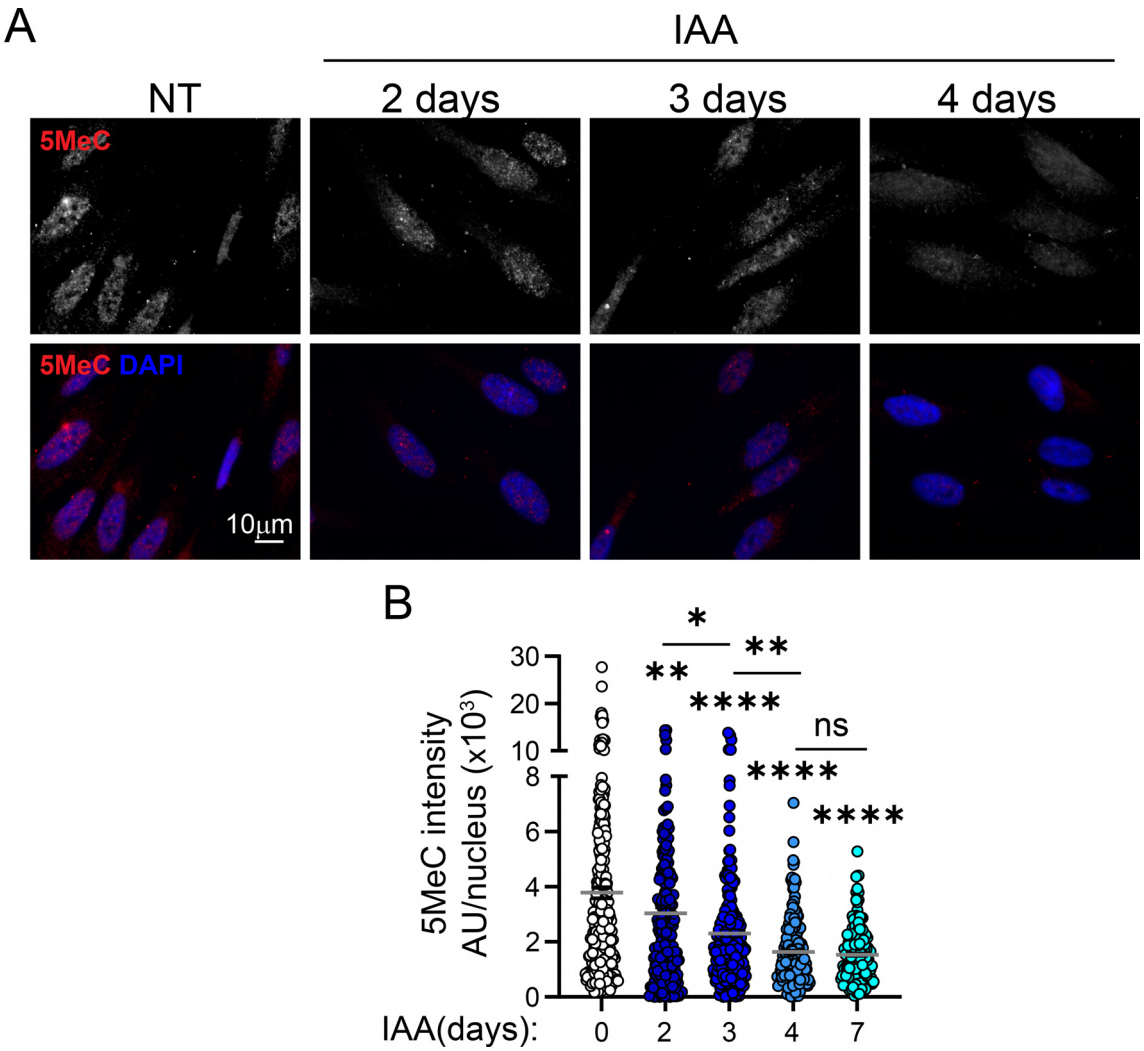

Fig. 4 DNMT1 inducible degradation causes global DNA demethylation. **A** Representative images of immunostaining for 5-Methyl-Cytosine (5MeC) displaying global DNA methylation reduction from 2 days up to 4 days of IAA treatment. Nuclei were counterstained with DAPI. **B** Single-cell nucleus quantification of 5MeC signal (AU: arbitrary unit) without (0 days) or with IAA (2, 3, 4 and 7 days) treatment. The scatter plot is cumulative of 6 independent experiments with at least 150 cells counted for each condition. Error bars represent the standard error of the mean SEM. Un-paired t-test between the samples: **** < 0.0001; ** < 0.01; * ≤ 0.05; ns > 0.05

Discussion

Studies on the role of DNMT1 in cell fitness, defined as the cells' ability to thrive in a specific environment, have shown varying results even within the same genetic background, making it challenging to determine its true importance in normal cells. These results might be due to the systems used to disable DNMT1. Here, we employed a cell model that we have recently published where DNMT1 endogenous protein can be rapidly and completely degraded using an inducible degron [32] in the non-tumoral RPE-1 cell line. This approach allows us to observe the direct and immediate effects of the protein absence in normal cells without potential biases from cytotoxicity caused by DNMT1-inhibiting drugs or siRNA transfection, or from cell adaptation to the gene knockout. We observed a gradual decrease in cell proliferation, culminating in a block occurring at the G1/S transition between days 4 and 7 in the absence of DNMT1. This suggests that DNMT1 protein is dispensable for cell proliferation for a few cell cycles (approximately 3–4 cell cycles), but its prolonged absence triggers a cell cycle arrest at the G1/S transition, inhibiting cells from replicating their DNA. In parallel, as the cells proliferate in the absence of DNMT1, passive DNA demethylation occurs and reaches its peak by day 4. This suggests that this methylation level may represent the maximum tolerance for maintaining the normal progression of the cell cycle. Indeed, major changes in both cell proliferation and cell cycle occur starting from day 4. However, upon restoring DNMT1 protein through IAA washout, cells exit the proliferation arrest and begin re-entering mitosis within 24 h, indicating that DNMT1 presence is perceived as a solution to restore cell proliferation. This observation could also imply that ensuring the maintenance of the minimal tolerable level of DNA methylation through rescued DNMT1 activity is sufficient to allow cell cycle progression. The minimal tolerable level of DNA methylation might constitute the threshold to avoid unrecoverable and dangerous genetic instability [6].

We also investigated the checkpoint triggered by DNMT1 prolonged absence and DNA methylation loss. Interestingly, despite the different types of arrest in the cell cycle observed so far in the previous literature, DNMT1 impairment often triggers the activation of cyclin-dependent kinase inhibitors, mainly p21 [12, 21, 24, 30, 44, 45]. We previously demonstrated that p21 activation and consequent cell cycle arrest is an immediate event in response to DNMT1 acute depletion in normal primary fibroblasts [12]. With the inducible degradation of DNMT1, we confirmed p21 activation even though it is not an immediate response but rather a delayed response to DNMT1's prolonged absence and DNA methylation loss. We also demonstrated that p21 activation is mostly triggered by p53 which is predominantly phosphorylated on serine 15, a marker of a stabilized and active p53 that cannot be inhibited by MDM2 [46]. Knocking-down of p53, as a consequence, releases cell proliferation arrest. Interestingly, p14ARF, which we previously showed to be responsible for the cell cycle arrest in the case of acute DNMT1 depletion by RNA interference, is activated only at day 7 in the absence of DNMT1. This activation likely occurs when DNA methylation conditions become critically compromised, necessitating stricter regulation of the cell cycle. Also, we did not observe an increase of γH2AX suggesting the occurrence of DNA damage that could have triggered p53 phosphorylation and activation, as previously reported [12].

Altogether, our results demonstrate that the prolonged absence of DNMT1 and consequent DNA methylation loss act as cellular stress signals that can endanger genome stability. This triggers p53-dependent p21 activation to halt cell proliferation before methylation reaches critical low levels. Notably, this proliferation arrest can be reversed when the stress source—such as DNMT1 loss—is resolved by restoring DNMT1 protein levels. Future research is needed to identify the specific cellular sensor responsible for detecting this stress and to explore whether this sensor can be modulated. This line of investigation could be particularly significant given that DNA methylation loss is a hallmark of numerous human diseases, including cancer. Understanding this stress-response pathway, and how it intersects with the fundamental processes of cell cycle control and genomic stability, could ultimately open new therapeutic avenues to target abnormal cell proliferation, offering hope for more effective treatments against diseases associated with DNA methylation loss.

Supplementary Information The online version contains supplementary material available at https://doi.org/10.1007/s00018-024-05547-y.

Acknowledgements We wish to thank Daniele Fachinetti, Institut Curie (Paris, France) for sharing and agreeing to the use of the engineered cells and for his helpful comments, and ATeN Center, University of Palermo (Italy), for acquiring flow cytometry data.

Author contributions Conceptualization: V.B.; Methodology: V.B. and A.D.L.; Formal analysis and investigation: S.M., S.G., P.S.C.; Writing—original draft preparation: V.B. and S.M.; Writing and editing: V.B., S.M., S.G., P.S.C.; Commenting draft: V.B. and A.D.L.; Supervision: V.B..

Funding This work was supported by FFR2023 and FFR2024 to VB.

Data availability The data that support the findings of this study are available within the article and its supplementary materials. Additional details are available from the corresponding author on request.

Declarations

Conflict of interests The authors have no relevant financial or non-financial interests to disclose.

Consent for publication All authors reviewed the results and contributed to the final manuscript. All authors approved this manuscript for publication.

References

1. Illingworth RS, Bird AP (2009) CpG islands—'A rough guide.' FEBS Lett 583:1713–1720. https://doi.org/10.1016/j.febslet.2009.04.012
2. Choy JS, Wei S, Lee JY et al (2010) DNA methylation increases nucleosome compaction and rigidity. J Am Chem Soc 132:1782–1783. https://doi.org/10.1021/ja910264z
3. Sharp AJ, Stathaki E, Migliavacca E et al (2011) DNA methylation profiles of human active and inactive X chromosomes. Genome Res 21:1592–1600. https://doi.org/10.1101/gr.112680.110
4. Sheaffer KL, Elliott EN, Kaestner KH (2016) DNA hypomethylation contributes to genomic instability and intestinal cancer initiation. Cancer Prev Res (Phila) 9:534–546. https://doi.org/10.1158/1940-6207.CAPR-15-0349
5. Tucci V, Isles AR, Kelsey G et al (2019) Genomic imprinting and physiological processes in mammals. Cell 176:952–965. https://doi.org/10.1016/j.cell.2019.01.043
6. Pappalardo XG, Barra V (2021) Losing DNA methylation at repetitive elements and breaking bad. Epigenetics Chromatin 14:25. https://doi.org/10.1186/s13072-021-00400-z
7. Carollo PS, Barra V (2023) Chromatin epigenetics and nuclear lamina keep the nucleus in shape: examples from natural and accelerated aging. Biol Cell 115:e2200023. https://doi.org/10.1111/boc.202200023
8. Martino S, Carollo PS, Barra V (2023) A glimpse into chromatin organization and nuclear lamina contribution in neuronal differentiation. Genes (Basel) 14:1046. https://doi.org/10.3390/genes14051046
9. Jackson-Grusby L, Laird PW, Magge SN et al (1997) Mutagenicity of 5-aza-2'-deoxycytidine is mediated by the mammalian DNA methyltransferase. Proc Natl Acad Sci U S A 94:4681–4685. https://doi.org/10.1073/pnas.94.9.4681
10. Unterberger A, Andrews SD, Weaver ICG, Szyf M (2006) DNA methyltransferase 1 knockdown activates a replication stress checkpoint. Mol Cell Biol 26:7575–7586. https://doi.org/10.1128/MCB.01887-05
11. Hollenbach PW, Nguyen AN, Brady H et al (2010) A comparison of azacitidine and decitabine activities in acute myeloid leukemia cell lines. PLoS ONE 5:e9001. https://doi.org/10.1371/journal.pone.0009001
12. Barra V, Schillaci T, Lentini L et al (2012) Bypass of cell cycle arrest induced by transient DNMT1 post-transcriptional silencing triggers aneuploidy in human cells. Cell Div 7:2. https://doi.org/10.1186/1747-1028-7-2
13. Costa G, Barra V, Lentini L et al (2016) DNA demethylation caused by 5-Aza-2'-deoxycytidine induces mitotic alterations and aneuploidy. Oncotarget 7(3):726–3739. https://doi.org/10.18632/oncotarget.6897
14. Kaji K, Factor VM, Andersen JB et al (2016) DNMT1 is a required genomic regulator for murine liver histogenesis and regeneration. Hepatology 64:582–598. https://doi.org/10.1002/hep.28563
15. Tang D, Zheng S, Zheng Z et al (2022) Dnmt1 is required for the development of auditory organs via cell cycle arrest and Fgf signalling. Cell Prolif 55:e13225. https://doi.org/10.1111/cpr.13225
16. Laranjeira ABA, Hollingshead MG, Nguyen D et al (2023) DNA damage, demethylation and anticancer activity of DNA methyltransferase (DNMT) inhibitors. Sci Rep 13:5964. https://doi.org/10.1038/s41598-023-32509-4
17. Li E, Bestor TH, Jaenisch R (1992) Targeted mutation of the DNA methyltransferase gene results in embryonic lethality. Cell 69:915–926. https://doi.org/10.1016/0092-8674(92)90611-f
18. Liao J, Karnik R, Gu H et al (2015) Targeted disruption of DNMT1, DNMT3A and DNMT3B in human embryonic stem cells. Nat Genet 47:469–478. https://doi.org/10.1038/ng.3258
19. DNMT1 DepMap Gene Summary. https://depmap.org/portal/gene/DNMT1?tab=overview. Accessed 25 Feb 2024
20. Zhang Z, Wang G, Li Y et al (2022) Recent progress in DNA methyltransferase inhibitors as anticancer agents. Front Pharmacol. https://doi.org/10.3389/fphar.2022.1072651
21. Palii SS, Van Emburgh BO, Sankpal UT et al (2008) DNA methylation inhibitor 5-Aza-2′-deoxycytidine induces reversible genome-wide DNA damage that is distinctly influenced by DNA methyltransferases 1 and 3B. Mol Cell Biol 28:752–771. https://doi.org/10.1128/MCB.01799-07
22. Qi D, Li J, Que B et al (2016) Long non-coding RNA DBCCR1-003 regulate the expression of DBCCR1 via DNMT1 in bladder cancer. Cancer Cell Int 16:81. https://doi.org/10.1186/s12935-016-0356-8
23. Wang X-Z, Cheng Y, Wang K-L et al (2016) Peperomin E reactivates silenced tumor suppressor genes in lung cancer cells by inhibition of DNA methyltransferase. Cancer Sci 107:1506–1519. https://doi.org/10.1111/cas.13029
24. Amatori S, Papalini F, Lazzarini R et al (2009) Decitabine, differently from DNMT1 silencing, exerts its antiproliferative activity through p21 upregulation in malignant pleural mesothelioma (MPM) cells. Lung Cancer 66:184–190. https://doi.org/10.1016/j.lungcan.2009.01.015
25. Tsujioka T, Yokoi A, Uesugi M et al (2013) Effects of DNA methyltransferase inhibitors (DNMTIs) on MDS-derived cell lines. Exp Hematol 41:189–197. https://doi.org/10.1016/j.exphem.2012.10.006
26. Chen T, Hevi S, Gay F et al (2007) Complete inactivation of DNMT1 leads to mitotic catastrophe in human cancer cells. Nat Genet 39:391–396. https://doi.org/10.1038/ng1982
27. Rhee I, Jair K-W, Yen R-WC et al (2000) CpG methylation is maintained in human cancer cells lacking DNMT1. Nature 404:1003–1007. https://doi.org/10.1038/35010000
28. Jiang C, Gong F (2016) DNA methyltransferase 1: a potential gene therapy target for hepatocellular carcinoma? Oncol Res Treat 39:448–452. https://doi.org/10.1159/000447414

29. Milutinovic S, Zhuang Q, Niveleau A, Szyf M (2003) Epigenomic stress response. Knockdown of DNA methyltransferase 1 triggers an intra-S-phase arrest of DNA replication and induction of stress response genes. J Biol Chem 278:14985–14995. https://doi.org/10.1074/jbc.M213219200
30. Wang H, Wu J, Meng X et al (2011) MicroRNA-342 inhibits colorectal cancer cell proliferation and invasion by directly targeting DNA methyltransferase 1. Carcinogenesis 32:1033–1042. https://doi.org/10.1093/carcin/bgr081
31. Snyder RD, Lachmann PJ (1989) Differential effects of 5-azacytidine and 5-azadeoxycytidine on cytotoxicity, DNA-strand breaking and repair of X-ray-induced DNA damage in HeLa cells. Mutat Res 226:185–190. https://doi.org/10.1016/0165-7992(89)90018-3
32. Scelfo A, Barra V, Abdennur N et al (2024) Tunable DNMT1 degradation reveals DNMT1/DNMT3B synergy in DNA methylation and genome organization. J Cell Biol 223:e202307026. https://doi.org/10.1083/jcb.202307026
33. Nishimura K, Yamada R, Hagihara S et al (2020) A super-sensitive auxin-inducible degron system with an engineered auxin-TIR1 pair. Nucleic Acids Res 48:e108. https://doi.org/10.1093/nar/gkaa748
34. Holland AJ, Fachinetti D, Han JS, Cleveland DW (2012) Inducible, reversible system for the rapid and complete degradation of proteins in mammalian cells. Proc Natl Acad Sci U S A 109:E3350-3357. https://doi.org/10.1073/pnas.1216880109
35. Carollo PS, Tutone M, Culletta G et al (2023) Investigating the inhibition of FTSJ1, a tryptophan tRNA-specific 2′-O-methyltransferase by NV TRIDs, as a mechanism of readthrough in nonsense mutated CFTR. Int J Mol Sci 24:9609. https://doi.org/10.3390/ijms24119609
36. Giacomini G, Piquet S, Chevallier O et al (2024) Aberrant DNA repair reveals a vulnerability in histone H3.3-mutant brain tumors. Nucleic Acids Res 52:2372–2388. https://doi.org/10.1093/nar/gkad1257
37. Said M, Barra V, Balzano E et al (2022) FANCD2 promotes mitotic rescue from transcription-mediated replication stress in SETX-deficient cancer cells. Commun Biol 5:1395. https://doi.org/10.1038/s42003-022-04360-2
38. Perriera R, Vitale E, Pibiri I et al (2023) Readthrough approach using NV translational readthrough-inducing drugs (TRIDs): A Study of the Possible Off-Target Effects on Natural Termination Codons (NTCs) on TP53 and Housekeeping Gene Expression. Int J Mol Sci 24:15084. https://doi.org/10.3390/ijms242015084
39. Veneziano L, Barra V, Lentini L et al (2016) p14(ARF) prevents proliferation of aneuploid cells by inducing p53-dependent apoptosis. J Cell Physiol 231:336–344. https://doi.org/10.1002/jcp.24976
40. Veneziano L, Barra V, Cilluffo D, Di Leonardo A (2019) Proliferation of aneuploid cells induced by CENP-E depletion is counteracted by the p14ARF tumor suppressor. Mol Genet Genomics 294:149–158. https://doi.org/10.1007/s00438-018-1495-5
41. Barra V, Chiavetta RF, Titoli S et al (2022) Specific irreversible cell-cycle arrest and depletion of cancer cells obtained by combining curcumin and the flavonoids quercetin and fisetin. Genes 13:1125. https://doi.org/10.3390/genes13071125
42. Aparicio T, Megías D, Méndez J (2012) Visualization of the MCM DNA helicase at replication factories before the onset of DNA synthesis. Chromosoma 121:499–507. https://doi.org/10.1007/s00412-012-0381-x
43. Shin H, Leung A, Costello KR et al (2023) Inhibition of DNMT1 methyltransferase activity via glucose-regulated O-GlcNAcylation alters the epigenome. Elife 12:e85595. https://doi.org/10.7554/eLife.85595
44. Young JI, Smith JR (2001) DNA methyltransferase I (DNMT1) inhibition induces a p21 dependent cell cycle arrest. ScientificWorldJournal 1:131. https://doi.org/10.1100/tsw.2001.232
45. Milutinovic S, Brown SE, Zhuang Q, Szyf M (2004) DNA methyltransferase 1 knock down induces gene expression by a mechanism independent of DNA methylation and histone deacetylation. J Biol Chem 279:27915–27927. https://doi.org/10.1074/jbc.M312823200
46. Shieh S-Y, Ikeda M, Taya Y, Prives C (1997) DNA damage-induced phosphorylation of p53 alleviates inhibition by MDM2. Cell 91:325–334. https://doi.org/10.1016/S0092-8674(00)80416-X

4 Results

4.1 DNMT1 inducible degradation causes global DNA demethylation, slowing-down of cell proliferation and aneuploidy in cancer cells

To ascertain that the ^{NA}DNMT1 inducible degradation was functional in DLD-1 ^{NA}DNMT1 cancer cells, the cells were treated with IAA. DNMT1 mNeonGreen protein absence was confirmed both by the fluorescence absence via fluorescence microscopy and by the absence of the protein through immunoblot assay (Figure 1A and 1B). Additionally, to confirm that DNMT1 loss correlated with a loss of DNA methylation in these cells, 5-methylcytosine immunostaining at 10 days of IAA treatment was performed (Figure 1C). The analysis revealed a significant decrease in global DNA methylation following the IAA treatment (Figure 1D), as also observed by Fachinetti's group [472]. The 5mC staining was performed on mitotic chromosomes as well to better evaluate where the methylation was lost along the chromosome. The analysis focused on long chromosomes (Supp. Figure 1A and 1B) and short chromosomes (Supp. Figure 1E and 1F) with a similar length in cells with or without IAA treatment. A plot profile of these grouped selected chromosomes was performed and the analysis revealed that 5mC staining was in fact reduced across the whole chromatids, however the centromere was the most affected region (Supp. Figure 1C, 1D, 1G, 1H).

Depending on the cell line and the strategy used to disable DNMT1, DNMT1 absence can lead to different phenotypes [476]. By using the inducible degradation of the protein, which is almost immediate (1 hour) [472]. The effect of DNMT1 absence *per se* in the fitness of DLD-1 ^{NA}DNMT1 cells was evaluated. The trypan blue staining revealed that the cells did not die upon the IAA treatment and, thus, there was no negative effect on the survival (data not shown). Instead, DLD-1 cells continue to normally proliferate until slowing down in a significant way at the 10th day of treatment upon prolonged DNMT1 absence, specifically from the 7th to the 10th day (Figure 1E). An even longer treatment, 21 days of DNMT1 absence, highly reduces the ability to form colonies in the cancer cell line (Supp Figure 2A).

As attached to this thesis, my already published paper, which discuss about my thesis results on the effect of DNMT1 absence on RPE-1 cells, demonstrated that DNMT1 induced degradation leads to p53-p21waf1/cip1 pathway activation in normal human cells (Martino *et al.*, 2024). DLD-1 cell line is characterized by a point mutation in one of p53 alleles, a C -> T missense mutation leading to Ser -> Phe change at position 241 (ATCC database) [477] and resulting in the impairment of the binding of p53 to DNA. With this in mind, p53-p21waf1/cip1 pathway activation was

evaluated in DLD-1 cancer cells upon DNMT1 induced degradation. No change was observed in the overall p53 protein level by immunoblot (Supp. Figure 2B), instead, the analysis revealed an increase in both the expression and protein level of p21waf1/cip1 (Figure 1F and Supp. Figure 2C), which suggests a residual p53 function or activation by other transcriptional factors.

It was reported that silencing or the complete degradation of DNMT1 by DNMTs inhibitor AZA or DAC, lead to aneuploidy [471,472,478]. To confirm this, a cytogenetic analysis was performed (Figure 1G). The experiment revealed a change of the chromosome number after 10 days of IAA treatment (Figure 1H), suggesting that the prolonged DNMT1 absence or the consequent DNA methylation loss allows the generation of aneuploidy in the cells. Aneuploidy can be induced when there are mitotic errors, such as lagging chromosomes. Hence, the percentage of cells with micronuclei that arise from lagging chromosomes was evaluated. Specifically, I reasoned that lagging chromosome should have been appeared before day 10 of treatment to generate aneuploidy. As such, the presence of micronuclei was analysed on the 4th day of IAA treatment. The experiment revealed no significant differences with the control (P value 0,0746) (Supp. Figure 2D and 2E). This suggests no induction of lagging chromosomes upon DNA methylation loss or DNMT1 absence.

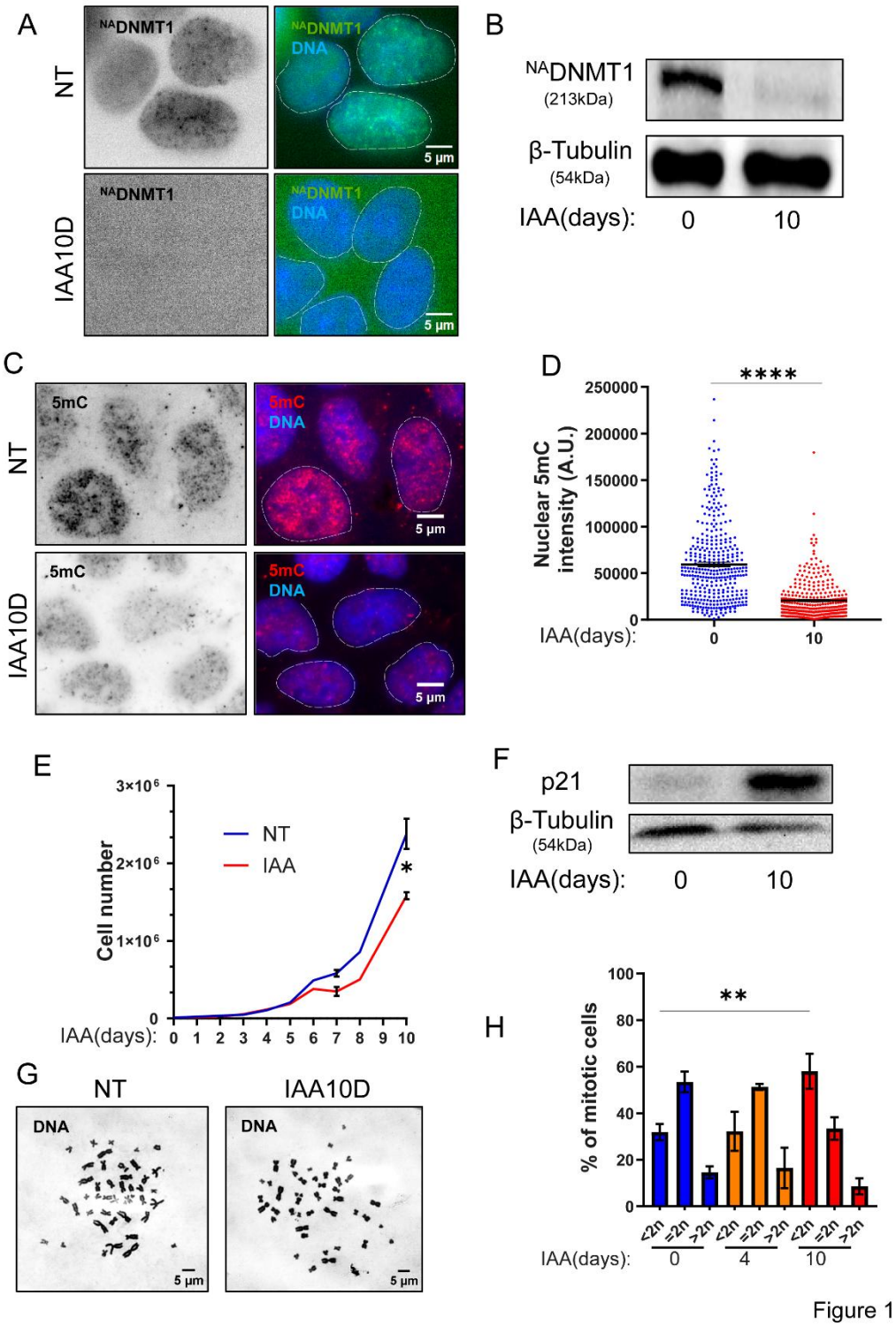

Figure 1

Figure 1: AID system induces the degradation of DNMT1 with subsequent DNA methylation loss and aneuploidy. **A** The DLD-1 endogenous fluorescence of ^{NA}DNMT1 is lost upon the IAA treatment. **B** Immunoblot shows ^{NA}DNMT1 successfully degraded at 10 days of IAA treatment in DLD-1 ^{NA}DNMT1 cells. **C** Immunostaining of 5mC in the untreated and 10 days IAA-treated DLD-1 ^{NA}DNMT1 cells. **D** Graph summarising the results in C shows that ^{NA}DNMT1 degradation highly reduces the 5mC level in DLD-1 ^{NA}DNMT1 cells. The graph shows the mean of 3 independent experiments. The error bars represent the standard error of the mean, SEM. At least 150 nuclei for each condition and each replicate were evaluated. Unpaired t-test between samples **** < 0.0001. **E** Graph reveals DLD-1 ^{NA}DNMT1 cells slow down proliferation. The graph shows the mean of 3 independent experiments. The error bars represent the standard error of the mean, SEM. Unpaired t-test between samples: * ≤ 0.05; ns > 0.05. **F** Immunoblot shows the increase of p21 protein amount upon 10 days of IAA treatment in DLD-1 ^{NA}DNMT1 cells. **G** Representative images of metaphase spreads of untreated and IAA-treated DLD-1 ^{NA}DNMT1

cells. The nuclei and chromosomes were stained with Giemsa. **H** Graph summarising the data in G. Numerical aneuploidy is achieved upon 10 days of IAA treatment in DLD-1 ^{NA}DNMT1 cells. The graph shows the mean of at least 3 independent experiments. The error bars represent the standard error of the mean, SEM. At least 20 metaphase spreads for each condition and each replicate were evaluated. Unpaired t-test between the samples: ** < 0.01; ns > 0.05.

4.2 DNMT1 inducible degradation improves the recruitment of centromere protein CENP-A and CENP-C of cancer cells

The alteration of the chromosome number strongly suggests that the prolonged absence of DNMT1 or the loss of DNA methylation can induce errors in chromosome segregation. This finding is not correlated with the presence of lagging chromosomes. DNA methylation is heavily recurrent at the repetitive DNA of the centromere, and the kinetochore complex, which has a central role in chromosome segregation, is assembled at the centromere. Thus, the centromere functioning and kinetochore recruitment were investigated in DLD-1 ^{NA}DNMT1 cells upon DNMT1 degradation as a possible cause of segregation errors.

To evaluate if the cells had difficulties in congressing the chromosomes to the metaphase plate, DLD-1 ^{NA}DNMT1 cells were first treated with STLC to synchronize them in mitosis with a monopolar-spindle state and then released in the presence of MG132 to block progression of mitosis over the metaphase (Supp. Figure 2F). At 7 days of IAA treatment, only about 25% of cells showed chromosomes at the metaphase plate compared to 50% of the control cells (Figure 2A-B). Although at 4 days treated cells showed no statistical difference compared to the controls, the P value 0,06 suggested that the alteration in the chromosome congression (only 30% of cells with chromosomes reaching the metaphase plate) starts even before the 7th day (Figure 2A-B).
Additionally, the cells with congressed chromosomes at the metaphase plate were analysed (Figure 2C) and, compared to the control, the IAA treated cells showed a higher incidence of misaligned chromosomes at both time points (Figure 2D).

Cells treated with STLC-MG132 were stained for the presence of CENP-A and CENP-T to check their recruitment at the mitotic uncongressed and misaligned chromosomes (Figure 2E). Indeed, both CENP-A/CENP-C and CENP-T are able to recruit the kinetochore complex at centromeres. The analysis revealed a dynamic rearrangement for CENP-T as it was increased at the 4th day of treatment but normalised at the 7th day compared to the control (Figure 2F). This could be explained by some compensatory mechanism at the centromeric region, or it could be due to technical issues. However, CENP-A was characterised by an increased intensity at the

centromere of the misaligned/uncongressed chromosomes at both 4 and 7 days of IAA treatment (Figure 2G).

Since CENP-A intensity was higher at the errors of all time points, DLD-1 ^{NA}DNMT1 cells CENP-A regulation and dynamics were further analysed. Since it is known that CENP-A is loaded onto centromere during the early G1 phase, immunostaining of interphase nuclei was performed (Figure 3A). DLD-1 ^{NA}DNMT1 cells asynchronous population was characterised by a clear increase in CENP-A spot intensity in the nuclei upon 10 days of IAA treatment (Figure 3B). To avoid any bias due to the presence of S-phase cells where CENP-A spots start to split and become double with halved intensity, a 24h of serum starvation experiment was performed. The serum starvation synchronises the cells in G1 phase. The synchronised populations of DLD-1 ^{NA}DNMT1 cells were characterised by increased CENP-A as well (Supp. Figure 3A), confirming the previous results. Surprisingly, the increase in intensity of CENP-A spots in the nuclei observed upon 10 days of IAA treatment did not correlate with a significant increase in the protein level (Figure 3C-D).

Next, the intensity of CENP-A spots at mitotic chromosomes was evaluated (Figure 3E). The analysis showed that at 10 days of treatment, CENP-A was increased at chromosomes (Figure 3F).

To characterise the timing of CENP-A increase, immunostaining experiments were performed at different time points and-revealed that CENP-A higher intensity is already noticeable at the 3rd day of IAA treatment (Figure 3G, Supp. Figure 3B).

To better understand this, the mRNA and the protein levels were evaluated. CENP-A gene expression was increased only on the first day of IAA treatment (Figure 3H), which suggests the need to produce more CENP-A and justify the observed increased intensity at the centromere. However, the protein levels did not change across different days of treatment even upon mitotic synchronization with colcemid (Supp. Figure 3C-D-E-F). These results would suggest that only CENP-A recruitment at centromeres is increased upon prolonged DNMT1 degradation, and not the whole protein level.

Since CENP-A recruitment was increased at all time points both in interphase nuclei and in mitotic chromosomes, the recruitment of the kinetochore was evaluated. I first focused on CENP-C, both in G1 nuclei and in mitosis (Supp. Figure 3G and Figure 4A). To select cells in G1 phase, CENP-A spots appearance as single (G1) or double (S/G2) spots were used. At the 4th day of IAA treatment, CENP-C was less intense in the G1 nuclei (Supp. Figure 3H). On the contrary, in mitosis CENP-C signal in IAA treated cells increases more than 15% compared to the non-treated cells (Figure 4A-B), showing that DNMT1 prolonged degradation deregulated CENP-C dynamics.

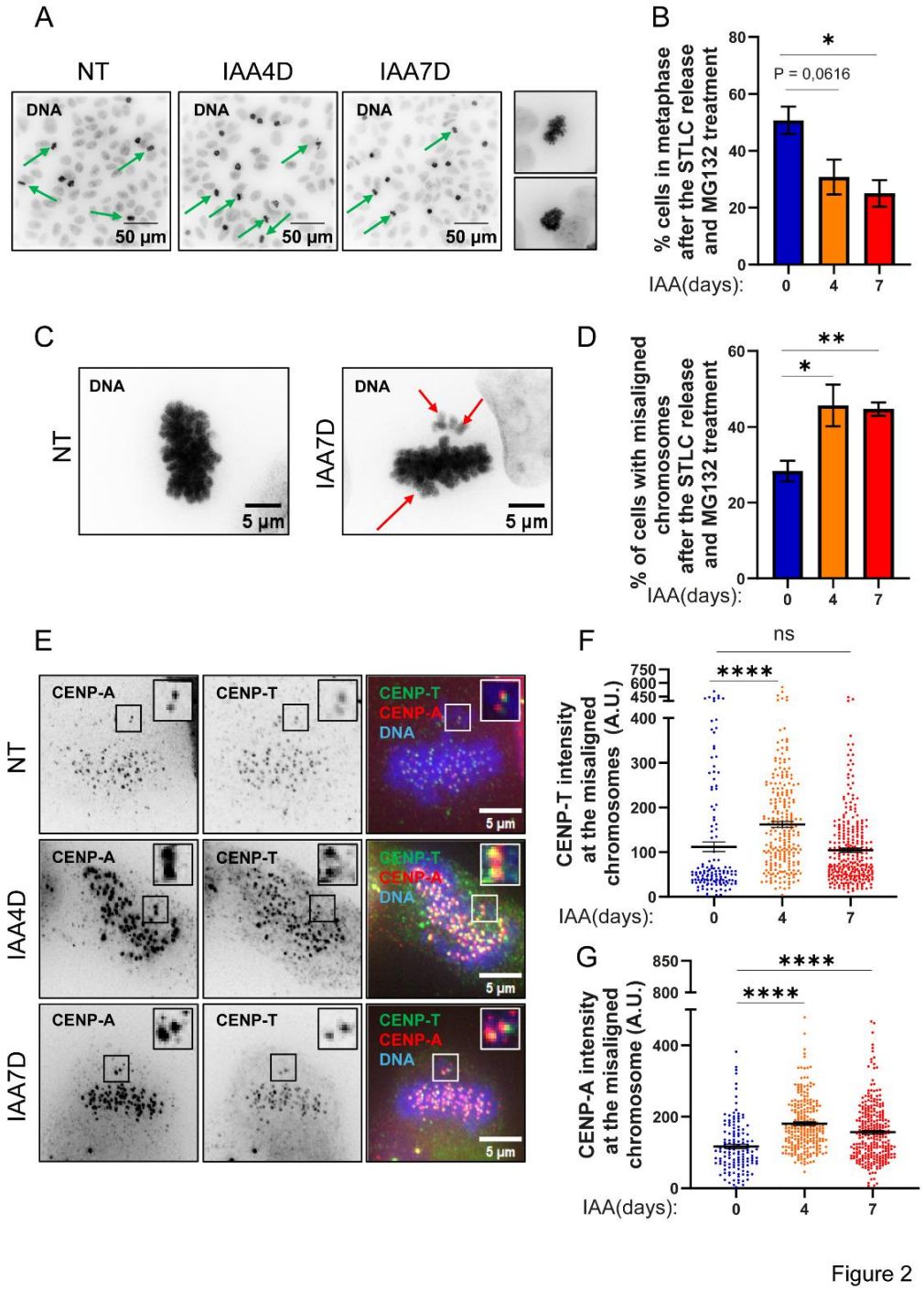

Figure 2

Figure 2: DNMT1 absence induces difficulties in chromosome congression, and mitotic errors characterised by higher CENPs intensity. **A** DAPI staining to evaluate the number of cells that reach the metaphase plate after STLC incubation and release into MG132 in the untreated and IAA-treated DLD-1 ^{NA}DNMT1 cells. The zooms show representative cells with or without, congressed and aligned chromosomes at the metaphase plate. **B** Graph summarising the results of A, reveals that the 4 days and 7 days IAA treated DLD-1 ^{NA}DNMT1 cells have difficulty in reaching the metaphase. The graph shows the mean of 3 independent experiments. The error bars represent the standard error of the mean, SEM. At least 17 mitotic cells for each condition and each replicate were evaluated. Unpaired t-test between the samples: * ≤ 0.05; P = 0.0616. **C** DAPI staining of untreated and 7 days IAA-treated DLD-1 ^{NA}DNMT1 cells. **D** Graph summarising the results in C shows that ^{NA}DNMT1 degradation induces uncongressed and misaligned chromosomes in DLD-1 ^{NA}DNMT1 cells. The graph shows the mean of 3 independent experiments. The error bars represent the standard error of the mean, SEM. At least 25 mitoses for each condition and each replica were evaluated. Unpaired t-test between samples ** < 0,01 and * ≤ 0.05. **E** Immunostaining of CENP-A and CENP-T in control, 4 days and 7 days IAA treated DLD-1 ^{NA}DNMT1 cells upon STLC incubation and release in MG132. **F**

Graph summarising the results in E reveals higher intensity of CENP-T at the mitotic errors at 4 days of IAA treatment. The graph shows the mean of 3 independent experiments. The error bars represent the standard error of the mean, SEM. At least 40 spots for each condition and each replica were evaluated. Unpaired t-test between samples **** < 0.0001; ns > 0.05. **G** Graph summarising the results in E, reveals higher intensity of CENP-A at the mitotic errors at 4 and 7 IAA days. The graph shows the mean of 3 independent experiments. The error bars represent the standard error of the mean, SEM. At least 40 spots for each condition and each replica were evaluated. Unpaired t-test between samples **** < 0.0001.

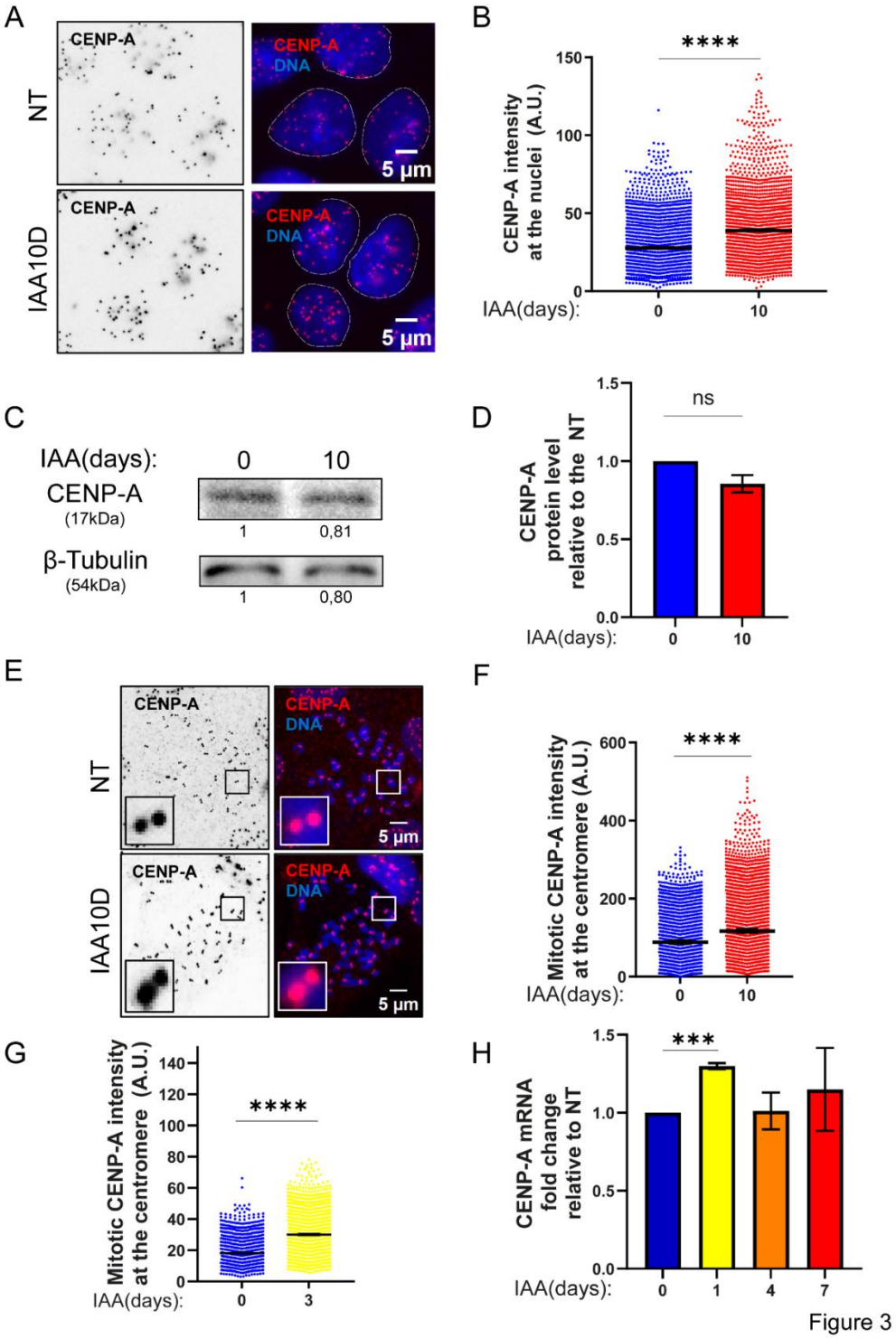

Figure 3

Figure 3: CENP-A higher recruitment is induced upon IAA treatment. **A** Immunostaining of CENP-A at the interphase nuclei in the untreated and 10 days IAA treated DLD-1 ^{NA}DNMT1 cells **B** Graph showing the results of A, reveals that CENP-A is increased at the nuclei of 10 days IAA treated DLD-1 ^{NA}DNMT1 cells. The graph shows the mean of

3 independent experiments. The error bars represent the standard error of the mean, SEM. At least 700 spots for each condition and each replica were evaluated. Unpaired t-test between the samples: **** < 0.0001. **C** Immunoblot of CENP-A in untreated and 10 days IAA treated DLD-1 ^{NA}DNMT1 cells. **D** Graph summarising the results in E shows that CENP-A protein amount does not change in DLD-1 ^{NA}DNMT1 cells upon IAA treatment. The graph shows the mean of 3 independent experiments. The error bars represent the standard error of the mean, SEM. Unpaired t-test between samples: ns > 0.05. **E** Immunostaining for CENP-A to evaluate the signal in mitotic chromosomes. **F** Graph summarising the results in E reveals higher signal of CENP-A at the centromere in mitosis of 10 days IAA treated DLD-1 ^{NA}DNMT1 cells. The graph shows the mean of 3 independent experiments. The error bars represent the standard error of the mean, SEM. At least 2000 spots for each condition and each replica were evaluated. Unpaired t-test between the samples: **** < 0.0001. **G** Graph reveals higher signal of CENP-A at the centromere in mitosis of 3 days IAA treated DLD-1 ^{NA}DNMT1 cells. The graph shows the mean of 3 independent experiments. The error bars represent the standard error of the mean, SEM. At least 700 spots for each condition and each replica were evaluated. Unpaired t-test between the samples: **** < 0.0001. **H** Graph showing the results of the RT-qPCR, reveals that CENP-A mRNA is increased at the first day of IAA treatment in DLD-1 ^{NA}DNMT1 cells. The graph shows the mean of 3 independent experiments. The error bars represent the standard error of the mean, SEM. Unpaired t-test between the samples: *** < 0.001; ns > 0.05.

4.3 DNMT1 inducible degradation does not impair the functionality of the kinetochore and the attachment formation

The observed CENP-A/CENP-C increase suggests that the whole kinetochore complex may be affected together with its function. To investigate this, Hec1 intensity was evaluated in DLD-1 ^{NA}DNMT1 cells in metaphase at 4 and 7 days of IAA treatment. The analysis revealed no change in the intensity (Figure 4C-D). This finding suggests no negative effect on the kinetochore structure at those timepoints. In parallel, the total protein level analysed by immunoblot assay revealed a reduction of Hec1 only at the first day of IAA treatment, similarly to what was observed for CENP-A (Figure 4F-4G). The same results occurred when MG132 (Supp. Figure 4A-B) or colcemid (Supp. Figure 4C-D) were used to synchronise the cells in mitosis.

To evaluate if the attachments were faithful, the proteins recruited when the end-on attachment is matured were analysed. In the same immunofluorescence experiment of Hec1, Astrin (Figure 4C), which is a signature of mature attachments was analysed. The immunofluorescence experiment revealed that the intensity of the signal of Astrin, located at the analysed Hec1 spots, was higher upon DNMT1/DNA methylation loss at 4 and 7 days of IAA treatment, respectively 20% and 15% higher than the control (Figure 4E).
To corroborate this result, the SKA complex, which is another signature protein of a proper attachment was also analysed. The experiment revealed an increase of the Ska3 intensity at each time point (Supp. Figure 4E-F). Ska3 data correlated with the one observed for Astrin.

No effect on the kinetochore complex and an increase of protein related to a stable attachment should, in principle, not affect kinetochore-microtubule attachment stability. To further confirm this hypothesis, a cold treatment assay for 15 min was performed on DLD-1 ^{NA}DNMT1 cells to

evaluate the k-fiber persistence. The low temperature can induce depolymerization of microtubules and only specialised structures like the stable interactions between the kinetochore and the microtubule will be maintained. At all timepoints analysed the microtubules were still attached to the kinetochore, confirming no negative effect on the attachment itself when it is already established (Figure 5A-B).

Since some researchers correlated the distance between the two poles and the metaphase plate thickness (Supp. Figure 5D) with the kinetochore-microtubule attachment stability [235], these distances were analysed, but no variation was observed (Supp. Figure 5E-F). This confirmed that DNA methylation loss or DNMT1 absence did not alter the realisation of stable attachments.

Finally, I observed the phenotype of the spindle poles upon cold treatment was analysed. Normally, the stable spindle appeared as k-fibers arising from the disk-shaped poles where tubulin had high intensity. Upon cold exposure, some unstable mitoses were characterised by k-fibers still present that, however, did not arise from a pole, which, instead, appears broken (Figure 5C). The phenotypes of the spindle pole were analysed. The experiment revealed an increased stability upon IAA treatments (Figure 5D). However, phenotypes in between the two conditions were also present. These phenotypes were classified as variant A and B. In variant A, the k-fibers were not connected to the pole, even if the tubulin disk is present, thus, potentially unstable (Supp. Figure A). In variant B, instead of k-fibers connected to the pole, which appeared linear and not as a disk, suggesting instead, stability (Supp. Figure A). The quantification of the regular broken or stable spindle poles plus the relative variants showed no statistical significance but a tendency to stability (Supp. Figure 5B-5C). All these support the idea of a positive impact on the spindle pole stability upon DNMT1 absence or DNA methylation loss.

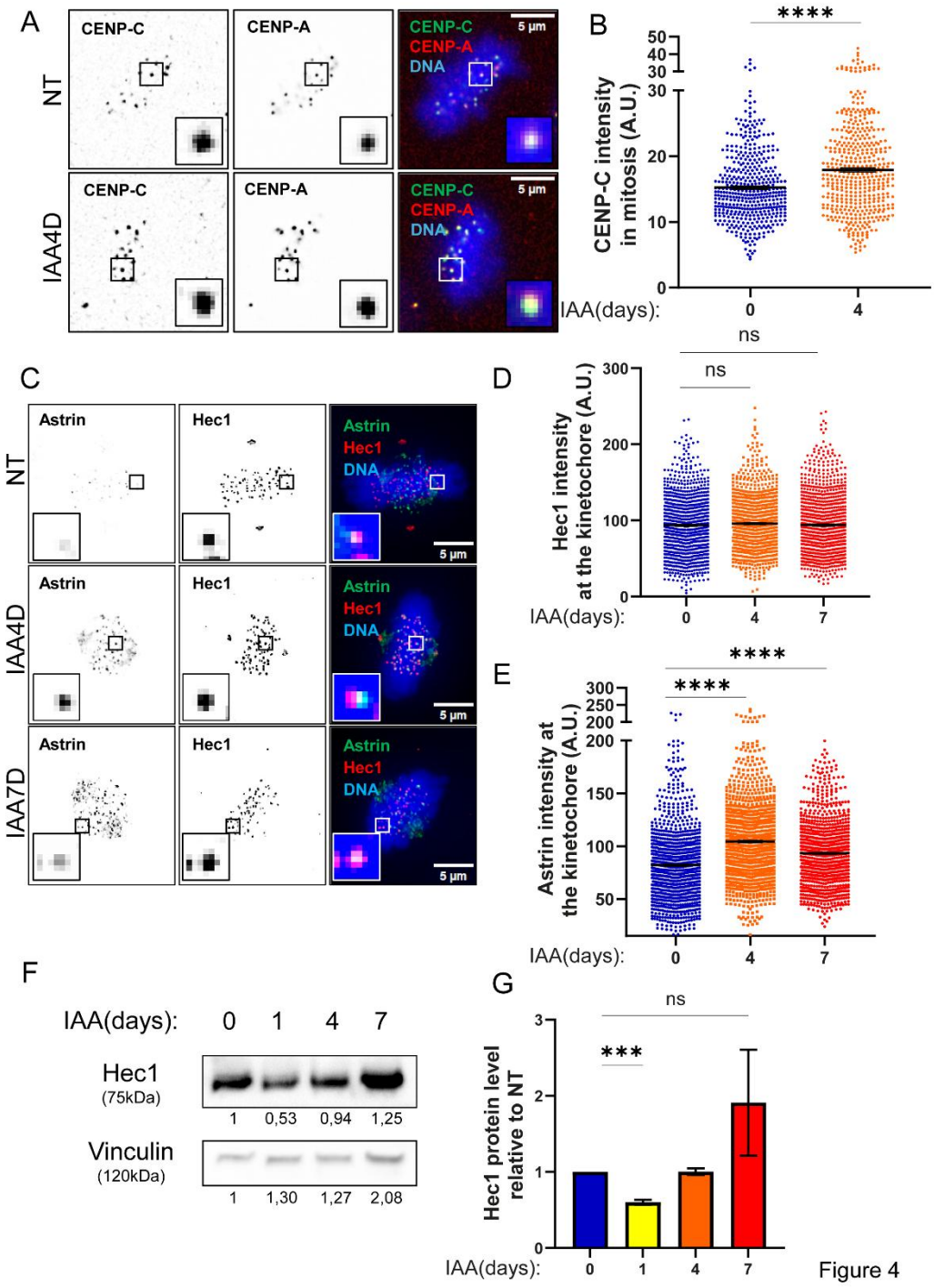

Figure 4

Figure 4: DNMT1 degradation improves the recruitment of CENP-C and Astrin. **A** Immunostaining for CENP-C and CENP-A in the untreated and 4 days IAA treated DLD-1 ^{NA}DNMT1 cells **B** Graph summarising the results in A, reveals higher intensity of CENP-C at the centromere of metaphase cells at 4 days of IAA treatment in DLD-1 ^{NA}DNMT1 cells. The graph shows the mean of 3 independent experiments. The error bars represent the standard error of the mean, SEM. At least 150 spots for each condition and each replicate were evaluated. Unpaired t-test between the samples: **** < 0.0001. **C** Immunostaining of Hec1 and Astrin at the metaphase in untreated, 4 days and 7 days of IAA treatment in DLD-1 ^{NA}DNMT1 cells. **D** Graph showing the results of C reveals that Hec1 does not change. The graph shows the mean of 3 independent experiments. The error bars represent the standard error of the mean, SEM. At least 315 spots for each condition and each replicate were evaluated. Unpaired t-test between the samples: ns > 0.05. **E** Graph showing the results of C reveals that Astrin increases at 4 and 7 days of IAA treatment in DLD-1 ^{NA}DNMT1 cells. The graph shows the mean of 3 independent experiments. The error bars represent the standard error of the mean, SEM. At least 315 spots for each condition and each replicate were evaluated. Unpaired t-test between the

samples: **** < 0.0001. **F** Immunoblot of Hec1 in untreated, 1 day, 4 days and 7 days of IAA treatment in DLD-1 ^{NA}DNMT1 cells. **G** Graph summarising the results in F reveals a reduction in Hec1 protein amount at the first day of IAA treatment. The graph shows the mean of 3 independent experiments. The error bars represent the standard error of the mean, SEM. Unpaired t-test between the samples: ***< 0.001; ns > 0.05.

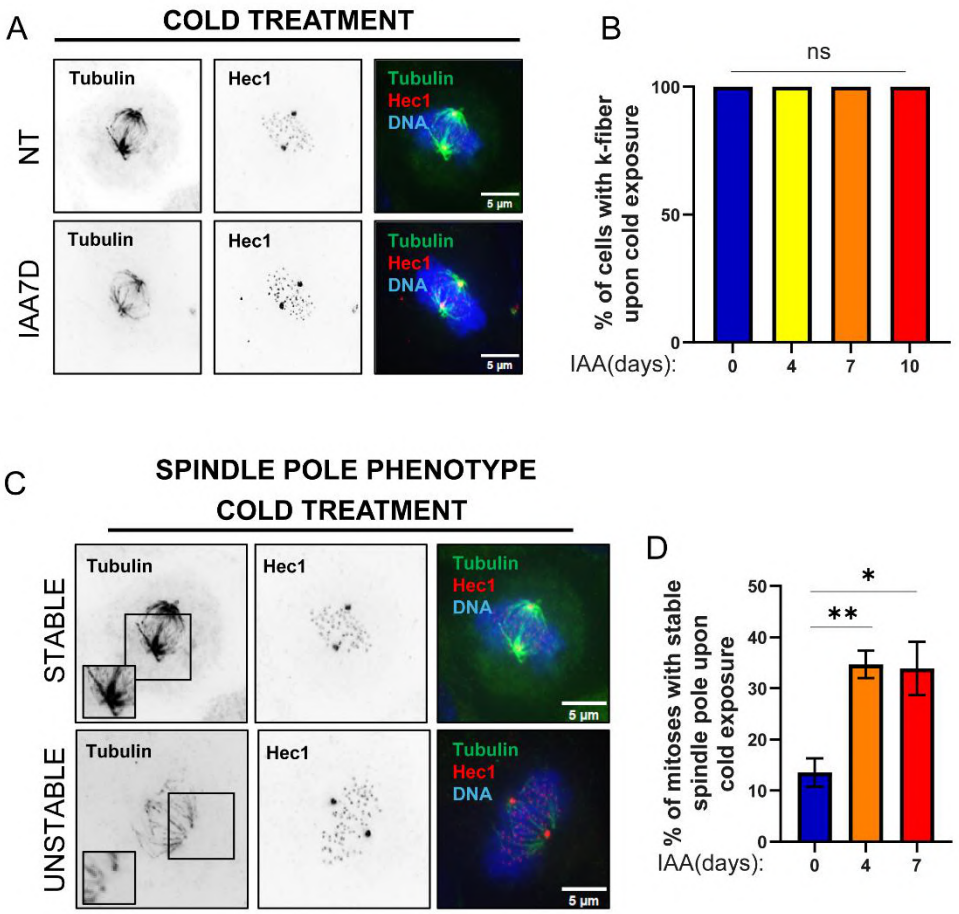

Figure 5

Figure 5: Kinetochore-microtubule attachment stability is not impaired upon DNMT1 absence or DNA methylation loss. **A** Immunostaining for Tubulin and Hec1 in the untreated and 7 days IAA treated DLD-1 ^{NA}DNMT1 cells upon 15 min of cold exposure **B** Graph summarising the results in A reveals the persistence of k-fibers at all observed IAA treated samples. The graph shows the mean of 3 independent experiments. The error bars represent the standard error of the mean, SEM. At least 25 mitoses for each condition and each replicate were evaluated. Unpaired t-test between the samples: ns > 0.05. **C** Immunostaining of Tubulin and Hec1 upon cold exposure, reveals different spindle pole phenotype in DLD-1 ^{NA}DNMT1 cells: STABLE, The pole is present and the mitotic spindle is connected to the pole; UNSTABLE, the mitotic spindle is not connected to a pole **D** Graph showing the results of C, reveals that the spindle poles are more stable in the 4 days and 7 days IAA treated DLD-1 ^{NA}DNMT1 cells. The graph shows the mean of 3 independent experiments. The error bars represent the standard error of the mean, SEM. At least 25 mitoses for each condition and each replica were evaluated. Unpaired t-test between the samples: ** < 0,01; * ≤ 0.05.

4.4 DNMT1 inducible degradation does not impair the stripping of the fibrous corona proteins in cancer cells

Since the kinetochore-microtubule attachment is still permitted but congression defects are present, I reasoned that the errors could arise before the formation of the attachment, possibly due to alterations of the fibrous corona or to defects in the cytoskeletal motor proteins. Hence, the effect of DNA methylation loss on P150Glued was evaluated. P150Glued is a component of the dynactin complex, which is required for the dynein molecular motor to strip off the fibrous corona proteins once stable, end-on kinetochore-microtubule connections are established. Immunoblot revealed no significant change in P150Glued protein level in both asynchronous and colcemid-synchronised cell population upon IAA treatment (Figure 6A-B and Supp. Figure 6A-B). Even if the protein level was not altered, the localisation of dynein complex which is important to ensure proper chromosome segregation was analysed. No variation in the number of P150Glued spots at metaphase in the cells at 10 days of IAA treatment was observed (Figure 6C-D). However, by measuring the intensity of P150Glued signal throughout the metaphase area between the two poles, an increase of P150Glued intensity was observed (Supp. Figure 5G and Figure 6E). This data shows a high persistence of dynein onto the microtubules and thus, an incomplete formation of kinetochore-microtubule attachment despite the occurrence of functional mature attachments. Higher presence of dynein on microtubules could suggest a premature stripping of fibrous corona proteins.

Another important molecular motor required for chromosome segregation is CENP-E, which allows the formation of lateral, immature attachments and is also required to maintain chromosomes at the metaphase plate. Difficulties in congressing the chromosomes may arise from a lack of CENP-E. CENP-E transcript and protein levels were evaluated and no change was observed neither in the asynchronous or in the synchronised cell population (Figure 6F-G-H and Supp. Figure 6C-D). Even if not significant Figures 6G-H show an increase of CENP-E protein level upon IAA treatment at every time point, which could be due to technical issues, but it could also be a symptom of the cells attempting to improve the congression of chromosomes.

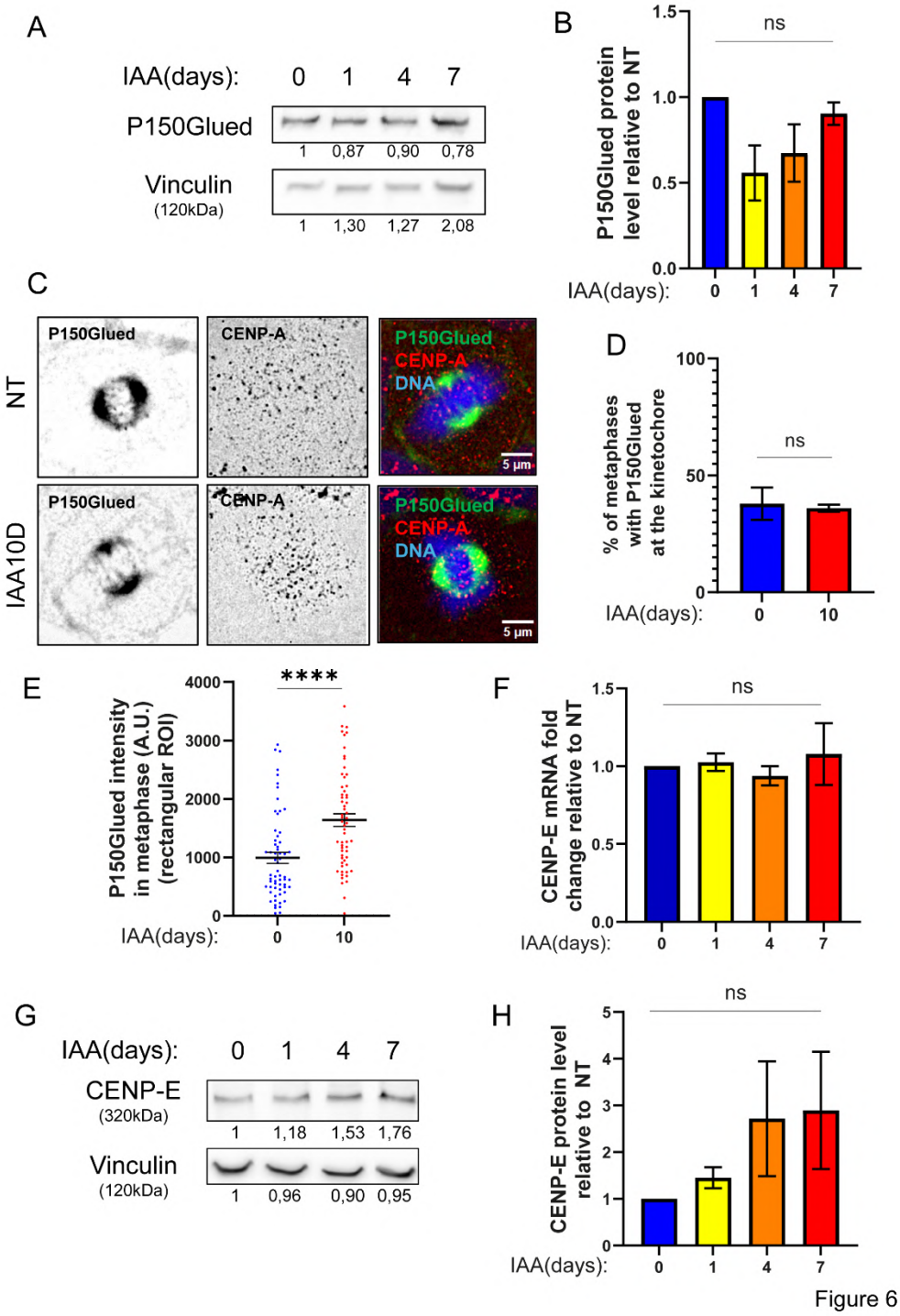

Figure 6

Figure 6: Loss of DNMT1 or DNA methylation may affect dynein and CENP-E. **A** Immunoblot for P150Glued in the untreated, 1 day, 4 days and 7 days IAA treated DLD-1 ^{NA}DNMT1 cells **B** Graph summarising the results in A, reveals no change on P150Glued protein amount. The graph shows the mean of 3 independent experiments. The error bars represent the standard error of the mean, SEM. Unpaired t-test between the samples: ns > 0.05. **C** Immunostaining of P150Glued and CENP-A in untreated and 10 days IAA treated DLD-1 ^{NA}DNMT1 cells. **D** Graph showing the results of C reveals the % of metaphase with P150Glued spots does not change upon IAA treatment in DLD-1 ^{NA}DNMT1 cells. The graph shows the mean of 3 independent experiments. The error bars represent the standard error of the mean, SEM. 20 mitoses for each condition and each replica were evaluated. Unpaired t-test between the samples: ns > 0.05. **E** Graph showing the results of C, reveals higher intensity of P150Glued (rectangular ROI located between the 2 poles) in 10 days IAA treated DLD-1 ^{NA}DNMT1 cells. The graph shows the mean of 3 independent experiments. The error bars represent the standard error of the mean, SEM. At least 20 mitoses for each condition and each replica were evaluated. Unpaired t-test between the samples: **** < 0.0001. **F** Graph shows no variation on the gene

expression of CENP-E in 1, 4 and 7 days IAA treated DLD-1 ^{NA}DNMT1 cells. **G** Immunoblotting for CENP-E in untreated and 1, 4 and 7 days IAA treated DLD-1 ^{NA}DNMT1 cells. **H** Graph summarising the results in G reveals no statistical significance at all timepoints in IAA treated DLD-1 ^{NA}DNMT1 cells. The graph shows the mean of 3 independent experiments. The error bars represent the standard error of the mean, SEM. Unpaired t-test between the samples: ns > 0.05.

4.5 DNMT1 inducible degradation does not impair the SAC

Since DLD-1 cells fail to establish the right conditions to segregate the chromosomes, which results in aneuploidy generation, SAC disfunction was reasoned. Thus, the cells were treated with nocadozole to trigger the checkpoint and an immunostaining for MAD1 at the 4th and 7th days of IAA treatment was performed. A significant yet only slight variability was observed: at 4 days there is a 15% increase, while at 7 days there is a reduction of less than 10% in respect to the control (Figure 7A-B). To evaluate further the eventual SAC impairment, MAD2 in both asynchronous and colcemid-synchronized cell population at different timepoints upon IAA treatment was analysed (Figure 7C-D and Supp. Figure 6E-F). No change in any of these conditions was observed. These results suggested that DNMT1 absence and loss of DNA methylation did not impair SAC proteins MAD1 or MAD2 functions.

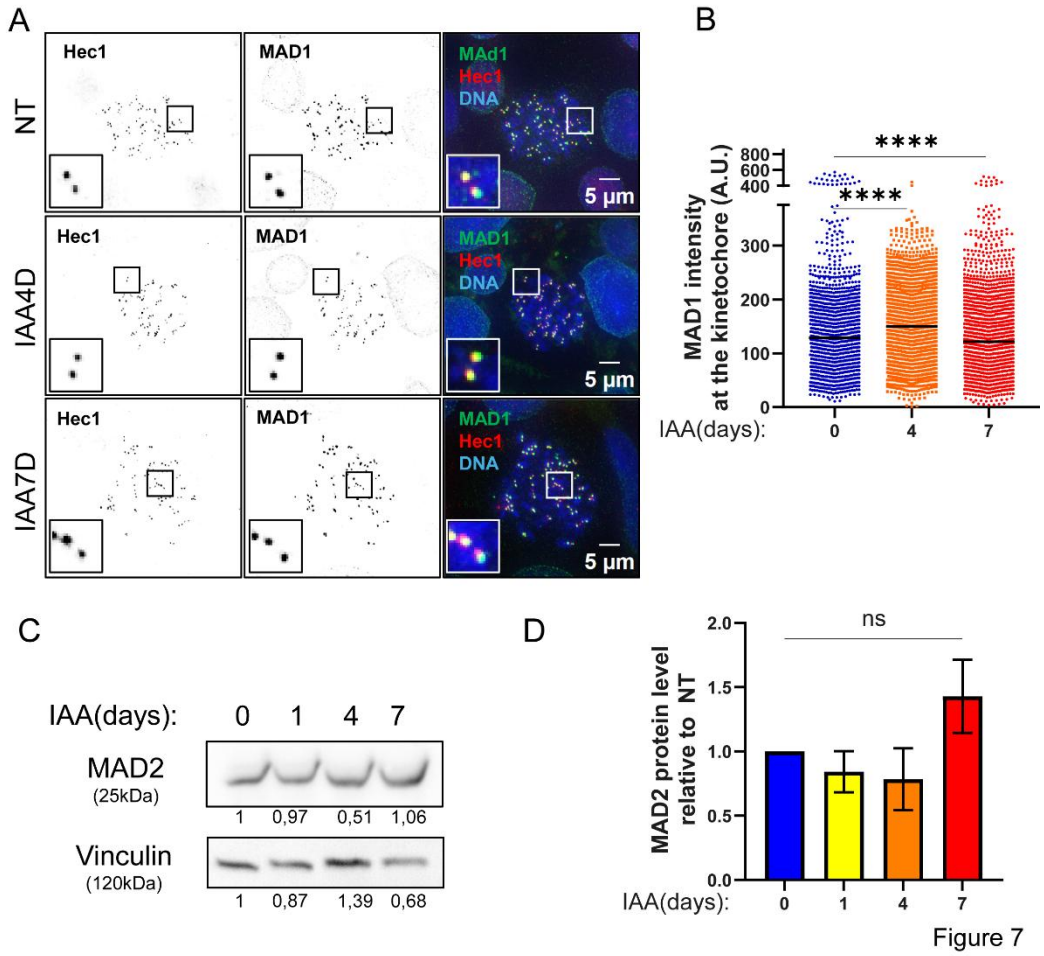

Figure 7

(Previous page) Figure 7: Loss of DNMT1 or DNA methylation does not impair SAC activity. **A** Immunostaining of MAD1 in the untreated, 4 days and 7 days IAA-treated DLD-1 ^{NA}DNMT1 cells **B** Graph summarising the results in A. The graph shows the mean of 3 independent experiments. The error bars represent the standard error of the mean, SEM. At least 650 spots for each condition and each replicate were analysed. Unpaired t-test between the samples: **** < 0.0001. **C** Immunoblot of MAD2 in untreated, 1 day, 4 days and 7 days IAA treated DLD-1 ^{NA}DNMT1 cells. **D** Graph showing the results of C as the mean of 3 independent experiments. The error bars represent the standard error of the mean, SEM. Unpaired t-test between the samples: **** < 0.0001; ns > 0.05.

4.6 DNMT1 inducible degradation alters Aurora B recruitment

The observed alteration of the kinetochore-microtubule interaction could suggest that Aurora B kinase, which is involved in the regulation of the attachments, may be altered.

To evaluate this, Aurora B protein level was analysed and a slight reduction was observed (average 20%) upon IAA treatment (Figure 8A-B). The same analysis performed on MG132 or colcemid-synchronised cells confirmed the reduction up to 7 days of IAA treatment, however, at 10 days Aurora B level came back to the one of the untreated conditions (Figure 8C-D and Supp. Figure 7A-B).

The observed reduction of Aurora B during 7 days of IAA treatment suggested the idea that the correction of improper kinetochore-microtubule attachments could be inaccurate in DNMT1-degraded cells, leading to aneuploidy. To confirm such hypothesis, the localisation of Aurora B and its scaffold protein INCENP onto mitotic chromosomes after treatment with colcemid were analysed (Figure 8E and 8H). No changes in the number of chromosomes stained with Aurora B or INCENP upon 10 days of IAA treatment were observed (Supp. Figure 7C and Figure 8H). However, the immunofluorescence experiment revealed that Aurora B intensity was increased at the centromere in IAA treated cells in comparison with the untreated cells (Figure 8F), which would suggest an enhancing of error correction.

To confirm that the highly recruited Aurora B was actually functional, the phosphorylation of one of its main targets Serine55 of Hec1 was evaluated.

To check this, immunoblot in both colcemid-synchronised and asynchronous populations was performed. Since colcemid depolymerizes microtubules, no attachments and alignment of chromosomes are present, thus, this condition allows measurement of Hec1 S55p level at the entry in mitosis. When the Hec1 S55p signals of IAA-treated population was compared with the colcemid-treated NT, an increase was observed at every analysed time point, except for the 4 days IAA treatment, probably due to technical issues (Figure 9A-B and Supp. Figure 7E). To further understand the dynamics of Hec1 S55p, a western blot assay of asynchronous populations at

different time points (Figure 9C) and the MG132-synchronised populations at 10 days of IAA treatment (Figure 9E) were performed. In both these conditions, the tubulin is able to interact with the kinetochore and chromosomes will reach the metaphase plate. Also, when MG132 is administered, the cells arrest in metaphase 3h, having more time to correct the errors. The analyses revealed that Hec1 S55p was increased, though not significantly in the asynchronous population (Figure 9D and Supp. Figure 7F). When MG132 is present, Hec1 S55p is reduced in IAA-treated cells to the levels of the untreated condition (Figure 9F and Supp. Figure 7D). Since the amount of mitotic cells could influence the protein level of Hec1 S55p, the mitotic index and the percentage of cells at metaphase in the MG132-treated population were evaluated. The number of mitoses ~~is~~ was not significantly altered (Supp. Figure 7G-H-I). Altogether, these results show that Aurora B is increased in both the recruitment at the centromere and the phosphorylation activity on Hec1 S55 upon DNMT1 prolonged absence.

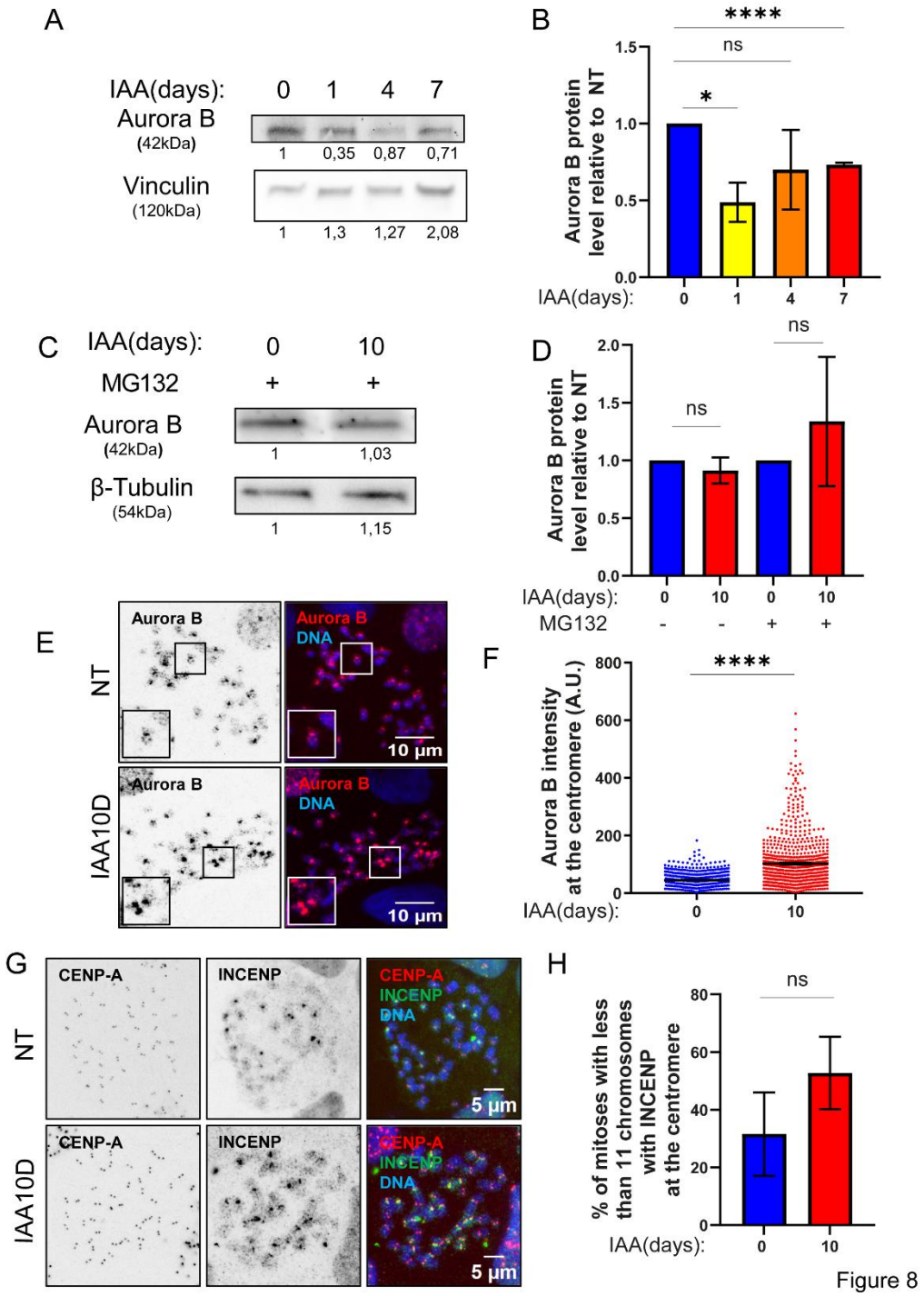

Figure 8

Figure 8: Loss of DNMT1 or DNA methylation alters Aurora B kinase. **A** Immunoblot of Aurora B kinase in untreated, 1 day, 4 days and 7 days IAA treated DLD-1 ^{NA}DNMT1 cells. **B** Graph summarizing the results in E, shows Aurora B protein reduction at the first and at the 7th days of IAA treatment. The graph shows the mean of 3 independent experiments. The error bars represent the standard error of the mean, SEM. Unpaired t-test between the samples: **** < 0.0001; * ≤ 0.05; ns > 0.05. **C** Immunoblot of Aurora B in the untreated, and 10 days IAA treated DLD-1 ^{NA}DNMT1 cells synchronised in mitosis with MG132. **D** Graph shows no change on the Aurora B protein levels at 10 days of IAA treatment in asynchronised and MG132 synchronised cells. The graph shows the mean of 3 independent experiments. The error bars represent the standard error of the mean, SEM. Unpaired t-test between the samples: ns > 0.05. **E** Immunostaining of Aurora B kinase in untreated and 10 days IAA treated DLD-1 ^{NA}DNMT1 cells. **F** Graph showing the results of E reveals increase of Aurora B intensity at the centromere upon IAA treatment in DLD-1 ^{NA}DNMT1 cells. The Aurora B intensity was taken by using a big circle spot that includes CENP-A doublets. CENP-A was used as centromeric marker. The graph shows the mean of 3 independent experiments. The error bars

represent the standard error of the mean, SEM. At least 200 spots for each condition and each replicate were evaluated. Unpaired t-test between the samples: **** < 0.0001. G Immunostaining of INCENP in untreated and 10 days IAA treated DLD-1 ^{NA}DNMT1 cells. **H** Graph summarizing the results in G. The cutoff number of chromosomes was established as the mode number of chromosomes decorated with INCENP in the untreated condition. The graph shows the mean of 4 independent experiments. The error bars represent the standard error of the mean, SEM. At least 20 mitoses for each condition and each replica were evaluated. Unpaired t-test between the samples: ns > 0.05.

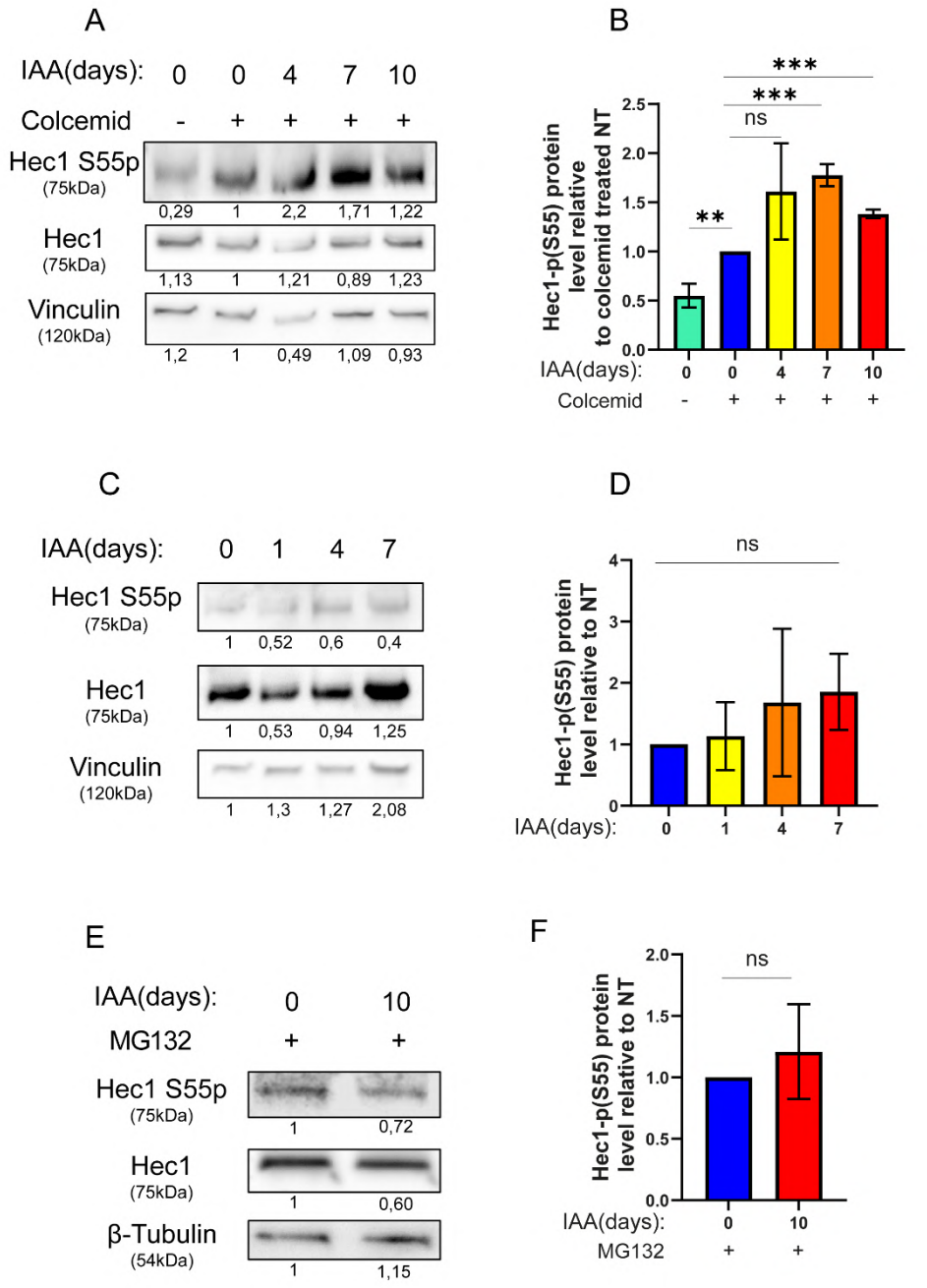

Figure 9

Figure 9: Loss of DNMT1 and DNA methylation alters Hec1 phosphorylation dynamics. **A** Immunoblot of Hec1 S55p and Hec1 in asynchronous untreated DLD-1 ^{NA}DNMT1 cells and colcemid-synchronized population of untreated, 4 days, 7 days and 10 days of IAA treated DLD-1 ^{NA}DNMT1 cells. **B** Graph summarising the results in A reveals the increase of Hec1 S55p at 7 and 10 days of IAA treatment in DLD-1 ^{NA}DNMT1 cells synchronised with colcemid. The graph shows the mean of 3 independent experiments. The error bars represent the standard error of the mean, SEM. Unpaired t-test between the samples: ** <0.001, * ≤ 0.05; ns > 0.05. **C** Immunoblot of Hec1 S55p and Hec1 in

untreated, 1 days, 4 days and 7 days IAA treated DLD-1 ^{NA}DNMT1 cells. **D** Graph summarising the results in C. The graph shows the mean of 3 independent experiments. The error bars represent the standard error of the mean, SEM. Unpaired t-test between the samples: ns > 0.05. **E** Immunoblot of Hec1 S55p and Hec1 in untreated, and 10 days IAA treated DLD-1 ^{NA}DNMT1 cells synchronised with MG132. **F** Graph summarising the results in E. The graph shows the mean of 3 independent experiments. The error bars represent the standard error of the mean, SEM. Unpaired t-test between the samples: ns > 0.05.

4.7 DNMT1 presence and DNA methylation loss improve error correction efficiency

The obtained data showed that DNMT1 prolonged degradation enhanced the stability of the existing kinetochore-microtubule attachments. However, it also sensitised the cells to microtubule depolymerization (colcemid treatment) with increased Aurora B recruitment and activity (Hec1 phosphorylation), which could suggest that microtubule dynamics is the key threat of this altered condition. If this is the case, IAA treatment should cause misaligned chromosomes rather than lagging chromosomes. To confirm this hypothesis, mitotic errors were checked focusing on lagging chromosomes in both IAA treated cells and DNMT1 rescued cells where IAA washout (WO) was performed (Supp. Figure 8A). As expected, no change in the percentage of mitotic cells characterised by lagging chromosomes was observed, confirming the results obtained with the observation of micronuclei (Supp. Figure 8B-C and Supp. Figure 2D). Then, misaligned chromosomes were evaluated, the percentage of cells with misaligned chromosomes were increased up to about 40% in the IAA treated cells, while reduced though not significantly in the DNMT1-rescued cells (WO) (Figure 10A-B). This observation confirmed that DNMT1 absence caused problems in chromosome congression. It remained unclear whether DNA methylation is involved as well in this process.

The recruitment of both Hec1 S55p and Aurora B at the misaligned chromosomes were analysed. At misaligned chromosomes, Hec1 S55p was higher in both IAA-treated and the DNMT1-rescued cells (Figure 10C-D). On the contrary, Aurora B intensity at errors did not significantly change either in the IAA-treated or in the DNMT1-rescued cells (Figure 10C-E). To further characterise Aurora B activity, the ratio between the intensity of Aurora B and Hec1 S55p signals at the errors was graphed. The graph shows a significant reduction of the ratio between Aurora B and Hec1 S55p at the IAA-treated and DNMT1-rescued cells (Figure 10F). Altogether, these results show that the cells tried to correct the misaligned chromosomes - caused by DNMT1 prolonged degradation - by activating Hec1 S55 phosphorylation, which likely is Aurora B-dependent.

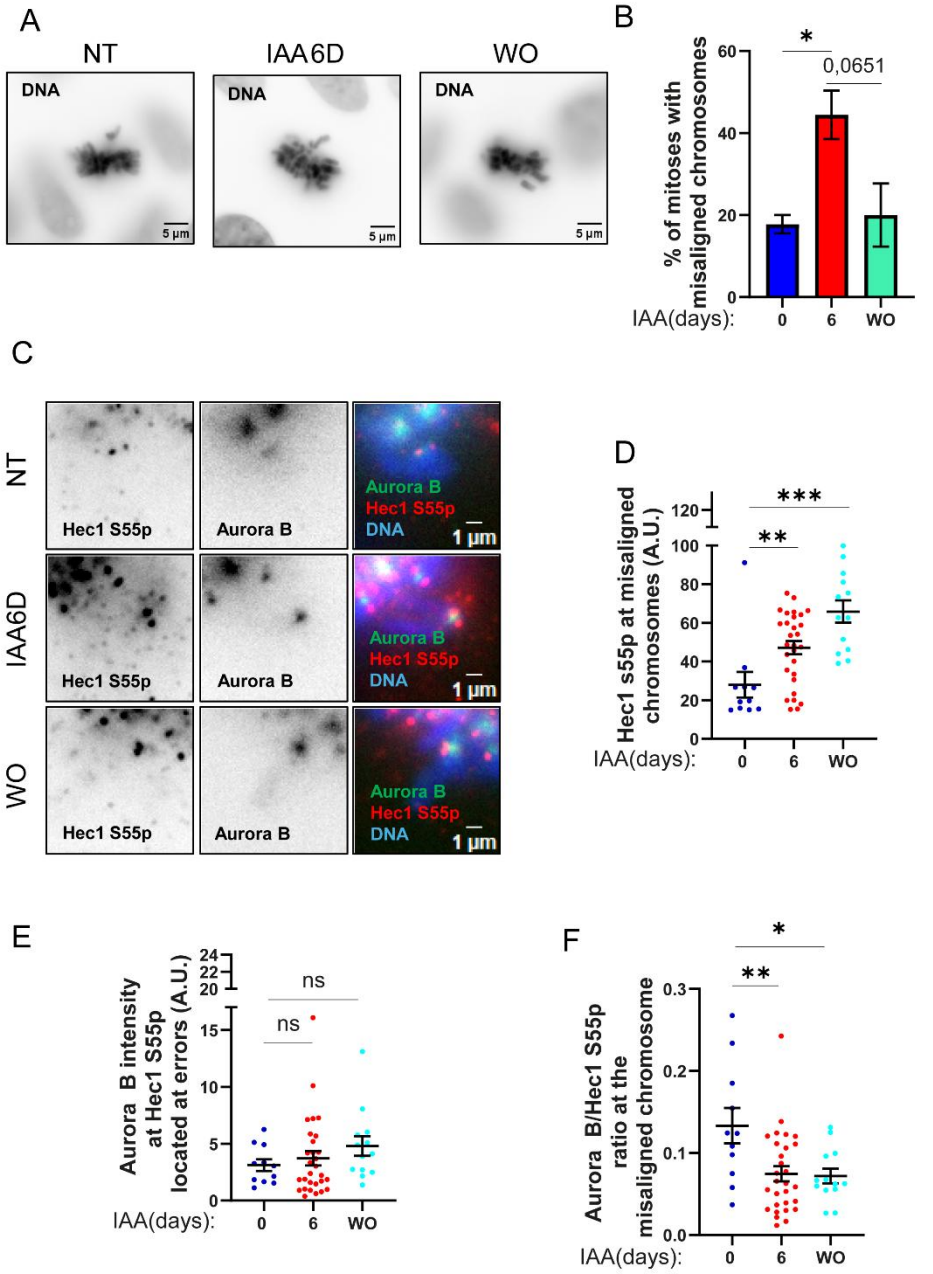

Figure 10

Figure 10: DNA methylation alters the Aurora B / Hec1 S55p ratio at the mitotic errors. **A** DAPI staining to evaluate the percentage of mitoses with misaligned chromosomes in untreated, 6 days IAA treated and 2 days DNMT1-rescued (WO) DLD-1 ^{NA}DNMT1 cells. **B** Graph summarising the results in A, reveals a rescue of errors upon DNMT1 restoration. The graph shows the mean of 3 independent experiments. The error bars represent the standard error of the mean, SEM. At least 15 mitoses for each condition and each replicate were evaluated. Unpaired t-test between the samples: * ≤ 0.05; P = 0,0651. **C** Immunostaining of Hec1 S55p and Aurora B in the misaligned chromosomes of untreated, 6 days IAA treated and WO DLD-1 ^{NA}DNMT1 cells. **D** Graph summarising the results in C shows the increase of Hec1 S55p at the misaligned chromosomes of 6 days IAA treated or DNMT1-rescued DLD-1 ^{NA}DNMT1 cells. The graph shows the mean of 3 independent experiments. The error bars represent the standard error of the mean, SEM. All the available spots for each condition and each replicate were evaluated. Unpaired t-test between the samples: *** < 0.01; ** < 0.1. **E** Graph summarising the results in C, shows no Aurora B intensity change at the

kinetochore complex. The graph shows the mean of 3 independent experiments. The error bars represent the standard error of the mean, SEM. All the available spots for each condition and each replicate were evaluated. Unpaired t-test between the samples: ns > 0.05. **F** Graph summarising the results in C shows a decrease in Aurora B/Hec1 S55p ratio in at the misaligned chromosomes of 6 days IAA treated or DNMT1-rescued DLD-1 ^{NA}DNMT1 cells. The graph shows the mean of 3 independent experiments. The error bars represent the standard error of the mean, SEM. All the available spots for each condition and each replicate were evaluated. Unpaired t-test between the samples: ** < 0.01; * ≤ 0.05.

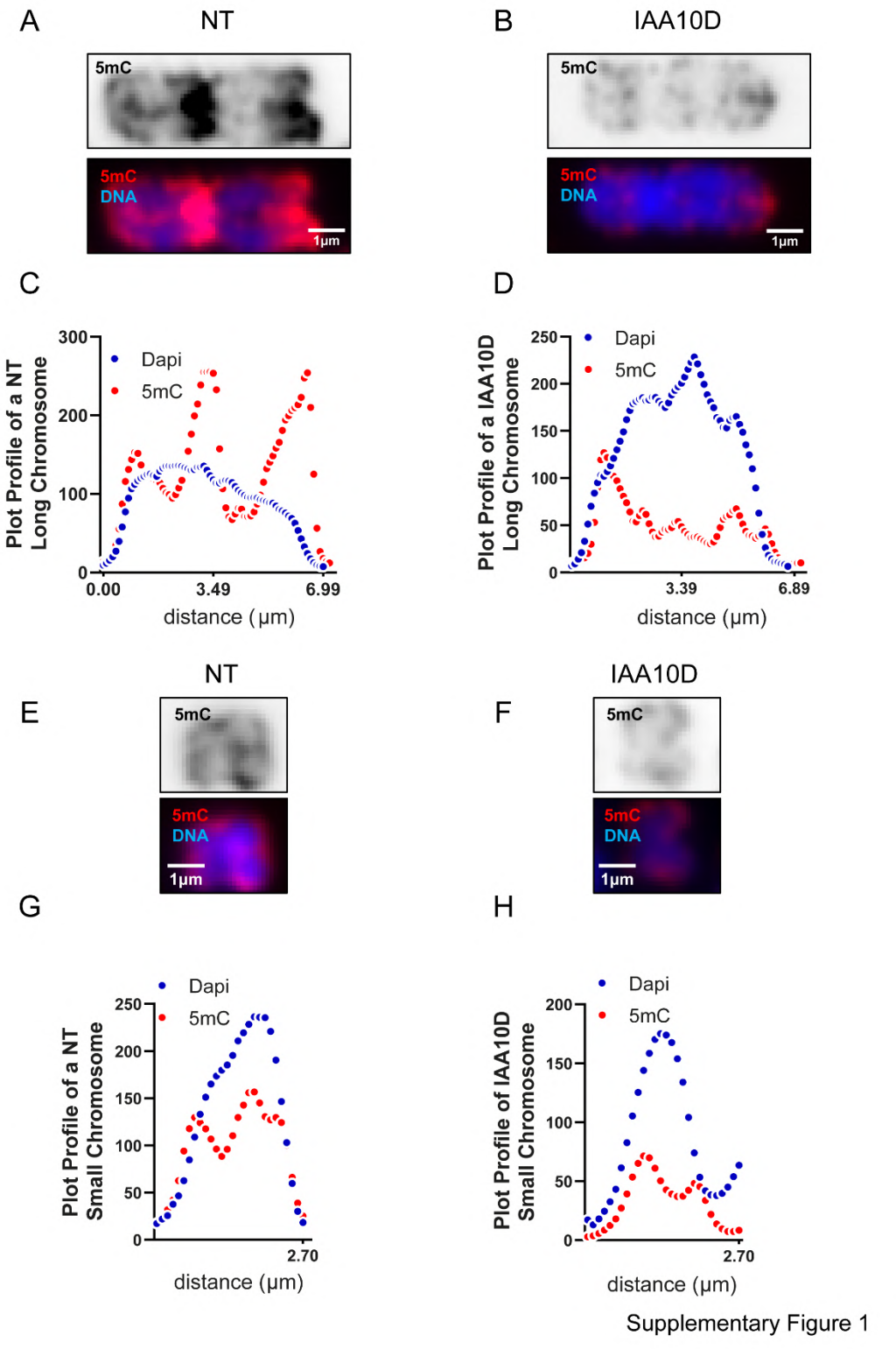

Supplementary Figure 1: **A** 5mC Immunostaining on a long chromosome of untreated DLD-1 ^{NA}DNMT1. **B** -5mC immunostaining on a long chromosome of 10 days IAA treated DLD-1 ^{NA}DNMT1. **C** Graph showing the plot profile of the-5mC at the chromatid of the selected untreated long chromosome. **D** Graph showing the plot profile of the 5mC at the chromatid of the selected IAA treated long chromosome. **E**-5mC immunostaining on a short chromosome of untreated DLD-1 ^{NA}DNMT1. **F** –5mC immunostaining on a short chromosome of 10 days IAA treated DLD-1 ^{NA}DNMT1. **G** Graph showing the plot profile of the–5mC at the chromatid of the selected untreated short chromosome. **H** Graph showing the plot profile of the–5mC at the chromatid of the selected IAA treated short chromosome.

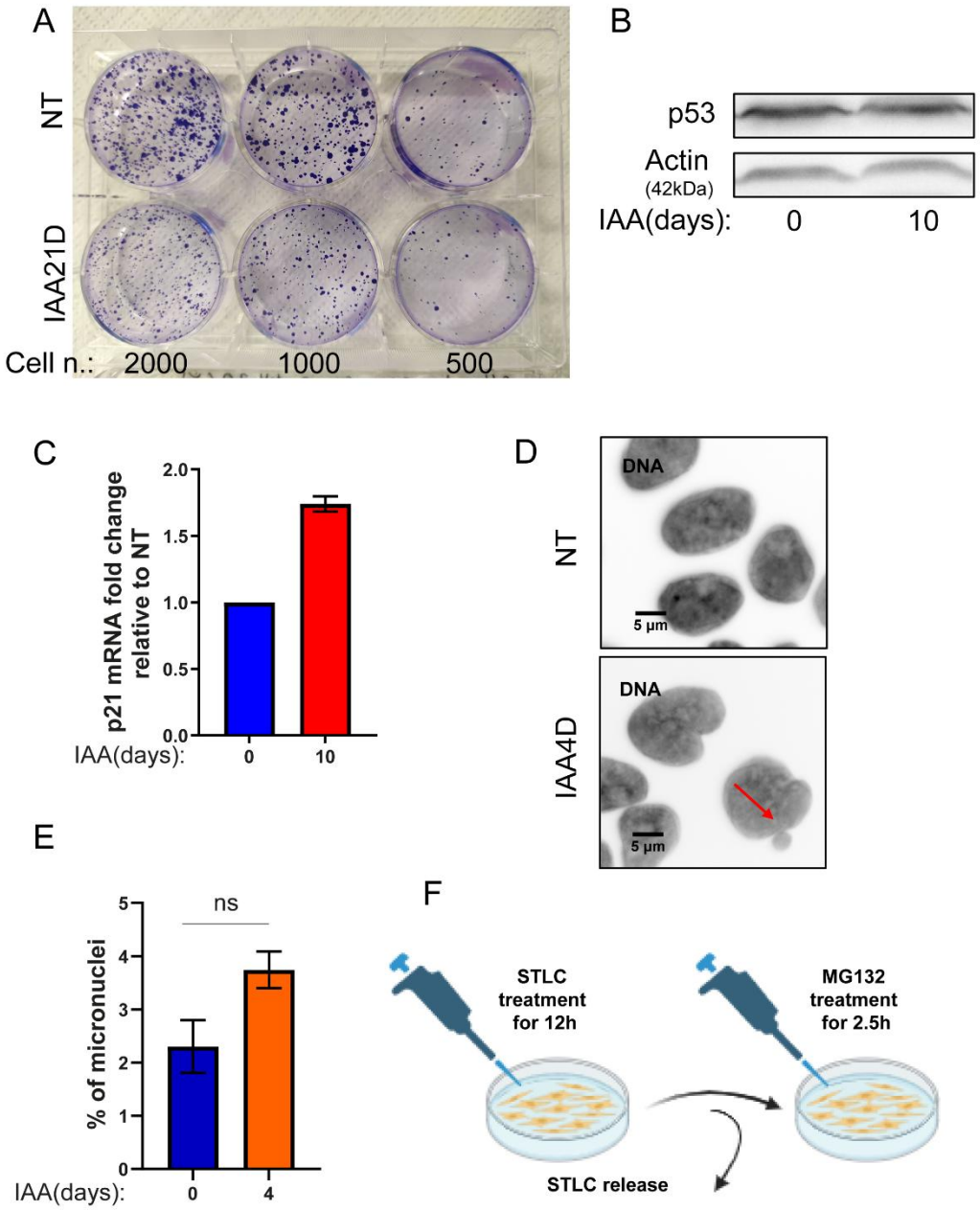

Supplementary Figure 2

Supplementary Figure 2: **A** Colony assay shows that a prolonged ^{NA}DNMT1 absence upon 21 days of IAA treatment impairs colony formation in DLD-1 ^{NA}DNMT1 cells. The experiment has been performed in 3 replicates. Number of seeded cells: 2000, 1000, and 500. **B** Immunoblot of p53 in untreated and 10 days of IAA treated DLD-1 ^{NA}DNMT1. **C** Graph showing p21 mRNA fold change upon 10 days of IAA treatment in DLD-1 ^{NA}DNMT1. The graph shows the mean of 2 independent experiments. The error bars represent the standard error of the mean, SEM. **D** DAPI staining to evaluate micronuclei formation upon 4 days of IAA treatment in DLD-1 ^{NA}DNMT1. **E** Graph summarising the results in E, shows no significant increase of micronuclei upon 4 days of IAA treatment in DLD-1 ^{NA}DNMT1 cells. The graph shows the mean of 3 independent experiments. The error bars represent the standard error of the mean, SEM. At least 190 nuclei for each condition and each replica were evaluated. Unpaired t-test between samples: ns > 0.05. **F** The representative image displays how STLC treatment and release into MG132 experiments were performed. The image was created in https://BioRender.com.

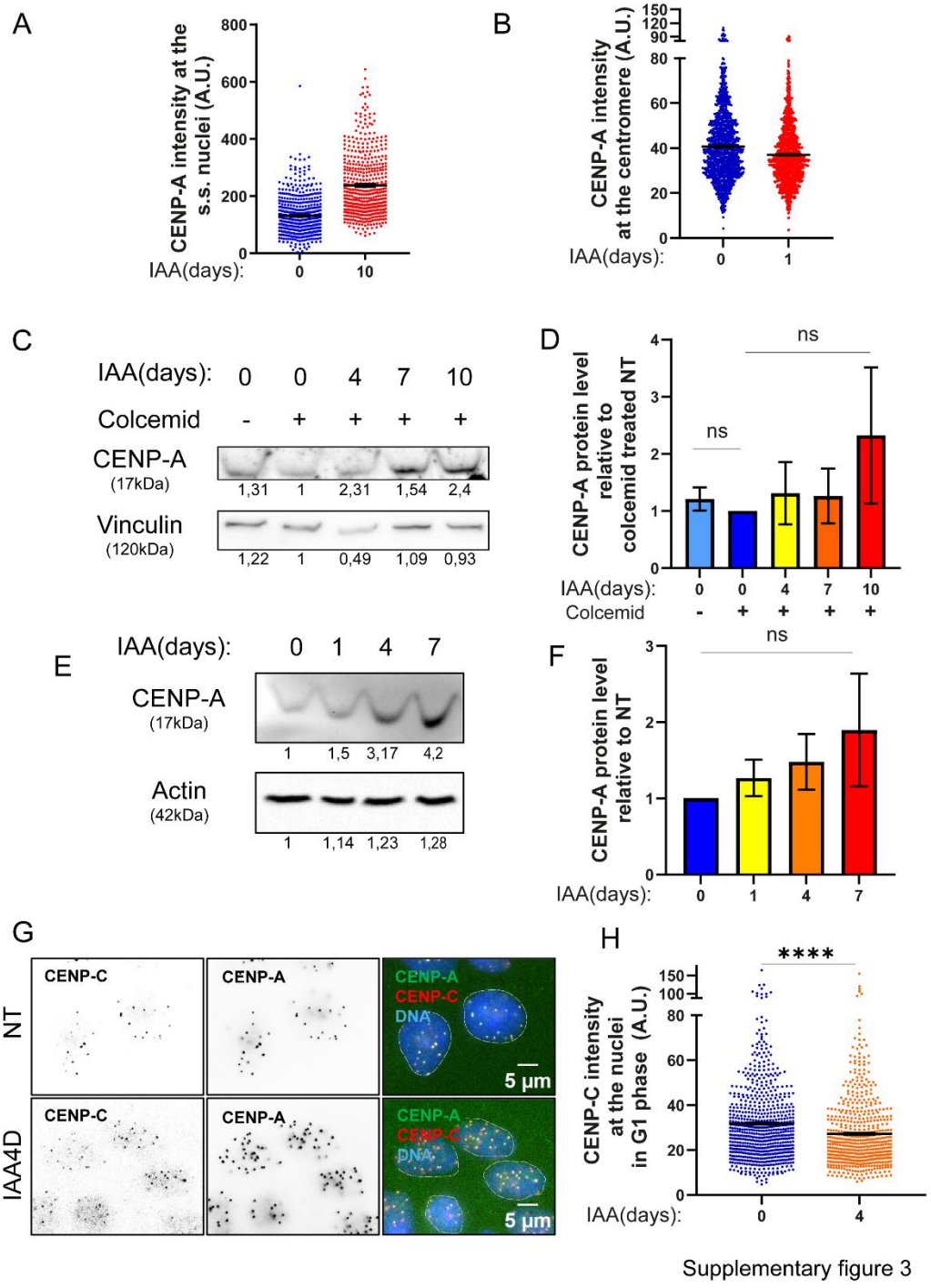

Supplementary figure 3

Supplementary Figure 3: **A** Graph reveals an increase of CENP-A intensity at the serum starved (s.s.) nuclei upon 10 days of IAA treatment in DLD-1 ^{NA}DNMT1 cells. The graph shows the mean of 1 independent experiment. At least 480 spots were evaluated. **B** Graph reveals a slightly decrease of CENP-A intensity at the centromere upon 1 days of IAA treatment in DLD-1 ^{NA}DNMT1 cells. The graph shows the mean of 2 independent experiments. The error bars represent the standard error of the mean, SEM. At least 700 spots for each condition and each replica were evaluated. **C** Immunoblot of CENP-A in asynchronous untreated DLD-1 ^{NA}DNMT1 cells and colcemid synchronized population of untreated, 4 days, 7 days and 10 days of IAA treated DLD-1 ^{NA}DNMT1 cells. **D** Graph summarizing the result in C, reveals no significant difference in the levels of CENP-A protein at any timepoints in DLD-1 ^{NA}DNMT1 cells. The graph shows the mean of 3 independent experiments. The error bars represent the standard error of the mean, SEM. Unpaired t-test between the samples: ns > 0.05. **E** Immunoblot of CENP-A in untreated, 1 day, 4 days and 7 days IAA treated DLD-1 ^{NA}DNMT1 cells. **F** Graph summarizing the result in D reveals no significant difference in the levels of

CENP-A protein at any timepoints in DLD-1 ^{NA}DNMT1 cells. The graph shows the mean of 3 independent experiments. The error bars represent the standard error of the mean, SEM. Unpaired t-test between the samples: ns > 0.05. **G** Immunostaining of CENP-C and CENP-A at the interphase nuclei in the untreated and 4 days IAA treated DLD-1 ^{NA}DNMT1 cells. H Graph showing the results of H reveals that CENP-C is reduced at the centromere of 4 days IAA treated DLD-1 ^{NA}DNMT1 nuclei. The graph shows the mean of 3 independent experiments. The error bars represent the standard error of the mean, SEM. At least 250 spots for each condition and each replica were evaluated. Unpaired t-test between the samples: **** < 0.0001.

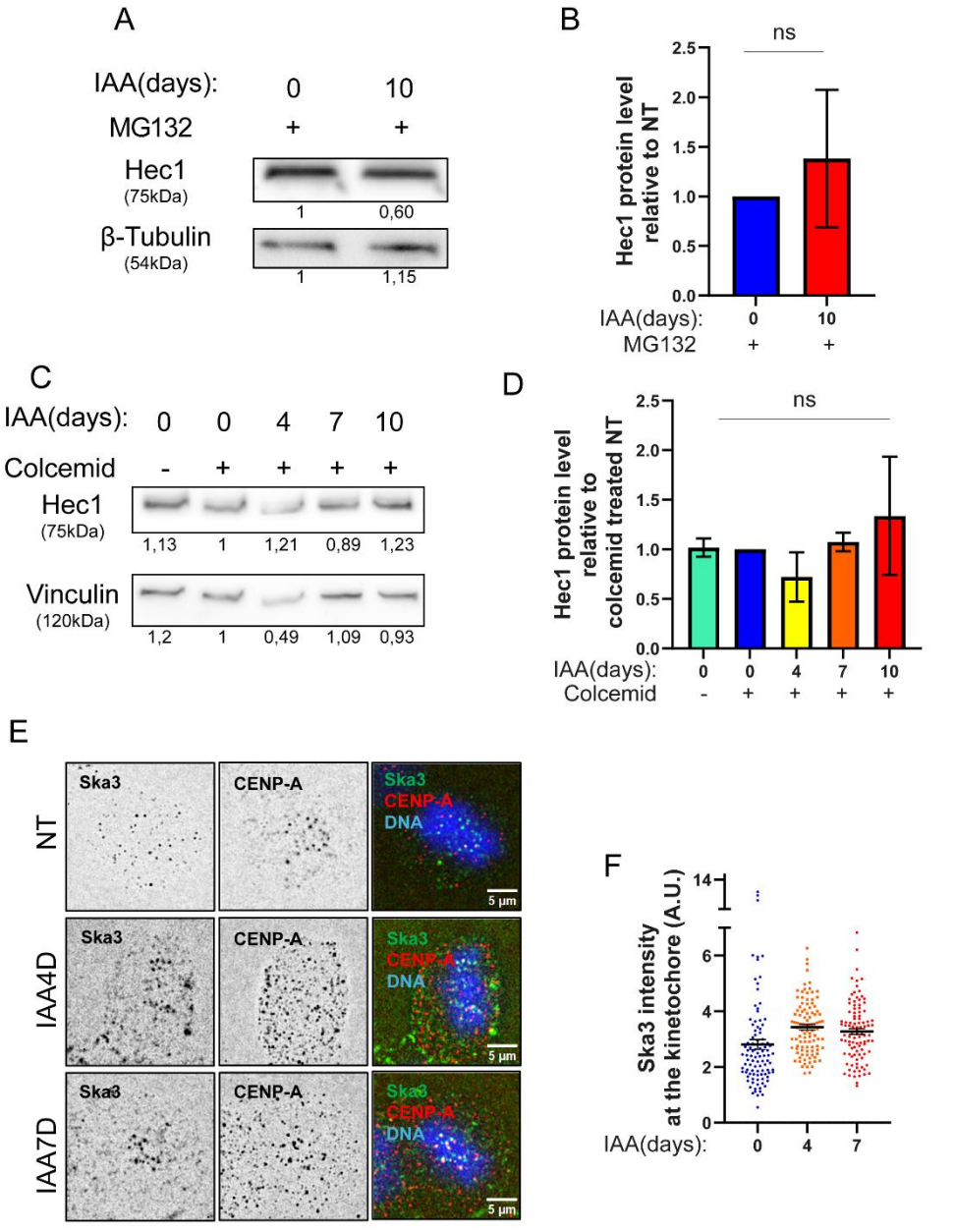

Supplementary Figure 4

Supplementary Figure 4: **A** Immunoblot of Hec1 in untreated and 10 days of IAA treatment in DLD-1 ^{NA}DNMT1 cells synchronized with MG132 **B** Graph summarising the results in A, shows no change on Hec1 protein amount. The graph shows the mean of 3 independent experiments. The error bars represent the standard error of the mean, SEM. Unpaired t-test between the samples: ns > 0.05. **C** Immunoblot of Hec1 in asynchronous untreated DLD-1

[NA]DNMT1 cells and colcemid synchronized population of untreated, 4 days, 7 days and 10 days of IAA treatment. **D** Graph summarising the results in C. The graph shows the mean of 3 independent experiments. The error bars represent the standard error of the mean, SEM. Unpaired t-test between the samples: ns > 0.05. **E** Immunostaining of CENP-A and Ska3 in untreated, 4 days and 7 days of IAA treatment in DLD-1 [NA]DNMT1 cells. **F** Graph summarising the results in E reveals an increase in Ska3 recruitment at the centromeric region. The graph shows the mean of 1 independent experiment. The error bars represent the standard error of the mean, SEM. At least 150 spots were evaluated.

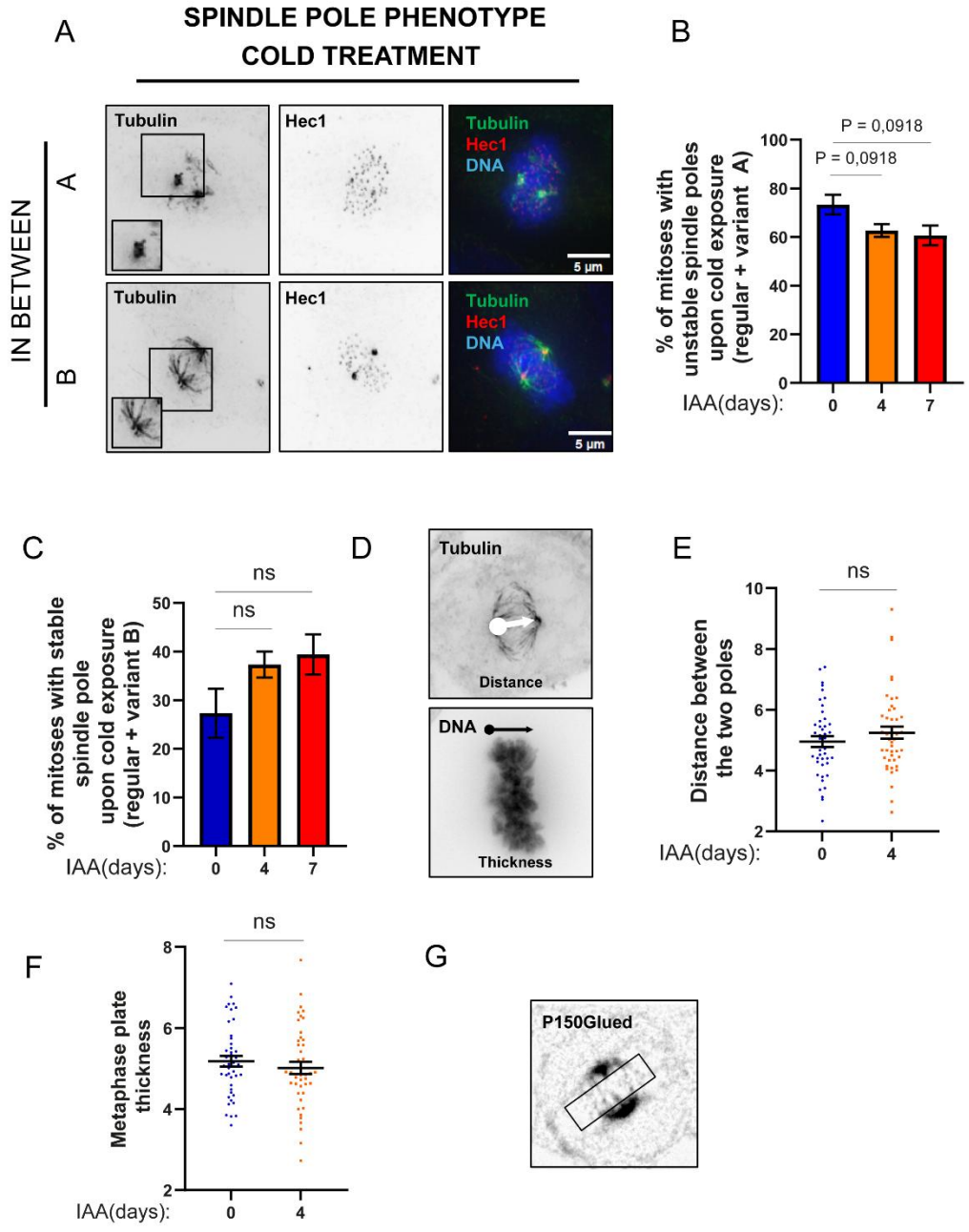

Supplementary Figure 5

Supplementary Figure 5: **A** Immunostaining of Tubulin and Hec1 upon cold exposure, reveals partially stable and partially unstable spindle pole phenotype in DLD-1 [NA]DNMT1 cells: VARIANT A, the pole is present, but the mitotic spindle is not connected to it; VARIANT B, the spindle binds the pole even if not in a disk shape. **B** Graph showing the results of Figure 5C unstable phenotype together with the partially variant A, reveals that the spindle poles do not

change in stability at the 4 days and 7 days IAA treated DLD-1 ^{NA}DNMT1 cells. The graph shows the mean of 3 independent experiments. The error bars represent the standard error of the mean, SEM. At least 25 mitoses for each condition and each replica were evaluated. Unpaired t-test between the samples: ns > 0.05. **C** Graph showing the results of Figure 5C stable phenotype together with the partially variant B, reveals that the spindle poles do not change in stability at the 4 days and 7 days IAA treated DLD-1 ^{NA}DNMT1 cells. The graph shows the mean of 3 independent experiments. The error bars represent the standard error of the mean, SEM. At least 25 mitoses for each condition and each replica were evaluated. Unpaired t-test between the samples: ns > 0.05. **D** Immunostaining for tubulin to evaluate the distance between the poles and the metaphase plate thickness upon cold treatment in untreated and IAA treated DLD-1 ^{NA}DNMT1 cells. **E** Graph summarising the results in A reveals no change in the distance between the poles at 4 days of IAA treatment in DLD-1 ^{NA}DNMT1 cells. The graph shows the mean of 3 independent experiments. The error bars represent the standard error of the mean, SEM. At least 15 mitoses for each condition and each replicate were evaluated. Unpaired t-test between the samples: ns > 0.05. **F** Graph summarising the results in A reveals no change in the metaphase plate thickness at 4 days of IAA treatment in DLD-1 ^{NA}DNMT1 cells. The graph shows the mean of 3 independent experiments. The error bars represent the standard error of the mean, SEM. At least 15 mitoses for each condition and each replicate were evaluated. Unpaired t-test between the samples: ns > 0.05. **G** Representative image to shows how the quantification of P150Glued at the metaphase plate was performed. The used ROI is located between the two poles.

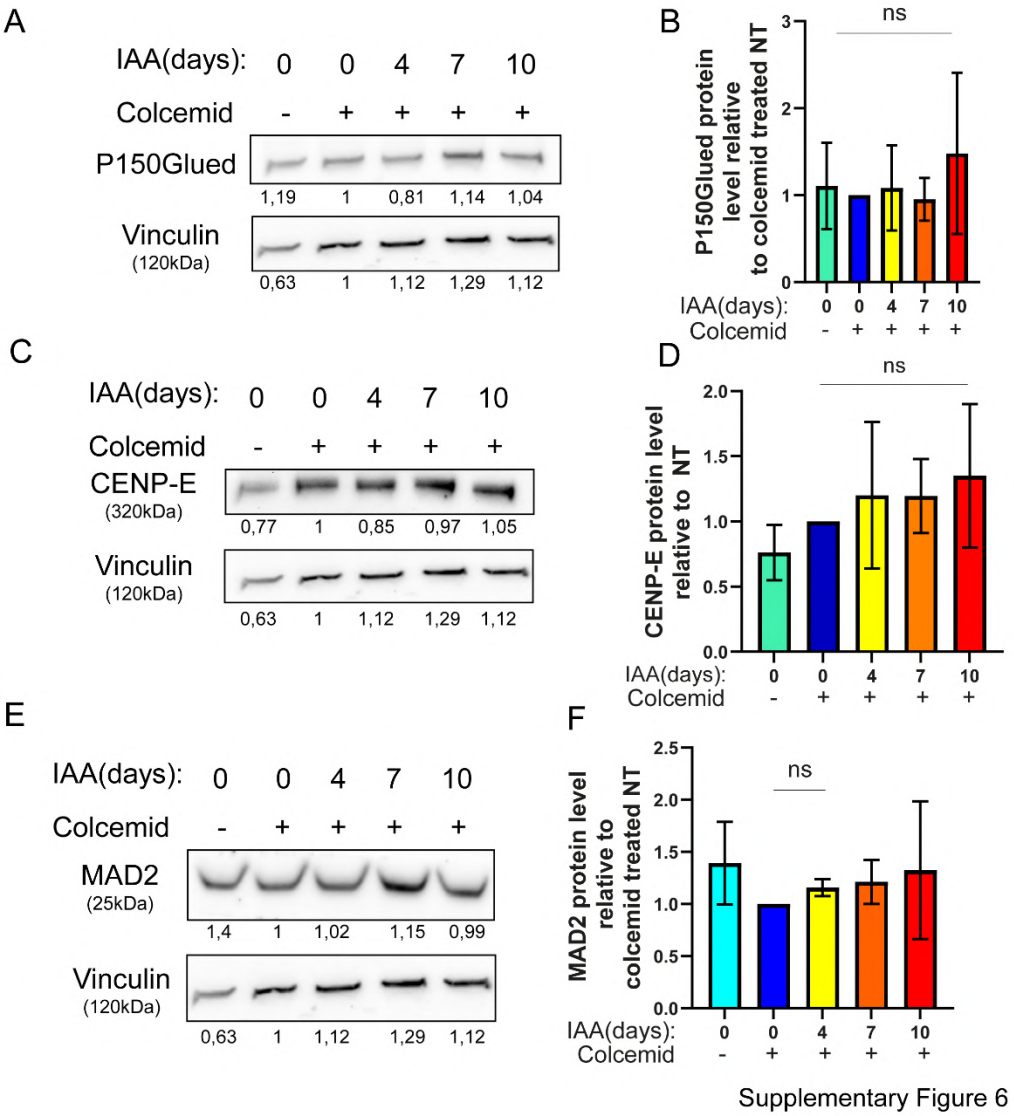

Supplementary Figure 6

Supplementary Figure 6: **A** Immunoblot for P150Glued in asynchronous untreated DLD-1 ^{NA}DNMT1 cells and colcemid synchronized population of untreated, 4 days, 7 days and 10 days of IAA treated DLD-1 ^{NA}DNMT1 cells. **B** Graph summarising the results in D reveals no statistical relevance at all time points in DLD-1 ^{NA}DNMT1 cells synchronised with colcemid. The graph shows the mean of 3 independent experiments. The error bars represent the standard error of the mean, SEM. Unpaired t-test between the samples: ns > 0.05. **C** Immunoblot for CENP-E in

asynchronous untreated DLD-1 ^{NA}DNMT1 cells and colcemid synchronized population of untreated, 4 days, 7 days and 10 days of IAA treated DLD-1 ^{NA}DNMT1 cells. **D** Graph summarising the results in F reveals no statistical relevance in DLD-1 ^{NA}DNMT1 cells synchronised with colcemid. The graph shows the mean of 3 independent experiments. The error bars represent the standard error of the mean, SEM. Unpaired t-test between the samples: ns > 0.05. **E** Immunoblot for MAD2 in asynchronous untreated DLD-1 ^{NA}DNMT1 cells and colcemid synchronized population of untreated, 4 days, 7 days and 10 days of IAA treated DLD-1 ^{NA}DNMT1 cells. **F** Graph summarising the results in H reveals no statistical relevance at any time point in DLD-1 ^{NA}DNMT1 cells synchronised with colcemid. The graph shows the mean of 3 independent experiments. The error bars represent the standard error of the mean, SEM. Unpaired t-test between the samples: ns > 0.05.

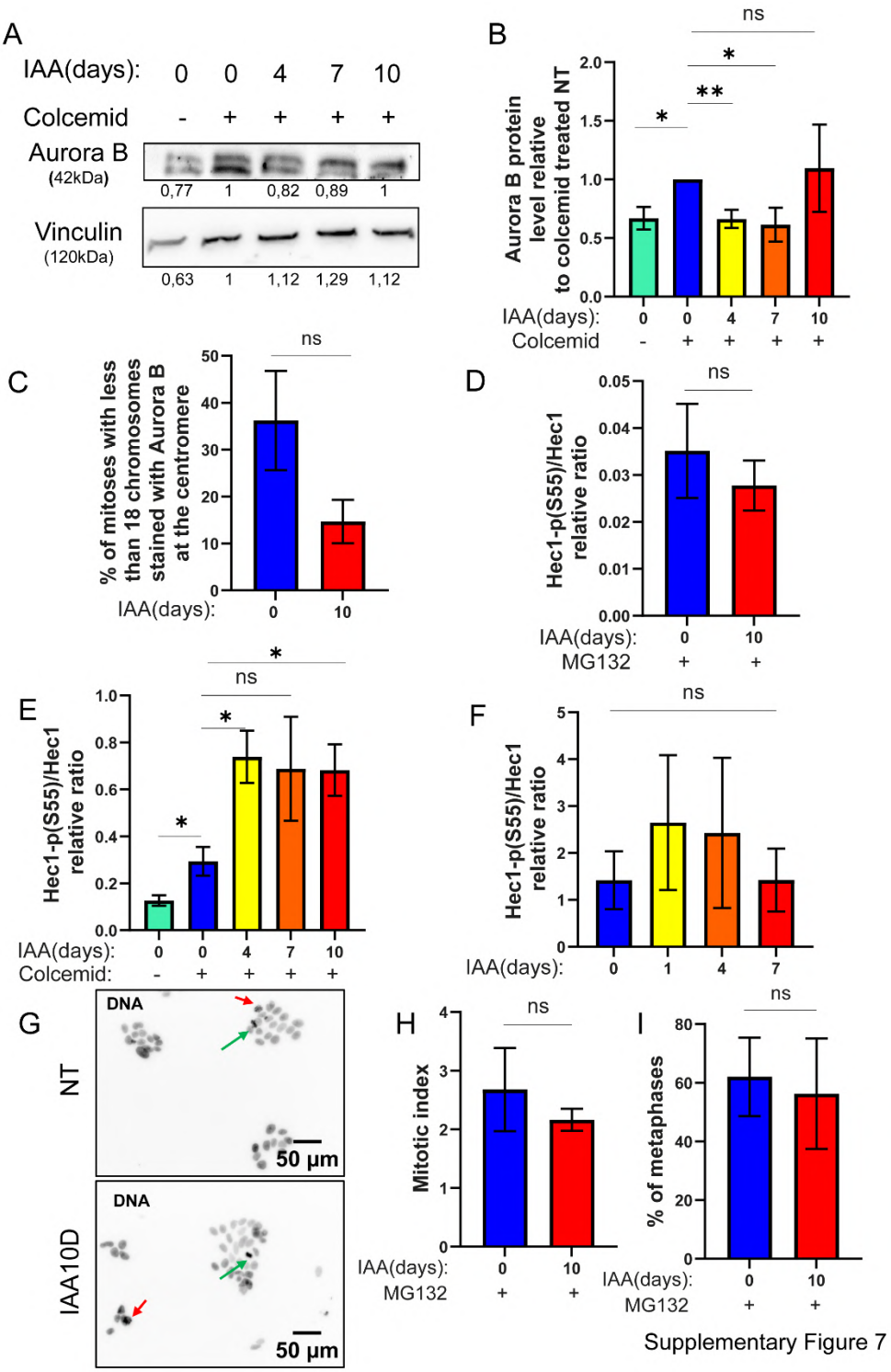

Supplementary Figure 7

Supplementary Figure 7: **A** Immunoblot of Aurora B in asynchronous untreated DLD-1 ^{NA}DNMT1 cells and colcemid synchronized population of untreated, 4 days, 7 days and 10 days of IAA treated DLD-1 ^{NA}DNMT1 cells. **B** Graph

summarising the results in A reveals the reduction of Aurora B at 4 and 7 days of IAA treatment in DLD-1 ^{NA}DNMT1 cells synchronised with colcemid. The graph shows the mean of 3 independent experiments. The error bars represent the standard error of the mean, SEM. Unpaired t-test between the samples: ** <0,001, * ≤ 0.05; ns > 0.05. **C** Graph summarizing the results in Figure 8 E. The cutoff number of chromosomes was established as the mode number of chromosomes decorated with Aurora B in the untreated condition. The graph shows the mean of 3 independent experiments. The error bars represent the standard error of the mean, SEM. At least 20 mitoses for each condition and each replica were evaluated. Unpaired t-test between the samples: ns > 0.05. **D** Graph summarising the result in Fig 9E shows no change in Hec1p/Hec1 ratio. The graph shows the mean of 3 independent experiments. The error bars represent the standard error of the mean, SEM. Unpaired t-test between the samples: ns > 0.05. **E** Graph, summarising the result in Fig. 9A shows the increase in Hec1p/Hec1 ratio in 4 days, 7 days and 10 days IAA treated DLD-1 ^{NA}DNMT1 cells. The graph shows the mean of 3 independent experiments. The error bars represent the standard error of the mean, SEM. Unpaired t-test between samples: * ≤ 0.05; ns > 0.05. **F** Graph summarising the result in Fig 9C shows no change in Hec1p/Hec1 ratio. The graph shows the mean of 3 independent experiments. The error bars represent the standard error of the mean, SEM. Unpaired t-test between the samples: ns > 0.05. **G** DAPI staining to evaluate the mitotic index and the percentage of cells in metaphase in MG132-synchronized untreated and 10 days IAA treated DLD-1 ^{NA}DNMT1 cells. **H** Graph summarizing the results in G. The graph shows the mean of 3 independent experiments. The error bars represent the standard error of the mean, SEM. At least 480 nuclei for each condition and each replicate were evaluated. Unpaired t-test between the samples: ns > 0.05. **I** Graph summarising the results in F The graph shows the mean of 3 independent experiments. The error bars represent the standard error of the mean, SEM. At least 8 mitoses for each condition and each replica were evaluated. Unpaired t-test between the samples: ns > 0.05.

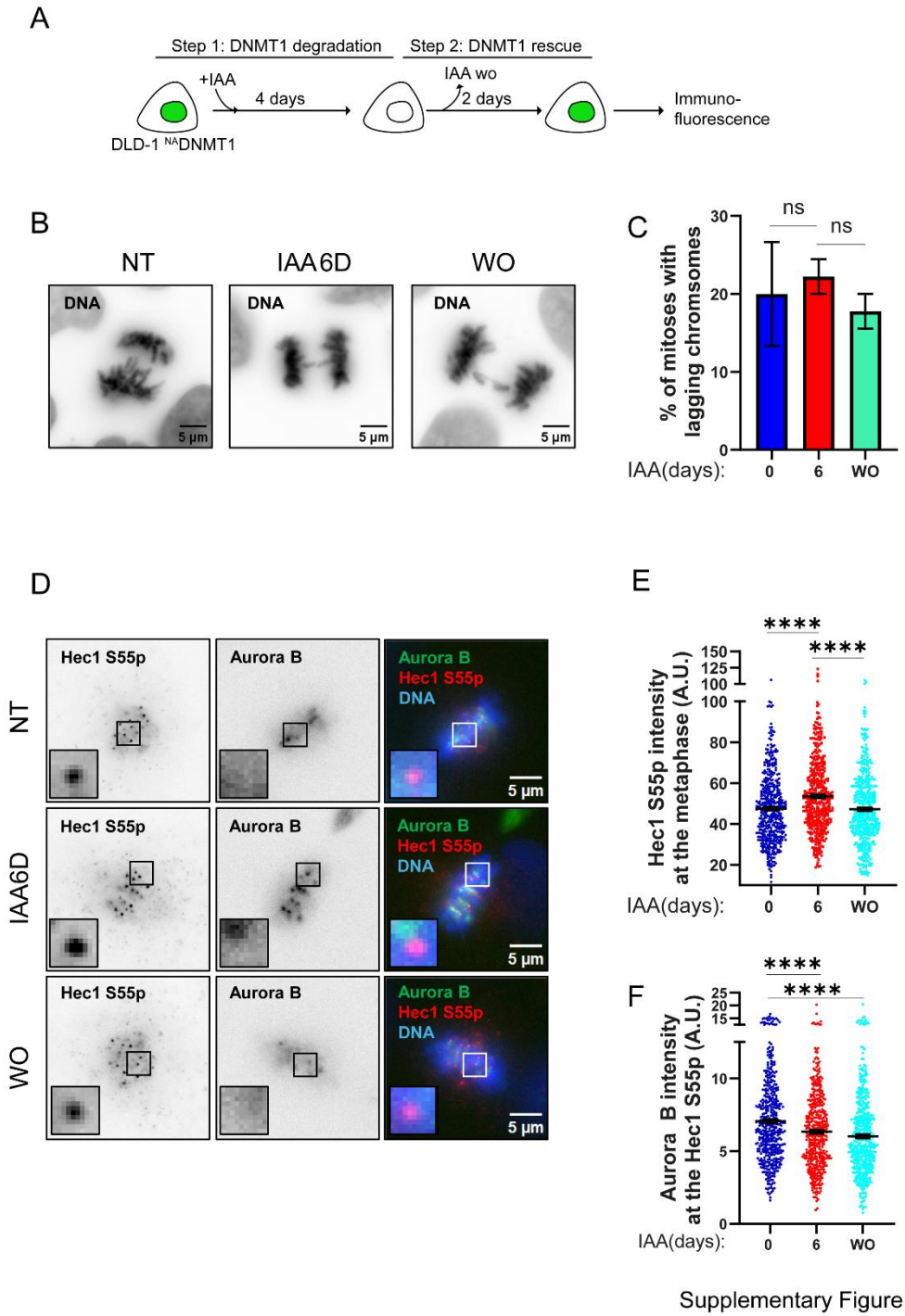

Supplementary Figure 8

Supplementary Figure 8: **A** Schematics to shows how the rescue experiments were performed. **B** DAPI staining to evaluate the percentage of mitoses with lagging chromosomes in untreated, 6 days IAA treated and 2 days DNMT1-rescued (WO) DLD-1 ^{NA}DNMT1 cells. **C** Graph summarising the results in B, reveals no significant change at all samples. The graph shows the mean of 3 independent experiments. The error bars represent the standard error of the mean, SEM. At least 15 mitoses for each condition and each replicate has been evaluated. Unpaired t-test between the samples: ns > 0.05. **D** Immunostaining of Hec1 S55p and Aurora B in untreated, 6 days IAA treated and WO DLD-1 ^{NA}DNMT1 cells. **E** Graph summarising the results in D reveals increase of Hec1 S55p at the metaphase plate upon DNMT1 absence and a restore of the signal when DNMT1 is rescued. The graph shows the mean of 3 independent experiments. The error bars represent the standard error of the mean, SEM. At least 150 spots for each condition and each replicate were evaluated. Unpaired t-test between the samples: **** < 0,1. **F** Graph summarising the results in D reveals reduction of Aurora B kinase at the kinetochore of the metaphase plate. The graph shows the mean of 3 independent experiments. The error bars represent the standard error of the mean, SEM. At least 150 spots for each condition and each replicate were evaluated. Unpaired t-test between the samples: **** < 0.1.

5 Discussion and conclusion

DNA methylation is essential to ensure the fitness of the cells and its alteration is associated to several human diseases. Both aging cells and cancer are characterised by a change in DNA methylation pattern with DNA hypomethylation specifically observed at the repetitive DNA. Thus, evaluating the role of DNA methylation at such region is important to understand the biology behind these human conditions.

To investigate the effect of a global DNA methylation loss, I used cell models where endogenous DNMT1 protein can be rapidly and completely degraded using an inducible degron in both tumoral colon-rectum DLD-1 cells and immortalized human retinal pigment epithelial RPE-1 cells. This approach allows me to observe the direct and immediate effects of the protein absence without potential biases due to the cytotoxicity caused by DNMT1-inhibiting drugs or siRNA transfection, or to the cell adaptation to the gene knockout. The aim in the first part of the thesis is to evaluate the effect of DNMT1 absence or DNA methylation loss on cell cycle progression. A gradual decrease in cell proliferation was observed with a significant reduction at the 4^{th} or 10^{th} day of treatment (depending on the cell line), with consequent upregulation of p21waf1/cip1. In the thesis results published in the attached paper, DNMT1 protein is dispensable for normal cell proliferation for a few cell cycles (approximately 3-4 cell cycles), and the prolonged absence and consequentially loss of DNA methylation, triggers a cell cycle arrest at the G1/S transition. Accordingly, the DLD-1 cell line is also characterized by G1 arrest, though slower [472]. As such, DLD-1 can still proliferate longer under DNMT1 degradation. Indeed, while normal cells are characterized by a fixed tolerance in DNA methylation levels for maintaining the normal progression of the cell cycle, DLD-1 cell line could tolerate lower levels of DNA methylation as the proliferation is reduced only after 10 days in DNMT1 absence. This could be explained by the upregulation of DNMT3B that occurs upon DNMT1 degradation [472]. DNMT3B could methylate important regions of the genome required to sustain the fitness of the cell; thus, tumour cell lines may be adapted to a hypomethylated phenotype due to a compensatory mechanism. Ensuring the maintenance of the minimal tolerable level of DNA methylation is, however, required for cell survival.

One of the most methylated regions of DNA is the centromere, which is involved in the recruitment of the kinetochore complex, which, in turn, allows chromosome segregation during mitosis. Loss of DNA methylation could impair the centromere and thus the kinetochore functioning, leading to mitotic errors. To evaluate such a context, the cells must undergo mitosis. The activation of the p53/p21waf1/cip1 axis makes the RPE-1 unsuitable for analysis upon

prolonged DNMT1 absence and DNA methylation loss. Instead, DLD-1 can keep proliferating longer upon prolonged DNMT1 absence, until the tolerable minimal level of DNA methylation is reached in these cells. Moreover, DLD-1 cells have a pseudo-diploid chromosome asset, but most importantly, they are stable and prone to keep a 2n DNA content. Thus, DLD-1 cells are suitable for experiments aiming to evaluate chromosome segregation upon DNMT1 and DNA methylation loss.

The degradation of DNMT1 and the induction of DNA methylation loss in DLD-1 ^{NA}DNMT1 cells was firstly confirmed. DNA methylation loss was global; however, a marked reduction of the 5mC was observed at the centromere, which consolidates the initial hypothesis of a potential impact at such region. Indeed, a promising role of DNA methylation in regulating the centromere has been recently confirmed [473]. Also, DNMT1 silencing, DNMTs' inhibitors and degradation of DNMT1 have been all correlated with aneuploidy [471,472,479]. However, the connection between loss of DNA methylation and aneuploidy, likely through the formation of mitotic errors, is not fully elucidated. My aim, in the second part of my thesis, is to characterise the changes that occur upon DNA global hypomethylation that can regulate chromosome segregation.

Upon prolonged IAA treatment and, thus, DNMT1 absence, DLD-1 cells are characterised by difficulties in congressing the chromosomes, with the appearance of mitotic errors, specifically misaligned chromosomes, and a change in the chromosome number. This phenotype suggests alteration of chromosomes segregation which relies on the kinetochore and the microtubules of the mitotic spindle. To further investigate on this, the recruitment of the proteins involved in the centromere functioning, kinetochore recruitment, kinetochore-microtubule attachment and in its regulation were evaluated.

First, an enhanced recruitment of CENP-A at the centromere starting from the 3rd day of IAA treatment was observed. CENP-A is normally recruited at the hypomethylated region of the methylated and active HORs of the centromere [307]. Therefore, the loss of DNA methylation may expand the hypomethylated region that recruits CENP-A. The recently published paper of Fachinetti's group used a CRISPR system to guide a TET1 enzyme to the pericentromere and confirmed that, in fact, DNA methylation loss correlates with increased CENP-A recruitment due to a loss of centromere boundaries [473]. Thus, the DNA methylation loss achieved in the DLD-1 ^{NA}DNMT1 cells could induce a similar phenotype. However, while their system is specific for the pericentromere, the ^{NA}DNMT1 degradation induces a global DNA hypomethylation which mimics the more physiological condition observed upon aging and cancer.

The presence of higher CENP-A intensity at the centromere suggests that DNMT1 prolonged absence alter the centromere. This phenotype could lead to chromosome segregation defects. Thus, SAC proteins MAD1 and MAD2 were analysed with the hypothesis that the SAC impairment may be the cause of misaligned chromosomes. Both proteins were present and not altered upon DNMT1 degradation which suggests that the SAC is functional and should stop the cells if the kinetochore-microtubule attachments are not ideal.

Next, I focused on the characterisation of the pathway for the recruitment of the kinetochore complex upon DNMT1 prolonged absence. CENP-A is required for the recruitment of the kinetochore and, in the first place, CENP-C. However, the increase of CENP-A did not directly correlate with increased CENP-C. During G1, CENP-C signal was, instead, reduced in DNMT1-degraded cells compared to the normal condition. Nevertheless, CENP-C intensity increased when cells reached mitosis. Interestingly, this increase did not induce increase of Hec1 at the kinetochore.

No impact on the kinetochore should permit the formation of stable kinetochore-microtubule attachments. Indeed, the exposure to cold, which depolymerises the microtubules that are not involved in stable attachments, reveals no negative effect on the kinetochore-microtubule interaction when DNMT1 is absent. Thus, the interaction seems to be stable and, to further confirm this, the intensity of Astrin and Ska3 which characterise mature and stable end-on kinetochore-microtubule interactions were analysed. Both proteins were increased and recruited more efficiently at the kinetochore of hypomethylated cells. This suggested that DLD-1 cells are characterised by higher stability at the attachments upon the prolonged loss of DNMT1, hence, the kinetochore is correctly recruited and functional.

The mature end-on interaction between Hec1 and the microtubule plus end is permitted and ensured upon prolonged DNMT1 absence. However, as discussed above, the cells show congression defects, which suggests that the problems potentially arise prior to the end-on maturation of the attachment, thus, at the lateral kinetochore-microtubule interaction. To explore this possibility, CENP-E, which ensures the lateral attachments and permits both the timely chromosome maintenance at the metaphase plate and faithful chromosome segregation [413] was analysed. CENP-E protein level-tends to increase, though without statistical significance. To have a better understanding, then, Aurora B kinase, which is known to regulate the end-on maturation and also to allow the formation of the lateral attachments [415,431,467] was evaluated. Aurora B protein level was reduced upon prolonged DNMT1 absence in both synchronised and asynchronous cells, which may indicate defective Aurora B function. To deepen this point, the Aurora B localization

was verified by immunostaining. At the kinetochore of chromosomes that were congressed at the metaphase plate Aurora B was reduced. The reduction of Aurora B at the kinetochore is supplied by the increase of Astrin and Ska3 at the formed attachment [425,480]. At the misaligned chromosomes, instead, Aurora B did not change at the kinetochore complex. These data still did not disclose whether the kinase activity of Aurora B was functional. To directly evaluate this, the phosphorylation of Hec1 S55 which is targeted by Aurora B, was evaluated. Hec1 S55p is high at the unattached and unaligned kinetochore and is reduced as the cells progress through mitosis, reaching a minimal value in metaphase where the attachments are fully matured. Hec1 S55p is only slightly increased at the metaphase plate of DNMT1-degraded cells. At the misaligned chromosomes, instead, Hec1 S55p is highly enhanced suggesting increased Aurora B activity at the kinetochore. Thus, Aurora B is specifically active at the kinetochore of unaligned chromosomes.

Since at the metaphase plate, Hec1 phosphorylation is low and at the misaligned chromosomes is high, I hypothesise that the problem in the attachment could arise from lack of microtubules and thus, that microtubules could rescue the defects induced upon DNMT1 prolonged absence. To test this hypothesis, the microtubules were removed by using a depolymerising drug. Hec1 S55p was, in fact, higher compared to the control. This confirms that upon entry on early mitosis, the kinetochore is actively targeted by Aurora B when DNMT1 is degraded. To further validate such hypothesis, Aurora B was analysed in the absence of microtubules. An increase of Aurora B was observed specifically at the centromere.

Altogether, the results suggest that DNMT1 absence leads to increased activity of Aurora B kinase at the centromere where it strongly phosphorylates Hec1 on S55 to facilitate the initial lateral interaction with the microtubules plus end. Thus, upon DNMT1 absence, Aurora B is more prone to correct uncongressed chromosomes. I speculated that the highly negative charge of Hec1 could be used to improve the binding of the kinetochore to the microtubules. As soon as the chromosome reaches the metaphase plate, the presence of the attached microtubules induces the removal of Aurora B at the kinetochore, leading to higher stabilisation of the attachment by Astrin and Ska3 recruitment. The stabilisation of the kinetochore-microtubule attachment seems to be a phenotype induced by the DNA methylation loss and not by the mere absence of DNMT1, as DNMT1 rescue experiments show no recovery of Aurora B at the kinetochore of chromosomes aligned at the metaphase plate.

At the misaligned chromosomes, instead, Aurora B does not change and Hec1 phosphorylation remains high which suggests a failure of the microtubules to recognise/find some kinetochores.

Even if the activity of other kinases in phosphorylating Hec1 cannot be excluded, the increase of S55p is strongly connected to DNA methylation loss as DNMT1 rescue experiments reveal the persistence of Hec1 phosphorylation at misaligned chromosomes. However, upon DNMT1 rescue the misaligned chromosomes seems to be partially reduced. Thus, the aneuploidy could arise not from misaligned chromosomes but from a combination of events which favours aneuploid cells:

1) The activation of p21waf1/cip1 arrests the tumor cells that are sensitive to DNMT1 absence. Thus, the pool of 2n cells is reduced over time favouring the proliferation of already present aneuploid cells, which succeed in adaptation;
2) The difficulty in creating the initial binding by the microtubules to the kinetochore;
3) Misaligned chromosomes not recognised by the SAC could be lost inducing aneuploidy.

My Ph.D. research revealed that both normal and tumoral cells can sustain DNMT1 absence until the level of DNA methylation is reduced to toxic levels. RPE-1 normal cells sense this minimal level earlier than DLD-1 cancer cells. This suggests that DNMTs inhibitors as chemotherapy may not be that efficient in cancer therapy. Moreover, the study unveiled a possible mechanism by which DNA methylation ensures faithful chromosome segregation through the correct identification and binding between microtubules and kinetochores. Futures studies will fulfil the gaps about the role played by both DNMT1 and DNA methylation in the biorientation of chromosomes and in error correction.

6 ACKNOWLEDGEMENTS

I declare no conflict of interest. I would like to acknowledge the professional help that I received during these 3 years of PhD:

I would like to thank Professors Andrea Fuso and Alessandra Pollice for their suggestions and professional support in reviewing my thesis.

I would like to express my gratitude to Prof Aldo Di Leonardo. He's retired, but he keeps joining us from time to time to bring jokes, joy, and professional suggestions.

I would like to acknowledge the support I received at the University of Palermo from Professor Laura Lentini, who offered professional support, suggestions, and many items required for my research.

I would like to acknowledge the support of Dr Pietro Salvatore Carollo who offered professional support enriching the days of the PhD years

I would like to acknowledge the support I received at Queen Mary University of London. Professor Viji Draviam and the Center for Cell Dynamics supported many experiments with their antibodies and high-technology microscopes. In this regard, I would like to acknowledge EMBO for its economic support during my stay at London, which helped me to focus on the experiments.

Special thanks go to Prof Salvatore Feo, who, close to retirement, accepted me as his PhD student, supporting my research career.

I would like to acknowledge the work of my PhD course coordinator and the Academic Board, who supported each PhD student with workshops and courses aimed at improving our knowledge. Moreover, I would like to thank the academic board for the comments received during the annual exams, which helped me to progress on my research.

Special thanks to the post-doc researchers, PhD and Master's students who fulfilled these years. They offered many suggestions, emotional and technical support

Finally, my 3 years were supported by Dr Viviana Barra. She trained me during my Master's thesis and enriched my growth as an incredible full of ideas researcher and a wonderful co-tutor. I would suggest her as top tutor and recommend her to any new PhD student at the University of Palermo. PhD can be stressful; we all know that. Dr Barra helped me to stay "sane". PhD students can fail the experiments, but she never failed to support me. Thank you for everything.

7 REFERENCES

1. Watson, J. D. & Crick, F. H. Molecular structure of nucleic acids; a structure for deoxyribose nucleic acid. *Nature* **171**, 737–738 (1953).
2. Rothbart, S. B. & Strahl, B. D. Interpreting the language of histone and DNA modifications. *Biochim. Biophys. Acta* **1839**, 627–643 (2014).
3. Clark, D. J. & Kimura, T. Electrostatic mechanism of chromatin folding. *J. Mol. Biol.* **211**, 883–896 (1990).
4. Wolffe, A. P. *Chromatin: Structure and Function*. (Academic Press, 2012).
5. Luger, K. & Hansen, J. C. Nucleosome and chromatin fiber dynamics. *Curr. Opin. Struct. Biol.* **15**, 188–196 (2005).
6. Richmond, T. J. & Davey, C. A. The structure of DNA in the nucleosome core. *Nature* **423**, 145–150 (2003).
7. Simpson, R. T. Structure of the chromatosome, a chromatin particle containing 160 base pairs of DNA and all the histones. *Biochemistry* **17**, 5524–5531 (1978).
8. Oudet, P., Gross-Bellard, M. & Chambon, P. Electron microscopic and biochemical evidence that chromatin structure is a repeating unit. *Cell* **4**, 281–300 (1975).
9. Ou, H. D. *et al.* ChromEMT: Visualizing 3D chromatin structure and compaction in interphase and mitotic cells. *Science* **357**, eaag0025 (2017).
10. Waddington, C. H. The epigenotype. 1942. *Int. J. Epidemiol.* **41**, 10–13 (2012).
11. Dupras, C., Saulnier, K. M. & Joly, Y. Epigenetics, ethics, law and society: A multidisciplinary review of descriptive, instrumental, dialectical and reflexive analyses. *Soc. Stud. Sci.* **49**, 785–810 (2019).
12. Goldberg, A. D., Allis, C. D. & Bernstein, E. Epigenetics: a landscape takes shape. *Cell* **128**, 635–638 (2007).
13. Bove, G., Del Gaudio, N. & Altucci, L. Epitranscriptomics and epigenetics: two sides of the same coin? *Clin. Epigenetics* **16**, 121 (2024).
14. Peserico, A. & Simone, C. Physical and functional HAT/HDAC interplay regulates protein acetylation balance. *J. Biomed. Biotechnol.* **2011**, 371832 (2011).
15. Hyun, K., Jeon, J., Park, K. & Kim, J. Writing, erasing and reading histone lysine methylations. *Exp. Mol. Med.* **49**, e324 (2017).
16. Riggs, A. D. X inactivation, differentiation, and DNA methylation. *Cytogenet. Cell Genet.* **14**, 9–25 (1975).
17. Laurent, L. *et al.* Dynamic changes in the human methylome during differentiation. *Genome Res.* **20**, 320–331 (2010).
18. Guo, J. U. *et al.* Distribution, recognition and regulation of non-CpG methylation in the adult mammalian brain. *Nat. Neurosci.* **17**, 215–222 (2014).
19. Ramsahoye, B. H. *et al.* Non-CpG methylation is prevalent in embryonic stem cells and may be mediated by DNA methyltransferase 3a. *Proc. Natl. Acad. Sci. U. S. A.* **97**, 5237–5242 (2000).
20. Jones, P. A. Functions of DNA methylation: islands, start sites, gene bodies and beyond. *Nat. Rev. Genet.* **13**, 484–492 (2012).
21. Song, C. *et al.* DNA methylation reader MECP2: cell type- and differentiation stage-specific protein distribution. *Epigenetics Chromatin* **7**, 17 (2014).
22. Holwerda, S. J. B. & de Laat, W. CTCF: the protein, the binding partners, the binding sites and their chromatin loops. *Philos. Trans. R. Soc. Lond. B. Biol. Sci.* **368**, 20120369 (2013).
23. Kamakaka, R. T. & Biggins, S. Histone variants: deviants? *Genes Dev.* **19**, 295–310 (2005).
24. Bannister, A. J. & Kouzarides, T. Regulation of chromatin by histone modifications. *Cell Res.* **21**, 381–395 (2011).
25. Capell, B. C. & Berger, S. L. Genome-wide epigenetics. *J. Invest. Dermatol.* **133**, e9 (2013).
26. Allfrey, V. G., Pogo, B. G., Littau, V. C., Gershey, E. L. & Mirsky, A. E. Histone acetylation in insect chromosomes. *Science* **159**, 314–316 (1968).
27. Peixoto, P., Cartron, P.-F., Serandour, A. A. & Hervouet, E. From 1957 to Nowadays: A Brief History of Epigenetics. *Int. J. Mol. Sci.* **21**, 7571 (2020).
28. Lee, D. Y., Hayes, J. J., Pruss, D. & Wolffe, A. P. A positive role for histone acetylation in transcription factor access to nucleosomal DNA. *Cell* **72**, 73–84 (1993).
29. Eberharter, A. & Becker, P. B. Histone acetylation: a switch between repressive and permissive chromatin. Second in review series on chromatin dynamics. *EMBO Rep.* **3**, 224–229 (2002).
30. Shi, Y. *et al.* Histone demethylation mediated by the nuclear amine oxidase homolog LSD1. *Cell* **119**, 941–953 (2004).
31. Zhang, J., Jing, L., Li, M., He, L. & Guo, Z. Regulation of histone arginine methylation/demethylation by methylase and demethylase (Review). *Mol. Med. Rep.* **19**, 3963–3971 (2019).
32. Musselman, C. A., Khorasanizadeh, S. & Kutateladze, T. G. Towards understanding methyllysine readout. *Biochim. Biophys. Acta* **1839**, 686–693 (2014).
33. Jambhekar, A., Dhall, A. & Shi, Y. Roles and regulation of histone methylation in animal development. *Nat. Rev. Mol. Cell Biol.* **20**, 625–641 (2019).

34. Bernstein, B. E. *et al.* Methylation of histone H3 Lys 4 in coding regions of active genes. *Proc. Natl. Acad. Sci. U. S. A.* **99**, 8695–8700 (2002).
35. Barski, A. *et al.* High-resolution profiling of histone methylations in the human genome. *Cell* **129**, 823–837 (2007).
36. Haynes, S. R. *et al.* The bromodomain: a conserved sequence found in human, Drosophila and yeast proteins. *Nucleic Acids Res.* **20**, 2603 (1992).
37. Ball, L. J. *et al.* Structure of the chromatin binding (chromo) domain from mouse modifier protein 1. *EMBO J.* **16**, 2473–2481 (1997).
38. Lachner, M., O'Carroll, D., Rea, S., Mechtler, K. & Jenuwein, T. Methylation of histone H3 lysine 9 creates a binding site for HP1 proteins. *Nature* **410**, 116–120 (2001).
39. Clapier, C. R., Iwasa, J., Cairns, B. R. & Peterson, C. L. Mechanisms of action and regulation of ATP-dependent chromatin-remodelling complexes. *Nat. Rev. Mol. Cell Biol.* **18**, 407–422 (2017).
40. Fire, A. *et al.* Potent and specific genetic interference by double-stranded RNA in Caenorhabditis elegans. *Nature* **391**, 806–811 (1998).
41. Khvorova, A., Reynolds, A. & Jayasena, S. D. Functional siRNAs and miRNAs exhibit strand bias. *Cell* **115**, 209–216 (2003).
42. Mello, C. C. & Conte, D. Revealing the world of RNA interference. *Nature* **431**, 338–342 (2004).
43. Kornienko, A. E., Guenzl, P. M., Barlow, D. P. & Pauler, F. M. Gene regulation by the act of long non-coding RNA transcription. *BMC Biol.* **11**, 59 (2013).
44. Lee, H., Zhang, Z. & Krause, H. M. Long Noncoding RNAs and Repetitive Elements: Junk or Intimate Evolutionary Partners? *Trends Genet. TIG* **35**, 892–902 (2019).
45. Ferrer, J. & Dimitrova, N. Transcription regulation by long non-coding RNAs: mechanisms and disease relevance. *Nat. Rev. Mol. Cell Biol.* **25**, 396–415 (2024).
46. Perry, R. P. & Kelley, D. E. Existence of methylated messenger RNA in mouse L cells. *Cell* **1**, 37–42 (1974).
47. Dubin, D. T. & Taylor, R. H. The methylation state of poly A-containing messenger RNA from cultured hamster cells. *Nucleic Acids Res.* **2**, 1653–1668 (1975).
48. Yang, Y., Hsu, P. J., Chen, Y.-S. & Yang, Y.-G. Dynamic transcriptomic m6A decoration: writers, erasers, readers and functions in RNA metabolism. *Cell Res.* **28**, 616–624 (2018).
49. Sendinc, E. *et al.* PCIF1 Catalyzes m6Am mRNA Methylation to Regulate Gene Expression. *Mol. Cell* **75**, 620-630.e9 (2019).
50. Flamand, M. N., Tegowski, M. & Meyer, K. D. The Proteins of mRNA Modification: Writers, Readers, and Erasers. *Annu. Rev. Biochem.* **92**, 145–173 (2023).
51. Pombo, A. & Dillon, N. Three-dimensional genome architecture: players and mechanisms. *Nat. Rev. Mol. Cell Biol.* **16**, 245–257 (2015).
52. Banushi, B., Collova, J. & Milroy, H. Epigenetic Echoes: Bridging Nature, Nurture, and Healing Across Generations. *Int. J. Mol. Sci.* **26**, 3075 (2025).
53. Morrison, O. & Thakur, J. Molecular Complexes at Euchromatin, Heterochromatin and Centromeric Chromatin. *Int. J. Mol. Sci.* **22**, 6922 (2021).
54. Keating, S. T. & El-Osta, A. Epigenetics and Metabolism. *Circ. Res.* **116**, 715–736 (2015).
55. Hotchkiss, R. D. The quantitative separation of purines, pyrimidines, and nucleosides by paper chromatography. *J. Biol. Chem.* **175**, 315–332 (1948).
56. Bird, A. DNA methylation patterns and epigenetic memory. *Genes Dev.* **16**, 6–21 (2002).
57. Lyko, F. The DNA methyltransferase family: a versatile toolkit for epigenetic regulation. *Nat. Rev. Genet.* **19**, 81–92 (2018).
58. Timinskas, A., Butkus, V. & Janulaitis, A. Sequence motifs characteristic for DNA [cytosine-N4] and DNA [adenine-N6] methyltransferases. Classification of all DNA methyltransferases. *Gene* **157**, 3–11 (1995).
59. Jin, B. & Robertson, K. D. DNA Methyltransferases (DNMTs), DNA Damage Repair, and Cancer. *Adv. Exp. Med. Biol.* **754**, 3–29 (2013).
60. Klimasauskas, S., Kumar, S., Roberts, R. J. & Cheng, X. HhaI methyltransferase flips its target base out of the DNA helix. *Cell* **76**, 357–369 (1994).
61. Goll, M. G. *et al.* Methylation of tRNAAsp by the DNA methyltransferase homolog Dnmt2. *Science* **311**, 395–398 (2006).
62. Dhe-Paganon, S., Syeda, F. & Park, L. DNA methyl transferase 1: regulatory mechanisms and implications in health and disease. *Int. J. Biochem. Mol. Biol.* **2**, 58–66 (2011).
63. Ciechomska, M., Roszkowski, L. & Maslinski, W. DNA Methylation as a Future Therapeutic and Diagnostic Target in Rheumatoid Arthritis. *Cells* **8**, 953 (2019).
64. Yoder, J. A. & Bestor, T. H. A candidate mammalian DNA methyltransferase related to pmt1p of fission yeast. *Hum. Mol. Genet.* **7**, 279–284 (1998).
65. Dong, A. *et al.* Structure of human DNMT2, an enigmatic DNA methyltransferase homolog that displays denaturant-resistant binding to DNA. *Nucleic Acids Res.* **29**, 439–448 (2001).

66. Okano, M., Xie, S. & Li, E. Dnmt2 is not required for de novo and maintenance methylation of viral DNA in embryonic stem cells. *Nucleic Acids Res.* **26**, 2536–2540 (1998).
67. Jeltsch, A. *et al.* Mechanism and biological role of Dnmt2 in Nucleic Acid Methylation. *RNA Biol.* **14**, 1108–1123 (2017).
68. Du, J., Johnson, L. M., Jacobsen, S. E. & Patel, D. J. DNA methylation pathways and their crosstalk with histone methylation. *Nat. Rev. Mol. Cell Biol.* **16**, 519–532 (2015).
69. Kareta, M. S., Botello, Z. M., Ennis, J. J., Chou, C. & Chédin, F. Reconstitution and mechanism of the stimulation of de novo methylation by human DNMT3L. *J. Biol. Chem.* **281**, 25893–25902 (2006).
70. Lei, H. *et al.* De novo DNA cytosine methyltransferase activities in mouse embryonic stem cells. *Development* **122**, 3195–3205 (1996).
71. Okano, M., Xie, S. & Li, E. Cloning and characterization of a family of novel mammalian DNA (cytosine-5) methyltransferases. *Nat. Genet.* **19**, 219–220 (1998).
72. Okano, M., Bell, D. W., Haber, D. A. & Li, E. DNA methyltransferases Dnmt3a and Dnmt3b are essential for de novo methylation and mammalian development. *Cell* **99**, 247–257 (1999).
73. Jimenji, T., Matsumura, R., Kori, S. & Arita, K. Structure of PCNA in complex with DNMT1 PIP box reveals the basis for the molecular mechanism of the interaction. *Biochem. Biophys. Res. Commun.* **516**, 578–583 (2019).
74. Syeda, F. *et al.* The Replication Focus Targeting Sequence (RFTS) Domain Is a DNA-competitive Inhibitor of Dnmt1*. *J. Biol. Chem.* **286**, 15344–15351 (2011).
75. Zhang, Z.-M. *et al.* Crystal Structure of Human DNA Methyltransferase 1. *J. Mol. Biol.* **427**, 2520–2531 (2015).
76. Song, J., Rechkoblit, O., Bestor, T. H. & Patel, D. J. Structure of DNMT1-DNA complex reveals a role for autoinhibition in maintenance DNA methylation. *Science* **331**, 1036–1040 (2011).
77. Easwaran, H. P., Schermelleh, L., Leonhardt, H. & Cardoso, M. C. Replication-independent chromatin loading of Dnmt1 during G2 and M phases. *EMBO Rep.* **5**, 1181–1186 (2004).
78. Haggerty, C. *et al.* Dnmt1 has de novo activity targeted to transposable elements. *Nat. Struct. Mol. Biol.* **28**, 594–603 (2021).
79. Kim, D. J. The Role of the DNA Methyltransferase Family and the Therapeutic Potential of DNMT Inhibitors in Tumor Treatment. *Curr. Oncol.* **32**, 88 (2025).
80. Bird, A., Taggart, M., Frommer, M., Miller, O. J. & Macleod, D. A fraction of the mouse genome that is derived from islands of nonmethylated, CpG-rich DNA. *Cell* **40**, 91–99 (1985).
81. Mariño-Ramírez, L., Spouge, J. L., Kanga, G. C. & Landsman, D. Statistical analysis of over-represented words in human promoter sequences. *Nucleic Acids Res.* **32**, 949–958 (2004).
82. Illingworth, R. S. & Bird, A. P. CpG islands – 'A rough guide'. *FEBS Lett.* **583**, 1713–1720 (2009).
83. Proffitt, J. H., Davie, J. R., Swinton, D. & Hattman, S. 5-Methylcytosine is not detectable in Saccharomyces cerevisiae DNA. *Mol. Cell. Biol.* **4**, 985–988 (1984).
84. Simpson, V. J., Johnson, T. E. & Hammen, R. F. Caenorhabditis elegans DNA does not contain 5-methylcytosine at any time during development or aging. *Nucleic Acids Res.* **14**, 6711–6719 (1986).
85. Chen, Z. & Riggs, A. D. DNA methylation and demethylation in mammals. *J. Biol. Chem.* **286**, 18347–18353 (2011).
86. Zhang, H., Lang, Z. & Zhu, J.-K. Dynamics and function of DNA methylation in plants. *Nat. Rev. Mol. Cell Biol.* **19**, 489–506 (2018).
87. Hung, M. S. *et al.* Drosophila proteins related to vertebrate DNA (5-cytosine) methyltransferases. *Proc. Natl. Acad. Sci. U. S. A.* **96**, 11940–11945 (1999).
88. Robertson, K. D. DNA methylation and human disease. *Nat. Rev. Genet.* **6**, 597–610 (2005).
89. Reik, W., Dean, W. & Walter, J. Epigenetic reprogramming in mammalian development. *Science* **293**, 1089–1093 (2001).
90. Dean, W. Pathways of DNA Demethylation. in *DNA Methyltransferases - Role and Function* (eds Jeltsch, A. & Jurkowska, R. Z.) 211–238 (Springer International Publishing, Cham, 2022). doi:10.1007/978-3-031-11454-0_9.
91. Dusadeemeelap, C., Rojasawasthien, T., Matsubara, T., Kokabu, S. & Addison, W. N. Inhibition of TET-mediated DNA demethylation suppresses osteoblast differentiation. *FASEB J.* **36**, e22153 (2022).
92. Conticello, S. G., Thomas, C. J. F., Petersen-Mahrt, S. K. & Neuberger, M. S. Evolution of the AID/APOBEC family of polynucleotide (deoxy)cytidine deaminases. *Mol. Biol. Evol.* **22**, 367–377 (2005).
93. Tahiliani, M. *et al.* Conversion of 5-Methylcytosine to 5-Hydroxymethylcytosine in Mammalian DNA by MLL Partner TET1. *Science* **324**, 930–935 (2009).
94. Ito, S. *et al.* Role of Tet proteins in 5mC to 5hmC conversion, ES-cell self-renewal and inner cell mass specification. *Nature* **466**, 1129–1133 (2010).
95. He, Y.-F. *et al.* Tet-mediated formation of 5-carboxylcytosine and its excision by TDG in mammalian DNA. *Science* **333**, 1303–1307 (2011).
96. Bhutani, N., Burns, D. M. & Blau, H. M. DNA Demethylation Dynamics. *Cell* **146**, 866–872 (2011).

97. Klein, C. J. *et al.* Mutations in DNMT1 cause hereditary sensory neuropathy with dementia and hearing loss. *Nat. Genet.* **43**, 595–600 (2011).
98. Winkelmann, J. *et al.* Mutations in DNMT1 cause autosomal dominant cerebellar ataxia, deafness and narcolepsy. *Hum. Mol. Genet.* **21**, 2205–2210 (2012).
99. Liu, C. C. *et al.* Global DNA methylation, DNMT1, and MBD2 in patients with systemic lupus erythematosus. *Lupus* **20**, 131–136 (2011).
100. Pappalardo, X. G. & Barra, V. Losing DNA methylation at repetitive elements and breaking bad. *Epigenetics Chromatin* **14**, 25 (2021).
101. Wijmenga, C. *et al.* Localization of the ICF Syndrome to Chromosome 20 by Homozygosity Mapping. *Am. J. Hum. Genet.* **63**, 803–809 (1998).
102. Kiaee, F. *et al.* Clinical, Immunologic and Molecular Spectrum of Patients with Immunodeficiency, Centromeric Instability, and Facial Anomalies (ICF) Syndrome: A Systematic Review. *Endocr. Metab. Immune Disord. Drug Targets* **21**, 664–672 (2021).
103. Jeanpierre, M. *et al.* An embryonic-like methylation pattern of classical satellite DNA is observed in ICF syndrome. *Hum. Mol. Genet.* **2**, 731–735 (1993).
104. Schuffenhauer, S. *et al.* DNA, FISH and complementation studies in ICF syndrome: DNA hypomethylation of repetitive and single copy loci and evidence for a trans acting factor. *Hum. Genet.* **96**, 562–571 (1995).
105. Miniou, P. *et al.* alpha-satellite DNA methylation in normal individuals and in ICF patients: heterogeneous methylation of constitutive heterochromatin in adult and fetal tissues. *Hum. Genet.* **99**, 738–745 (1997).
106. Sagie, S. *et al.* Non-random length distribution of individual telomeres in immunodeficiency, centromeric instability and facial anomalies syndrome, type I. *Hum. Mol. Genet.* **26**, 4244–4256 (2017).
107. Gisselsson, D. *et al.* Interphase chromosomal abnormalities and mitotic missegregation of hypomethylated sequences in ICF syndrome cells. *Chromosoma* **114**, 118–126 (2005).
108. Ehrlich, M. The ICF syndrome, a DNA methyltransferase 3B deficiency and immunodeficiency disease. *Clin. Immunol.* **109**, 17–28 (2003).
109. Kwabi-Addo, B. *et al.* Age-related DNA methylation changes in normal human prostate tissues. *Clin. Cancer Res. Off. J. Am. Assoc. Cancer Res.* **13**, 3796–3802 (2007).
110. Fuke, C. *et al.* Age related changes in 5-methylcytosine content in human peripheral leukocytes and placentas: an HPLC-based study. *Ann. Hum. Genet.* **68**, 196–204 (2004).
111. Drinkwater, R. D., Blake, T. J., Morley, A. A. & Turner, D. R. Human lymphocytes aged in vivo have reduced levels of methylation in transcriptionally active and inactive DNA. *Mutat. Res.* **219**, 29–37 (1989).
112. Wilson, V. L., Smith, R. A., Ma, S. & Cutler, R. G. Genomic 5-methyldeoxycytidine decreases with age. *J. Biol. Chem.* **262**, 9948–9951 (1987).
113. Jones, M. J., Goodman, S. J. & Kobor, M. S. DNA methylation and healthy human aging. *Aging Cell* **14**, 924–932 (2015).
114. Horvath, S. *et al.* Aging effects on DNA methylation modules in human brain and blood tissue. *Genome Biol.* **13**, R97 (2012).
115. Pappalardo, X. G. & Barra, V. Losing DNA methylation at repetitive elements and breaking bad. *Epigenetics Chromatin* **14**, 25 (2021).
116. Mays-Hoopes, L. L., Brown, A. & Huang, R. C. Methylation and rearrangement of mouse intracisternal a particle genes in development, aging, and myeloma. *Mol. Cell. Biol.* **3**, 1371–1380 (1983).
117. Masser, D. R. *et al.* Sexually divergent DNA methylation patterns with hippocampal aging. *Aging Cell* **16**, 1342–1352 (2017).
118. Unnikrishnan, A. *et al.* The role of DNA methylation in epigenetics of aging. *Pharmacol. Ther.* **195**, 172–185 (2019).
119. Bollati, V. *et al.* Decline in genomic DNA methylation through aging in a cohort of elderly subjects. *Mech. Ageing Dev.* **130**, 234–239 (2009).
120. De Cecco, M. *et al.* Genomes of replicatively senescent cells undergo global epigenetic changes leading to gene silencing and activation of transposable elements. *Aging Cell* **12**, 247–256 (2013).
121. Enukashvily, N. I., Donev, R., Waisertreiger, I. S.-R. & Podgornaya, O. I. Human chromosome 1 satellite 3 DNA is decondensed, demethylated and transcribed in senescent cells and in A431 epithelial carcinoma cells. *Cytogenet. Genome Res.* **118**, 42–54 (2007).
122. Feng, Y., Jankovic, J. & Wu, Y.-C. Epigenetic mechanisms in Parkinson's disease. *J. Neurol. Sci.* **349**, 3–9 (2015).
123. Fuso, A. & Lucarelli, M. CpG and Non-CpG Methylation in the Diet–Epigenetics–Neurodegeneration Connection. *Curr. Nutr. Rep.* **8**, 74–82 (2019).
124. Smith, R. G. & Lunnon, K. DNA Modifications and Alzheimer's Disease. in *Neuroepigenomics in Aging and Disease* (ed. Delgado-Morales, R.) 303–319 (Springer International Publishing, Cham, 2017). doi:10.1007/978-3-319-53889-1_16.
125. Martinez-Feduchi, P., Jin, P. & Yao, B. Epigenetic modifications of DNA and RNA in Alzheimer's disease. *Front. Mol. Neurosci.* **17**, 1398026 (2024).

126. Dolinar, A., Ravnik-Glavač, M. & Glavač, D. Epigenetic mechanisms in amyotrophic lateral sclerosis: A short review. *Mech. Ageing Dev.* **174**, 103–110 (2018).
127. Nicolia, V., Lucarelli, M. & Fuso, A. Environment, epigenetics and neurodegeneration: Focus on nutrition in Alzheimer's disease. *Exp. Gerontol.* **68**, 8–12 (2015).
128. Fuso, A. The 'golden age' of DNA methylation in neurodegenerative diseases. *Clin. Chem. Lab. Med.* **51**, 523–534 (2013).
129. Miranda-Morales, E. *et al.* Implications of DNA Methylation in Parkinson's Disease. *Front. Mol. Neurosci.* **10**, 225 (2017).
130. Matsumoto, L. *et al.* CpG demethylation enhances alpha-synuclein expression and affects the pathogenesis of Parkinson's disease. *PloS One* **5**, e15522 (2010).
131. Ai, S. *et al.* Hypomethylation of SNCA in blood of patients with sporadic Parkinson's disease. *J. Neurol. Sci.* **337**, 123–128 (2014).
132. Masliah, E., Dumaop, W., Galasko, D. & Desplats, P. Distinctive patterns of DNA methylation associated with Parkinson disease: identification of concordant epigenetic changes in brain and peripheral blood leukocytes. *Epigenetics* **8**, 1030–1038 (2013).
133. Fuso, A. *et al.* Changes in Presenilin 1 gene methylation pattern in diet-induced B vitamin deficiency. *Neurobiol. Aging* **32**, 187–199 (2011).
134. Fuso, A. *et al.* S-adenosylmethionine reduces the progress of the Alzheimer-like features induced by B-vitamin deficiency in mice. *Neurobiol. Aging* **33**, 1482.e1–16 (2012).
135. Raia, T. *et al.* One-carbon metabolism modulates miR-29a–DNA methylation crosstalk in Alzheimer's disease. *Alzheimers Dement.* **21**, e70703 (2025).
136. Lunnon, K. *et al.* Methylomic profiling implicates cortical deregulation of ANK1 in Alzheimer's disease. *Nat. Neurosci.* **17**, 1164–1170 (2014).
137. Younesian, S., Yousefi, A.-M., Momeny, M., Ghaffari, S. H. & Bashash, D. The DNA Methylation in Neurological Diseases. *Cells* **11**, 3439 (2022).
138. Shireby, G. *et al.* DNA methylation signatures of Alzheimer's disease neuropathology in the cortex are primarily driven by variation in non-neuronal cell-types. *Nat. Commun.* **13**, 5620 (2022).
139. Matrisciano, F. *et al.* Epigenetic modifications of GABAergic interneurons are associated with the schizophrenia-like phenotype induced by prenatal stress in mice. *Neuropharmacology* **68**, 184–194 (2013).
140. Alvarez-Nuñez, F. *et al.* PTEN Promoter Methylation in Sporadic Thyroid Carcinomas. *Thyroid*® **16**, 17–23 (2006).
141. Choi, S. H. *et al.* Changes in DNA methylation of tandem DNA repeats are different from interspersed repeats in cancer. *Int. J. Cancer J. Int. Cancer* **125**, 723–729 (2009).
142. Feinberg, A. P. & Vogelstein, B. Hypomethylation distinguishes genes of some human cancers from their normal counterparts. *Nature* **301**, 89–92 (1983).
143. Gama-Sosa, M. A. *et al.* The 5-methylcytosine content of DNA from human tumors. *Nucleic Acids Res.* **11**, 6883–6894 (1983).
144. Costello, J. F. *et al.* Aberrant CpG-island methylation has non-random and tumour-type-specific patterns. *Nat. Genet.* **24**, 132–138 (2000).
145. Nishiyama, R. *et al.* A DNA repeat, NBL2, is hypermethylated in some cancers but hypomethylated in others. *Cancer Biol. Ther.* **4**, 440–448 (2005).
146. Ehrlich, M. DNA hypomethylation in cancer cells. *Epigenomics* **1**, 239–259 (2009).
147. Nunes, S. P., Henrique, R., Jerónimo, C. & Paramio, J. M. DNA Methylation as a Therapeutic Target for Bladder Cancer. *Cells* **9**, 1850 (2020).
148. Tompkins, J. D. Discovering DNA Methylation, the History and Future of the Writing on DNA. *J. Hist. Biol.* **55**, 865–887 (2022).
149. Borchiellini, M., Ummarino, S. & Di Ruscio, A. The Bright and Dark Side of DNA Methylation: A Matter of Balance. *Cells* **8**, 1243 (2019).
150. Heredia-Mendez, A. J., Sánchez-Sánchez, G. & López-Camarillo, C. Reprogramming of the Genome-Wide DNA Methylation Landscape in Three-Dimensional Cancer Cell Cultures. *Cancers* **15**, 1991 (2023).
151. Nishino, K. *et al.* Non-CpG methylation occurs in the regulatory region of the Sry gene. *J. Reprod. Dev.* **57**, 586–593 (2011).
152. Patil, V., Ward, R. L. & Hesson, L. B. The evidence for functional non-CpG methylation in mammalian cells. *Epigenetics* **9**, 823–828 (2014).
153. Lomvardas, S. *et al.* Interchromosomal interactions and olfactory receptor choice. *Cell* **126**, 403–413 (2006).
154. Pinney, S. E. Mammalian Non-CpG Methylation: Stem Cells and Beyond. *Biology* **3**, 739–751 (2014).
155. Angeloni, A. & Bogdanovic, O. Enhancer DNA methylation: implications for gene regulation. *Essays Biochem.* **63**, 707–715 (2019).
156. Edrei, Y. *et al.* Methylation-directed regulatory networks determine enhancing and silencing of mutation disease driver genes and explain inter-patient expression variation. *Genome Biol.* **24**, 264 (2023).

157. Kreibich, E. & Krebs, A. R. Relevance of DNA methylation at enhancers for the acquisition of cell identities. *FEBS Lett.* **597**, 1805–1817 (2023).
158. Hellman, A. & Chess, A. Gene body-specific methylation on the active X chromosome. *Science* **315**, 1141–1143 (2007).
159. Rauch, T. A., Wu, X., Zhong, X., Riggs, A. D. & Pfeifer, G. P. A human B cell methylome at 100−base pair resolution. *Proc. Natl. Acad. Sci. U. S. A.* **106**, 671–678 (2009).
160. Neri, F. *et al.* Intragenic DNA methylation prevents spurious transcription initiation. *Nature* **543**, 72–77 (2017).
161. Agirre, E. *et al.* A chromatin code for alternative splicing involving a putative association between CTCF and HP1α proteins. *BMC Biol.* **13**, 31 (2015).
162. Merkenschlager, M. & Nora, E. P. CTCF and Cohesin in Genome Folding and Transcriptional Gene Regulation. *Annu. Rev. Genomics Hum. Genet.* **17**, 17–43 (2016).
163. Shukla, S. *et al.* CTCF-promoted RNA polymerase II pausing links DNA methylation to splicing. *Nature* **479**, 74–79 (2011).
164. Bernstein, C. DNA Methylation and Establishing Memory. *Epigenetics Insights* **15**, 25168657211072499 (2022).
165. Shimizu, M., Mori, T., Sakurai, T. & Shindo, H. Destabilization of nucleosomes by an unusual DNA conformation adopted by poly(dA)·poly(dT) tracts in vivo. *EMBO J.* **19**, 3358–3365 (2000).
166. Suter, B., Schnappauf, G. & Thoma, F. Poly(dA·dT) sequences exist as rigid DNA structures in nucleosome-free yeast promoters in vivo. *Nucleic Acids Res.* **28**, 4083–4089 (2000).
167. Davey, C. S., Pennings, S., Reilly, C., Meehan, R. R. & Allan, J. A determining influence for CpG dinucleotides on nucleosome positioning in vitro. *Nucleic Acids Res.* **32**, 4322–4331 (2004).
168. Davey, C., Pennings, S. & Allan, J. CpG methylation remodels chromatin structure in vitro. *J. Mol. Biol.* **267**, 276–288 (1997).
169. Li, S., Peng, Y. & Panchenko, A. R. DNA methylation: Precise modulation of chromatin structure and dynamics. *Curr. Opin. Struct. Biol.* **75**, 102430 (2022).
170. Geahigan, K. B., Meints, G. A., Hatcher, M. E., Orban, J. & Drobny, G. P. The dynamic impact of CpG methylation in DNA. *Biochemistry* **39**, 4939–4946 (2000).
171. Choy, J. S. *et al.* DNA Methylation Increases Nucleosome Compaction and Rigidity. *J. Am. Chem. Soc.* **132**, 1782–1783 (2010).
172. Georgel, P. T. *et al.* Chromatin compaction by human MeCP2. Assembly of novel secondary chromatin structures in the absence of DNA methylation. *J. Biol. Chem.* **278**, 32181–32188 (2003).
173. Chua, G. N. L. *et al.* Differential dynamics specify MeCP2 function at nucleosomes and methylated DNA. *Nat. Struct. Mol. Biol.* **31**, 1789–1797 (2024).
174. Liu, Y. *et al.* MECP2 directly interacts with RNA polymerase II to modulate transcription in human neurons. *Neuron* **112**, 1943-1958.e10 (2024).
175. Gabel, H. W. *et al.* Disruption of DNA-methylation-dependent long gene repression in Rett syndrome. *Nature* **522**, 89–93 (2015).
176. Chin, E. W. M. & Goh, E. L. K. MeCP2 Dysfunction in Rett Syndrome and Neuropsychiatric Disorders. *Methods Mol. Biol. Clifton NJ* **2011**, 573–591 (2019).
177. Horike, S., Cai, S., Miyano, M., Cheng, J.-F. & Kohwi-Shigematsu, T. Loss of silent-chromatin looping and impaired imprinting of DLX5 in Rett syndrome. *Nat. Genet.* **37**, 31–40 (2005).
178. Singleton, M. K. *et al.* MeCP2 is required for global heterochromatic and nucleolar changes during activity-dependent neuronal maturation. *Neurobiol. Dis.* **43**, 190–200 (2011).
179. Linhoff, M. W., Garg, S. K. & Mandel, G. A high-resolution imaging approach to investigate chromatin architecture in complex tissues. *Cell* **163**, 246–255 (2015).
180. Yearim, A. *et al.* HP1 is involved in regulating the global impact of DNA methylation on alternative splicing. *Cell Rep.* **10**, 1122–1134 (2015).
181. Dinant, C. & Luijsterburg, M. S. The emerging role of HP1 in the DNA damage response. *Mol. Cell. Biol.* **29**, 6335–6340 (2009).
182. Bártová, E. *et al.* Function of heterochromatin protein 1 during DNA repair. *Protoplasma* **254**, 1233–1240 (2017).
183. Chakraborty, A. & Prasanth, S. G. Phosphorylation–dephosphorylation cycle of HP1α governs accurate mitotic progression. *Cell Cycle* **13**, 1663–1670 (2014).
184. Jackson-Grusby, L. *et al.* Loss of genomic methylation causes p53-dependent apoptosis and epigenetic deregulation. *Nat. Genet.* **27**, 31–39 (2001).
185. Tomizawa, S. *et al.* Dynamic stage-specific changes in imprinted differentially methylated regions during early mammalian development and prevalence of non-CpG methylation in oocytes. *Dev. Camb. Engl.* **138**, 811–820 (2011).
186. Xie, W. *et al.* Base-resolution analyses of sequence and parent-of-origin dependent DNA methylation in the mouse genome. *Cell* **148**, 816–831 (2012).

187. DeChiara, T. M., Robertson, E. J. & Efstratiadis, A. Parental imprinting of the mouse insulin-like growth factor II gene. *Cell* **64**, 849–859 (1991).
188. Barlow, D. P., Stöger, R., Herrmann, B. G., Saito, K. & Schweifer, N. The mouse insulin-like growth factor type-2 receptor is imprinted and closely linked to the Tme locus. *Nature* **349**, 84–87 (1991).
189. Wutz, A. & P. Barlow, D. Imprinting of the mouse *Igf2r* gene depends on an intronic CpG island. *Mol. Cell. Endocrinol.* **140**, 9–14 (1998).
190. Dean, W. *et al.* Conservation of methylation reprogramming in mammalian development: aberrant reprogramming in cloned embryos. *Proc. Natl. Acad. Sci. U. S. A.* **98**, 13734–13738 (2001).
191. Monk, M., Boubelik, M. & Lehnert, S. Temporal and regional changes in DNA methylation in the embryonic, extraembryonic and germ cell lineages during mouse embryo development. *Dev. Camb. Engl.* **99**, 371–382 (1987).
192. Howlett, S. K. & Reik, W. Methylation levels of maternal and paternal genomes during preimplantation development. *Dev. Camb. Engl.* **113**, 119–127 (1991).
193. Rougier, N. *et al.* Chromosome methylation patterns during mammalian preimplantation development. *Genes Dev.* **12**, 2108–2113 (1998).
194. Bogdanović, O. & Lister, R. DNA methylation and the preservation of cell identity. *Curr. Opin. Genet. Dev.* **46**, 9–14 (2017).
195. Heard, E. & Disteche, C. M. Dosage compensation in mammals: fine-tuning the expression of the X chromosome. *Genes Dev.* **20**, 1848–1867 (2006).
196. Schulz, W. A., Steinhoff, C. & Florl, A. R. Methylation of endogenous human retroelements in health and disease. *Curr. Top. Microbiol. Immunol.* **310**, 211–250 (2006).
197. Kuster, J. E., Guarnieri, M. H., Ault, J. G., Flaherty, L. & Swiatek, P. J. IAP insertion in the murine LamB3 gene results in junctional epidermolysis bullosa. *Mamm. Genome Off. J. Int. Mamm. Genome Soc.* **8**, 673–681 (1997).
198. Gwynn, B., Lueders, K., Sands, M. S. & Birkenmeier, E. H. Intracisternal A-particle element transposition into the murine beta-glucuronidase gene correlates with loss of enzyme activity: a new model for beta-glucuronidase deficiency in the C3H mouse. *Mol. Cell. Biol.* **18**, 6474–6481 (1998).
199. Haase, A. D. *et al.* PIWI-interacting RNAs: who, what, when, where, why, and how. *EMBO J.* **43**, 5335–5339 (2024).
200. Kuramochi-Miyagawa, S. *et al.* DNA methylation of retrotransposon genes is regulated by Piwi family members MILI and MIWI2 in murine fetal testes. *Genes Dev.* **22**, 908–917 (2008).
201. Anvar, Z. *et al.* DNA Methylation Dynamics in the Female Germline and Maternal-Effect Mutations That Disrupt Genomic Imprinting. *Genes* **12**, 1214 (2021).
202. Polo, J. M. *et al.* A molecular roadmap of reprogramming somatic cells into iPS cells. *Cell* **151**, 1617–1632 (2012).
203. Lister, R. *et al.* Hotspots of aberrant epigenomic reprogramming in human induced pluripotent stem cells. *Nature* **471**, 68–73 (2011).
204. Matthews, H. K., Bertoli, C. & de Bruin, R. A. M. Cell cycle control in cancer. *Nat. Rev. Mol. Cell Biol.* **23**, 74–88 (2022).
205. Pardee, A. B. G1 Events and Regulation of Cell Proliferation. *Science* **246**, 603–608 (1989).
206. Paweletz, N. Walther Flemming: pioneer of mitosis research. *Nat. Rev. Mol. Cell Biol.* **2**, 72–75 (2001).
207. Holloway, S. L., Glotzer, M., King, R. W. & Murray, A. W. Anaphase is initiated by proteolysis rather than by the inactivation of maturation-promoting factor. *Cell* **73**, 1393–1402 (1993).
208. Sudakin, V. *et al.* The cyclosome, a large complex containing cyclin-selective ubiquitin ligase activity, targets cyclins for destruction at the end of mitosis. *Mol. Biol. Cell* **6**, 185–197 (1995).
209. Campisi, J. & d'Adda di Fagagna, F. Cellular senescence: when bad things happen to good cells. *Nat. Rev. Mol. Cell Biol.* **8**, 729–740 (2007).
210. Cj, S. Mammalian G1 cyclins. *Cell* **73**, (1993).
211. Quelle, D. E. *et al.* Overexpression of mouse D-type cyclins accelerates G1 phase in rodent fibroblasts. *Genes Dev.* **7**, 1559–1571 (1993).
212. V, B., J, L., Mj, M., M, P. & G, D. Cyclin D1 is a nuclear protein required for cell cycle progression in G1. *Genes Dev.* **7**, (1993).
213. J, K., H, M., Sw, H., Me, E. & Cj, S. Direct binding of cyclin D to the retinoblastoma gene product (pRb) and pRb phosphorylation by the cyclin D-dependent kinase CDK4. *Genes Dev.* **7**, (1993).
214. Weintraub, S. J., Prater, C. A. & Dean, D. C. Retinoblastoma protein switches the E2F site from positive to negative element. *Nature* **358**, 259–261 (1992).
215. Schafer, K. A. The cell cycle: a review. *Vet. Pathol.* **35**, 461–478 (1998).
216. Engeland, K. Cell cycle regulation: p53-p21-RB signaling. *Cell Death Differ.* **29**, 946–960 (2022).
217. Sherr, C. J. G1 phase progression: Cycling on cue. *Cell* **79**, 551–555 (1994).
218. Ra, W. The retinoblastoma protein and cell cycle control. *Cell* **81**, (1995).
219. Cj, S. Cancer cell cycles. *Science* **274**, (1996).

220. Ka, W. & Si, R. Activation of cyclin E/CDK2 is coupled to site-specific autophosphorylation and ubiquitin-dependent degradation of cyclin E. *EMBO J.* **15**, (1996).
221. Dynlacht, B. D., Flores, O., Lees, J. A. & Harlow, E. Differential regulation of E2F transactivation by cyclin/cdk2 complexes. *Genes Dev.* **8**, 1772–1786 (1994).
222. Nishitani, H. & Lygerou, Z. DNA replication licensing. *Front. Biosci. J. Virtual Libr.* **9**, 2115–2132 (2004).
223. Barnum, K. J. & O'Connell, M. J. Cell Cycle Regulation by Checkpoints. *Methods Mol. Biol. Clifton NJ* **1170**, 29–40 (2014).
224. D, G. *et al.* Cyclin A2 regulates nuclear-envelope breakdown and the nuclear accumulation of cyclin B1. *Curr. Biol. CB* **17**, (2007).
225. Tk, F., Ht, M. & Ry, P. Specialized roles of the two mitotic cyclins in somatic cells: cyclin A as an activator of M phase-promoting factor. *Mol. Biol. Cell* **18**, (2007).
226. Laoukili, J. *et al.* Activation of FoxM1 during G2 requires cyclin A/Cdk-dependent relief of autorepression by the FoxM1 N-terminal domain. *Mol. Cell. Biol.* **28**, 3076–3087 (2008).
227. Ll, P. & H, P.-W. Inactivation of the p34cdc2-cyclin B complex by the human WEE1 tyrosine kinase. *Science* **257**, (1992).
228. Pr, M., Tr, C., A, K. & Wg, D. Myt1: a membrane-associated inhibitory kinase that phosphorylates Cdc2 on both threonine-14 and tyrosine-15. *Science* **270**, (1995).
229. Pines, J. & Hunter, T. Human cyclins A and B1 are differentially located in the cell and undergo cell cycle-dependent nuclear transport. *J. Cell Biol.* **115**, 1–17 (1991).
230. Draviam, V. M., Orrechia, S., Lowe, M., Pardi, R. & Pines, J. The Localization of Human Cyclins B1 and B2 Determines Cdk1 Substrate Specificity and Neither Enzyme Requires Mek to Disassemble the Golgi Apparatus. *J. Cell Biol.* **152**, 945 (2001).
231. Bentley, A. M., Normand, G., Hoyt, J. & King, R. W. Distinct Sequence Elements of Cyclin B1 Promote Localization to Chromatin, Centrosomes, and Kinetochores during Mitosis. *Mol. Biol. Cell* **18**, 4847–4858 (2007).
232. Valles, S. Y., Godek, K. M. & Compton, D. A. Cyclin A/Cdk1 promotes chromosome alignment and timely mitotic progression. *bioRxiv* 2023.12.21.572788 (2023) doi:10.1101/2023.12.21.572788.
233. Sciortino, S. *et al.* The cyclin B1 gene is actively transcribed during mitosis in HeLa cells. *EMBO Rep.* **2**, 1018–1023 (2001).
234. Strauss, B. *et al.* Cyclin B1 is essential for mitosis in mouse embryos, and its nuclear export sets the time for mitosis. *J. Cell Biol.* **217**, 179 (2018).
235. Zheng, X.-F. *et al.* CDK5–cyclin B1 regulates mitotic fidelity. *Nature* **633**, 932–940 (2024).
236. Chen, Q., Zhang, X., Jiang, Q., Clarke, P. R. & Zhang, C. Cyclin B1 is localized to unattached kinetochores and contributes to efficient microtubule attachment and proper chromosome alignment during mitosis. *Cell Res.* **18**, 268–280 (2008).
237. Yamano, H., Gannon, J., Mahbubani, H. & Hunt, T. Cell Cycle-Regulated Recognition of the Destruction Box of Cyclin B by the APC/C in Xenopus Egg Extracts. *Mol. Cell* **13**, 137–147 (2004).
238. Nasmyth, K. & Haering, C. H. Cohesin: its roles and mechanisms. *Annu. Rev. Genet.* **43**, 525–558 (2009).
239. Morgan, D. O. Principles of CDK regulation. *Nature* **374**, 131–134 (1995).
240. Et, C. *et al.* INK4 proteins, a family of mammalian CDK inhibitors with novel biological functions. *IUBMB Life* **59**, (2007).
241. Morris-Hanon, O. *et al.* The Cell Cycle Inhibitors p21Cip1 and p27Kip1 Control Proliferation but Enhance DNA Damage Resistance of Glioma Stem Cells. *Neoplasia N. Y. N* **19**, 519 (2017).
242. Di Leonardo, A., Linke, S. P., Clarkin, K. & Wahl, G. M. DNA damage triggers a prolonged p53-dependent G1 arrest and long-term induction of Cip1 in normal human fibroblasts. *Genes Dev.* **8**, 2540–2551 (1994).
243. Kastenhuber, E. R. & Lowe, S. W. Putting p53 in Context. *Cell* **170**, 1062–1078 (2017).
244. Borrero, L. J. H. & El-Deiry, W. S. Tumor Suppressor p53: Biology, Signaling Pathways, and Therapeutic Targeting. *Biochim. Biophys. Acta Rev. Cancer* **1876**, 188556 (2021).
245. Lane, D. P. Cancer. p53, guardian of the genome. *Nature* **358**, 15–16 (1992).
246. Waga, S., Hannon, G. J., Beach, D. & Stillman, B. The p21 inhibitor of cyclin-dependent kinases controls DNA replication by interaction with PCNA. *Nature* **369**, 574–578 (1994).
247. Umar, A. *et al.* Requirement for PCNA in DNA mismatch repair at a step preceding DNA resynthesis. *Cell* **87**, 65–73 (1996).
248. Delavaine, L. & La Thangue, N. B. Control of E2F activity by p21Waf1/Cip1. *Oncogene* **18**, 5381–5392 (1999).
249. Coqueret, O. & Gascan, H. Functional interaction of STAT3 transcription factor with the cell cycle inhibitor p21WAF1/CIP1/SDI1. *J. Biol. Chem.* **275**, 18794–18800 (2000).
250. Dotto, G. P. p21(WAF1/Cip1): more than a break to the cell cycle? *Biochim. Biophys. Acta* **1471**, M43-56 (2000).
251. Kitaura, H. *et al.* Reciprocal Regulation via Protein-Protein Interaction between c-Myc and p21 cip1/waf1/sdi1 in DNA Replication and Transcription *. *J. Biol. Chem.* **275**, 10477–10483 (2000).

252. Tom, S., Ranalli, T. A., Podust, V. N. & Bambara, R. A. Regulatory roles of p21 and apurinic/apyrimidinic endonuclease 1 in base excision repair. *J. Biol. Chem.* **276**, 48781–48789 (2001).
253. Roninson, I. B. Oncogenic functions of tumour suppressor p21(Waf1/Cip1/Sdi1): association with cell senescence and tumour-promoting activities of stromal fibroblasts. *Cancer Lett.* **179**, 1–14 (2002).
254. Besson, A., Dowdy, S. F. & Roberts, J. M. CDK inhibitors: cell cycle regulators and beyond. *Dev. Cell* **14**, 159–169 (2008).
255. Whittaker, S. R., Mallinger, A., Workman, P. & Clarke, P. A. Inhibitors of Cyclin-Dependent Kinases as Cancer Therapeutics. *Pharmacol. Ther.* **173**, 83–105 (2017).
256. Gralewska, P., Gajek, A., Marczak, A. & Rogalska, A. Participation of the ATR/CHK1 pathway in replicative stress targeted therapy of high-grade ovarian cancer. *J. Hematol. Oncol.J Hematol Oncol* **13**, 39 (2020).
257. Blackford, A. N. & Jackson, S. P. ATM, ATR, and DNA-PK: The Trinity at the Heart of the DNA Damage Response. *Mol. Cell* **66**, 801–817 (2017).
258. Singleton, B. K., Torres-Arzayus, M. I., Rottinghaus, S. T., Taccioli, G. E. & Jeggo, P. A. The C terminus of Ku80 activates the DNA-dependent protein kinase catalytic subunit. *Mol. Cell. Biol.* **19**, 3267–3277 (1999).
259. Falck, J., Coates, J. & Jackson, S. P. Conserved modes of recruitment of ATM, ATR and DNA-PKcs to sites of DNA damage. *Nature* **434**, 605–611 (2005).
260. Yang, J. *et al.* ATM and ATR: Sensing DNA damage. *World J. Gastroenterol.* **10**, 155–160 (2004).
261. Jazayeri, A. *et al.* ATM- and cell cycle-dependent regulation of ATR in response to DNA double-strand breaks. *Nat. Cell Biol.* **8**, 37–45 (2006).
262. Mirza-Aghazadeh-Attari, M. *et al.* DNA damage response and repair in colorectal cancer: Defects, regulation and therapeutic implications. *DNA Repair* **69**, 34–52 (2018).
263. O'Connor, M. J. Targeting the DNA Damage Response in Cancer. *Mol. Cell* **60**, 547–560 (2015).
264. Rayess, H., Wang, M. B. & Srivatsan, E. S. Cellular senescence and tumor suppressor gene p16. *Int. J. Cancer J. Int. Cancer* **130**, 1715–1725 (2012).
265. Pavel, M. *et al.* Contact inhibition controls cell survival and proliferation via YAP/TAZ-autophagy axis. *Nat. Commun.* **9**, 2961 (2018).
266. Mao, Z., Ke, Z., Gorbunova, V. & Seluanov, A. Replicatively senescent cells are arrested in G1 and G2 phases. *Aging* **4**, 431 (2012).
267. Yamashiro, Y. *et al.* Cyclin-Dependent Kinase Inhibitor p16 and p21 Expression, and Cell Cycle Change in Human Lens Epithelial Cell Line SRA 01/04 following Contact Inhibition in Normal Culture. *Ophthalmic Res.* **46**, 38–43 (2011).
268. Sun, P. Contact inhibition against senescence. *Oncotarget* **5**, 7212 (2014).
269. Mazouzi, A., Velimezi, G. & Loizou, J. I. DNA replication stress: causes, resolution and disease. *Exp. Cell Res.* **329**, 85–93 (2014).
270. Zeman, M. K. & Cimprich, K. A. Causes and consequences of replication stress. *Nat. Cell Biol.* **16**, 2–9 (2014).
271. Magnaghi-Jaulin, L., Eot-Houllier, G., Gallaud, E. & Giet, R. Aurora A Protein Kinase: To the Centrosome and Beyond. *Biomolecules* **9**, 28 (2019).
272. Compton, D. A. Focusing on spindle poles. *J. Cell Sci.* **111 (Pt 11)**, 1477–1481 (1998).
273. Tamura, N. & Draviam, V. M. Microtubule plus-ends within a mitotic cell are 'moving platforms' with anchoring, signalling and force-coupling roles. *Open Biol.* **2**, 120132 (2012).
274. Akhmanova, A. & Steinmetz, M. O. Tracking the ends: a dynamic protein network controls the fate of microtubule tips. *Nat. Rev. Mol. Cell Biol.* **9**, 309–322 (2008).
275. Prosser, S. L. & Pelletier, L. Mitotic spindle assembly in animal cells: a fine balancing act. *Nat. Rev. Mol. Cell Biol.* **18**, 187–201 (2017).
276. Karki, S. & Holzbaur, E. L. Affinity chromatography demonstrates a direct binding between cytoplasmic dynein and the dynactin complex. *J. Biol. Chem.* **270**, 28806–28811 (1995).
277. Li, Y., Yu, W., Liang, Y. & Zhu, X. Kinetochore dynein generates a poleward pulling force to facilitate congression and full chromosome alignment. *Cell Res.* **17**, 701–712 (2007).
278. Yang, Z., Tulu, U. S., Wadsworth, P. & Rieder, C. L. Kinetochore dynein is required for chromosome motion and congression independent of the spindle checkpoint. *Curr. Biol. CB* **17**, 973–980 (2007).
279. Dwivedi, D. & Sharma, M. Multiple Roles, Multiple Adaptors: Dynein During Cell Cycle. *Adv. Exp. Med. Biol.* **1112**, 13–30 (2018).
280. Dujardin, D. *et al.* Evidence for a Role of CLIP-170 in the Establishment of Metaphase Chromosome Alignment. *J. Cell Biol.* **141**, 849–862 (1998).
281. Akhmanova, A. *et al.* Clasps are CLIP-115 and -170 associating proteins involved in the regional regulation of microtubule dynamics in motile fibroblasts. *Cell* **104**, 923–935 (2001).
282. Pierre, P., Scheel, J., Rickard, J. E. & Kreis, T. E. CLIP-170 links endocytic vesicles to microtubules. *Cell* **70**, 887–900 (1992).
283. Weisbrich, A. *et al.* Structure-function relationship of CAP-Gly domains. *Nat. Struct. Mol. Biol.* **14**, 959–967 (2007).

284. Desai, A., Verma, S., Mitchison, T. J. & Walczak, C. E. Kin I kinesins are microtubule-destabilizing enzymes. *Cell* **96**, 69–78 (1999).
285. Hunter, A. W. *et al.* The kinesin-related protein MCAK is a microtubule depolymerase that forms an ATP-hydrolyzing complex at microtubule ends. *Mol. Cell* **11**, 445–457 (2003).
286. Moore, A. T. *et al.* MCAK associates with the tips of polymerizing microtubules. *J. Cell Biol.* **169**, 391–397 (2005).
287. Lee, T., Langford, K. J., Askham, J. M., Brüning-Richardson, A. & Morrison, E. E. MCAK associates with EB1. *Oncogene* **27**, 2494–2500 (2008).
288. Andrews, P. D. *et al.* Aurora B regulates MCAK at the mitotic centromere. *Dev. Cell* **6**, 253–268 (2004).
289. Gorbsky, G. J. Mitosis: MCAK under the aura of Aurora B. *Curr. Biol. CB* **14**, R346-348 (2004).
290. Lan, W. *et al.* Aurora B phosphorylates centromeric MCAK and regulates its localization and microtubule depolymerization activity. *Curr. Biol. CB* **14**, 273–286 (2004).
291. Ohno, S. So much 'junk' DNA in our genome. *Brookhaven Symp. Biol.* **23**, 366–370 (1972).
292. Zuckerkandl, E. Revisiting junk DNA. *J. Mol. Evol.* **34**, 259–271 (1992).
293. Lander, E. S. *et al.* Initial sequencing and analysis of the human genome. *Nature* **409**, 860–921 (2001).
294. International Human Genome Sequencing Consortium. Finishing the euchromatic sequence of the human genome. *Nature* **431**, 931–945 (2004).
295. Altemose, N. A classical revival: Human satellite DNAs enter the genomics era. *Semin. Cell Dev. Biol.* **128**, 2–14 (2022).
296. Altemose, N., Miga, K. H., Maggioni, M. & Willard, H. F. Genomic Characterization of Large Heterochromatic Gaps in the Human Genome Assembly. *PLOS Comput. Biol.* **10**, e1003628 (2014).
297. Nurk, S. *et al.* The complete sequence of a human genome. *Science* **376**, 44–53 (2022).
298. Thakur, J., Packiaraj, J. & Henikoff, S. Sequence, Chromatin and Evolution of Satellite DNA. *Int. J. Mol. Sci.* **22**, 4309 (2021).
299. Liao, X. *et al.* Repetitive DNA sequence detection and its role in the human genome. *Commun. Biol.* **6**, 954 (2023).
300. Lee, C., Wevrick, R., Fisher, R. B., Ferguson-Smith, M. A. & Lin, C. C. Human centromeric DNAs. *Hum. Genet.* **100**, 291–304 (1997).
301. Podgornaya, O., Dey, R., Lobov, I. & Enukashvili, N. Human satellite 3 (HS3) binding protein from the nuclear matrix: isolation and binding properties. *Biochim. Biophys. Acta* **1497**, 204–214 (2000).
302. Komissarov, A. S., Gavrilova, E. V., Demin, S. J., Ishov, A. M. & Podgornaya, O. I. Tandemly repeated DNA families in the mouse genome. *BMC Genomics* **12**, 531 (2011).
303. Musacchio, A. & Desai, A. A Molecular View of Kinetochore Assembly and Function. *Biology* **6**, 5 (2017).
304. Ozkan, E. & Lacerda, M. P. Genetics, Cytogenetic Testing And Conventional Karyotype. in *StatPearls* (StatPearls Publishing, Treasure Island (FL), 2025).
305. Westhorpe, F. G. & Straight, A. F. Functions of the centromere and kinetochore in chromosome segregation. *Curr. Opin. Cell Biol.* **25**, 334–340 (2013).
306. McNulty, S. M. & Sullivan, B. A. Alpha satellite DNA biology: Finding function in the recesses of the genome. *Chromosome Res. Int. J. Mol. Supramol. Evol. Asp. Chromosome Biol.* **26**, 115–138 (2018).
307. Altemose, N. *et al.* Complete genomic and epigenetic maps of human centromeres. *Science* **376**, eabl4178 (2022).
308. Willard, H. F. Chromosome-specific organization of human alpha satellite DNA. *Am. J. Hum. Genet.* **37**, 524–532 (1985).
309. Waye, J. S. & Willard, H. F. Nucleotide sequence heterogeneity of alpha satellite repetitive DNA: a survey of alphoid sequences from different human chromosomes. *Nucleic Acids Res.* **15**, 7549–7569 (1987).
310. Miga, K. H. *et al.* Telomere-to-telomere assembly of a complete human X chromosome. *Nature* **585**, 79–84 (2020).
311. Logsdon, G. A. *et al.* The structure, function and evolution of a complete human chromosome 8. *Nature* **593**, 101–107 (2021).
312. Gershman, A. *et al.* Epigenetic Patterns in a Complete Human Genome. *Science* **376**, eabj5089 (2022).
313. Alexandrov, I., Kazakov, A., Tumeneva, I., Shepelev, V. & Yurov, Y. Alpha-satellite DNA of primates: old and new families. *Chromosoma* **110**, 253–266 (2001).
314. Shepelev, V. A., Alexandrov, A. A., Yurov, Y. B. & Alexandrov, I. A. The Evolutionary Origin of Man Can Be Traced in the Layers of Defunct Ancestral Alpha Satellites Flanking the Active Centromeres of Human Chromosomes. *PLoS Genet.* **5**, e1000641 (2009).
315. Jones, K. W., Prosser, J., Corneo, G. & Ginelli, E. The chromosomal location of human satellite DNA 3. *Chromosoma* **42**, 445–451 (1973).
316. Palmer, D. K., O'Day, K., Wener, M. H., Andrews, B. S. & Margolis, R. L. A 17-kD centromere protein (CENP-A) copurifies with nucleosome core particles and with histones. *J. Cell Biol.* **104**, 805–815 (1987).

317. Palmer, D. K., O'Day, K., Trong, H. L., Charbonneau, H. & Margolis, R. L. Purification of the centromere-specific protein CENP-A and demonstration that it is a distinctive histone. *Proc. Natl. Acad. Sci. U. S. A.* **88**, 3734–3738 (1991).
318. Sullivan, K. F., Hechenberger, M. & Masri, K. Human CENP-A contains a histone H3 related histone fold domain that is required for targeting to the centromere. *J. Cell Biol.* **127**, 581–592 (1994).
319. Meluh, P. B., Yang, P., Glowczewski, L., Koshland, D. & Smith, M. M. Cse4p is a component of the core centromere of Saccharomyces cerevisiae. *Cell* **94**, 607–613 (1998).
320. Oegema, K., Desai, A., Rybina, S., Kirkham, M. & Hyman, A. A. Functional Analysis of Kinetochore Assembly in Caenorhabditis elegans. *J. Cell Biol.* **153**, 1209–1226 (2001).
321. Barnhart, M. C. *et al.* HJURP is a CENP-A chromatin assembly factor sufficient to form a functional de novo kinetochore. *J. Cell Biol.* **194**, 229–243 (2011).
322. Mendiburo, M. J., Padeken, J., Fülöp, S., Schepers, A. & Heun, P. Drosophila CENH3 is sufficient for centromere formation. *Science* **334**, 686–690 (2011).
323. Fachinetti, D. *et al.* A two-step mechanism for epigenetic specification of centromere identity and function. *Nat. Cell Biol.* **15**, 1056–1066 (2013).
324. Stellfox, M. E., Bailey, A. O. & Foltz, D. R. Putting CENP-A in its place. *Cell. Mol. Life Sci. CMLS* **70**, 387–406 (2013).
325. Hoffmann, S. *et al.* CENP-A Is Dispensable for Mitotic Centromere Function after Initial Centromere/Kinetochore Assembly. *Cell Rep.* **17**, 2394–2404 (2016).
326. Mahlke, M. A. *et al.* Evolution and instability of human centromeres are accelerated by heterochromatin boundary loss and CENP-A overexpression. *BioRxiv Prepr. Serv. Biol.* 2025.02.03.636285 (2025) doi:10.1101/2025.02.03.636285.
327. Amor, D. J. *et al.* Human centromere repositioning 'in progress'. *Proc. Natl. Acad. Sci. U. S. A.* **101**, 6542–6547 (2004).
328. Logsdon, G. A. *et al.* Both tails and the centromere targeting domain of CENP-A are required for centromere establishment. *J. Cell Biol.* **208**, 521–531 (2015).
329. Dunleavy, E. M. *et al.* HJURP is a cell-cycle-dependent maintenance and deposition factor of CENP-A at centromeres. *Cell* **137**, 485–497 (2009).
330. Foltz, D. R. *et al.* Centromere-specific assembly of CENP-a nucleosomes is mediated by HJURP. *Cell* **137**, 472–484 (2009).
331. Bernad, R. *et al.* Xenopus HJURP and condensin II are required for CENP-A assembly. *J. Cell Biol.* **192**, 569–582 (2011).
332. Fujita, Y. *et al.* Priming of centromere for CENP-A recruitment by human hMis18alpha, hMis18beta, and M18BP1. *Dev. Cell* **12**, 17–30 (2007).
333. Rošić, S., Köhler, F. & Erhardt, S. Repetitive centromeric satellite RNA is essential for kinetochore formation and cell division. *J. Cell Biol.* **207**, 335–349 (2014).
334. Wang, J. *et al.* Mitotic regulator Mis18β interacts with and specifies the centromeric assembly of molecular chaperone holliday junction recognition protein (HJURP). *J. Biol. Chem.* **289**, 8326–8336 (2014).
335. McNulty, S. M., Sullivan, L. L. & Sullivan, B. A. Human centromeres produce chromosome-specific and array-specific alpha satellite transcripts that are complexed with CENP-A and CENP-C. *Dev. Cell* **42**, 226-240.e6 (2017).
336. Black, B. E. *et al.* Centromere identity maintained by nucleosomes assembled with histone H3 containing the CENP-A targeting domain. *Mol. Cell* **25**, 309–322 (2007).
337. Fachinetti, D. *et al.* A two-step mechanism for epigenetic specification of centromere identity and function. *Nat. Cell Biol.* **15**, 1056–1066 (2013).
338. Shelby, R. D., Vafa, O. & Sullivan, K. F. Assembly of CENP-A into Centromeric Chromatin Requires a Cooperative Array of Nucleosomal DNA Contact Sites. *J. Cell Biol.* **136**, 501–513 (1997).
339. Shelby, R. D., Monier, K. & Sullivan, K. F. Chromatin Assembly at Kinetochores Is Uncoupled from DNA Replication. *J. Cell Biol.* **151**, 1113–1118 (2000).
340. Jansen, L. E. T., Black, B. E., Foltz, D. R. & Cleveland, D. W. Propagation of centromeric chromatin requires exit from mitosis. *J. Cell Biol.* **176**, 795–805 (2007).
341. Silva, M. C. C. *et al.* Cdk activity couples epigenetic centromere inheritance to cell cycle progression. *Dev. Cell* **22**, 52–63 (2012).
342. McKinley, K. L. & Cheeseman, I. M. Polo-like kinase 1 licenses CENP-A deposition at centromeres. *Cell* **158**, 397–411 (2014).
343. Müller, S. *et al.* Phosphorylation and DNA binding of HJURP determine its centromeric recruitment and function in CenH3(CENP-A) loading. *Cell Rep.* **8**, 190–203 (2014).
344. Yu, Z. *et al.* Dynamic phosphorylation of CENP-A at Ser68 orchestrates its cell-cycle-dependent deposition at centromeres. *Dev. Cell* **32**, 68–81 (2015).

345. Masumoto, H., Masukata, H., Muro, Y., Nozaki, N. & Okazaki, T. A human centromere antigen (CENP-B) interacts with a short specific sequence in alphoid DNA, a human centromeric satellite. *J. Cell Biol.* **109**, 1963–1973 (1989).
346. Hudson, D. F. *et al.* Centromere Protein B Null Mice are Mitotically and Meiotically Normal but Have Lower Body and Testis Weights. *J. Cell Biol.* **141**, 309–319 (1998).
347. Kapoor, M. *et al.* The cenpB gene is not essential in mice. *Chromosoma* **107**, 570–576 (1998).
348. Perez-Castro, A. V. *et al.* Centromeric protein B null mice are viable with no apparent abnormalities. *Dev. Biol.* **201**, 135–143 (1998).
349. Fachinetti, D. *et al.* DNA Sequence-Specific Binding of CENP-B Enhances the Fidelity of Human Centromere Function. *Dev. Cell* **33**, 314–327 (2015).
350. Mitra, S., Srinivasan, B. & Jansen, L. E. T. Stable inheritance of CENP-A chromatin: Inner strength versus dynamic control. *J. Cell Biol.* **219**, e202005099 (2020).
351. Suzuki, N. *et al.* CENP-B interacts with CENP-C domains containing Mif2 regions responsible for centromere localization. *J. Biol. Chem.* **279**, 5934–5946 (2004).
352. French, B. T. & Straight, A. F. Swapping CENP-A at the centromere. *Nat. Cell Biol.* **15**, 1028–1030 (2013).
353. Chan, F. L. *et al.* Active transcription and essential role of RNA polymerase II at the centromere during mitosis. *Proc. Natl. Acad. Sci. U. S. A.* **109**, 1979–1984 (2012).
354. Blower, M. D. Centromeric transcription regulates Aurora-B localization and activation. *Cell Rep.* **15**, 1624–1633 (2016).
355. Grenfell, A. W., Heald, R. & Strzelecka, M. Mitotic noncoding RNA processing promotes kinetochore and spindle assembly in Xenopus. *J. Cell Biol.* **214**, 133 (2016).
356. Perea-Resa, C. & Blower, M. D. Centromere Biology: Transcription Goes on Stage. *Mol. Cell. Biol.* **38**, e00263-18 (2018).
357. Peters, A. H. *et al.* Loss of the Suv39h histone methyltransferases impairs mammalian heterochromatin and genome stability. *Cell* **107**, 323–337 (2001).
358. Zhu, Q. *et al.* BRCA1 tumour suppression occurs via heterochromatin-mediated silencing. *Nature* **477**, 179–184 (2011).
359. Peters, A. H. F. M. *et al.* Loss of the Suv39h Histone Methyltransferases Impairs Mammalian Heterochromatin and Genome Stability. *Cell* **107**, 323–337 (2001).
360. Lehnertz, B. *et al.* Suv39h-mediated histone H3 lysine 9 methylation directs DNA methylation to major satellite repeats at pericentric heterochromatin. *Curr. Biol. CB* **13**, 1192–1200 (2003).
361. Bulut-Karslioglu, A. *et al.* Suv39h-Dependent H3K9me3 Marks Intact Retrotransposons and Silences LINE Elements in Mouse Embryonic Stem Cells. *Mol. Cell* **55**, 277–290 (2014).
362. Fuks, F., Hurd, P. J., Deplus, R. & Kouzarides, T. The DNA methyltransferases associate with HP1 and the SUV39H1 histone methyltransferase. *Nucleic Acids Res.* **31**, 2305–2312 (2003).
363. Johnson, W. L. *et al.* RNA-dependent stabilization of SUV39H1 at constitutive heterochromatin. *eLife* **6**, e25299 (2017).
364. Johnson, L., Cao, X. & Jacobsen, S. Interplay between two epigenetic marks. DNA methylation and histone H3 lysine 9 methylation. *Curr. Biol. CB* **12**, 1360–1367 (2002).
365. Carroll, C. W., Milks, K. J. & Straight, A. F. Dual recognition of CENP-A nucleosomes is required for centromere assembly. *J. Cell Biol.* **189**, 1143–1155 (2010).
366. McKinley, K. L. *et al.* The CENP-L-N Complex Forms a Critical Node in an Integrated Meshwork of Interactions at the Centromere-Kinetochore Interface. *Mol. Cell* **60**, 886–898 (2015).
367. Rago, F., Gascoigne, K. E. & Cheeseman, I. M. Distinct organization and regulation of the outer kinetochore KMN network downstream of CENP-C and CENP-T. *Curr. Biol. CB* **25**, 671–677 (2015).
368. Suzuki, A., Badger, B. L. & Salmon, E. D. A quantitative description of Ndc80 complex linkage to human kinetochores. *Nat. Commun.* **6**, 8161 (2015).
369. Huis In 't Veld, P. J. *et al.* Molecular basis of outer kinetochore assembly on CENP-T. *eLife* **5**, e21007 (2016).
370. Takenoshita, Y., Hara, M. & Fukagawa, T. Recruitment of two Ndc80 complexes via the CENP-T pathway is sufficient for kinetochore functions. *Nat. Commun.* **13**, 851 (2022).
371. Saitoh, H. *et al.* CENP-C, an autoantigen in scleroderma, is a component of the human inner kinetochore plate. *Cell* **70**, 115–125 (1992).
372. Tomkiel, J., Cooke, C. A., Saitoh, H., Bernat, R. L. & Earnshaw, W. C. CENP-C is required for maintaining proper kinetochore size and for a timely transition to anaphase. *J. Cell Biol.* **125**, 531–545 (1994).
373. Sugimoto, K., Yata, H., Muro, Y. & Himeno, M. Human centromere protein C (CENP-C) is a DNA-binding protein which possesses a novel DNA-binding motif. *J. Biochem. (Tokyo)* **116**, 877–881 (1994).
374. Politi, V. *et al.* CENP-C binds the alpha-satellite DNA in vivo at specific centromere domains. *J. Cell Sci.* **115**, 2317–2327 (2002).
375. Trazzi, S. *et al.* In vivo functional dissection of human inner kinetochore protein CENP-C. *J. Struct. Biol.* **140**, 39–48 (2002).

376. Song, K., Gronemeyer, B., Lu, W., Eugster, E. & Tomkiel, J. E. Mutational analysis of the central centromere targeting domain of human centromere protein C, (CENP-C). *Exp. Cell Res.* **275**, 81–91 (2002).
377. Trazzi, S. *et al.* The C-Terminal Domain of CENP-C Displays Multiple and Critical Functions for Mammalian Centromere Formation. *PLoS ONE* **4**, e5832 (2009).
378. Sugimoto, K., Kuriyama, K., Shibata, A. & Himeno, M. Characterization of internal DNA-binding and C-terminal dimerization domains of human centromere/kinetochore autoantigen CENP-C in vitro: role of DNA-binding and self-associating activities in kinetochore organization. *Chromosome Res. Int. J. Mol. Supramol. Evol. Asp. Chromosome Biol.* **5**, 132–141 (1997).
379. Cohen, R. L. *et al.* Structural and Functional Dissection of Mif2p, a Conserved DNA-binding Kinetochore Protein. *Mol. Biol. Cell* **19**, 4480–4491 (2008).
380. Lanini, L. & McKeon, F. Domains required for CENP-C assembly at the kinetochore. *Mol. Biol. Cell* **6**, 1049–1059 (1995).
381. Milks, K. J., Moree, B. & Straight, A. F. Dissection of CENP-C-directed centromere and kinetochore assembly. *Mol. Biol. Cell* **20**, 4246–4255 (2009).
382. Screpanti, E. *et al.* Direct binding of Cenp-C to the Mis12 complex joins the inner and outer kinetochore. *Curr. Biol. CB* **21**, 391–398 (2011).
383. Kato, H. *et al.* A conserved mechanism for centromeric nucleosome recognition by centromere protein CENP-C. *Science* **340**, 1110–1113 (2013).
384. Klare, K. *et al.* CENP-C is a blueprint for constitutive centromere–associated network assembly within human kinetochores. *J. Cell Biol.* **210**, 923–934 (2015).
385. Hori, T. *et al.* CCAN makes multiple contacts with centromeric DNA to provide distinct pathways to the outer kinetochore. *Cell* **135**, 1039–1052 (2008).
386. Gascoigne, K. E. *et al.* Induced ectopic kinetochore assembly bypasses the requirement for CENP-A nucleosomes. *Cell* **145**, 410–422 (2011).
387. Kim, S. & Yu, H. Multiple assembly mechanisms anchor the KMN spindle checkpoint platform at human mitotic kinetochores. *J. Cell Biol.* **208**, 181–196 (2015).
388. Petrovic, A. *et al.* Structure of the MIS12 Complex and Molecular Basis of Its Interaction with CENP-C at Human Kinetochores. *Cell* **167**, 1028-1040.e15 (2016).
389. Kiyomitsu, T., Obuse, C. & Yanagida, M. Human Blinkin/AF15q14 is required for chromosome alignment and the mitotic checkpoint through direct interaction with Bub1 and BubR1. *Dev. Cell* **13**, 663–676 (2007).
390. Petrovic, A. *et al.* The MIS12 complex is a protein interaction hub for outer kinetochore assembly. *J. Cell Biol.* **190**, 835–852 (2010).
391. Kiyomitsu, T., Obuse, C. & Yanagida, M. Human Blinkin/AF15q14 is required for chromosome alignment and the mitotic checkpoint through direct interaction with Bub1 and BubR1. *Dev. Cell* **13**, 663–676 (2007).
392. Musacchio, A. & Salmon, E. D. The spindle-assembly checkpoint in space and time. *Nat. Rev. Mol. Cell Biol.* **8**, 379–393 (2007).
393. Cheeseman, I. M., Chappie, J. S., Wilson-Kubalek, E. M. & Desai, A. The Conserved KMN Network Constitutes the Core Microtubule-Binding Site of the Kinetochore. *Cell* **127**, 983–997 (2006).
394. Ciferri, C. *et al.* Architecture of the human ndc80-hec1 complex, a critical constituent of the outer kinetochore. *J. Biol. Chem.* **280**, 29088–29095 (2005).
395. Wei, R. R. *et al.* Structure of a central component of the yeast kinetochore: the Spc24p/Spc25p globular domain. *Struct. Lond. Engl. 1993* **14**, 1003–1009 (2006).
396. Wei, R. R., Sorger, P. K. & Harrison, S. C. Molecular organization of the Ndc80 complex, an essential kinetochore component. *Proc. Natl. Acad. Sci. U. S. A.* **102**, 5363–5367 (2005).
397. Wei, R. R., Al-Bassam, J. & Harrison, S. C. The Ndc80/HEC1 complex is a contact point for kinetochore-microtubule attachment. *Nat. Struct. Mol. Biol.* **14**, 54–59 (2007).
398. Martin-Lluesma, S., Stucke, V. M. & Nigg, E. A. Role of Hec1 in spindle checkpoint signaling and kinetochore recruitment of Mad1/Mad2. *Science* **297**, 2267–2270 (2002).
399. Kops, G. J. P. L. & Gassmann, R. Crowning the Kinetochore: The Fibrous Corona in Chromosome Segregation. *Trends Cell Biol.* **30**, 653–667 (2020).
400. Mosalaganti, S. *et al.* Structure of the RZZ complex and molecular basis of its interaction with Spindly. *J. Cell Biol.* **216**, 961–981 (2017).
401. Vaughan, K. T. & Vallee, R. B. Cytoplasmic dynein binds dynactin through a direct interaction between the intermediate chains and p150Glued. *J. Cell Biol.* **131**, 1507–1516 (1995).
402. Schroer, T. A. Dynactin. *Annu. Rev. Cell Dev. Biol.* **20**, 759–779 (2004).
403. Dixit, R., Levy, J. R., Tokito, M., Ligon, L. A. & Holzbaur, E. L. F. Regulation of Dynactin through the Differential Expression of p150Glued Isoforms. *J. Biol. Chem.* **283**, 33611–33619 (2008).
404. Waterman-Storer, C. M., Karki, S. & Holzbaur, E. L. The p150Glued component of the dynactin complex binds to both microtubules and the actin-related protein centractin (Arp-1). *Proc. Natl. Acad. Sci. U. S. A.* **92**, 1634–1638 (1995).

405. Yao, X., Anderson, K. L. & Cleveland, D. W. The microtubule-dependent motor centromere-associated protein E (CENP-E) is an integral component of kinetochore corona fibers that link centromeres to spindle microtubules. *J. Cell Biol.* **139**, 435–447 (1997).
406. Magidson, V. *et al.* The spatial arrangement of chromosomes during prometaphase facilitates spindle assembly. *Cell* **146**, 555–567 (2011).
407. Conti, D. *et al.* How are Dynamic Microtubules Stably Tethered to Human Chromosomes? in *Cytoskeleton - Structure, Dynamics, Function and Disease* (IntechOpen, 2017). doi:10.5772/intechopen.68321.
408. Ault, J. G., Demarco, A. J., Salmon, E. D. & Rieder, C. L. Studies on the ejection properties of asters: astral microtubule turnover influences the oscillatory behavior and positioning of mono-oriented chromosomes. *J. Cell Sci.* **99**, 701–710 (1991).
409. Maiato, H., Gomes, A. M., Sousa, F. & Barisic, M. Mechanisms of Chromosome Congression during Mitosis. *Biology* **6**, 13 (2017).
410. Kapoor, T. M. *et al.* Chromosomes Can Congress to the Metaphase Plate Before Biorientation. *Science* **311**, 388–391 (2006).
411. Kim, Y., Holland, A. J., Lan, W. & Cleveland, D. W. Aurora kinases and protein phosphatase 1 mediate chromosome congression through regulation of CENP-E. *Cell* **142**, 444–455 (2010).
412. Eibes, S. *et al.* CENP-E activation by Aurora A and B controls kinetochore fibrous corona disassembly. *Nat. Commun.* **14**, 5317 (2023).
413. Shrestha, R. L. & Draviam, V. M. Lateral to end-on conversion of chromosome-microtubule attachment requires kinesins CENP-E and MCAK. *Curr. Biol. CB* **23**, 1514–1526 (2013).
414. DeLuca, J. G. *et al.* Hec1 and Nuf2 Are Core Components of the Kinetochore Outer Plate Essential for Organizing Microtubule Attachment Sites. *Mol. Biol. Cell* **16**, 519–531 (2005).
415. Shrestha, R. L. *et al.* Aurora-B kinase pathway controls the lateral to end-on conversion of kinetochore-microtubule attachments in human cells. *Nat. Commun.* **8**, 150 (2017).
416. Gergely, F., Draviam, V. M. & Raff, J. W. The ch-TOG/XMAP215 protein is essential for spindle pole organization in human somatic cells. *Genes Dev.* **17**, 336–341 (2003).
417. Maiato, H. *et al.* Human CLASP1 is an outer kinetochore component that regulates spindle microtubule dynamics. *Cell* **113**, 891–904 (2003).
418. Mimori-Kiyosue, Y. *et al.* Mammalian CLASPs are required for mitotic spindle organization and kinetochore alignment. *Genes Cells Devoted Mol. Cell. Mech.* **11**, 845–857 (2006).
419. Gaitanos, T. N. *et al.* Stable kinetochore-microtubule interactions depend on the Ska complex and its new component Ska3/C13Orf3. *EMBO J.* **28**, 1442–1452 (2009).
420. Miller, M. P., Asbury, C. L. & Biggins, S. A TOG Protein Confers Tension Sensitivity to Kinetochore-Microtubule Attachments. *Cell* **165**, 1428–1439 (2016).
421. Conti, D. *et al.* Kinetochores attached to microtubule-ends are stabilised by Astrin bound PP1 to ensure proper chromosome segregation. *eLife* **8**, e49325 (2019).
422. Polley, S. *et al.* Stable kinetochore-microtubule attachment requires loop-dependent Ndc80-Ndc80 binding. *EMBO J.* **42**, e112504 (2023).
423. Radhakrishnan, R. M., Stokes, L., Day, M., Veld, P. J. H. in 't & Volkov, V. A. Microtubule end stabilisation by cooperative oligomers of Ska and Ndc80 complexes. 2025.07.06.663352 Preprint at https://doi.org/10.1101/2025.07.06.663352 (2025).
424. Mack, G. J. & Compton, D. A. Analysis of mitotic microtubule-associated proteins using mass spectrometry identifies astrin, a spindle-associated protein. *Proc. Natl. Acad. Sci. U. S. A.* **98**, 14434–14439 (2001).
425. Schmidt, J. C. *et al.* Aurora B kinase controls the targeting of the Astrin-SKAP complex to bioriented kinetochores. *J. Cell Biol.* **191**, 269–280 (2010).
426. Liu, D. *et al.* Regulated targeting of protein phosphatase 1 to the outer kinetochore by KNL1 opposes Aurora B kinase. *J. Cell Biol.* **188**, 809–820 (2010).
427. Hanisch, A., Silljé, H. H. W. & Nigg, E. A. Timely anaphase onset requires a novel spindle and kinetochore complex comprising Ska1 and Ska2. *EMBO J.* **25**, 5504–5515 (2006).
428. Welburn, J. P. I. *et al.* The human kinetochore Ska1 complex facilitates microtubule depolymerization-coupled motility. *Dev. Cell* **16**, 374–385 (2009).
429. Daum, J. R. *et al.* Ska3 is required for spindle checkpoint silencing and the maintenance of chromosome cohesion in mitosis. *Curr. Biol. CB* **19**, 1467–1472 (2009).
430. Chan, G. K., Schaar, B. T. & Yen, T. J. Characterization of the kinetochore binding domain of CENP-E reveals interactions with the kinetochore proteins CENP-F and hBUBR1. *J. Cell Biol.* **143**, 49–63 (1998).
431. McVey, S. L., Cosby, J. K. & Nannas, N. J. Aurora B Tension Sensing Mechanisms in the Kinetochore Ensure Accurate Chromosome Segregation. *Int. J. Mol. Sci.* **22**, 8818 (2021).
432. Ruchaud, S., Carmena, M. & Earnshaw, W. C. Chromosomal passengers: conducting cell division. *Nat. Rev. Mol. Cell Biol.* **8**, 798–812 (2007).
433. DeLuca, K. F., Lens, S. M. A. & DeLuca, J. G. Temporal changes in Hec1 phosphorylation control kinetochore–microtubule attachment stability during mitosis. *J. Cell Sci.* **124**, 622–634 (2011).

434. Cheeseman, I. M. *et al.* Phospho-Regulation of Kinetochore-Microtubule Attachments by the Aurora Kinase Ipl1p. *Cell* **111**, 163–172 (2002).
435. DeLuca, J. G. *et al.* Kinetochore microtubule dynamics and attachment stability are regulated by Hec1. *Cell* **127**, 969–982 (2006).
436. Ideue, T., Cho, Y., Nishimura, K. & Tani, T. Involvement of satellite I noncoding RNA in regulation of chromosome segregation. *Genes Cells Devoted Mol. Cell. Mech.* **19**, 528–538 (2014).
437. Jambhekar, A., Emerman, A. B., Schweidenback, C. T. H. & Blower, M. D. RNA stimulates Aurora B kinase activity during mitosis. *PloS One* **9**, e100748 (2014).
438. Iemura, K., Yoshizaki, Y., Kuniyasu, K. & Tanaka, K. Attenuated Chromosome Oscillation as a Cause of Chromosomal Instability in Cancer Cells. *Cancers* **13**, 4531 (2021).
439. DeLuca, K. F. *et al.* Aurora A kinase phosphorylates Hec1 to regulate metaphase kinetochore-microtubule dynamics. *J. Cell Biol.* **217**, 163–177 (2018).
440. Iemura, K., Natsume, T., Maehara, K., Kanemaki, M. T. & Tanaka, K. Chromosome oscillation promotes Aurora A–dependent Hec1 phosphorylation and mitotic fidelity. *J. Cell Biol.* **220**, e202006116 (2021).
441. Gordon, D. J., Resio, B. & Pellman, D. Causes and consequences of aneuploidy in cancer. *Nat. Rev. Genet.* **13**, 189–203 (2012).
442. McIntosh, J. R. Structural and mechanical control of mitotic progression. *Cold Spring Harb. Symp. Quant. Biol.* **56**, 613–619 (1991).
443. Li, X. & Nicklas, R. B. Mitotic forces control a cell-cycle checkpoint. *Nature* **373**, 630–632 (1995).
444. Rieder, C. L., Cole, R. W., Khodjakov, A. & Sluder, G. The checkpoint delaying anaphase in response to chromosome monoorientation is mediated by an inhibitory signal produced by unattached kinetochores. *J. Cell Biol.* **130**, 941–948 (1995).
445. Lara-Gonzalez, P., Westhorpe, F. G. & Taylor, S. S. The Spindle Assembly Checkpoint. *Curr. Biol.* **22**, R966–R980 (2012).
446. Ma, H., L, T. & Bt, R. S. cerevisiae genes required for cell cycle arrest in response to loss of microtubule function. *Cell* **66**, (1991).
447. R, L. & Aw, M. Feedback control of mitosis in budding yeast. *Cell* **66**, (1991).
448. Weiss, E. & Winey, M. The Saccharomyces cerevisiae spindle pole body duplication gene MPS1 is part of a mitotic checkpoint. *J. Cell Biol.* **132**, 111–123 (1996).
449. Hoffman, D. B., Pearson, C. G., Yen, T. J., Howell, B. J. & Salmon, E. D. Microtubule-dependent changes in assembly of microtubule motor proteins and mitotic spindle checkpoint proteins at PtK1 kinetochores. *Mol. Biol. Cell* **12**, 1995–2009 (2001).
450. Iwanaga, Y. & Jeang, K.-T. Expression of mitotic spindle checkpoint protein hsMAD1 correlates with cellular proliferation and is activated by a gain-of-function p53 mutant. *Cancer Res.* **62**, 2618–2624 (2002).
451. Jeong, S.-J. *et al.* Transcriptional Abnormality of the hsMAD2 Mitotic Checkpoint Gene Is a Potential Link to Hepatocellular Carcinogenesis. *Cancer Res.* **64**, 8666–8673 (2004).
452. Karess, R. Rod-Zw10-Zwilch: a key player in the spindle checkpoint. *Trends Cell Biol.* **15**, 386–392 (2005).
453. Caldas, G. V. *et al.* The RZZ complex requires the N-terminus of KNL1 to mediate optimal Mad1 kinetochore localization in human cells. *Open Biol.* **5**, 150160 (2015).
454. Antoni, A. D. *et al.* The Mad1/Mad2 Complex as a Template for Mad2 Activation in the Spindle Assembly Checkpoint. *Curr. Biol.* **15**, 214–225 (2005).
455. Li, Y., Gorbea, C., Mahaffey, D., Rechsteiner, M. & Benezra, R. MAD2 associates with the cyclosome/anaphase-promoting complex and inhibits its activity. *Proc. Natl. Acad. Sci. U. S. A.* **94**, 12431–12436 (1997).
456. Fang, G., Yu, H. & Kirschner, M. W. The checkpoint protein MAD2 and the mitotic regulator CDC20 form a ternary complex with the anaphase-promoting complex to control anaphase initiation. *Genes Dev.* **12**, 1871–1883 (1998).
457. Ryan, S. D. *et al.* Up-regulation of the mitotic checkpoint component Mad1 causes chromosomal instability and resistance to microtubule poisons. *Proc. Natl. Acad. Sci. U. S. A.* **109**, E2205–E2214 (2012).
458. McAinsh, A. D. & Kops, G. J. P. L. Principles and dynamics of spindle assembly checkpoint signalling. *Nat. Rev. Mol. Cell Biol.* **24**, 543–559 (2023).
459. Buffin, E., Lefebvre, C., Huang, J., Gagou, M. E. & Karess, R. E. Recruitment of Mad2 to the Kinetochore Requires the Rod/Zw10 Complex. *Curr. Biol.* **15**, 856–861 (2005).
460. London, N., Ceto, S., Ranish, J. A. & Biggins, S. Phosphoregulation of Spc105 by Mps1 and PP1 regulates Bub1 localization to kinetochores. *Curr. Biol. CB* **22**, 900–906 (2012).
461. Shepperd, L. A. *et al.* Phosphodependent recruitment of Bub1 and Bub3 to Spc7/KNL1 by Mph1 kinase maintains the spindle checkpoint. *Curr. Biol. CB* **22**, 891–899 (2012).
462. Yamagishi, Y., Yang, C.-H., Tanno, Y. & Watanabe, Y. MPS1/Mph1 phosphorylates the kinetochore protein KNL1/Spc7 to recruit SAC components. *Nat. Cell Biol.* **14**, 746–752 (2012).
463. Primorac, I. *et al.* Bub3 reads phosphorylated MELT repeats to promote spindle assembly checkpoint signaling. *eLife* **2**, e01030 (2013).

464. Hiruma, Y. *et al.* Competition between MPS1 and microtubules at kinetochores regulates spindle checkpoint signaling. *Science* **348**, 1264–1267 (2015).
465. Etemad, B. & Kops, G. J. Attachment issues: kinetochore transformations and spindle checkpoint silencing. *Curr. Opin. Cell Biol.* **39**, 101–108 (2016).
466. Raisch, T. *et al.* Structure of the RZZ complex and molecular basis of Spindly-driven corona assembly at human kinetochores. *EMBO J.* **41**, e110411 (2022).
467. Murata-Hori, M. & Wang, Y. The Kinase Activity of Aurora B Is Required for Kinetochore-Microtubule Interactions during Mitosis. *Curr. Biol.* **12**, 894–899 (2002).
468. Ditchfield, C. *et al.* Aurora B couples chromosome alignment with anaphase by targeting BubR1, Mad2, and Cenp-E to kinetochores. *J. Cell Biol.* **161**, 267–280 (2003).
469. Hauf, S. *et al.* The small molecule Hesperadin reveals a role for Aurora B in correcting kinetochore–microtubule attachment and in maintaining the spindle assembly checkpoint. *J. Cell Biol.* **161**, 281–294 (2003).
470. Matsumura, S., Toyoshima, F. & Nishida, E. Polo-like kinase 1 facilitates chromosome alignment during prometaphase through BubR1. *J. Biol. Chem.* **282**, 15217–15227 (2007).
471. Costa, G., Barra, V., Lentini, L., Cilluffo, D. & Di Leonardo, A. DNA demethylation caused by 5-Aza-2'-deoxycytidine induces mitotic alterations and aneuploidy. *Oncotarget* **7**, 3726–3739 (2016).
472. Scelfo, A. *et al.* Tunable DNMT1 degradation reveals DNMT1/DNMT3B synergy in DNA methylation and genome organization. *J. Cell Biol.* **223**, e202307026 (2024).
473. Salinas-Luypaert, C. *et al.* DNA methylation influences human centromere positioning and function. *Nat. Genet.* **57**, 2509–2521 (2025).
474. Holland, A. J., Fachinetti, D., Han, J. S. & Cleveland, D. W. Inducible, reversible system for the rapid and complete degradation of proteins in mammalian cells. *Proc. Natl. Acad. Sci. U. S. A.* **109**, E3350-3357 (2012).
475. Nishimura, K. *et al.* A super-sensitive auxin-inducible degron system with an engineered auxin-TIR1 pair. *Nucleic Acids Res.* **48**, e108 (2020).
476. Martino, S., Gargano, S., Carollo, P. S., Di Leonardo, A. & Barra, V. DNMT1 prolonged absence is a tunable cellular stress that triggers cell proliferation arrest to protect from major DNA methylation loss. *Cell. Mol. Life Sci. CMLS* **82**, 7 (2024).
477. Rodrigues, N. R. *et al.* p53 mutations in colorectal cancer. *Proc. Natl. Acad. Sci. U. S. A.* **87**, 7555–7559 (1990).
478. Barra, V., Schillaci, T., Lentini, L., Costa, G. & Di Leonardo, A. Bypass of cell cycle arrest induced by transient DNMT1 post-transcriptional silencing triggers aneuploidy in human cells. *Cell Div.* **7**, 2 (2012).
479. Besselink, N. *et al.* The genome-wide mutational consequences of DNA hypomethylation. *Sci. Rep.* **13**, 6874 (2023).
480. Chan, Y. W., Jeyaprakash, A. A., Nigg, E. A. & Santamaria, A. Aurora B controls kinetochore-microtubule attachments by inhibiting Ska complex-KMN network interaction. *J. Cell Biol.* **196**, 563–571 (2012).